

NASA Contractor Report 3508

NASA
CR
3508
c.1

0062229



TECH LIBRARY KAFB, NM

Tests of a "D" Vented Thrust Deflecting Nozzle Behind a Simulated Turbofan Engine

T. L. Watson

TECHNICAL REPORT
AERONAUTICAL LIBRARY
KAFB, ALBUQUERQUE, NM

CONTRACT NAS3-21733
JANUARY 1982

NASA



0062229

NASA Contractor Report 3508

Tests of a "D" Vented Thrust Deflecting Nozzle Behind a Simulated Turbofan Engine

T. L. Watson
McDonnell Douglas Corporation
St. Louis, Missouri

Prepared for
Lewis Research Center
under Contract NAS3-21733



National Aeronautics
and Space Administration

Scientific and Technical
Information Branch

1982

TABLE OF CONTENTS

<u>Section</u>	<u>Title</u>	<u>Page</u>
I.	SUMMARY	1
II.	INTRODUCTION	3
III.	"D" VENTED NOZZLE CONCEPT	5
IV.	TEST APPARATUS	6
	Model Description	6
	Instrumentation	7
V.	EXPERIMENTAL PROCEDURES AND DATA REPEATABILITY	10
	Test Procedures	10
	Data Reduction	10
	Data Repeatability	12
VI.	DISCUSSION OF RESULTS	13
	Data Comparisons	13
	Exit Area Variation	15
	Core Configuration Comparison	17
	Hood Rotation	20
	Yaw Vane Removal	20
	Mismatched Nozzle Entrance Total Pressure	20
	Core Temperature Variation	21
	Thrust Moment Arm	22
	Flow Visualization	22
VII.	SUMMARY OF RESULTS	23
REFERENCES		24
APPENDIX A - "D" VENTED NOZZLE PERFORMANCE DATA		25
APPENDIX B - SYMBOL DEFINITIONS		26

I. SUMMARY

Tests were conducted at the NASA-Lewis Research Center on a 20% scale "D" vented, thrust deflecting, nozzle applicable to subsonic vertical/short take-off and landing (V/STOL) aircraft. The program objectives were to evaluate the effects of core nozzle geometry and exit location on the performance of the "D" vented nozzle. The emergency engine-out condition, in which the fan in a failed engine is driven mechanically through a cross shaft arrangement with power supplied by the operable engine, was also evaluated. Pressure loads design data were also sought for a large scale "D" vented nozzle to be evaluated behind a TF34 turbofan engine at the NASA-Ames Research Center in 1981 (Contract Number NAS2-10564).

Nozzle entrance flow conditions were representative of a turbofan engine (design bypass ratio = 5.5). Fan flow was provided by a tip-turbine fan. A separate, independently controlled air supply was introduced into the model to simulate turbofan engine gas generator (core) flow. Nozzle performance, surface static pressure and flow visualization data were obtained over a nozzle pressure ratio range (fan stream) of 1.1 to 1.35. Nozzle pressure ratio of the core stream was varied from 1.1 to 1.6. Tests were conducted with parametric variations of nozzle entrance Mach number from 0.30 to 0.55 and thrust deflection angle from approximately 0° (cruise) to 100°. Several core nozzle configurations were evaluated, as were the effects of core exit axial location, mismatch between the core and fan stream nozzle pressure ratios, and the presence of a yaw vane.

Results showed that the core nozzle hub shape affected overall nozzle performance. A slotted mixer type core configuration showed promise in improving nozzle performance under engine out conditions. Moving the core exit aft into the nozzle improved performance at engine out with only a minor effect when the core was flowing. An adverse trend on velocity coefficient with nozzle pressure ratio for the vectored nozzle was observed. This is attributed to total pressure or total temperature distortion in the nozzle entrance flow, or to geometry differences between the current hardware and the smaller model used to obtain the results reported in Reference 1. Consistent with results from previous tests, vectored nozzle performance was found to be sensitive to exit area, and the highest performance levels were achieved with matched core and fan nozzle pressure ratios. Performance decreased with mismatched pressure ratios.

The following recommendations are offered as a result of this test:

- o A slotted mixer type of core nozzle configuration should be evaluated further.
- o A parametric evaluation of the effects of total pressure and temperature distortion on vectored nozzle performance should be conducted.
- o Due to the sensitivity of ideal thrust and mass flow to nozzle pressure ratio at unchoked conditions, total pressure levels in the boundary layer should be included in the determination of nozzle entrance total pressure.

- o Tests at NASA-Lewis Research Center are currently planned to survey the nozzle exit flow. Results will provide a data base for analytical studies, diagnostic information, and insights into core stream location and mixing between core and fan streams. Additional analytical studies should be conducted to investigate flow processes within the nozzle. This would provide insight into secondary flows and how they are affected by distortion.

II. INTRODUCTION

The "D" vented nozzle is a lift/cruise thrust vectoring system designed for operation with low pressure ratio, high bypass ratio propulsion systems. The nozzle is a multi-function hood deflector which can be configured for either a conventional turbofan engine or a tip turbine fan system. It is shown installed on a twin engine, subsonic V/STOL configuration in Figure 1. In this installation, the thrust vector is located close to the aircraft center of gravity. Pitch control forces and moments are produced by reaction control system jets, located in the nose and tail. Yaw control is provided by differential vectoring of the two "D" vented nozzles and roll control is provided by thrust modulation.

Flight safety considerations for multi-engine VTOL aircraft have required that VTOL vehicle control capabilities must be maintained in the event of an engine failure. To meet this "engine out" requirement, the engine fans of the configuration shown in Figure 1 are cross-shafted. In the event of a core malfunction, the fan in the failed engine would be driven mechanically, with power being transferred from the other engine. With little or no core flow present, the "D" vented nozzle must operate well with the fan stream alone flowing over a base region. This is especially critical because engine out operation usually sizes the propulsion system for such VTOL aircraft.

The vented vectoring nozzle concept was identified by McDonnell Aircraft Company in 1973 after extensive investigations of thrust vectoring, lift/cruise nozzle systems. The study of nozzles for low fan pressure ratio V/STOL propulsion systems was initiated in 1971. Experimental tests have been carried out on a continuing basis up to the present, with a cumulative total of 1600 test occupancy hours. This effort has included screening tests of various nozzle concepts, detailed parametric studies of circular, rectangular and "D" shaped deflector nozzles, and extensive investigations of both "vented" and "unvented" nozzle concepts. The development history and performance for the "D" vented nozzle are summarized in Reference 1.

To further investigate the "D" vented nozzle concept, a test program was conducted at the NASA-Lewis Research Center. The primary objective was to investigate the effects of engine core flow conditions and nozzle geometry on the performance of the "D" vented nozzle configuration. This was achieved through evaluations of six core nozzle configurations, three exit locations and two core flow temperature levels. Design data were also sought for a large scale "D" vented nozzle to be evaluated behind a TF34 turbofan engine at the NASA-Ames Research Center in 1981 (Contract Number NAS2-10564).

McDonnell Aircraft Company designed the model and instrumentation, and fabricated the nozzle hardware. After the test was conducted on the Vertical Thrust Stand at the NASA-Lewis Research Center, test data were analyzed and an oral report and this written report were issued.

Most of the tests were conducted behind a simulated turbofan engine with design bypass ratio of 5.5. The total pressures of the fan and core streams were varied independently, and the engine out condition was simulated by shutting off the core flow.

The "D" vented nozzle concept is described in Section III. The model and instrumentation descriptions are provided in Section IV. The test and data reduction procedures along with an assessment of the data is presented in Section V.

Nozzle performance data are presented in Section VI over a range of nozzle pressure ratios at the matched, mismatched, and engine out conditions for six core nozzle geometries, and variations in exit area and hood rotation. The effects of mismatched nozzle pressure ratios, core temperature, and the presence of a yaw vane were also studied.

The basic nozzle performance data is given in the Appendix A. A definition of symbols is presented in Appendix B.

III. "D" VENTED NOZZLE CONCEPT

Developed as an efficient thrust deflecting device, the "D" vented nozzle is applicable to subsonic V/STOL aircraft powered by low pressure ratio turbo-fan engines. It also provides high levels of performance for long endurance cruise and loiter flight. Figure 2 illustrates the nozzle in both cruise and VTOL modes. The assembly consists of a fixed asymmetric hood, two movable deflector hoods and a split yaw vane/closure door assembly attached to a single support beam, centrally located on the bottom of the fixed nozzle hood. In the cruise mode, the yaw vane doors are closed to form a flat bottom duct and a single "D" shaped cruise exit area. For transition from conventional to vertical flight the closure doors are each rotated 90° to form a single split yaw vane after which longitudinal thrust vectoring is accomplished by rotation of the deflector hood elements. Vectoring in the side direction is obtained by deflecting the split yaw vane.

The nature of flows in a flow turning device such as the "D" vented nozzle are complex but have been understood qualitatively for some time. Investigations reported in References 2 and 3 describe the secondary flows that are induced as a stream is deflected in a bend. These secondary flows are normal to the main stream and are sources of thrust loss within the turning device.

Vented nozzle operating characteristics can be understood through a comparison with those of a short radius (unvented) elbow, Figure 3. In the initial turning section of an unvented deflector, the pressure decreases on the inner wall and increases on the outer wall due to centrifugal forces. The situation is reversed in the final turning section because the pressures have to meet a common ambient condition. The severity of the pressure gradients causes the boundary layer to thicken at the final section of the inner wall. This problem is further complicated by the secondary flows caused by the centrifugal forces. These secondary flows transport low momentum fluid to the inner wall. With these two combined effects, boundary layer separation at the inner wall often occurs.

In a vented nozzle, the static pressure in the elbow inner corner is constrained to near ambient, and the static pressure on the outer wall increases to maintain the required static pressure gradient to balance the centrifugal forces in the turn. Since no elbow inner wall surface is present, separation does not occur and the corresponding total pressure loss is avoided.

IV. TEST APPARATUS

MODEL DESCRIPTION

The experimental apparatus utilized in this test program consisted of an inlet bellmouth and a Tech Development Inc. Model 1109, 30.5 cm. (12 in.) diameter tip-turbine fan mated with a MCAIR designed exhaust system. The exhaust system was composed of a core engine duct, core nozzle assembly, and a "D" vented thrust vectoring nozzle. In addition, a portion of the testing was done with a convergent reference nozzle installed in place of the "D" nozzle.

A schematic of the combined fan/exhaust system test apparatus is shown in Figure 4. This arrangement provided an experimental means to measure vectoring nozzle performance under variations of the core engine flow rate, total pressure, temperature and exit geometry. Flow from the tip-turbine fan simulated the fan flow of a V/STOL turbofan engine, and heated air introduced into the core duct represented the turbofan turbine exhaust flow. Fan stream total pressure and flow were varied through fan speed, while the core flow properties were controlled by the air supply pressure and temperature level. Model normal and axial forces and pitching moment were measured by a six-component strain gage balance. The model was tested in the NASA-Lewis Vertical Thrust Stand, shown in Figure 5. A description of each of the major components of the exhaust system is presented below.

Fan/Core Duct - As shown in Figure 4, the duct hardware consisted of two concentric cylindrical duct sections in which the fan and the core air flow were routed to the lift/cruise vectoring nozzle entrance station. The outer duct connected the Model 1109 fan with the "D" vented nozzle and simulated the fan duct of a turbofan engine. This duct also incorporated the attachment bracket for the force balance used for measurement of the forces and moments. The outer duct accommodated an exit rake at the fan stator exit. Fan drive air was routed to the fan case as shown in the schematic of Figure 6.

The inner duct mated with the hub of the Model 1109 fan and the fan exit rake hub fairings. Heated air was introduced into the inner duct plenum through a strut located just downstream of the fan exit station, Figure 6. It was then routed from the plenum through a flow straightener to a core nozzle. The air used to drive the fan and to simulate core engine exhaust were obtained from the same source, which was heated to 149°C (300°F).

"D" Vented Nozzle - The "D" vented nozzle assembly consisted of five basic elements: a fixed hood, two rotating hoods, a venting lip, and a yaw vane/closure door. Figure 4 shows the "D" vented nozzle in the deflected position. The fixed hood is an asymmetric contoured component in which the fan duct transitions from the circular annulus just ahead of the nozzle entrance station to a "D" shaped exit cross section of the cruise configuration with the closure door installed. In the vectoring mode, the flow turning process is initiated in the fixed hood.

The "D" shaped rotating hoods nest within each other and are hinged at common points located on either side of the fixed hood. The two hoods in

combination provide a maximum geometric deflection angle of 120° from the horizontal fan centerline. The hood had deflection positions of 60°, 75°, 90°, 100° and 110°.

The venting lip determines nozzle exit area with the hoods rotated. This area is defined as the area in a waterline plane bounded by the downstream edge of the venting lip and the rotating hoods in the 110° position. The intersection of the exit plane with the rotating hood is shown by a dashed line in Figure 7. The exit area was assumed to be independent of hood rotation angle. Five venting lip elements of varying lengths were provided for exit area control. The variation ranged from 1.3 to 1.706 times the nozzle entrance flow area, as shown in Figure 7.

The "D" vented nozzle yaw vane/closure door assembly was simulated by fixed geometry hardware for this program. A single yaw vane was installed for vectored nozzle testing. For testing in the cruise mode, the yaw vane was removed and a flat plate closure was mounted to the yaw vane support beam.

Core Nozzle Configuration - A total of five core nozzle shroud/hub geometries were available. A core closure device was also provided. These are shown in Figure 8. The configurations included a Reference Nozzle, Alternate Nozzles 1 and 2, a Slotted Mixer, a 90° Elbow, and a Reference Closure. The Reference Nozzle consisted of an elliptical hub and a short shroud. Alternate No. 1 had a tapered hub with an extended shroud, while Alt. No. 2 had the same tapered hub with a short shroud.

The Slotted Mixer Nozzle was included to investigate a means to improve performance at the engine out condition. The slot flow area in the conical surface could be varied by rotating an interior concentric slotted sleeve with respect to the outer shell.

The 90° Elbow was a fixed structure which separated the fan and core flows in the vectored nozzle. The yaw vane was removed in order to test this configuration.

The Reference Closure Hub was a contoured centerbody which covered the entire core exit to provide a contoured, reference base shape for engine out investigations.

In addition to the above configurations, two sets of lengthened shrouds and corresponding hub spacers were available. This hardware allowed the core exit to be moved aft into the fixed hood.

Convergent Reference Nozzle - The nozzle, shown in Figure 9, is a contoured convergent design with a circular exit area.

INSTRUMENTATION

Instrumentation was provided in the model to measure nozzle thrust, fan operating characteristics, nozzle entrance flow conditions, and local wall static pressures. Forces and moments were determined from six-component

strain gage balance measurements. Fan drive and simulated core mass flows were measured with choked and unchoked calibrated venturis. High level and differential pressure measurements were made with pressure transducers that were read individually. Low level pressures were read using pressure transducers in Scanivalve modules. Temperatures were determined from thermocouple measurements. Accuracies for this instrumentation are summarized in Table 1.

A description of the instrumentation in each model component is presented below.

Force Balance - Model forces and moments were determined with output from a Task Corporation Mark VII, 10.2 cm. (4 in.) diameter strain gage balance. All six components and their second order interactions were used to determine normal force, axial force, and pitching moment. Nozzle forces were confined to the pitch plane throughout the program. Core and fan drive air lines that bridged the balance were routed to minimize normal force and pitching moment tares.

Bellmouth - Eight static pressure taps are located at two axial positions in the bellmouth, as shown in Figure 10. This bellmouth is geometrically similar to a smaller 14 cm. (5.5 in.) diameter bellmouth previously calibrated by the Colorado Engineering Experiment Station, Inc. Two sets of static pressure taps were included in the smaller design to determine the position that produced the best calibration. Fan stream mass flow for this test was calculated from pressure measurements at the downstream location and calibration coefficients from the smaller bellmouth.

Fan Exit - Instrumentation was provided at the exit of the fan stators by the rake shown in Figure 11. Flow properties in the tip-turbine and fan streams were measured just upstream of where they mixed in the fan duct. Turbine exit instrumentation consisted of eight total pressure probes, eight total temperature probes, and eight static pressure taps. Fan stream instrumentation consisted of forty total pressure probes, sixteen total temperature probes and eight static pressure taps.

Nozzle Entrance - Flow properties for the fan and core streams were determined from instrumentation shown in Figure 12. Total pressure and temperature probe locations were area weighted. Twenty-five total pressure probes, six total temperature probes, and six static pressure probes were located in the fan stream. In addition, twelve static pressure taps were located in the outer duct wall. Core stream instrumentation consisted of fifteen total pressure and three total temperature probes, with four static pressure taps located in the inner duct wall.

Fan Duct - Two rows of static pressure taps were located in the upper and lower surfaces of the outer wall as shown in Figure 13. The locations were selected to investigate static pressure gradients forward of the hoods and venting lip. Data were used for determining static pressure loads and for diagnostic purposes.

Core Nozzle - Each of the core nozzles contained static pressure instrumentation on both the outer walls of the nozzles and the hub centerbodies, as illustrated in Figure 8. Static pressures were measured at three circumferential positions - top, bottom and lefthand side. Measurements provided data on the aerodynamic loads induced across the core nozzles by the "D" vented nozzle and on the efficiency of the diffusion of the fan and core duct flow into the "D" nozzle.

Fixed Hood - A row of static pressure taps was provided along the top centerline of the fixed hood of the "D" vented nozzle. This instrumentation, shown in Figure 14, was installed to determine the static pressure distribution along the hood for loads and diagnostic information.

V. EXPERIMENTAL PROCEDURES AND DATA REPEATABILITY

TEST PROCEDURE

Each test run was initiated by first setting the nozzle geometric configuration. Following a warm-up period, fan stream NPR was set through rotor speed and the core stream NPR was set by a regulator adjustment. After allowing approximately one minute for the pressures to stabilize, data were recorded. Following this, a new fan/core NPR combination was selected. This procedure was repeated until all desired points were run. The air supply was then shut down to permit a model change. No flow (zero load) data were recorded with model temperatures stabilized at test (warm) conditions before and after a run for use in calculating thrust loads.

A wide range of test conditions were investigated during the program. Nozzle total pressure ratio (NPR) varied from 1.10 to 1.35, which resulted in a range of Mach number of 0.30 to 0.55 at the nozzle entrance. Runs were made with the total pressures in the fan and core streams matched and mismatched. Also, testing was conducted with the core flow shut off to simulate engine out operation. The latter condition occurs when the fan in an engine with an inoperative core is driven mechanically by the other engine. A total of 88 runs were made during the test period. The test program is summarized in Appendix A.

Tare forces and moments due to core and fan drive air flows which bridged the balance were determined prior to the start of the "D" vented nozzle tests. Corrections were then applied to force balance measurements to remove the effects of the bridging tares.

Data from each run were recorded on magnetic tape and processed through the data reduction program on a high speed digital computer. A brief summary of the key portions of the data reduction procedure is presented in the next section.

DATA REDUCTION

Nozzle performance was evaluated in terms of velocity coefficient, C_v , and discharge coefficient, C_w . Symbols are defined in Appendix B. Ideal thrust and ideal flow rate were calculated for separate (unmixed) core and fan stream flows. The nozzle sizing parameter is specific corrected flow, $W7S$, from which nozzle entrance Mach number can be calculated using isentropic relationships.

When the nozzle was tested in the normal turbofan operating mode (core flowing), calculations were referred to the mixing plane at the nozzle entrance, denoted Station 7. Nozzle station designations are shown in Figure 15. For example, the specific corrected flow with fan and core flowing is denoted $W7S$. At the engine out condition (core not flowing), properties were referred to the fan stream at the nozzle entrance, Station 16, e.g., the specific corrected flow at the engine out condition is denoted $W16S$.

Key performance parameters were calculated from the expressions below. The equations are presented for normal turbofan operation (core flowing), and, the station designation is "7".

Mass averaged nozzle entrance total pressure ratio

$$NPR7M = \frac{NPR16 * W16 + NPR56 * W56}{W16 + W56} \quad (1)$$

Mass averaged nozzle entrance total temperature (2)

$$TT7M = \frac{TT16 * W16 + TT56 * W56}{W16 + W56}$$

Ideal thrust

$$FGIyy = \frac{Wyy}{g} \sqrt{TTyy} \sqrt{\frac{2 \gamma R}{\gamma - 1}} \left[1 - \left(\frac{\gamma - 1}{\gamma} \right)^{\frac{1}{2}} \right] \quad (3)$$

where: yy = 16 - denotes fan stream
 yy = 56 - denotes core stream

Velocity coefficient

$$C_V = \frac{T}{FGI16 + FGI56} \quad (4)$$

In order to calculate the discharge coefficient, the ideal mass flow must be determined. It is not possible to calculate ideal flow for the separate streams because the exit area for each is unknown. Only the total exit area for both streams is known.

Consequently, a technique was used where an effective exit area for each stream could be calculated. The effective exit area is the area required by each stream if it were expanded isentropically to ambient pressure. These areas were added together, and the sum was divided by the physical exit area to determine a flow coefficient based on separate stream properties.

Effective exit area

$$AE8yy = \frac{Wyy \sqrt{Tyy}}{g \left[\frac{2\gamma}{R(\gamma-1)} \right]^{1/2} \left\{ (NPRyy)^{\frac{\gamma-1}{\gamma}} \left[(NPRyy)^{\frac{\gamma-1}{\gamma}} - 1 \right] \right\}^{1/2}} \quad (5)$$

where: yy = 16 - denotes fan stream
 yy = 56 - denotes core stream

Flow coefficient

$$C_w = \frac{AE816 + AE856}{A8} \quad (6)$$

Nozzle entrance specific corrected flow

$$W7S = \frac{(W16 + W56) * \sqrt{TT7M}}{NPR7M * P_{amb} * (A16 + A56)} * \frac{P_{std}}{\sqrt{\frac{T}{T_{std}}}} \quad (7)$$

The nozzle discharge coefficient can be determined from the specific corrected flow from the following relationship:

$$C_w = W7S * \frac{NPR7M * A7}{\frac{P_{std}}{\sqrt{T_{std}}} * A8 * g * \sqrt{\frac{2\gamma}{R(\gamma-1)}} \left[(NPR7M)^{\frac{\gamma-1}{\gamma}} (NPR7M)^{\frac{\gamma-1}{\gamma}} - 1 \right]^{1/2}} \quad (8)$$

DATA REPEATABILITY

Selected configurations were retested to ensure the repeatability of thrust and mass flow measurements. Repeatability was good, as exemplified by the results for a vectored configuration shown in Figure 16 and 17. Velocity coefficient repeatability was approximately ± 0.005 while the discharge coefficient was ± 0.002 . The thrust vector angle repeated within 1 degree.

The overall repeatability for the test is expressed in terms of a "standard error of the estimate" as defined in Figure 18. As shown, thrust and mass flow coefficients repeated within ± 0.0055 .

VI. DISCUSSION OF RESULTS

The "D" vented nozzle was tested behind a model tip-turbine fan with a separate core flow, which simulated an installation behind a turbofan engine. Performance is presented primarily in terms of velocity coefficient, C_v , i.e., the ratio of measured thrust to the ideal thrust of the unmixed fan and core streams. These velocity coefficients are presented as a function of either nozzle pressure ratio or entrance Mach number (specific corrected flow). The equations for these key parameters are defined in Section V. It should be noted that the computed "D" vented nozzle performance levels are reduced from 1% to 2% because the nozzle entrance total pressure did not include the lower pressure in the boundary layer.

The discussion that follows covers the effects on vectored and cruise nozzle performance of exit area variation, core nozzle geometry, hood rotation, yaw vane removal, variations in nozzle entrance conditions, and core stream temperature. Velocity coefficient, mass flow and thrust deflection results presented in the discussion were obtained from Figures 54 through 126, Appendix A. These figures are summarized in the Table 3 run schedule in Appendix A.

As will be shown, vectored nozzle performance is sensitive to nozzle entrance Mach number. In cases where comparisons are made, nozzle performance has been adjusted, if required, for slight differences in entrance Mach number, using sensitivities discussed below.

DATA COMPARISONS

Nozzle velocity coefficient characteristics measured during this test deviated from those measured earlier on the 10% scale, cold flow model described in Reference 1. The differences are attributed to nozzle entrance conditions and model hardware.

10% Scale Model Data - Representative results from Reference 1 are presented in Figure 19 for the "D" vented nozzle at the matched fan and core stream nozzle entrance total pressure ratio and the engine out conditions. At the matched condition, velocity coefficient increased with NPR7M from 0.955 at $NPR = 1.1$ to 0.965 at $NPR = 1.3$. Similarly, performance increased with fan stream nozzle pressure ratio at the engine out condition.

20% Scale Model Data - Typical results from tests behind the tip-turbine fan are presented in Figure 20 at the matched NPR and engine out conditions. At the matched condition, C_v decreased with $NPR7M$ from 0.95 at $NPR7M = 1.1$ to 0.94 at $NPR = 1.3$. Performance also decreased with nozzle pressure ratio at the engine out condition.

Comparisons - Differences between the 20% scale model results and those reported in Reference 1 for the 10% scale nozzle are attributed to three items: boundary layer at the nozzle entrance, total pressure and total temperature distortion at the nozzle entrance, and differences in model hardware.

The duct length upstream of the nozzle entrance in the 20% scale model resulted in a significant amount of boundary layer entering the nozzle. Thick boundary layer was not present in the Reference 1 tests. The effect of introducing this boundary layer flow into an unchoked nozzle is illustrated by examining the performance of the convergent reference nozzle (Figure 9).

At low (unchoked) pressure ratios, ideal thrust and mass flow are sensitive to total pressure. Since the nozzle entrance rake did not extend to the duct walls, total pressures in the boundary layer were not measured. One method of accounting for this is to estimate nozzle entrance total pressure from static pressures, mass flow, total temperatures and flow area measurements. Test results were adjusted in this manner and are shown in Figure 21. With the adjustment, C_V and C_W agree with the estimates provided by the General Electric Company.

Remaining velocity and discharge coefficients, and nozzle pressure ratios presented in this report have not been adjusted to account for boundary layer at the nozzle entrance. Adjusting for this would increase measured C_V and C_W approximately 2%.

Secondly, total pressure and temperature distortion were present at the nozzle entrance in this test program. Total pressure distortion was confined to the fan stream and was the result of the characteristically distorted flow profile at the exit of the model tip-turbine fan. Total temperature distortion was present because the core stream temperature was maintained about 111°C above that of the fan. Fan and core flows were obtained from a common source in the 10% scale test. Thus, the nozzle entrance conditions were uniform.

Fan stream total pressure distortion is illustrated in Figure 22 for the "D" vented nozzle at the matched pressure ratio condition. The distortion indices, shown in the figure were calculated from differences in the average of the total pressure readings from the legs (circumferential distortion) and averages of ring total pressure readings (radial distortion), rather than individual maximum minus minimum. The effect is to reduce the numerical distortion value. As is typical with the model fan, total pressure distortion increased with fan speed and was most severe in the radial direction. Distortion levels were found to correlate with fan stream Mach number. The variation of circumferential and radial distortion indices are presented as a function of fan stream Mach number in Figure 23 for the nozzle entrance stations. Radial distortion, especially, increased with Mach number.

Thirdly, differences in model geometry may have contributed to the deviation in performance trends. In the NASA-Lewis program, model hardware at the nozzle entrance simulated a high bypass ratio turbofan engine. Several turbine hub shapes were evaluated. Hardware simulating a turbine hub was not present during tests of the 10% scale model (Reference 1). Core flow completely filled the core nozzle shroud such that the bypass ratio was much lower. Presence of the hub in the simulated turbofan configuration altered the area distribution through the fixed hood. This may have altered the flow diffusion process.

According to descriptions of flows within bends presented in References 2 and 3, secondary flows induced within a turning device are a source of loss. Descriptions presented in these references apply to 90° elbows with an inner (suction) wall. Secondary flows within the "D" vented nozzle may differ from those described because of the lack of an inner wall.

The effects of entrance flow distortion on these secondary flows is not easily determined. Vorticity due to either pressure or temperature distortion, could influence the strength of the secondary flows and alter the thrust loss characteristics compared to the uniform entrance flow condition. For this reason, it is recommended that testing be performed to investigate parametrically the effects of distortion on vectored nozzle performance.

EXIT AREA VARIATION

Previous tests of the "D" vented nozzle, Reference 1, indicate that the velocity coefficient is strongly dependent on exit area variations, particularly in the vectored mode. Exit area and hood rotation angle were varied parametrically for the Reference Core (forward position) and Alternate No. 2 Core configurations. Results are presented below for the matched nozzle entrance pressure ratio and engine out conditions.

Reference Core - Forward - Performance for the vectored "D" vented nozzle is presented in the form of the map shown in Figure 24 for the Reference Core configuration in the forward position. Velocity coefficient is shown as a function of nozzle entrance specific corrected flow (Mach number). In this manner, both the nozzle performance, C_v , and the nozzle sizing parameter, specific corrected flow, are presented on the same map. Data in the figure have been interpolated to 90° of thrust deflection, which corresponds to the vertical take-off (VTOL) position. Lines of constant nozzle exit area (A_8/A_7) and nozzle entrance pressure ratio (NPR7M) are shown.

The relationship between exit area, entrance Mach number and velocity coefficient is explained through examination of the constant NPR7M and A_8/A_7 characteristics of Figure 24. Reducing the nozzle exit area at a constant value of nozzle pressure ratio decreases the nozzle entrance Mach number.

A similar result was obtained at the engine out condition, in that the velocity coefficient increased as the exit area was decreased. Nozzle performance for the Ref. Core-Forward is shown in Figure 25 at this condition. Velocity coefficients were lower than those in Figure 24, at the matched pressure ratio condition, because the fan stream entrance Mach number was higher for selected values of nozzle pressure ratio and exit area.

Nozzle exit area also influenced the model tip-turbine fan operating line. To allow sufficient stall margin when evaluating the effects of other configuration changes, a venting lip was selected that provided an exit area ratio, A_8/A_7 , of 1.578.

Alternate No. 2 Core - Results from tests with the Alt. No. 2 Core configuration are presented in Figure 26 for the matched pressure ratio condition,

showing the effects of exit area variation in the vectored mode. Data are presented for the 110° hood position which resulted in approximately 92° of thrust deflection. The performance map is similar to that for the Ref. Core configuration in that the velocity coefficient at a constant exit area decreased with increases in pressure ratio and was sensitive to changes in entrance Mach number at a constant pressure ratio.

Enough different hood rotation angles and nozzle exit areas were tested at the engine out condition to permit interpolation to 90° of thrust vectoring (VTOL configuration) and to nozzle exit area ratios of 1.3, 1.4, 1.5 and 1.6, Figure 27. A good example of the effect of nozzle exit area on velocity coefficient is shown by examining the results at a nozzle entrance pressure ratio of 1.35. At the baseline exit area ratio selected for the test, $A_g/A_7 = 1.578$, a velocity coefficient value of approximately 0.81 resulted. When the exit area was reduced to an area ratio of 1.3, velocity coefficient increased to approximately 0.94, a 16% increase. These results are consistent with those from previous tests, reported in Reference 1, in that, nozzle performance can be increased by reducing the entrance Mach number (i.e., by properly matching exit area to the reduced flow rate).

Discharge Coefficients - The vectored "D" vented nozzle exhibits a discharge coefficient characteristic similar to that for a sharp-edged orifice. Both are functions of pressure ratio.

Effective exit area is shown in Figure 28 for the vectored nozzle. Effective exit area is defined as the area required if the nozzle flow were expanded isentropically to ambient pressure. This parameter increases with nozzle pressure and explains the change in discharge coefficient with nozzle pressure ratio shown in Figure 17.

In contrast, the effective exit area and discharge coefficient for the cruise nozzle, presented in Figure 29 are relatively insensitive to nozzle pressure ratio, for the range evaluated.

Variable Exit Area - The use of a variable exit area with the vectored nozzle can be employed to increase nozzle performance. This is illustrated on the performance map of Figure 30. This map represents the nozzle exit area ratios tested.

Shown on the map is a velocity coefficient characteristic that would result if a variable geometry feature were included in the nozzle design. The exit area schedule assumed is that required to maintain a constant effective exit area. This would also produce a fan operating line corresponding to a fixed area. For illustration purposes, this schedule was applied for a geometric exit area ratio of 1.654.

Nozzle performance would increase about 0.5% over the pressure ratio range 1.1 to 1.3 instead of decreasing with a constant geometric exit area. Considering the increase (2%) in velocity coefficient when the effects of boundary layer on nozzle entrance total pressure ratio are considered, and the gains available with variable exit area, high nozzle performance ($C_V \geq 0.96$) can be achieved from the "D" vented nozzle in the VTOL configuration.

Vectored Nozzle Performance Sensitivities - Velocity coefficients for the vectored nozzle configurations are sensitive to nozzle entrance Mach number (specific corrected flow), as discussed above. In order for performance comparisions between configurations to be valid, the entrance Mach numbers must be equal. Sensitivities were derived from the data presented in Figure 24 for the matched pressure ratio condition and Figure 27 for the engine out condition to make the adjustments. These sensitivities are presented in Table 2 and represent the slopes of the constant nozzle pressure ratio lines from the above figures.

CORE CONFIGURATION COMPARISON

Six core configurations, shown in Figure 8, were evaluated to determine the effects on nozzle performance. The 90° elbow configuration was tested solely to evaluate any effects of isolating the core and fan streams.

Alternate No. 2 Core vs. Reference Core - Comparisons revealed an effect on performance due to the change in hub shape. Velocity coefficient is presented as a function of the nozzle pressure ratio for the vectored configuration for a single exit area ratio at the matched pressure ratio condition in Figure 31 and for the engine out case in Figure 32. Performance levels were nearly equal for both operating conditions, with the Alt. No. 2 Core being slightly higher (approximately 1%) at the matched pressure ratio condition and the reference core showing a slight advantage at the engine out condition. Effects of the change in core configuration can be obtained at additional exit area ratios by comparing Figures 24 and 26.

Performance comparisons are presented in Figure 33 for the cruise nozzle configuration at the matched pressure ratio condition. Again, the performance levels for the two core nozzle configurations are approximately equal, with the reference core performance being slightly higher (0.5% - 1%).

Slotted Mixer - The slotted mixer was designed to improve nozzle performance at the engine out condition. The slotted, conical shaped surface was intended to control the diffusion of the fan stream with the core not flowing. This is contrasted with the sudden diffusion of the fan stream at the nozzle entrance with either the Ref. or the Alt. No. 2 Core in the engine out condition. The slotted mixer also accelerates mixing between the core and fan streams when the core is flowing, and may result in some performance gains due to the mixing of the high temperature core and cold temperature fan streams in a turbofan engine.

For the matched pressure ratio condition, a bypass ratio of approximately 7.3 was achieved with the slotted mixer as compared to the design value of 5.5 achieved with the Ref. and Alt. No. 2 Core configurations. The bypass ratio was higher because the core flow was suppressed due to inadequate core nozzle exit area. In addition, the reduced core flow caused the fan operating line to shift, allowing higher fan flow at a given fan pressure ratio and exit area.

The performance levels for the slotted mixer are essentially equal in both the open and closed position as shown in Figure 34. Because the performance level was unaffected by the slot size, the slotted mixer can be used in the open position. This simplifies the design of the slotted mixer configuration, since variable geometry is not required.

Unlike Alt. No. 2 performance, also shown in Figure 34, the performance of the slotted mixer core nozzle remained constant at the higher pressure ratios. Velocity coefficient was 3% higher at NPR = 1.3. The static pressure distributions on the hub, Figure 35, indicate a separated region on the Alt. No. 2 Core, where the static pressure levels were constant with axial position along the hub. For the slotted mixer configuration, the static pressure level on the slotted shroud increased with axial distance along the nozzle, indicating a more efficient diffusion as the flow moved aft into the "D" vented nozzle. Static pressure levels on the hub inside the slotted shroud are higher than those on the exposed hub of the Alt. No. 2 Core, which is a further indication of better nozzle performance.

Performance levels of the slotted mixer are compared to those from the Alt. No. 2 Core for the cruise nozzle, at the engine out condition, in Figure 36. Velocity coefficients were approximately 1.5% higher with the slotted mixer.

Showing performance gains for both the vectored and the cruise nozzle configurations, the slotted mixer appears to be a promising core nozzle configuration for use with the "D" vented nozzle.

Alternate No. 1 Core - Performance levels for the Alt. No. 1 core fell between those for the Slotted Mixer and the Alt. No. 2 core for the higher fan stream nozzle pressure ratios as shown in Figure 37. The bypass ratio achieved with Alt. No. 1 core also exceeded the design value of 5.5 so that valid comparisons can be made only at the engine out condition. A slight adjustment to the velocity coefficient for the Alt. No. 1 core nozzle data was necessary to match entrance Mach numbers for the other two configurations. Hence, the abscissa is specific corrected flow instead of nozzle pressure ratio. The longer shroud on the Alt. No. 1 and Slotted Mixer core nozzles is thought to provide slight performance improvements at the higher nozzle pressure ratios.

90° Elbow - A 90° elbow configuration was tested to isolate the core stream from the fan stream within the vectored "D" vented nozzle. After the data was adjusted for removal of the yaw vane, performance levels for the 90° elbow were nearly equal to those for the slotted mixer and Alt. No. 1 Core nozzles at the matched pressure ratio condition, as shown in Figure 38. Comparisons are valid here because the bypass ratios with the three core configurations installed were nearly equal.

The presence of the elbow eliminated mixing of the core and fan streams and eliminated temperature gradients within the flow. In the 90° elbow, there are friction losses associated with boundary layer formation on both the inner and outer surfaces. Apparently these losses offset any gains associated with the elimination of interaction between the core and fan streams.

Core Axial Location - Moving the core exit aft into the nozzle could shorten the nacelle/nozzle length and save aircraft weight, as well as allow some flexibility in locating the VTOL thrust vector with respect to the aircraft center of gravity, which is of prime importance in the balance of VTOL configurations.

The exit of the Reference Core nozzle configuration was extended aft into the "D" vented nozzle to quantify the effects on nozzle performance. As shown in Figure 39, nozzle performance decreased only slightly.

The results for the engine out condition are presented in Figure 40. Nozzle performance was more sensitive to exit location at the engine out condition than at the matched pressure ratio condition. Performance increased about 2% as the nozzle was moved to the mid location, then decreased again as it was moved to the aft position.

The flow rate through the core nozzle is a function of the nozzle back pressure because the flow is subsonic throughout. Static pressures increased within the "D" vented nozzle as the flow was turned by the rotating hoods. As the reference core was moved aft, the higher static pressure reduced the amount of flow. In turn, the reduced core flow caused the fan operating line to shift, allowing higher fan flow at a given pressure ratio and exit area. These changes caused the bypass ratio to increase slightly.

Reference Closure Hub - An aerodynamically contoured closure was evaluated as a baseline for the engine out condition. The reference closure hub, Figure 8, completely closed off the core and provided a smooth area distribution through the fixed hood.

The thrust coefficient for the "D" vented nozzle with the Reference Closure Hub was lower than that for the turbofan configuration (Alt. No. 2 Core) at the engine out condition, Figure 41. Comparisons are made for the exit area ratios that provided the closest match in nozzle entrance Mach numbers. The presence of the Reference Closure Hub suppressed the fan flow when compared to the Alt. No. 2 Core at identical exit areas. Turning the flow across the hub also resulted in additional losses in total pressure, which adversely affected nozzle performance. The velocity coefficient characteristics with fan stream nozzle entrance total pressure ratio are similar.

Performance comparisons presented in Figure 42 for the cruise nozzle configuration show that the Reference Closure Hub provides approximately 1% performance increase over the Alt. No. 2 core at the engine out condition. Separation of the flow from the core shroud probably causes the performance penalty.

Summary of Results from Core Comparisons - Significant results from evaluation of the core nozzle configurations are as follows:

- o Moving the core downstream or extending the core shroud aft (e.g. the Slotted Mixer or Alt. No. 1 Core) improved the engine out performance in the vectored mode.

- o The slotted mixer core configuration improved vectored nozzle performance at the engine out condition at higher nozzle pressure ratios. An additional benefit may be gained at the matched pressure ratio condition in that mixing the cool fan and hot core streams in a turbofan engine may result in a higher thrust.
- o Hub shapes have an impact on "D" vented nozzle performance. The tapered hub resulted in higher vectored performance, while the elliptical shaped hub resulted in higher cruise performance.

HOOD ROTATION

The thrust vector is deflected in the "D" vented nozzle by rotating the two movable hoods. Typical results are presented in Figures 43 and 44 for the Alt. No. 2 core configuration and the baseline exit area ($A_8/A_7 = 1.578$). The thrust deflection angle was nearly linear with hood rotation angle, Figure 43, from the stowed position of 35.5° . Thrust vector angle was relatively insensitive to the nozzle entrance pressure ratio. For 90° of thrust vectoring, the VTOL configuration, approximately 107° of hood rotation was required.

The effects of hood rotation on nozzle performance are presented in Figure 44. The data show the effects of hood rotation on both the velocity coefficient and the nozzle entrance Mach number. Low performance levels at reduced thrust deflection angles are thought to result from a higher nozzle entrance Mach number.

The model hardware was designed for high performance levels at the VTOL condition. Therefore, the exit area was sized to provide a relatively low nozzle entrance Mach number. As the hood rotation angle was decreased with a fixed venting lip, effective nozzle exit area increased. This was accompanied by an increase in nozzle entrance Mach number and increased total pressure losses. Control of the nozzle exit area must be maintained throughout the thrust deflection range to maintain low entrance Mach numbers and high velocity coefficient.

YAW VANE REMOVAL

An alternate "D" vented nozzle concept under investigation does not use a yaw vane. Tests were performed during the NASA-Lewis program to document the effects of yaw vane removal. Nozzle performance improved about 1% with a matched nozzle pressure ratio and 2% at engine out conditions, as shown in Figures 45 and 46. The presence of the yaw vane causes a greater decrease in velocity coefficient at the engine out condition than at the matched pressure ratio condition.

MISMATCHED NOZZLE ENTRANCE TOTAL PRESSURE

The effects on nozzle performance of mismatched fan and core stream nozzle entrance total pressures were assessed for both the cruise and vectored configurations. As long as the core was flowing, cruise nozzle performance was not strongly affected. Results from tests of a vectored configuration are

presented in Figures 47 and 48. In these figures, the velocity coefficient is shown as a function of two different correlation parameters. Performance is correlated in Figure 47 as a function of a parameter based on fan and core stream nozzle entrance total pressures, $\lambda = (\text{NPR56} - \text{NPR16})/(\text{NPR7M} - 1)$. This parameter was also used to correlate smaller scale model data, as discussed in Reference 1.

The results are similar in that highest performance results at the matched pressure ratio condition. Velocity coefficient decreases as mismatches in total pressure occur in either stream corresponding to values of greater than or less than zero. Performance obtained at the engine out condition also correlates well with the other mismatched nozzle entrance pressure results.

Results of the correlation with a second mismatch parameter based on the dynamic pressure difference of the two streams is presented in Figure 48. Similar results were obtained. Similar results were also obtained from correlations involving velocity difference, velocity ratio, momentum difference, and kinetic energy difference with none providing any better correlation.

Velocity coefficients resulting from tests at the near-matched nozzle pressure ratio condition are also shown in Figures 47 and 48. With C_v varying about 3% over a small range of mismatch correlation parameter, different trends are apparent, comparing the near-matched and mismatched data. Similarly, a 3% variation is evident in the engine out data. As discussed under Data Comparisons, several items are thought to contribute to the trend of lower velocity coefficient with increasing nozzle pressure ratios as is evident in the near-matched and engine out data. An alternate correlation parameter, calculated for the near-matched condition, using maximum and minimum total pressures measured in the fan stream, did not improve the correlation. Therefore, it appears that the mechanisms discussed above affect C_v in a manner that is more severe than that resulting from NPR mismatch between the two streams.

Mismatched total pressures at the nozzle entrance did not strongly affect the performance of the "D" vented nozzle in the cruise configuration, as shown in Figure 49. When this result is compared with those discussed above, it appears that a mismatch in nozzle pressure ratio strongly affects performance only when nozzle flow is deflected. Additional losses are attributed to accelerated mixing between the two streams that is not present in the cruise configuration.

CORE TEMPERATURE VARIATION

The temperature of the core stream was varied to determine the effects on nozzle performance. Since the core and the fan drive air were supplied from a common source, core temperature could only be reduced approximately 28°C. The results for the vectored condition, Figure 50, show little effect of this small temperature variation. The remainder of the test was with 149°C core temperature.

THRUST MOMENT ARM

The distance between the gross thrust vector line of action and the aircraft center of gravity is critical to the design of V/STOL aircraft, in terms of both balance and control. The thrust moment arm is defined in Figure 51 as the distance measured along the engine centerline between the hood rotation point and the point where the gross thrust vector line of action and the engine centerline intersect. Variations of the thrust moment arm with nozzle pressure ratio and nozzle exit area are presented in Figure 52, where the thrust moment arm, L_T , has been normalized to the nozzle entrance diameter, D_7 . When the data are interpolated to a 90° thrust deflection angle, they indicate that the thrust vector moves aft with increasing nozzle pressure ratio.

Exit area was enlarged by moving the venting lip forward as shown in Figure 7. Increasing the exit area ratio from 1.5 to 1.6 apparently altered the static pressure distributions on the rotating hoods to cause the thrust vector to move aft slightly. The further increase to $A_8/A_7 = 1.7$ apparently altered the flow at the venting lip allowing more flow to exit here. The result was a forward shift of the thrust vector. These data indicate that there is only a slight sensitivity of the thrust vector location to nozzle exit area.

FLOW VISUALIZATION

Flow processes are extremely complex within the vectored "D" vented nozzle due to the three dimensional rotational nature of the flow field. Flow visualization tests were performed to determine the portion of the nozzle occupied by the hot (full scale turbofan engine) core. The position of the core is of concern because of the adverse effect on engine thrust of ingesting high temperature gas. In ground effects, flow from exhaust nozzles impinges on the ground and spreads radially. If the hot core exits in the forward portion of the exhaust stream, the spreading of the ground jet could carry the hot flow forward in the vicinity of the inlets. This condition would simplify the rotating hoods, in that, they can be designed to the relatively cool fan stream temperatures, rather than hot core stream temperatures.

Results from the flow visualization studies revealed that the core flow exited through the forward portion, near the venting lip, as shown in Figure 53. Colored oil was applied to a thin plate installed on the vertical centerline. The plate divided the nozzle into two halves. Different colors were applied to the leading edge of the plate in the fan and core streams. Color photographs taken after the run were used to define the boundary of the core. High core temperatures in a turbofan engine may change the location of the core stream.

VII. SUMMARY OF RESULTS

Results from tests of a 20% scale "D" vented nozzle behind a 30.5 cm. (12 in.) diameter tip-turbine fan with a separate core flow have yielded the following conclusions:

- o High nozzle performance ($C_V \geq 0.96$) can be achieved at both normal (core flowing) and engine out operating conditions through control of the nozzle entrance Mach number with variable exit area.
- o Core nozzle configurations affect performance at matched nozzle pressure ratios.
- o A mixer type nozzle is a promising configuration for engine out operation because the velocity coefficient was insensitive to nozzle pressure ratio over the range tested.
- o When compared with performance from a 10% scale model (Reference 1), results from tests of the 20% scale model indicated lower performance, an adverse trend of velocity coefficient with nozzle pressure ratio, and increased sensitivity to entrance Mach number. This is attributed to differences in model hardware, and total pressure distortion in the fan stream and different temperatures in the fan and core streams of the 20% scale model.
- o Highest vectored nozzle performance resulted when the core and fan stream nozzle pressure ratios are matched.
- o Due to the sensitivity of ideal thrust and mass flow to total pressure at unchoked conditions, total pressure loss in the boundary layer should be included in the determination of nozzle pressure ratio and the performance coefficients.
- o The core stream migrates forward with respect to the fan stream, in the vectored mode, for the core temperature range tested.

REFERENCES

1. Rosenberg, E.W., and Esker, D.W.: Development of the "D" Vented Thrust Deflecting Nozzle, AIAA-80-1856, August 1980.
2. Hawthorne, W.R.: Secondary Circulation in Fluid Flow, Proceedings of the Royal Society, A206, 1951.
3. Taylor, A.M.K.P., Whitelaw, J.H., and Yianneshis, M.: Measurements of Laminar and Turbulent Flow in a Curved Duct With Thin Inlet Boundary Layers, NASA CR 3367, 1981.

APPENDIX A

"D" VENTED NOZZLE PERFORMANCE DATA

Nozzle performance for all configurations are presented in Figures 54 through 126. A summary of the test configurations and the figures where the test results may be found are presented in Table 3.

Nozzle performance - velocity coefficient, C_v , specific corrected flow at the nozzle entrance, WSPC, and thrust deflection angle, PHI - are presented as a function of nozzle pressure ratio. For normal operating conditions, core flowing, the corrected flow at the nozzle entrance, $W\sqrt{\gamma}/\delta$, is divided by the sum of the core and fan stream flow areas. At the engine out condition, core not flowing, only the fan stream flow area is used. At the normal operating condition, "Nozzle Pressure Ratio" is the mass averaged value for the core and fan streams. At the engine out condition, it is the pressure ratio of the fan stream only.

A code is used to specify the operating condition and the run number as follows:

<u>10XX</u>	Engine out condition, core not flowing
<u>20XX</u>	Normal operating condition, core and fan streams operated at matched pressure ratios, NPR16 = NPR56.
<u>10XX</u>	Run number in Table 3.

REFERENCE CLOSURE HUB

For this configuration, only the fan was operating. Data are coded under 10XX or 30XX.

APPENDIX B

SYMBOL DEFINITIONS

AE816	Fan stream effective exit area, 627.9 cm^2 (97.33 in^2)
AE856	Core stream effective exit area, 131.7 cm^2 (20.41 in^2)
A16	Fan stream flow area at the nozzle entrance, cm^2 (in^2)
A56	Core stream flow area at the nozzle entrance, cm^2 (in^2)
A7	Nozzle entrance area, $A_{16} + A_{56}$, cm^2 (in^2)
A8	Nozzle exit area, cm^2 (in^2)
CD16	Circumferential distortion at the nozzle entrance based on average rake leg differences $[(\text{RAKE AVG})_{\text{HI}} - (\text{RAKE AVG})_{\text{LO}}]/\text{AVG NPR16}$
C_V	Velocity coefficient
C_W	Flow coefficient
D_7	Nozzle entrance diameter, 33.812 cm (13.312 in)
F_G	Nozzle thrust, newtons (1b)
FGI16	Fan stream ideal thrust, newtons (1b)
FGI56	Core Stream ideal thrust, newtons (1b)
FPRAV	Average fan exit total pressure ratio
L_T	Thrust moment arm, cm (in)
NPR	Nozzle pressure ratio, total pressure divided by ambient pressure/ (P_T/P_{amb})
NPR16	Total pressure ratio of the fan stream
NPR56	Total pressure ratio of the core stream
NPR7M	Mass weighted core and fan stream nozzle pressure ratio
P_{amb}	ambient static pressure, kilopascals (1b/in^2)
P_s	Static pressure, kilopascals (1b/in^2)
P_{std}	Standard pressure, 101.33 kilopascals (14.696 lb/in^2)
PHI	Thrust deflection angle measured from engine centerline, $\text{PHI} = \emptyset$, degrees
q_{16}	Fan stream dynamic pressure at the nozzle entrance, kilopascals (1b/in^2)
q_{56}	Core stream dynamic pressure at the nozzle entrance, kilopascals (1b/in^2)
RD16	Radial distortion of the fan stream at the nozzle entrance based on average ring differences, $[(\text{RING AVG})_{\text{HI}} - (\text{RING AVG})_{\text{LO}}]/\text{AVG NPR16}$
T	Measured nozzle thrust, newtons (1b)
T_{std}	Standard temperature, 287.8°K (518.7°R)
TT16	Fan stream total temperature, $^\circ\text{K}$ ($^\circ\text{R}$)
TT56	Core stream total temperature, $^\circ\text{K}$ ($^\circ\text{R}$)
TT7M	Mass weighted core and fan stream total temperature at the nozzle entrance, $^\circ\text{K}$ ($^\circ\text{R}$)
W16	Fan stream mass flow, kg/sec (1b/sec)
W56	Core stream mass flow kg/sec (1b/sec)
WSPC	Specific flow corrected to nozzle entrance conditions, $\text{WSPC} = \text{W75}$, kg/sec-cm^2 (1b/sec-in^2)
W7	Mass flow at the nozzle entrance - sum of core and fan stream mass flows, kg/sec (1b/sec)
W7S	Specific flow corrected to nozzle entrance conditions, $\text{W7S} = \text{WSPC}$, kg/sec-cm^2 (1b/sec-in^2)

γ Specific heat ratio
 δ Relative total pressure ratio, total pressure/standard pressure
 θ Relative total temperature ratio, total temperature/standard
temperature
 λ Total pressure ratio correlation parameter, $\frac{\text{NPR56} - \text{NPR16}}{\text{NPR7M} - 1}$
 ϕ Thrust deflection angle measured from engine centerline, $\phi = \text{PHI}$,
degrees

MEASURAND	INSTRUMENT	FULL SCALE MEASUREMENT	ESTIMATED ACCURACY
FORCES	6-COMPONENT STRAIN GAGE BALANCE	~4,448 NEWTONS (~1,000 LB)	±0.15% OF FULL SCALE
MASS FLOW (TURBINE DRIVE AND CORE STREAM)	UNCHOKED VENTURI	3.6 kg/sec (8 LB/SEC)	±0.15% OF READING
	CHOKED VENTURI	3.6 kg/sec (8 LB/SEC)	±0.15% OF READING
MASS FLOW (FAN)	BELLMOUTH	13.6 kg/sec (~30 LB/SEC)	±0.50% OF READING
DIFFERENTIAL PRESSURE (VENTURI)	TRANSDUCER	68.95 kPa (10 PSID)	±0.25% OF FULL SCALE
PRESSURE (MODEL TOTAL AND STATIC)	TRANSDUCER	34.47 kPa (25 PSIA)	±0.25% OF FULL SCALE
PRESSURE (VENTURI)	TRANSDUCER	3 447.38 kPa (500 PSIA)	±0.2% OF FULL SCALE
TEMPERATURE	THERMOCOUPLE	—	±0.25% OF READING

GP13-0132-130

TABLE 1
ESTIMATED INSTRUMENTATION ACCURACY

NPR16 = NPR56

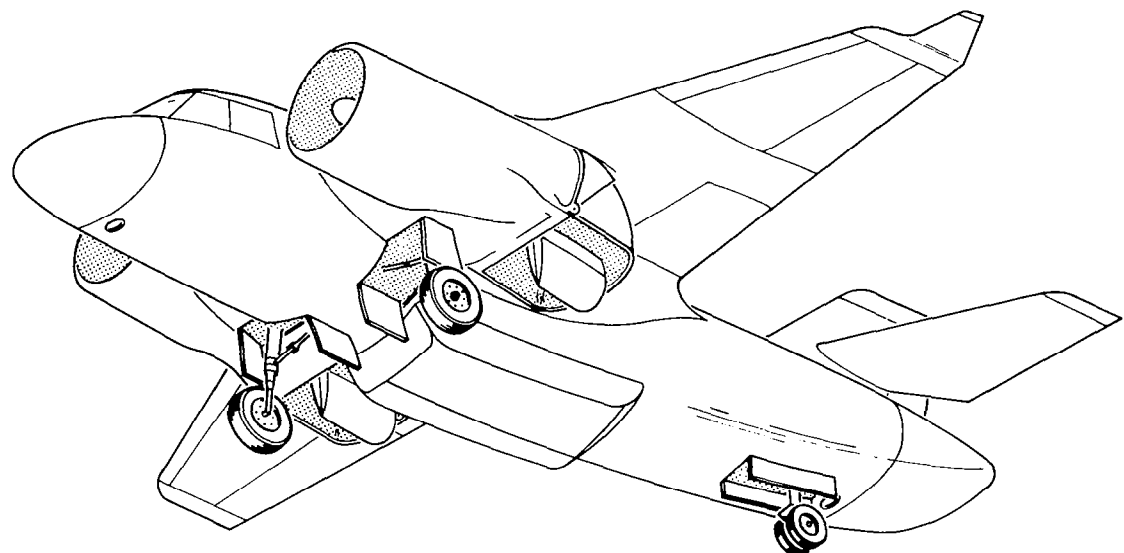
NOZZLE PRESSURE RATIO NPR7M	SENSITIVITY $\frac{\Delta C_V}{\Delta W_{7S}}$, $\frac{1}{\text{kg/sec-cm}^2}$
1.15	-33.1
1.20	-31.3
1.25	-27.5
1.30	-28.0

Engine Out

NOZZLE PRESSURE RATIO NPR16	SENSITIVITY $\frac{\Delta C_V}{\Delta W_{16S}}$, $\frac{1}{\text{kg/sec-cm}^2}$
1.15	-46.0
1.20	-45.6
1.25	-41.7
1.30	-42.2
1.35	-45.6

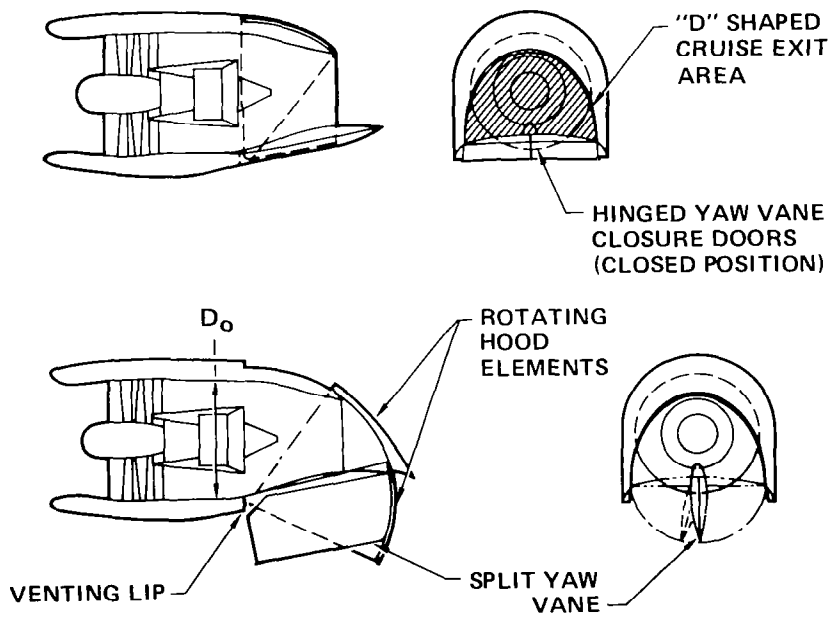
GP13-0132-11

TABLE 2
VECTORED NOZZLE PERFORMANCE SENSITIVITIES



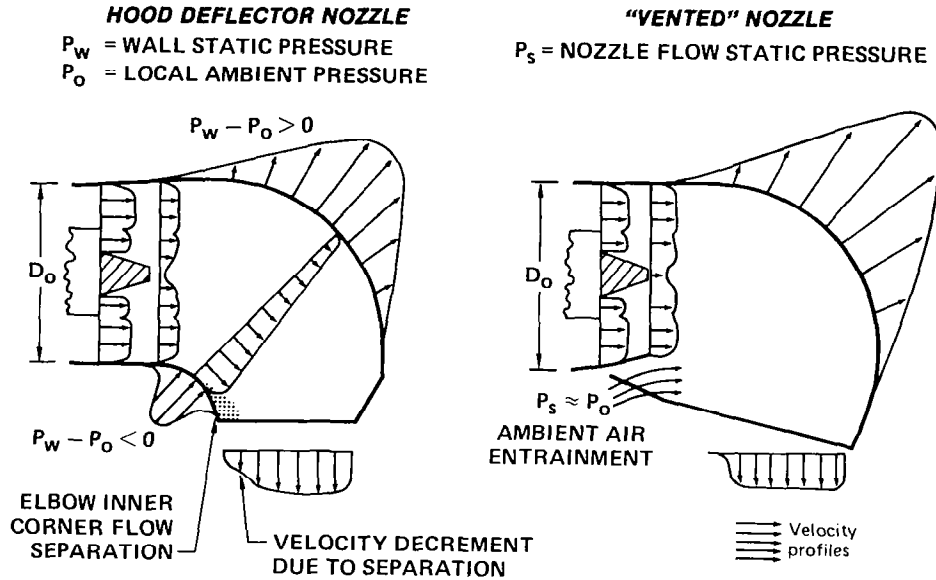
GP13-0132-107

FIGURE 1
SUBSONIC UTILITY CONCEPT WITH D-VENTED NOZZLES



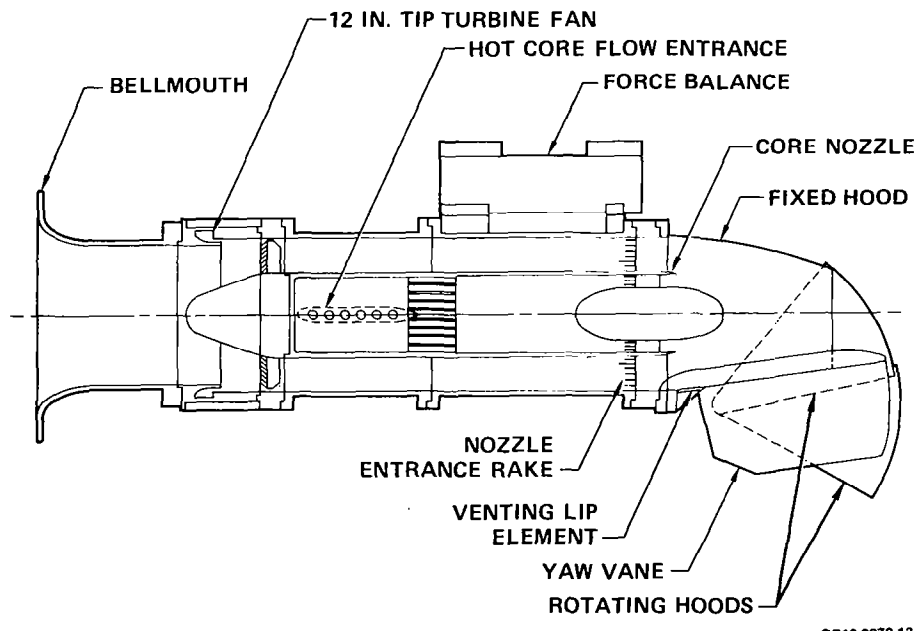
GP13-0272-28

FIGURE 2
"D" VENTED NOZZLE GEOMETRY



GP13-0132-109

FIGURE 3
NOZZLE FLOW CHARACTERISTICS



GP13-0272-13

FIGURE 4
CORE NOZZLE RESEARCH MODEL
"D" Vented Nozzle

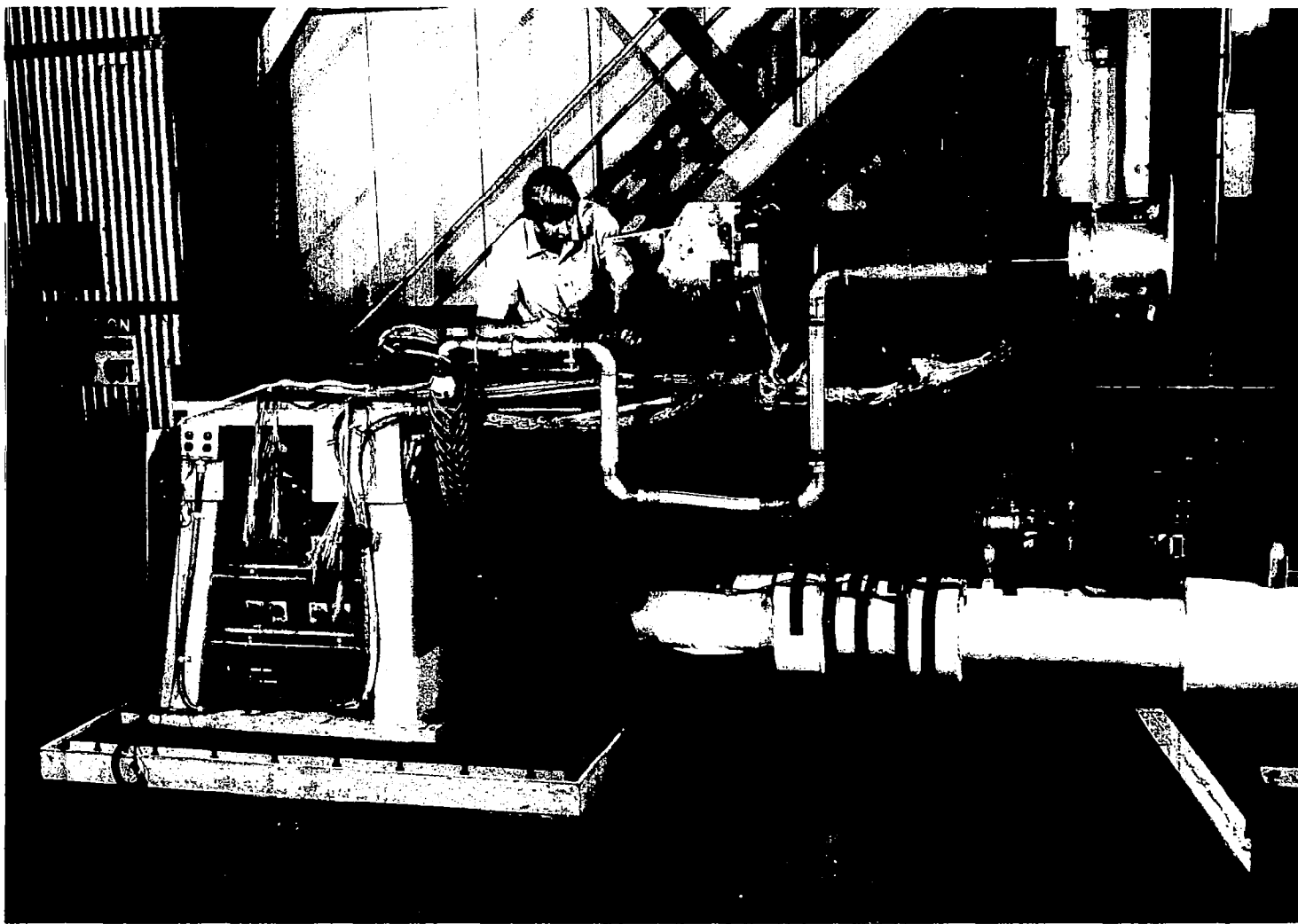


FIGURE 5
CORE NOZZLE RESEARCH MODEL INSTALLED ON VERTICAL THRUST STAND

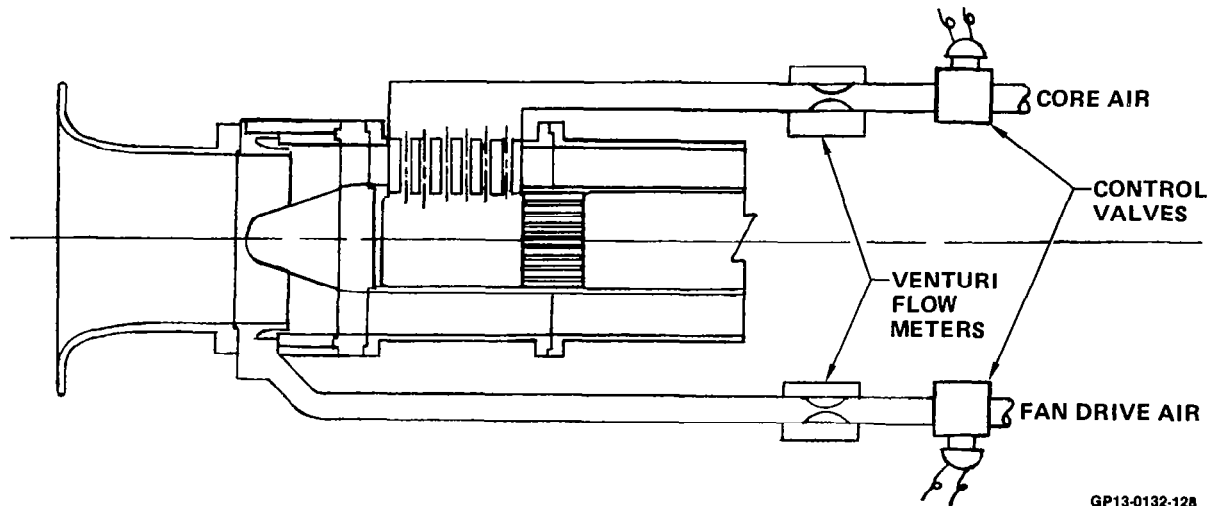


FIGURE 6
SCHEMATIC OF CORE AND FAN DRIVE AIR SYSTEMS

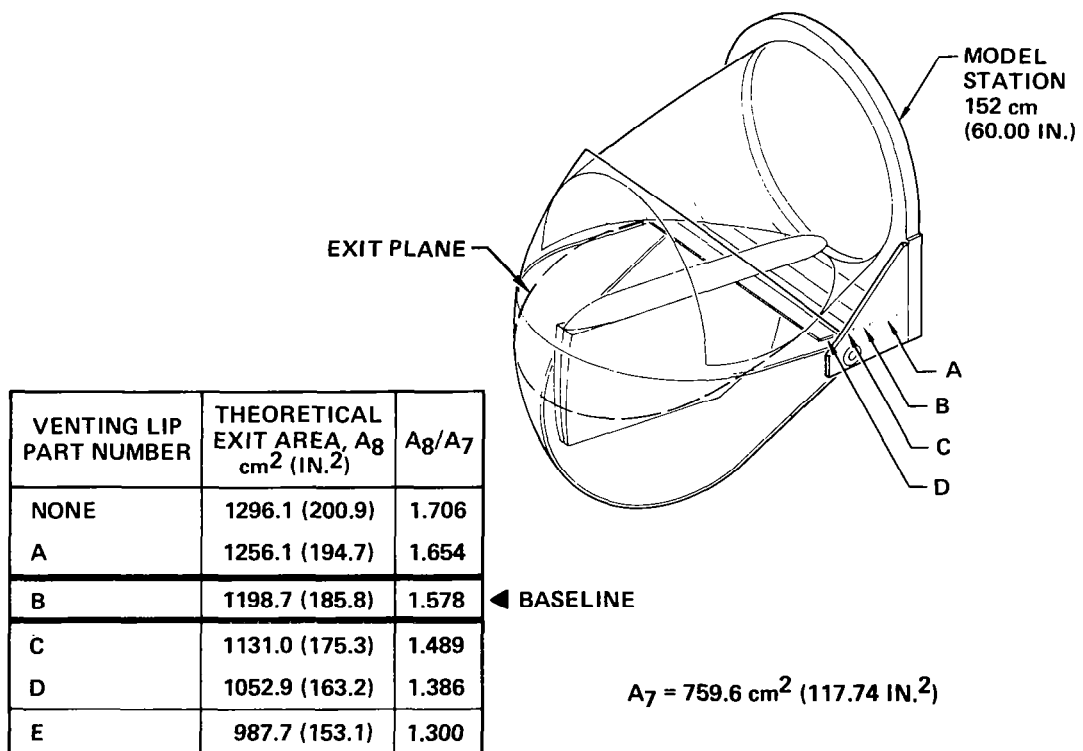
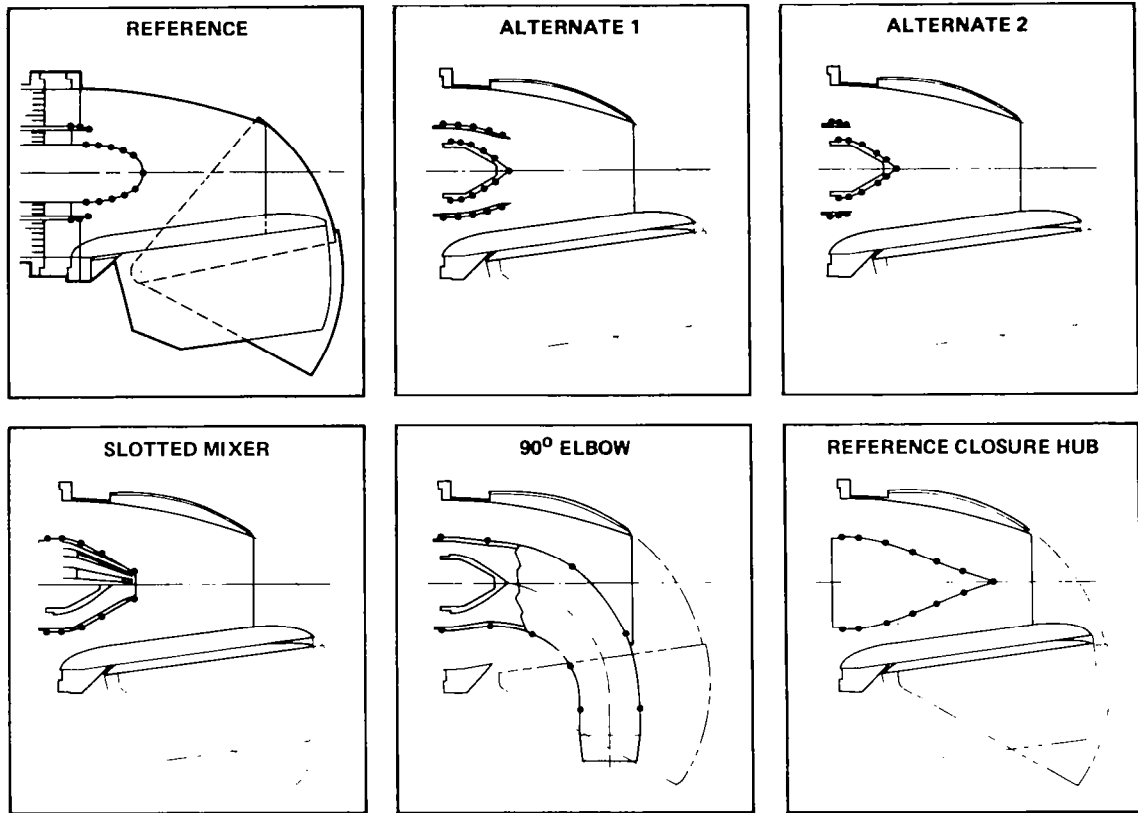


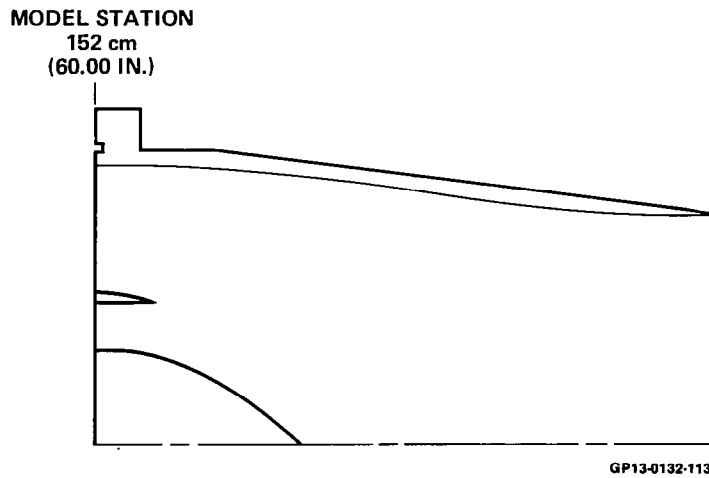
FIGURE 7
"D" VENTED NOZZLE EXIT AREA VARIATION



Note: Pressure tap locations indicated by dot (*)

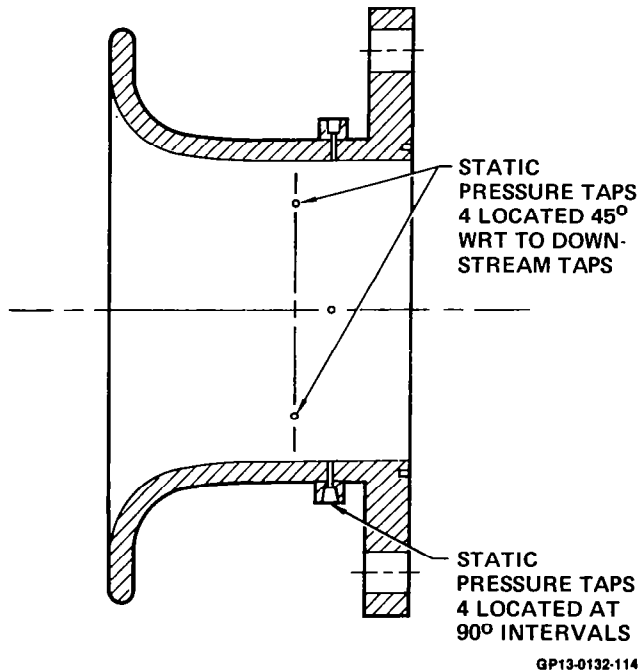
GP13-0272-15

FIGURE 8
CORE NOZZLE RESEARCH MODEL TEST
CORE NOZZLE CONFIGURATIONS



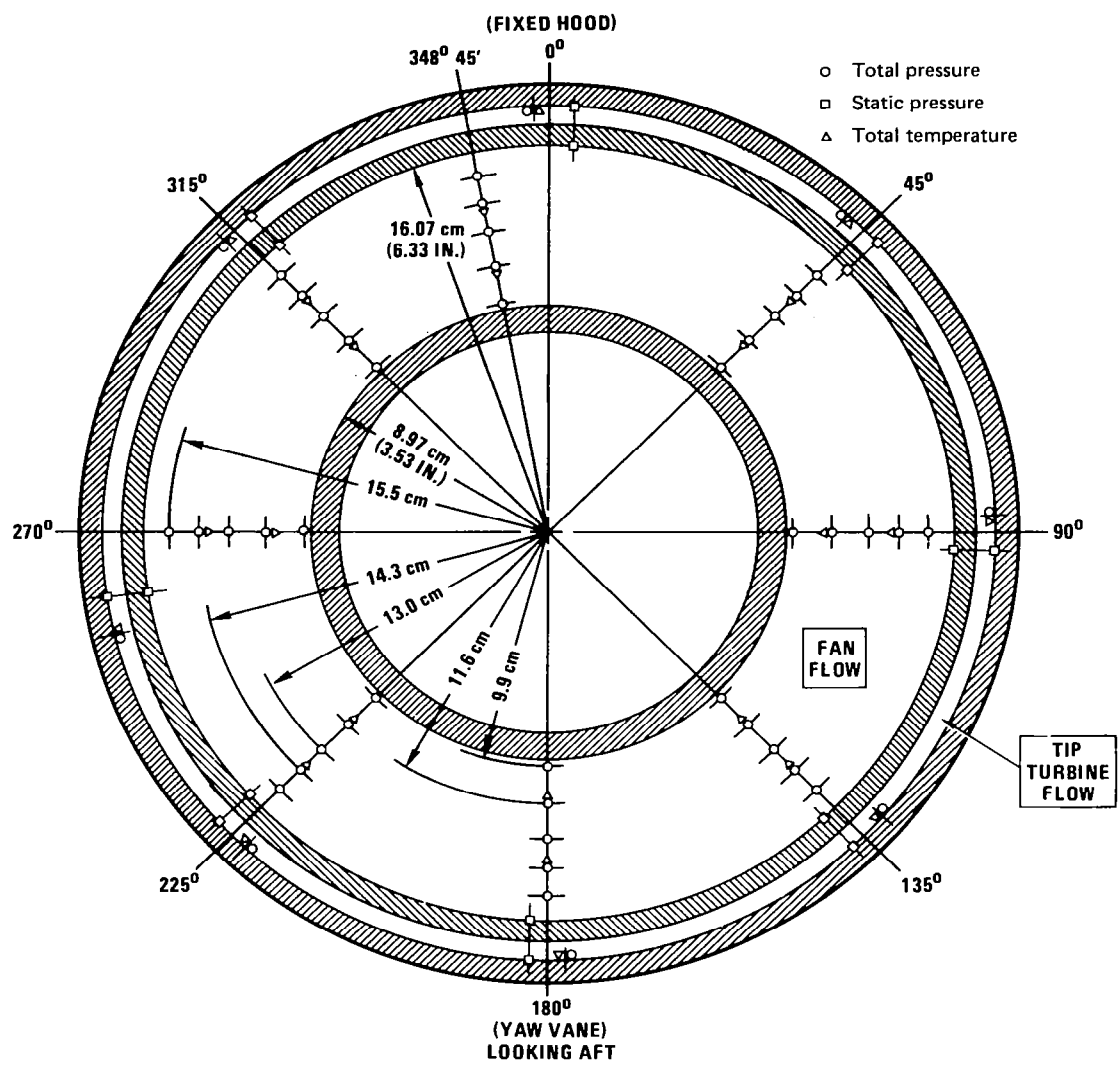
GP13-0132-113

FIGURE 9
CONVERGENT REFERENCE NOZZLE WITH ALTERNATE NO. 2 CORE



GP13-0132-114

FIGURE 10
BELLMOUTH STATIC PRESSURE INSTRUMENTATION



GP13-0132-115

FIGURE 11
FAN AND TIP TURBINE EXIT INSTRUMENTATION

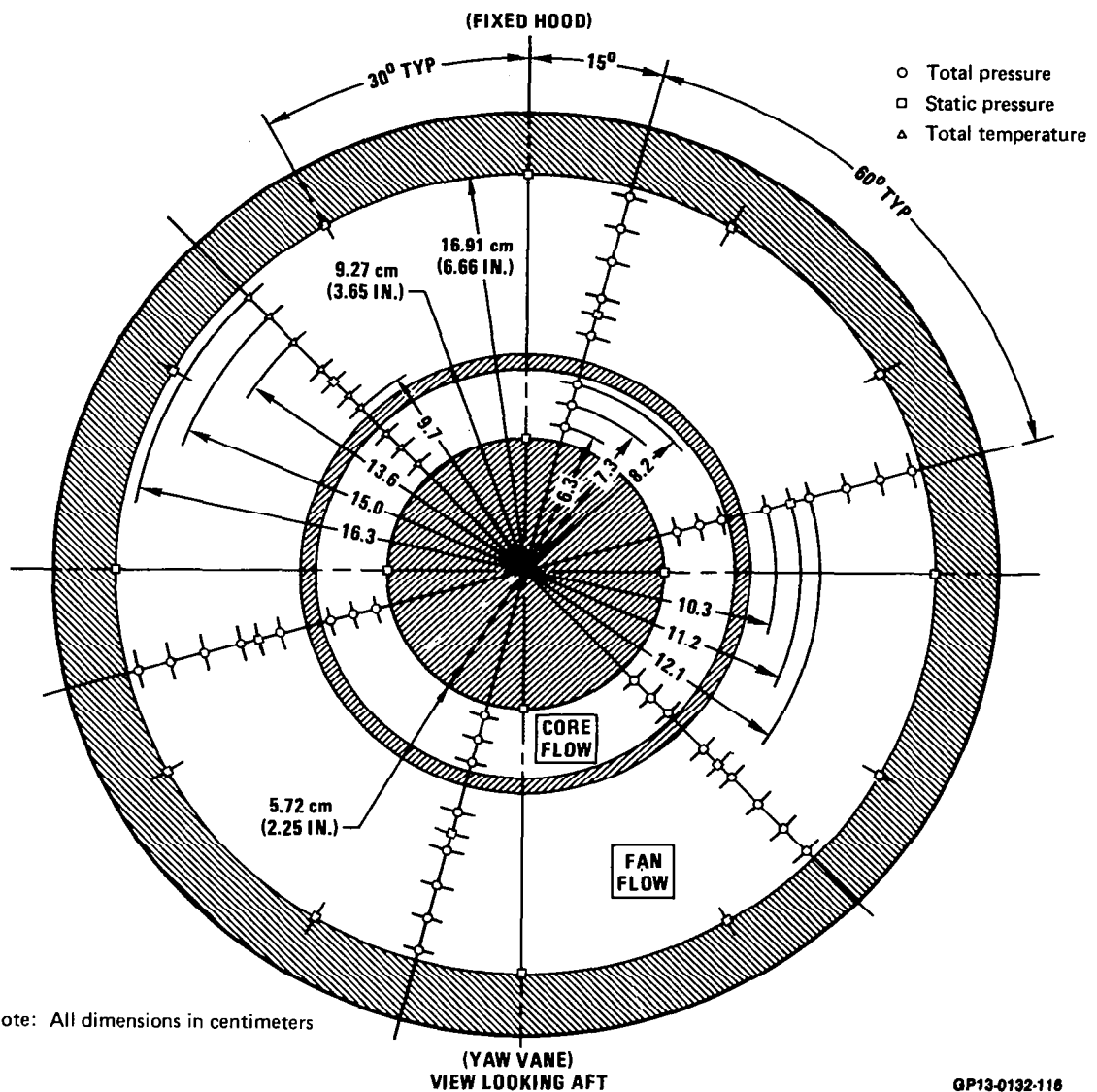
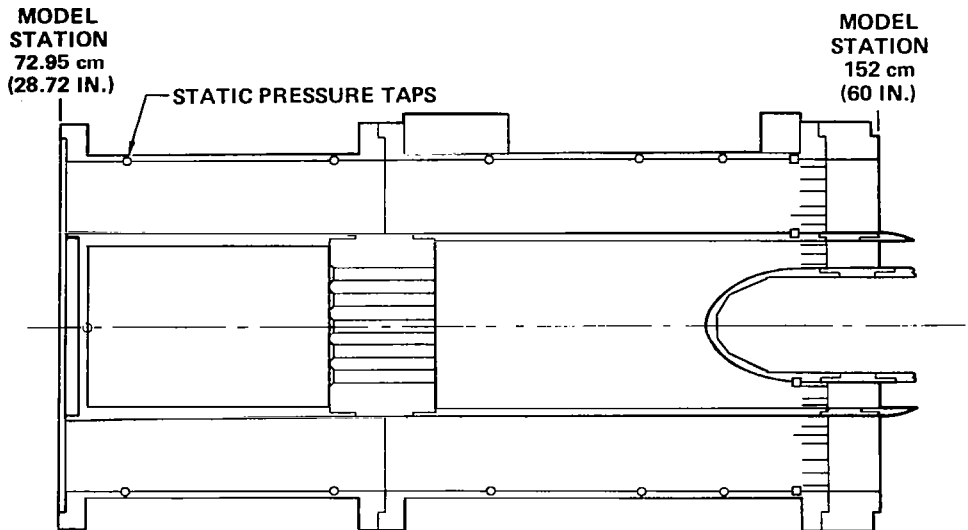


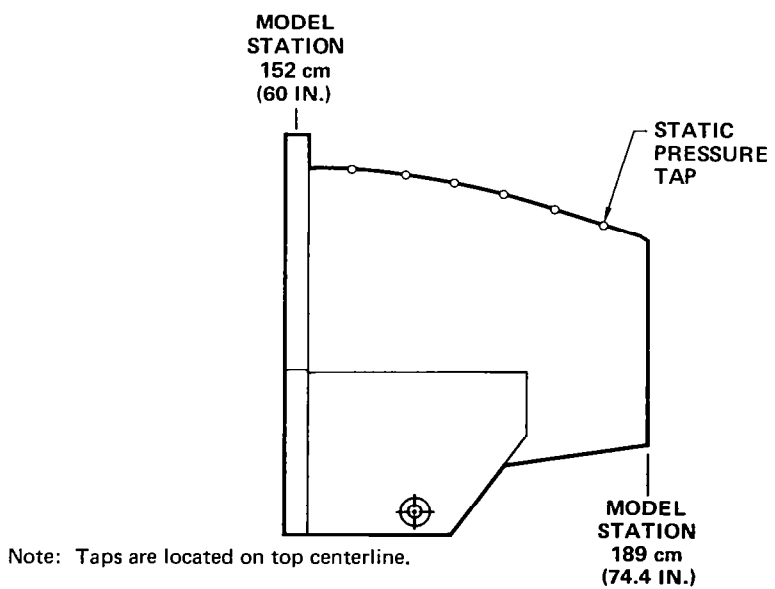
FIGURE 12
NOZZLE ENTRANCE STATION INSTRUMENTATION



SEE NOZZLE
ENTRANCE STATION
INSTRUMENTATION

GP13-0272-16

FIGURE 13
FAN DUCT STATIC PRESSURE TAP LOCATIONS



GP13-0272-17

FIGURE 14
FIXED HOOD STATIC PRESSURE INSTRUMENTATION

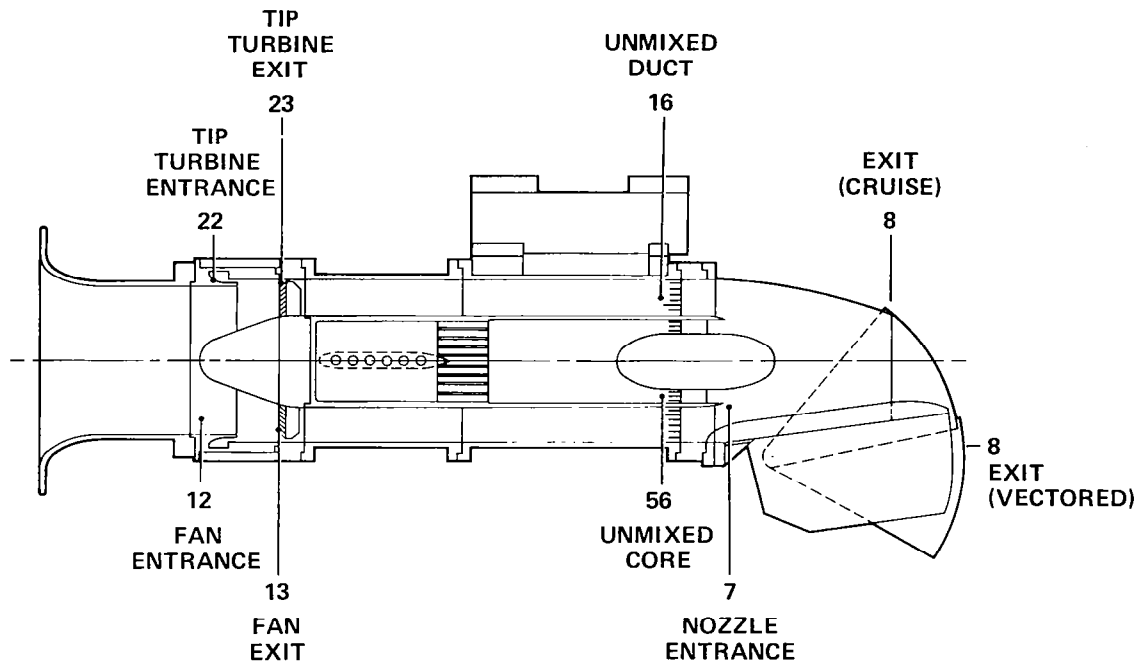


FIGURE 15
MODEL STATION DESIGNATIONS

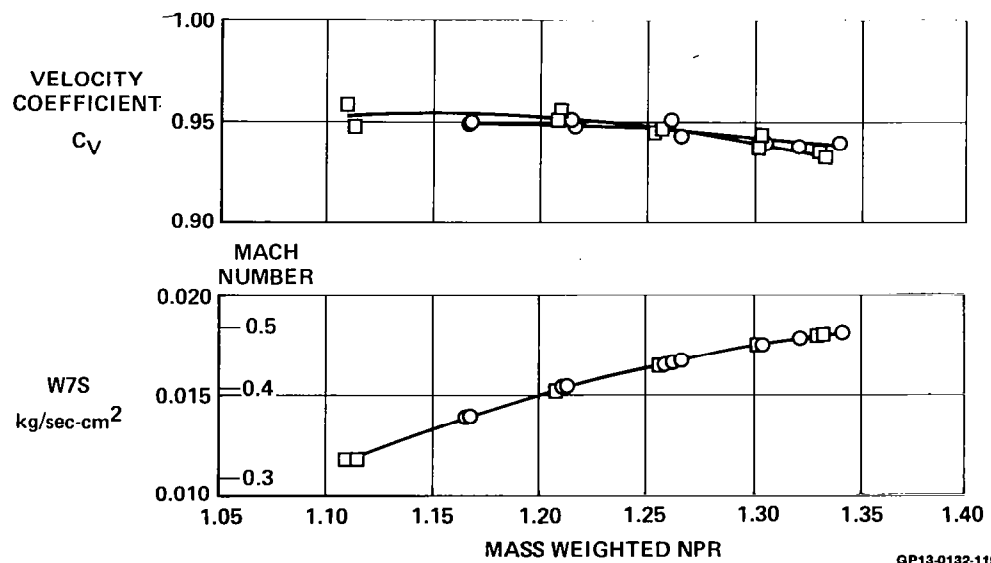
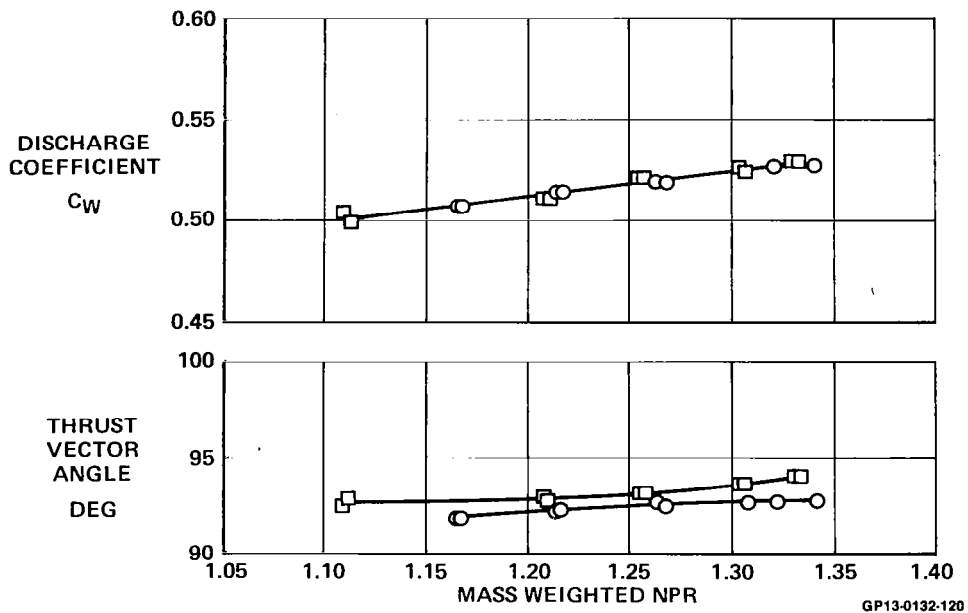


FIGURE 16
DATA REPEATABILITY
Runs 38 & 53 NPR16 = NPR56 Vectored Nozzle
110° Hood $A_8/A_7 = 1.578$ Alternate No. 2 Core



GP13-0132-120

FIGURE 17
DATA REPEATABILITY
Runs 38 & 53 NPR16 = NPR56 Vectored Nozzle
110° Hood $A_8/A_7 = 1.578$ Alternate No. 2 Core

$$\text{STANDARD ERROR OF THE ESTIMATE} = \sqrt{\frac{\sum_{i=1}^n (x_i - \bar{x})^2}{n - 1 - a}}$$

WHERE: n = NUMBER OF DATA POINTS

x_i = MEASURED VALUE

\bar{x} = CURVE FIT VALUE

a = DEGREE OF POLYNOMINAL THAT FITS DATA

	NUMBER OF DATA POINTS	STANDARD ERROR OF THE ESTIMATE	
		VELOCITY COEFFICIENT ΔC_V	DISCHARGE COEFFICIENT ΔC_W
NPR16 = NPR56	61	± 0.0040	± 0.004
ENGINE OUT	33	± 0.0055	± 0.003

GP13-0132-121

FIGURE 18
REPEATABILITY ASSESSMENT

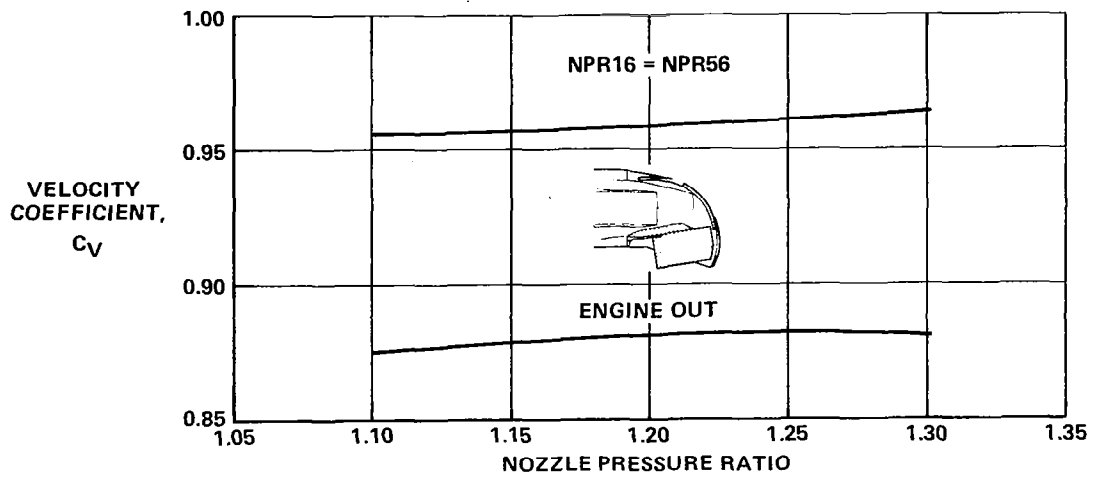


FIGURE 19
10% SCALE MODEL VECTORED NOZZLE PERFORMANCE
MATCHED PRESSURE RATIO AND ENGINE OUT
 $\phi = 90^\circ \quad A_8/A_7 = 1.578$

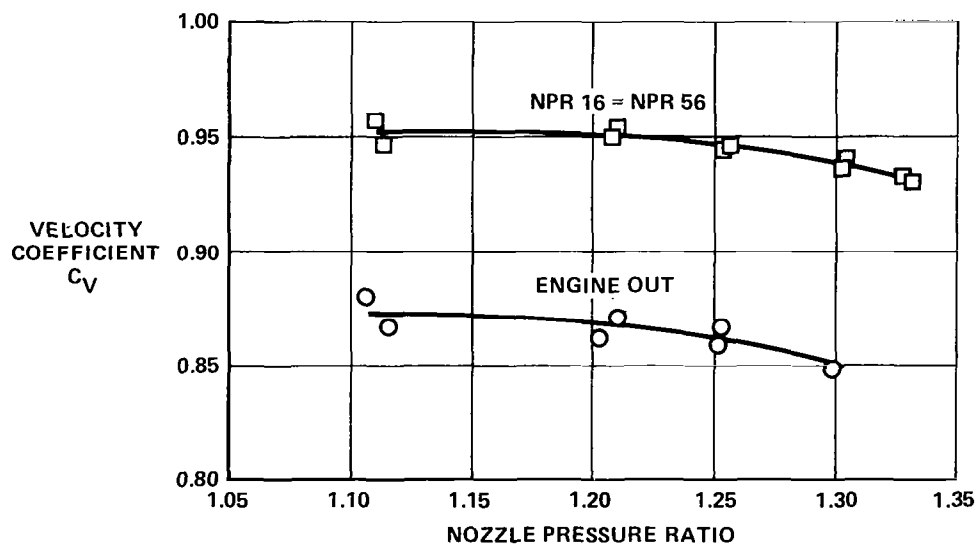


FIGURE 20
VECTORED NOZZLE PERFORMANCE
MATCHED PRESSURE RATIO AND ENGINE OUT
 110° Hood $A_8/A_7 = 1.578$ Alternate No. 2 Core

ALTERNATE 2

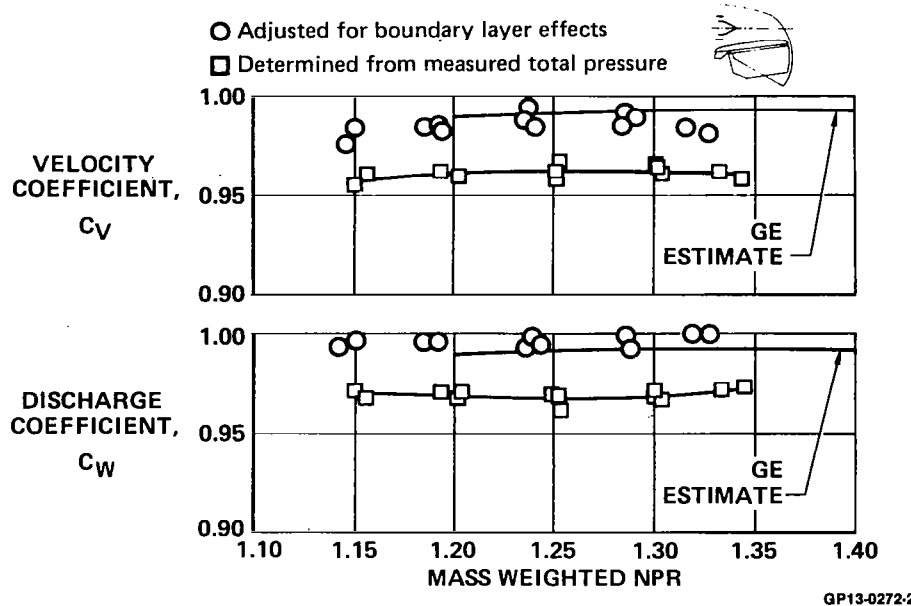


FIGURE 21
NOZZLE VELOCITY AND DISCHARGE COEFFICIENTS

NPR16 = NPR56 Convergent Reference Nozzle

Hood = 0° $A_8/A_7 = 0.7788$ Alternate No. 2 Core

RDG HOOD A_8/A_7 NPR7M ALT NO. 2 CORE
 664 110.00 1.5781 1.3320

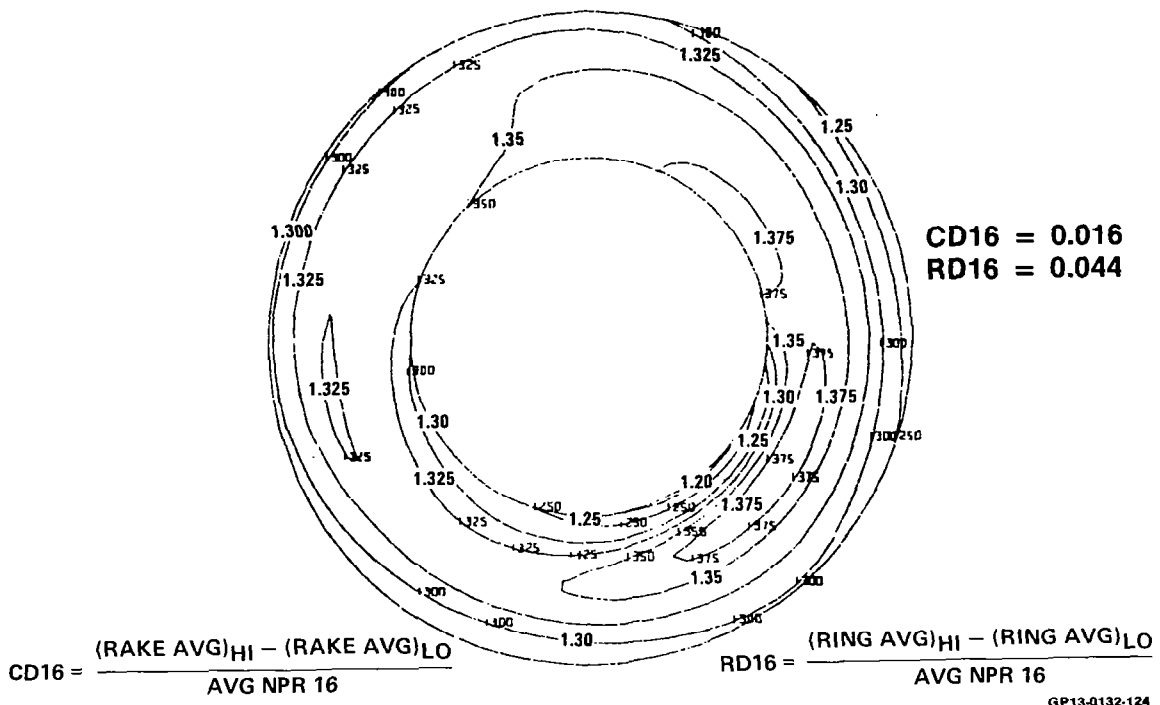
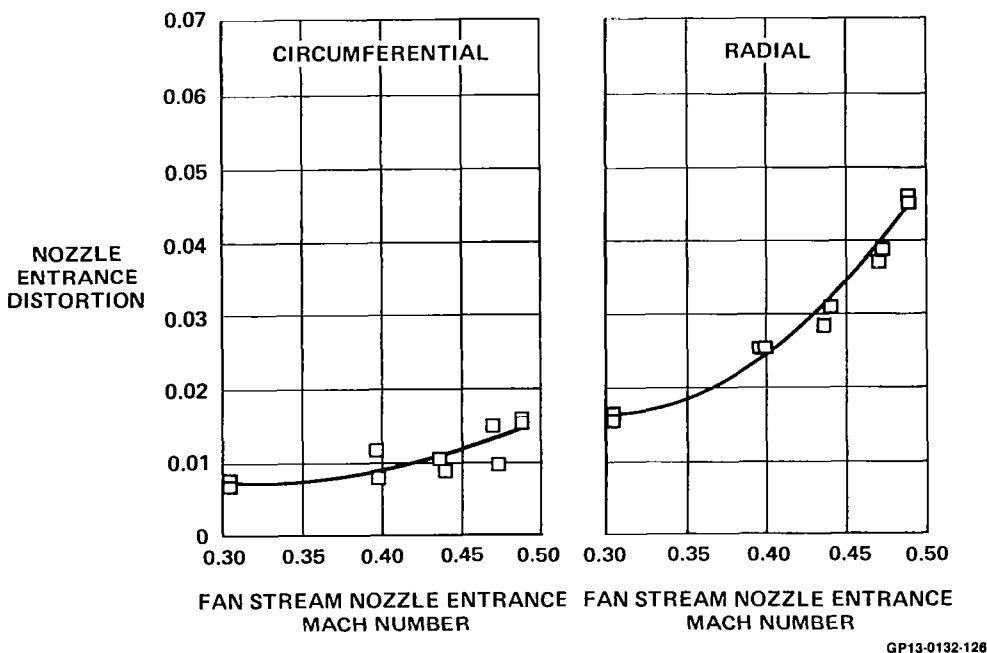
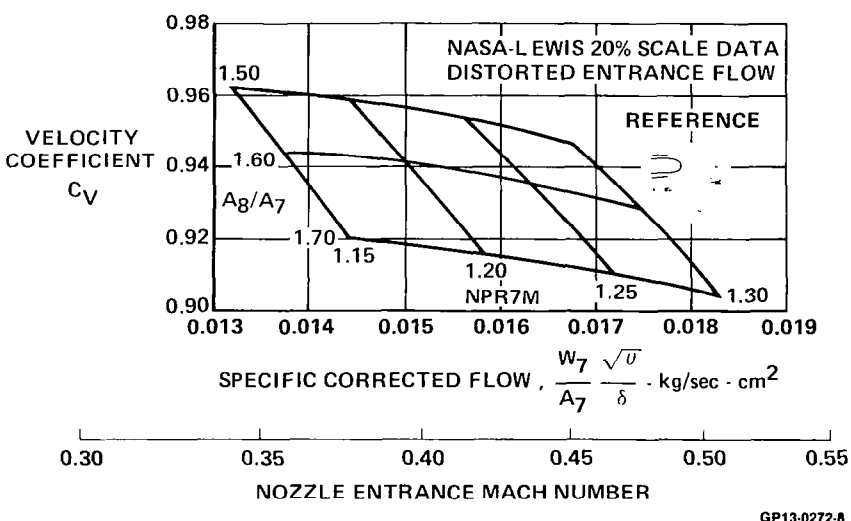


FIGURE 22
CONTOURS OF CONSTANT P_{T16}/P_{AMB}
 NPR16 = NPR56 Fan Stream at Nozzle Entrance



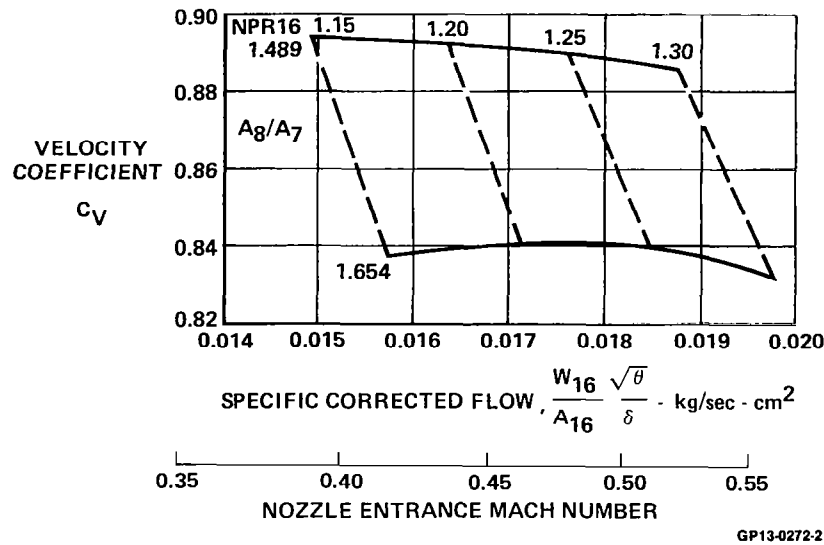
GP13-0132-128

FIGURE 23
FAN STREAM DISTORTION AT NOZZLE ENTRANCE
NPR16 = NPR56 110° Hood $A_8/A_7 = 1.578$ Alternate No. 2 Core



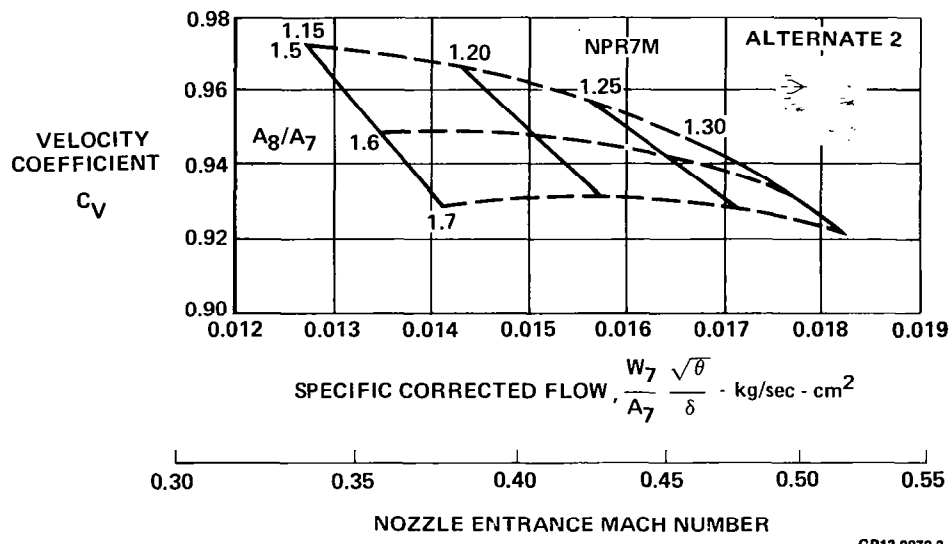
GP13-0272-8

FIGURE 24
EFFECT OF AREA VARIATION
NPR16 = NPR56 Reference Core-Forward $\phi = 90^\circ$



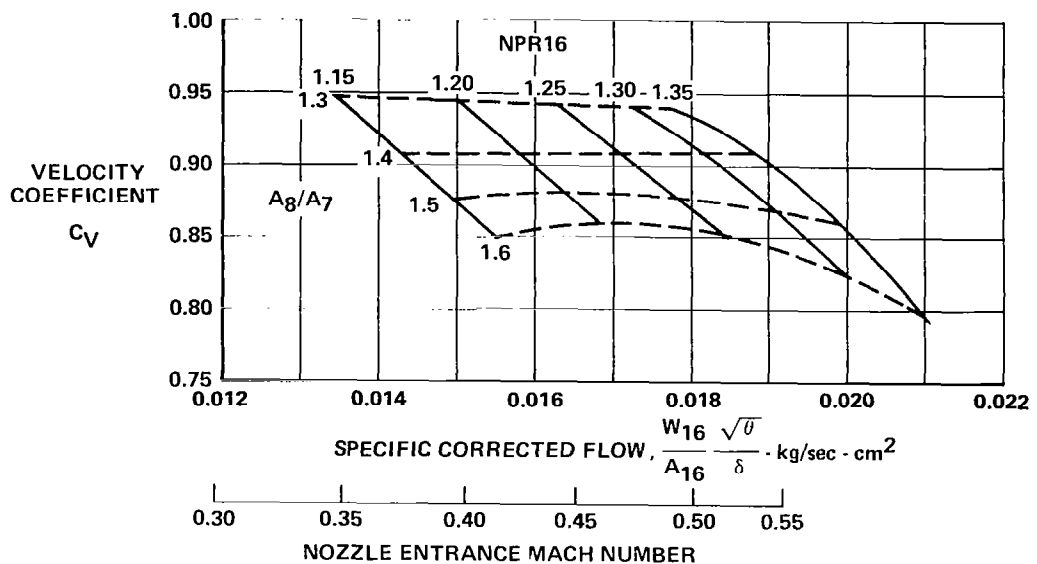
GP13-0272-2

FIGURE 25
EFFECT OF EXIT AREA VARIATION
Engine Out Reference Core - Forward $\phi = 90^\circ$



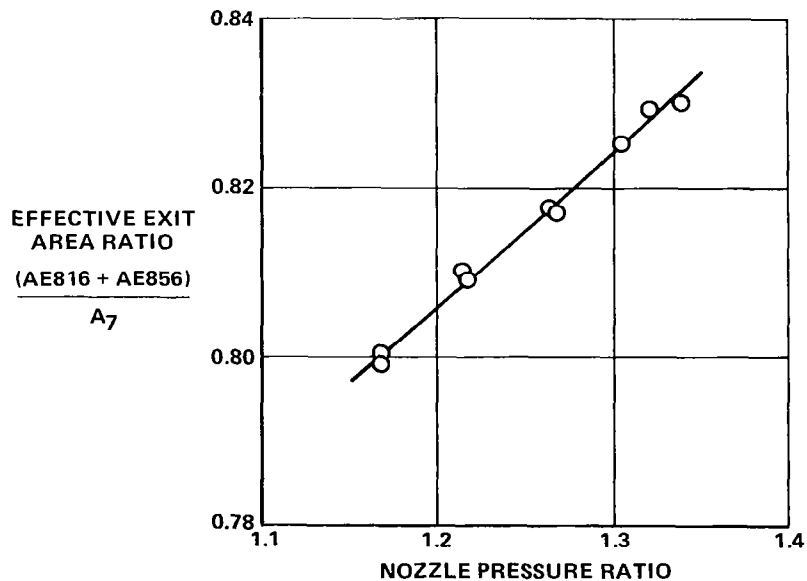
GP13-0272-3

FIGURE 26
EFFECT OF EXIT AREA VARIATION
NPR16 = NPR56 110° Hood Alternate No. 2 Core $\phi \approx 92^\circ$



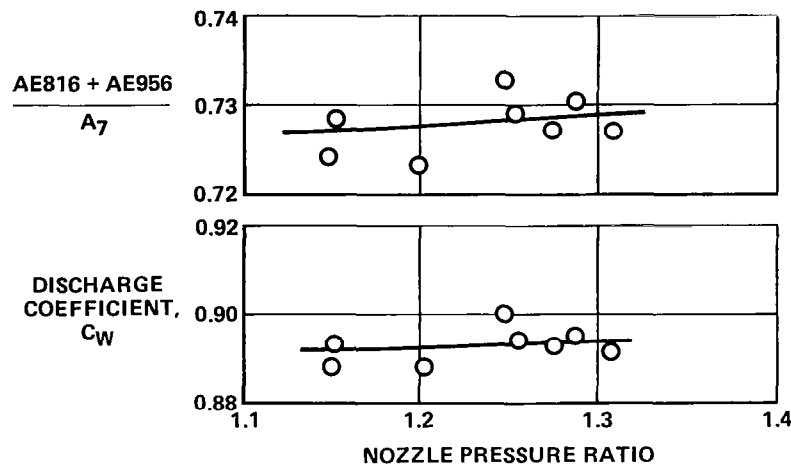
GP13-0272-4

FIGURE 27
EFFECT OF AREA VARIATION
Engine Out Alternate No. 2 Core $\phi = 90^\circ$



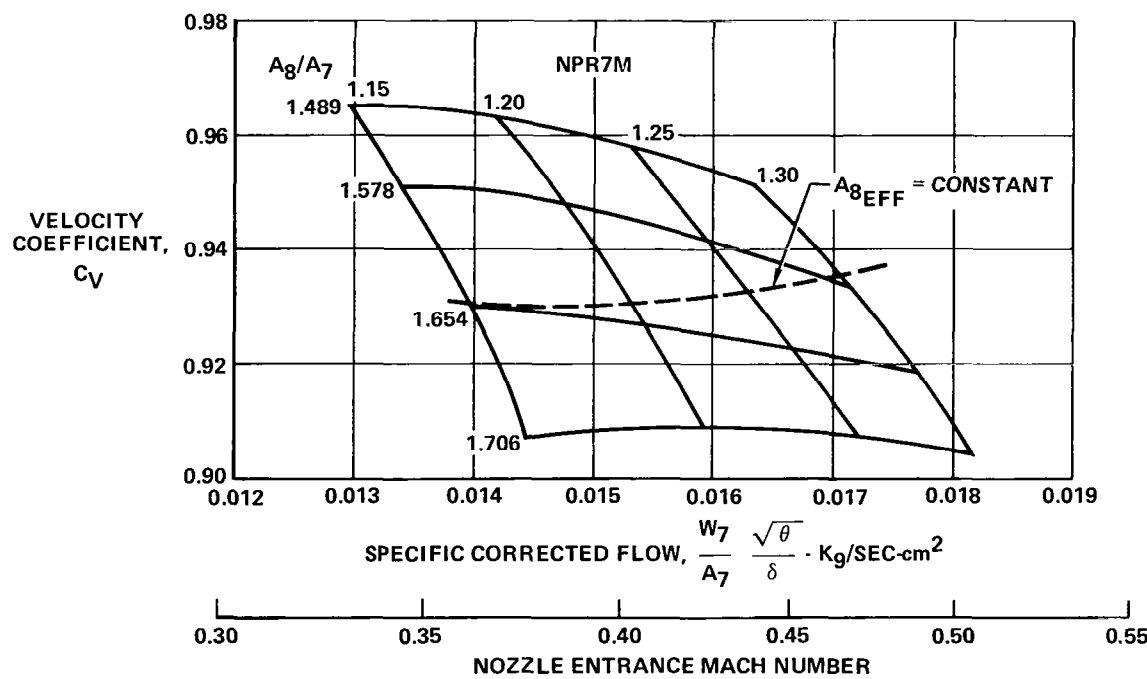
GP13-0272-36

FIGURE 28
VECTORED NOZZLE EFFECTIVE EXIT AREA
NPR16 = NPR56 110° Hood Alternate No. 2 Core $A_8/A_7 = 1.578$



GP13-0272-34

FIGURE 29
CRUISE NOZZLE EFFECTIVE EXIT AREA AND DISCHARGE COEFFICIENT
 $NPR_{16} = NPR_{56}$ Alt No. 2 Core $A_8/A_7 = 0.816$



GP13-0272-33

FIGURE 30
VECTORED NOZZLE PERFORMANCE AT CONSTANT EFFECTIVE EXIT AREA
 $NPR_{16} = NPR_{56}$ Hood = 110° Reference Core Forward

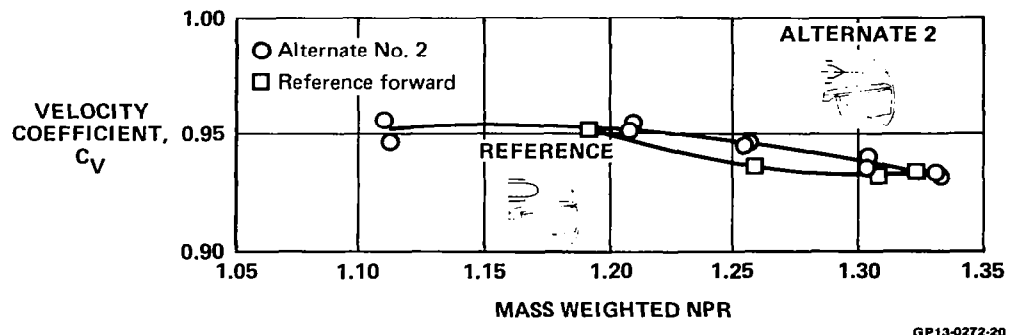


FIGURE 31
COMPARISON OF CORE NOZZLE CONFIGURATIONS
ALTERNATE NO. 2 CORE AND REFERENCE CORE - FORWARD
 $NPR_{16} = NPR_{56}$ Hood = 110° $A_8/A_7 = 1.578$

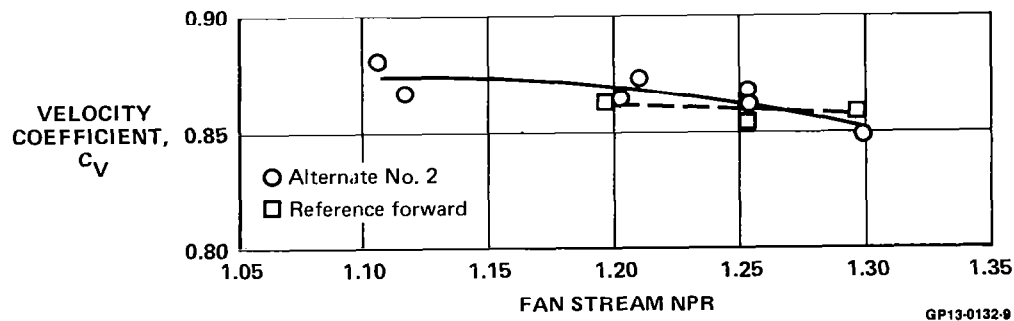


FIGURE 32
COMPARISON OF CORE NOZZLE CONFIGURATIONS
ALTERNATE NO. 2 CORE AND REFERENCE CORE
Engine Out Hood = 110° $A_8/A_7 = 1.578$

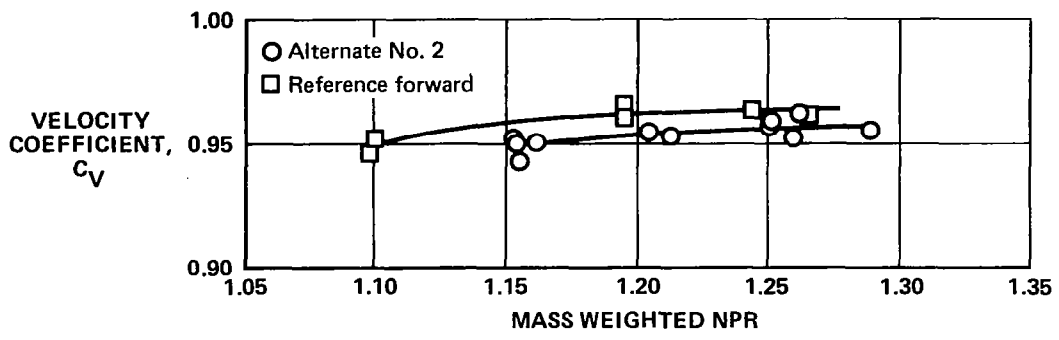


FIGURE 33
COMPARISON OF CORE NOZZLE CONFIGURATIONS
ALTERNATE NO. 2 CORE AND REFERENCE CORE - FORWARD
 $NPR_{16} = NPR_{56}$ Cruise Nozzle $A_8/A_7 = 0.816$

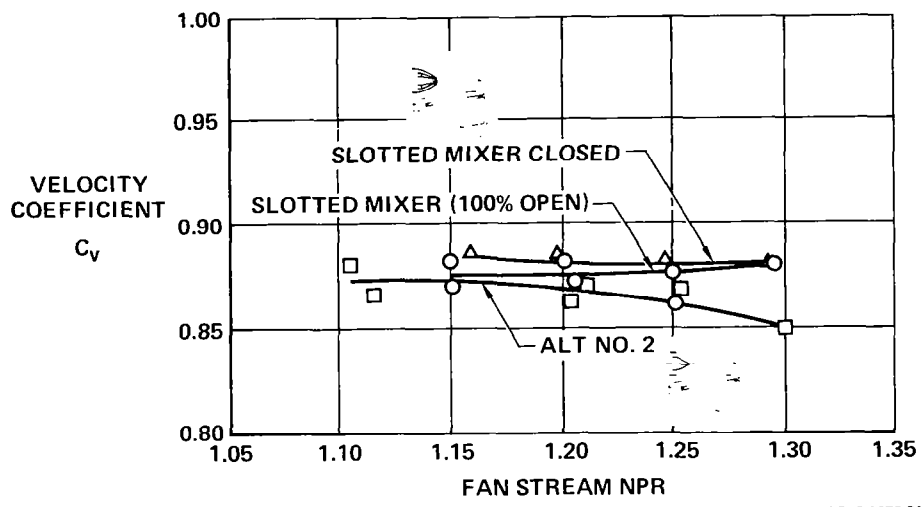
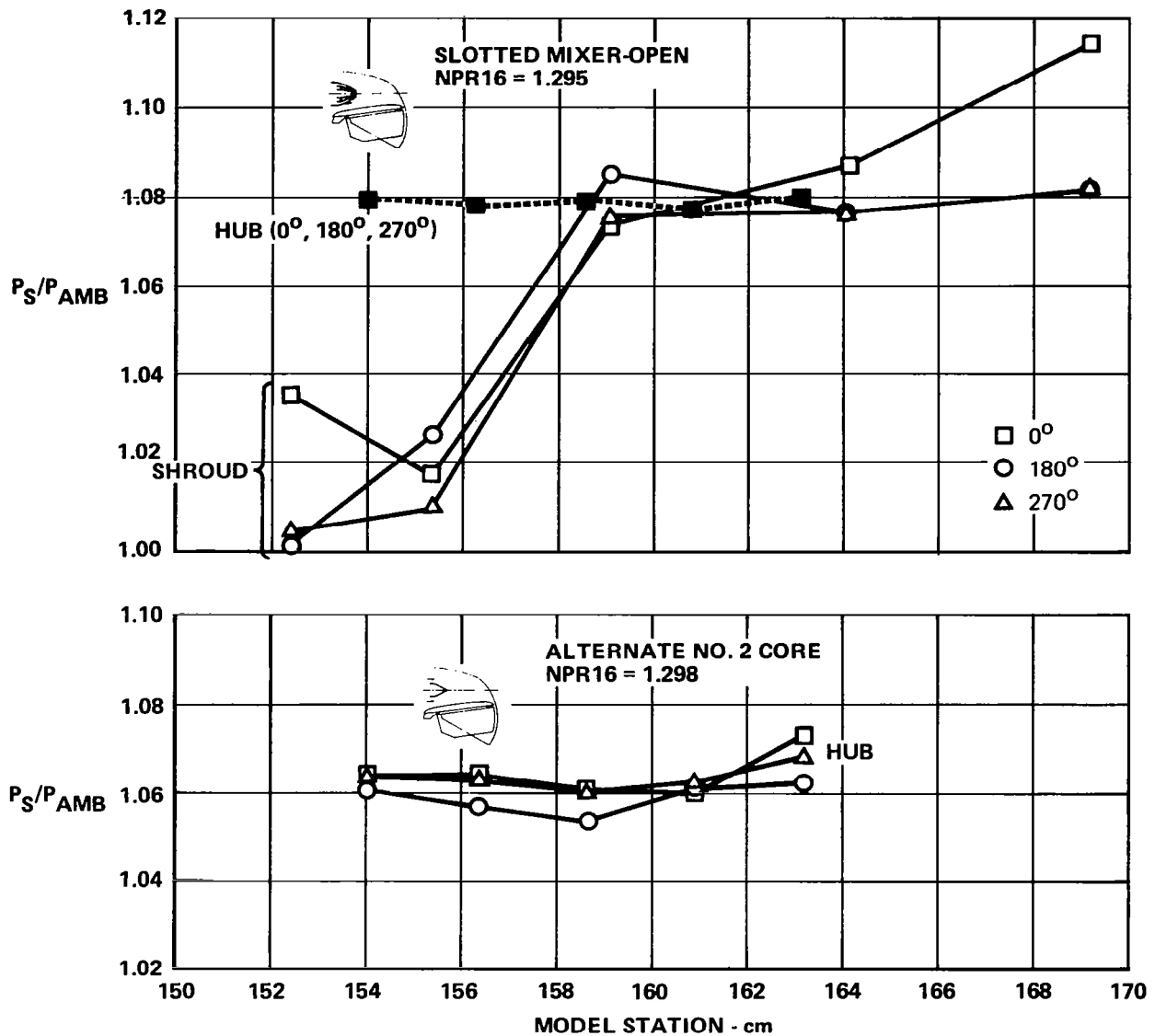
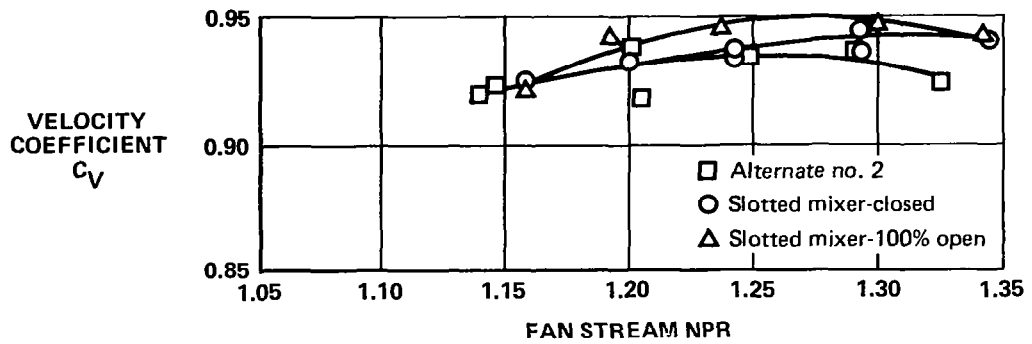


FIGURE 34
NOZZLE PERFORMANCE COMPARISON
Engine Out Slotted Mixer and Alternate No. 2 Core
Hood = 110° $A_8/A_7 = 1.578$



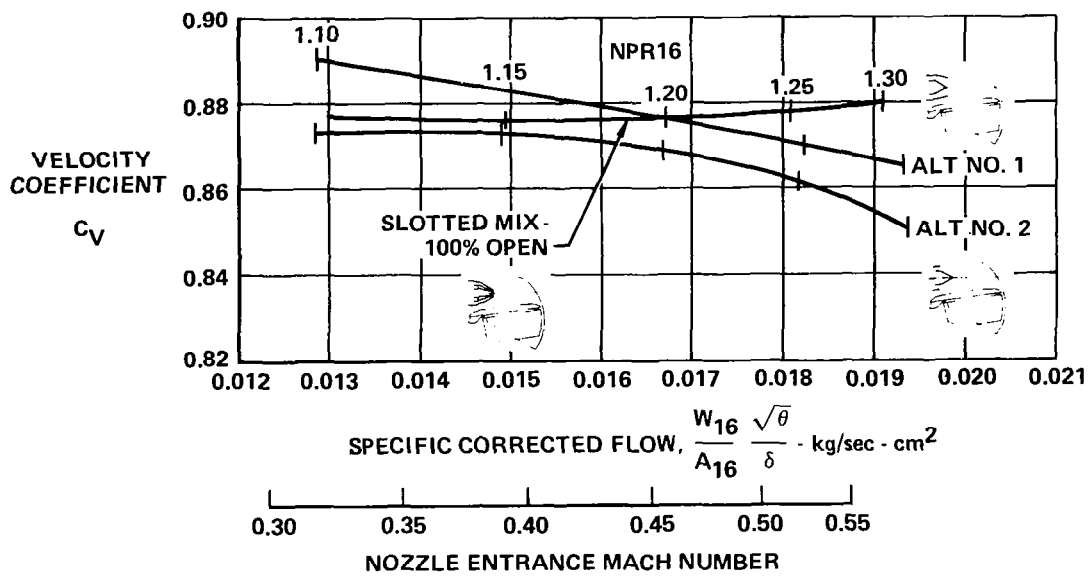
GP13-0272-22

FIGURE 35
CORE NOZZLE STATIC PRESSURE DISTRIBUTIONS
SLOTTED MIXER AND ALTERNATE NO. 2 CORE
 Engine Out Hood = 110° $A_8/A_7 = 1.578$



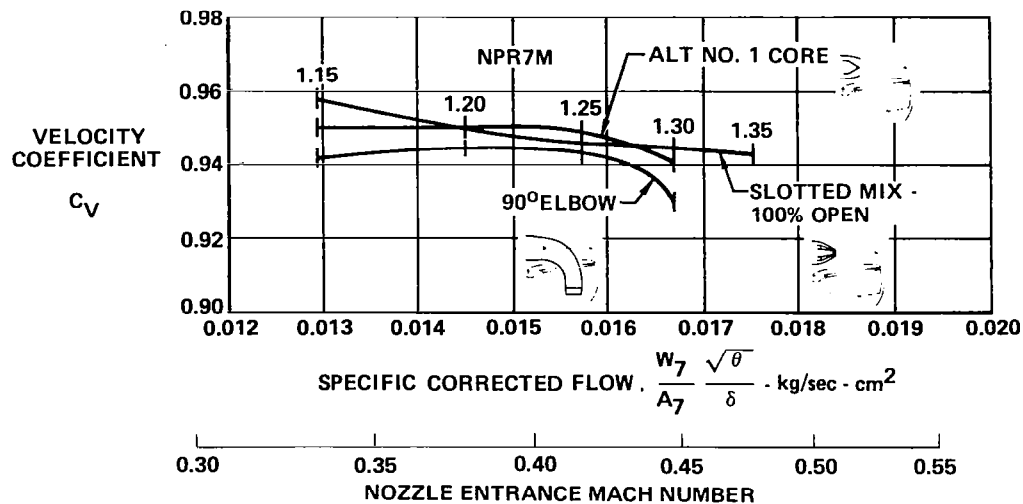
GP13-0272-39

FIGURE 36
COMPARISON OF CORE NOZZLE CONFIGURATIONS
SLOTTED MIXER AND ALTERNATE NO. 2 CORE
Engine Out Cruise Nozzle $A_8/A_7 = 0.816$



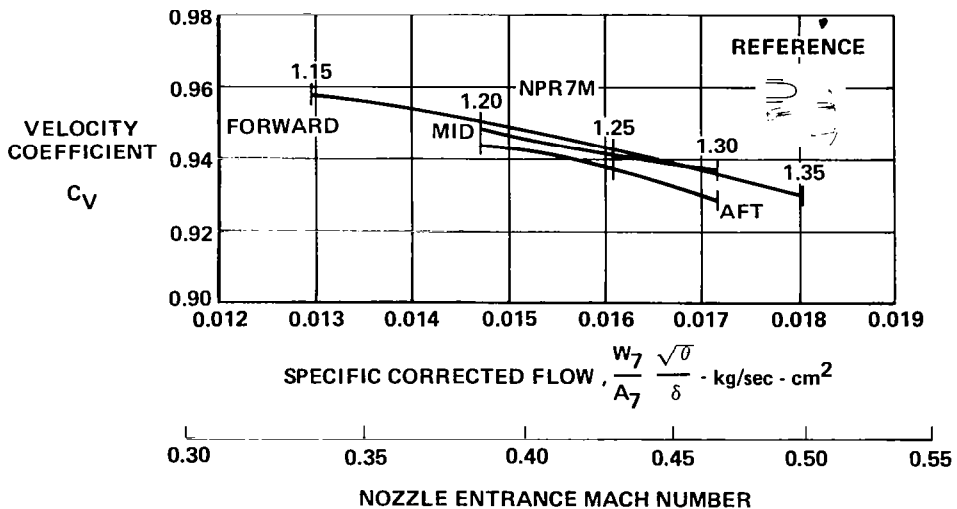
GP13-0272-11

FIGURE 37
CORE NOZZLE COMPARISON
SLOTTED MIXER, ALTERNATE 1, ALTERNATE 2
Engine Out Hood = 110° $A_8A_7 = 1.578$



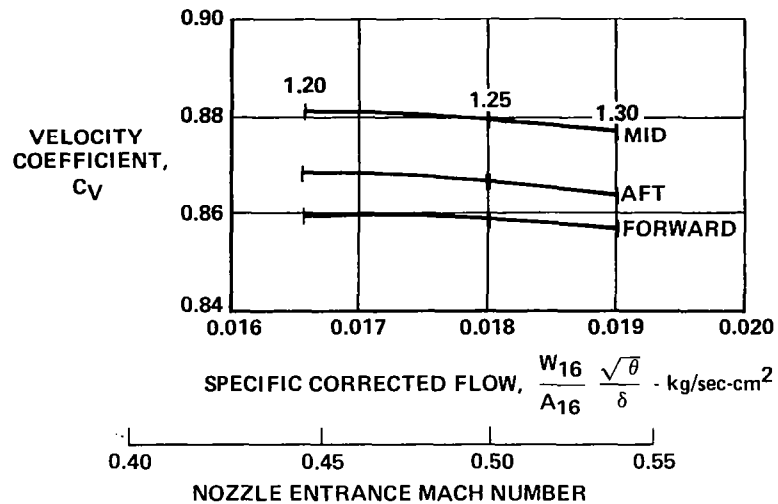
GP13-0272-10

FIGURE 38
CORE NOZZLE COMPARISON
SLOTTED MIXER, ALTERNATE 1, 90° ELBOW
 NPR16 = NPR56 110° Hood $A_8/A_7 = 1.578$



GP13-0272-5

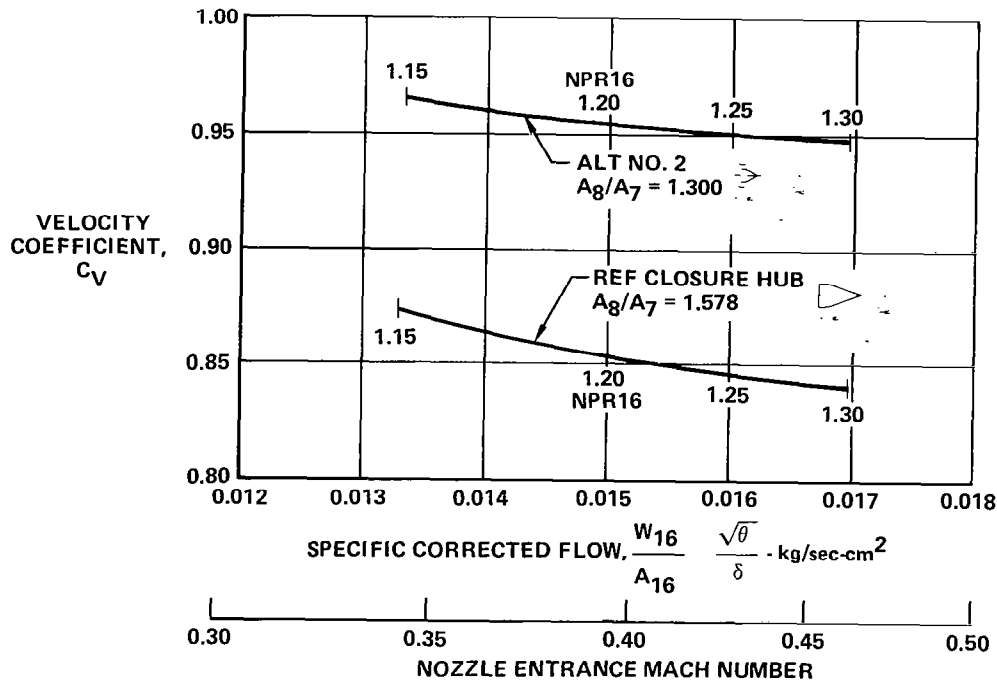
FIGURE 39
EFFECT OF CORE AXIAL LOCATION
 Reference Core
 NPR16 = NPR56 Hood = 110° $A_8/A_7 = 1.578$



GP13-0272-6

FIGURE 40
EFFECT OF CORE AXIAL LOCATION

Engine Out Reference Core
110° Hood $A_8/A_7 = 1.578$



GP13-0272-23

FIGURE 41
CORE NOZZLE COMPARISON
Alt No. 2 and Reference Closure Hub
Engine Out 110° Hood

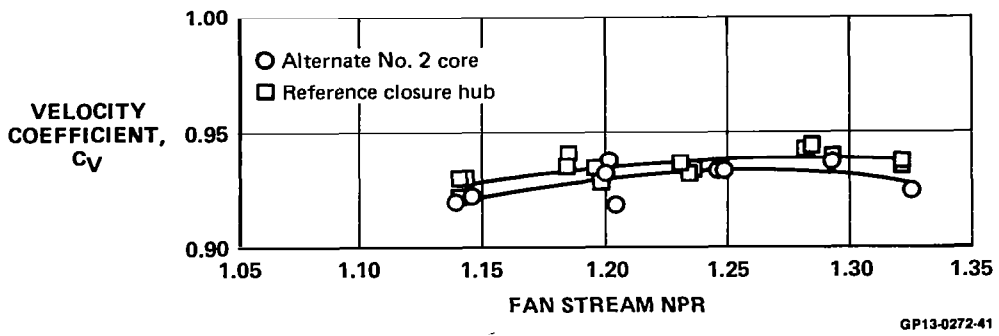


FIGURE 42
COMPARISON OF CORE NOZZLE CONFIGURATIONS
REFERENCE CLOSURE HUB AND ALTERNATE NO. 2 CORE
 Engine Out Cruise Nozzle $A_8/A_7 = 0.816$

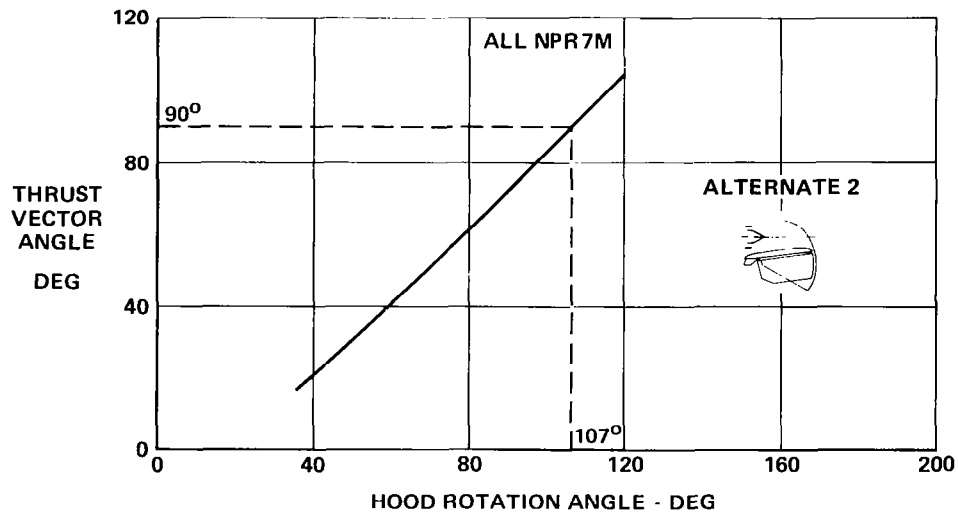


FIGURE 43
EFFECT OF HOOD ROTATION ON THRUST VECTOR ANGLE
 $NPR16 = NPR56$ Alternate No. 2 Core $A_8/A_7 = 1.578$

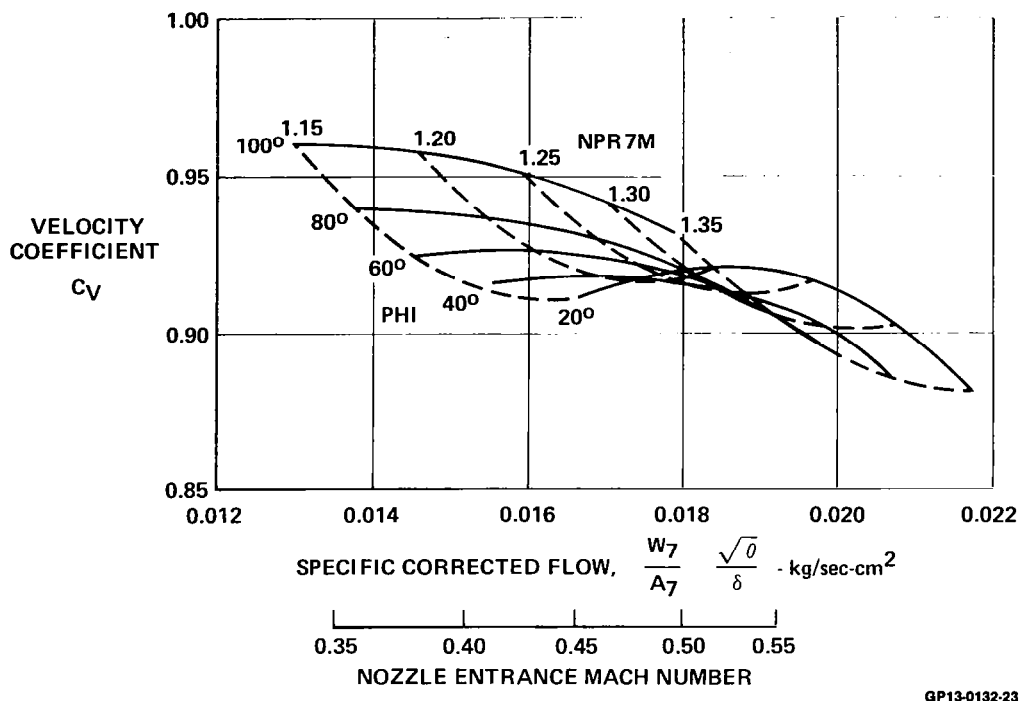


FIGURE 44
EFFECT OF HOOD ROTATION ON PERFORMANCE
NPR16 = NPR56 Alternate No. 2 Core $A_8/A_7 = 1.578$

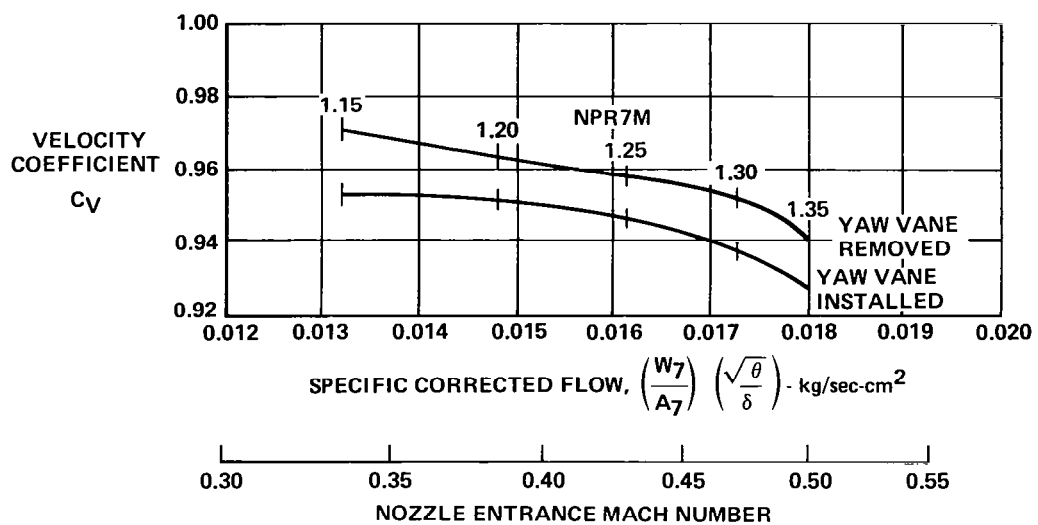


FIGURE 45
EFFECT OF YAW VANE REMOVAL
NPR16 = NPR56 Alternate No. 2 Core
110° Hood $A_8/A_7 = 1.578$

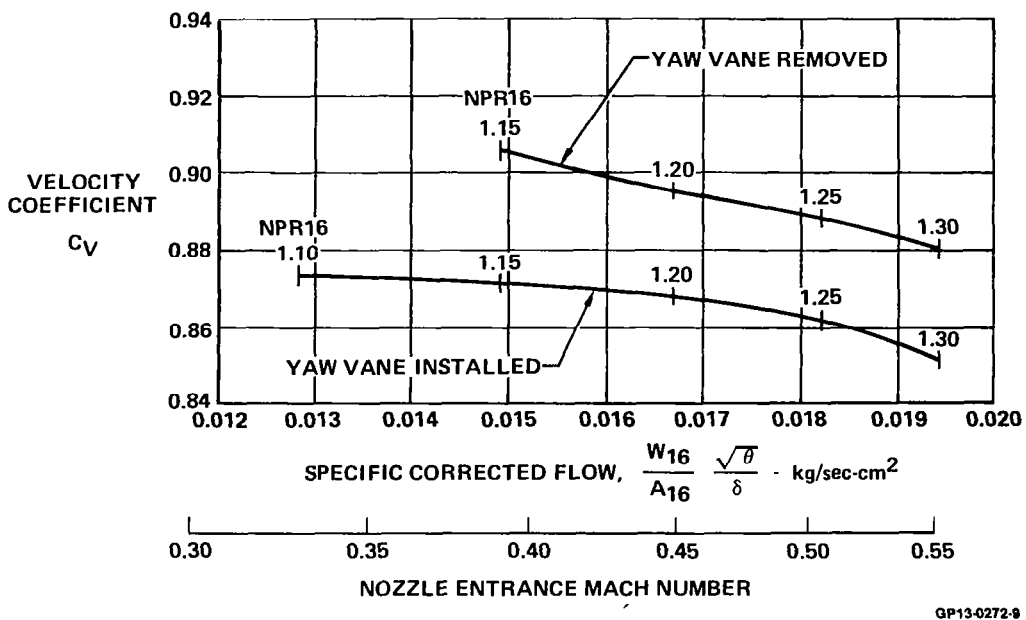


FIGURE 46
EFFECT OF YAW VANE REMOVAL
Engine Out Alternate No. 2 Core Hood = 110°
 $A_8/A_7 = 1.578$

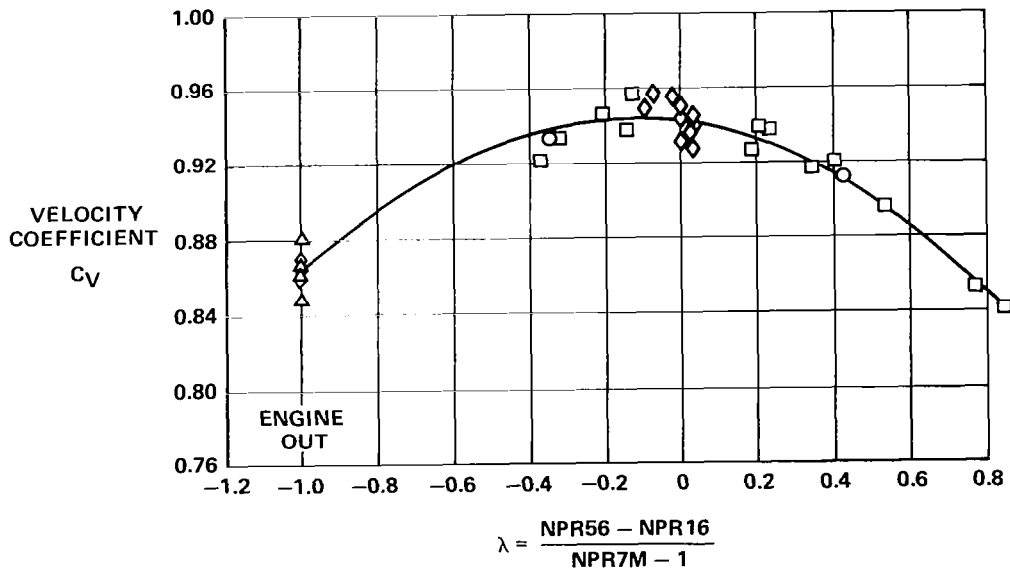


FIGURE 47
EFFECT OF MISMATCHED NPR ON THRUST COEFFICIENT
Nozzle Total Pressure Ratio Correlation
Hood = 110° $A_8/A_7 = 1.578$ Alternate No. 2 Core

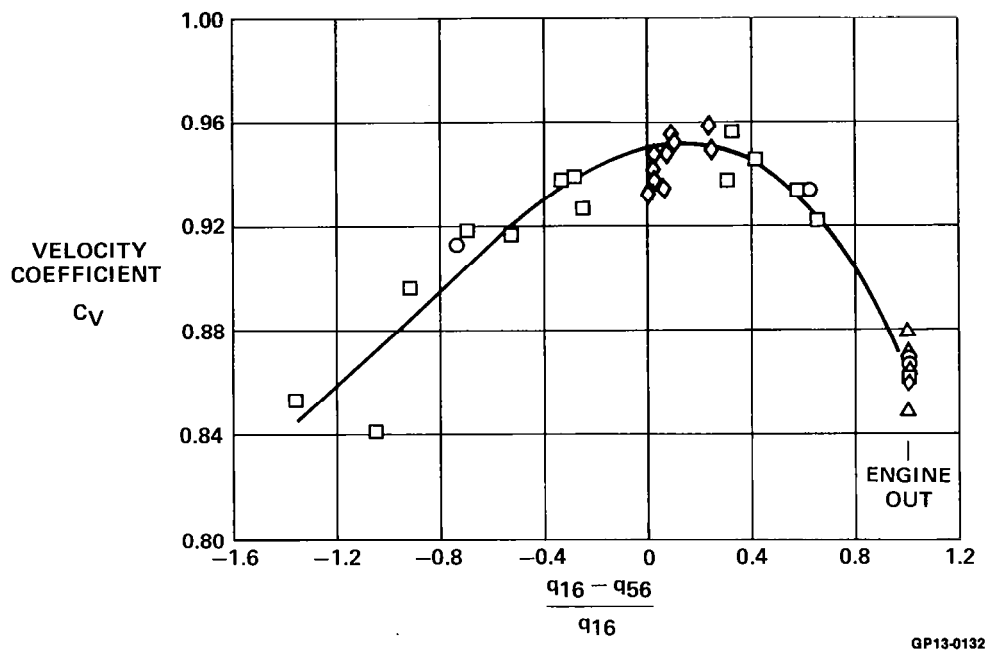


FIGURE 48
EFFECT OF MISMATCHED NPR ON THRUST COEFFICIENT

Nozzle Entrance Dynamic Pressure Correlation
Hood = 110° A₈/A₇ = 1.578 Alternate No. 2 Core

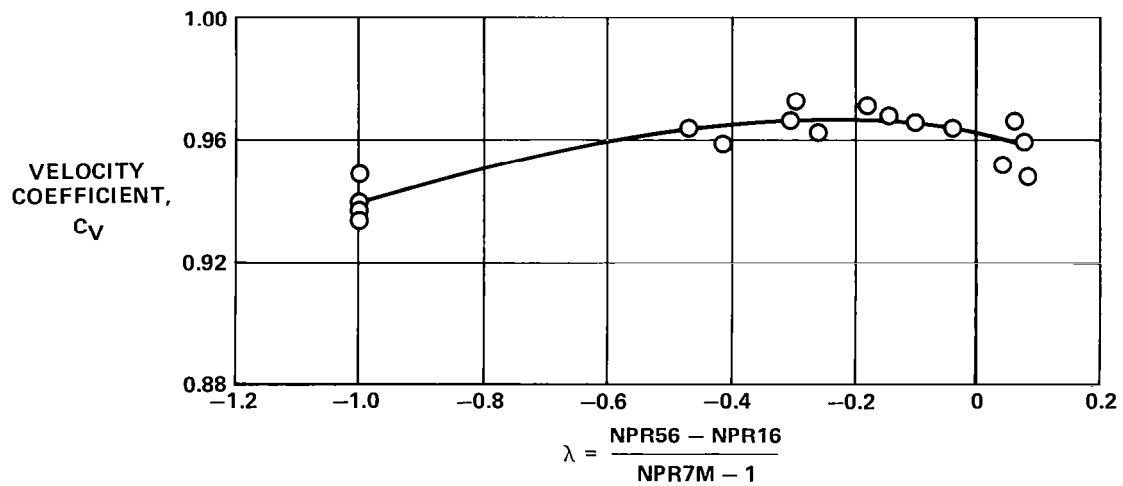
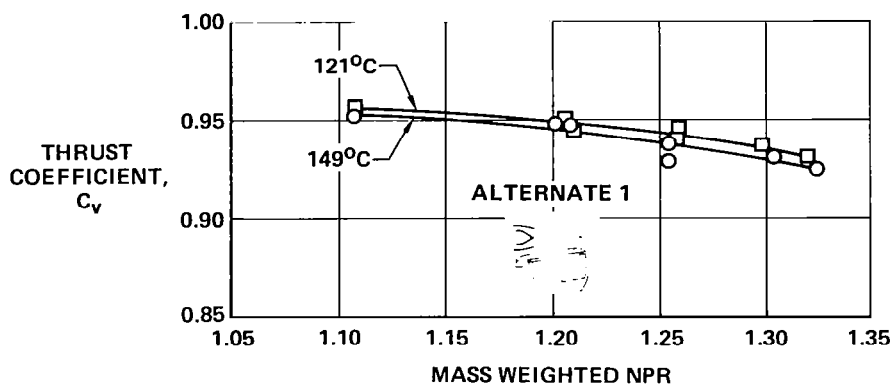
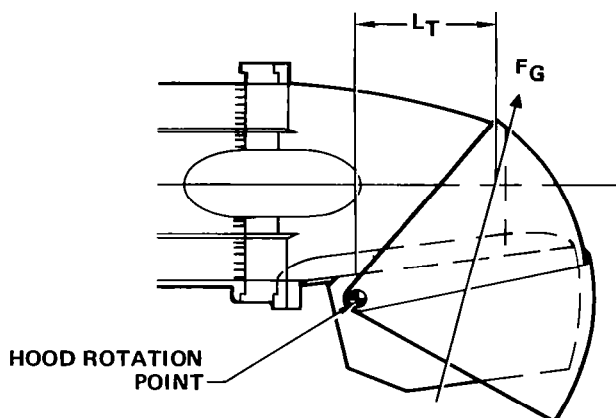


FIGURE 49
EFFECT OF MISMATCHED NPR ON CRUISE NOZZLE THRUST COEFFICIENT
Nozzle Total Pressure Ratio Correlation
Reference Core Forward A₈/A₇ = 0.816



GP13-0272-19

FIGURE 50
Effect of Core Temperature (T_{T56})
NPR16 = NPR56 Hood = 110° $A_8/A_7 = 1.578$ Alt No. 1 Core



GP13-0132-30

FIGURE 51
DEFINITION OF THRUST MOMENT ARM

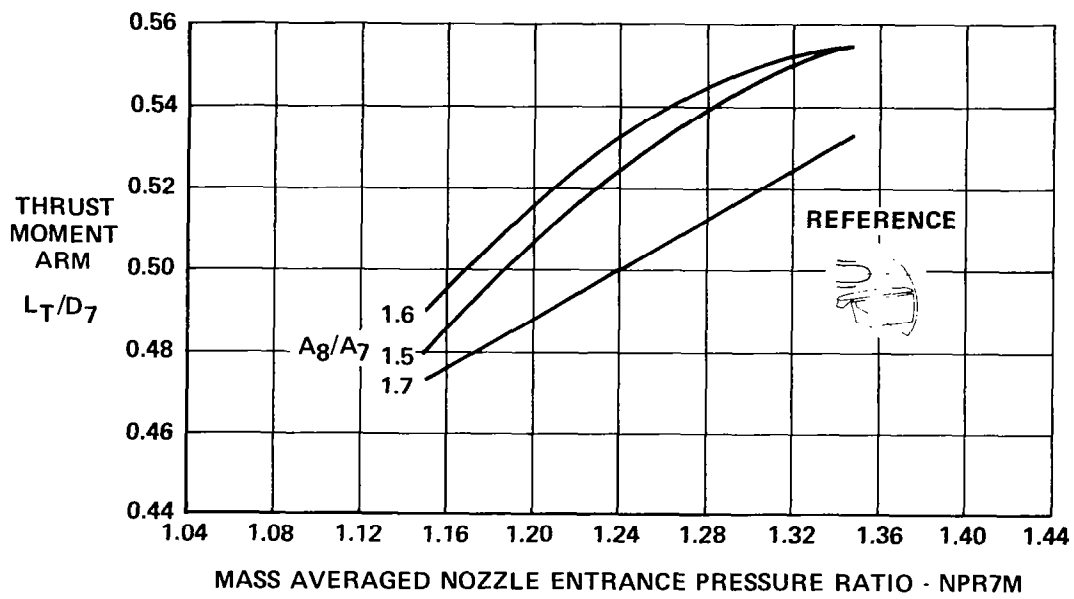
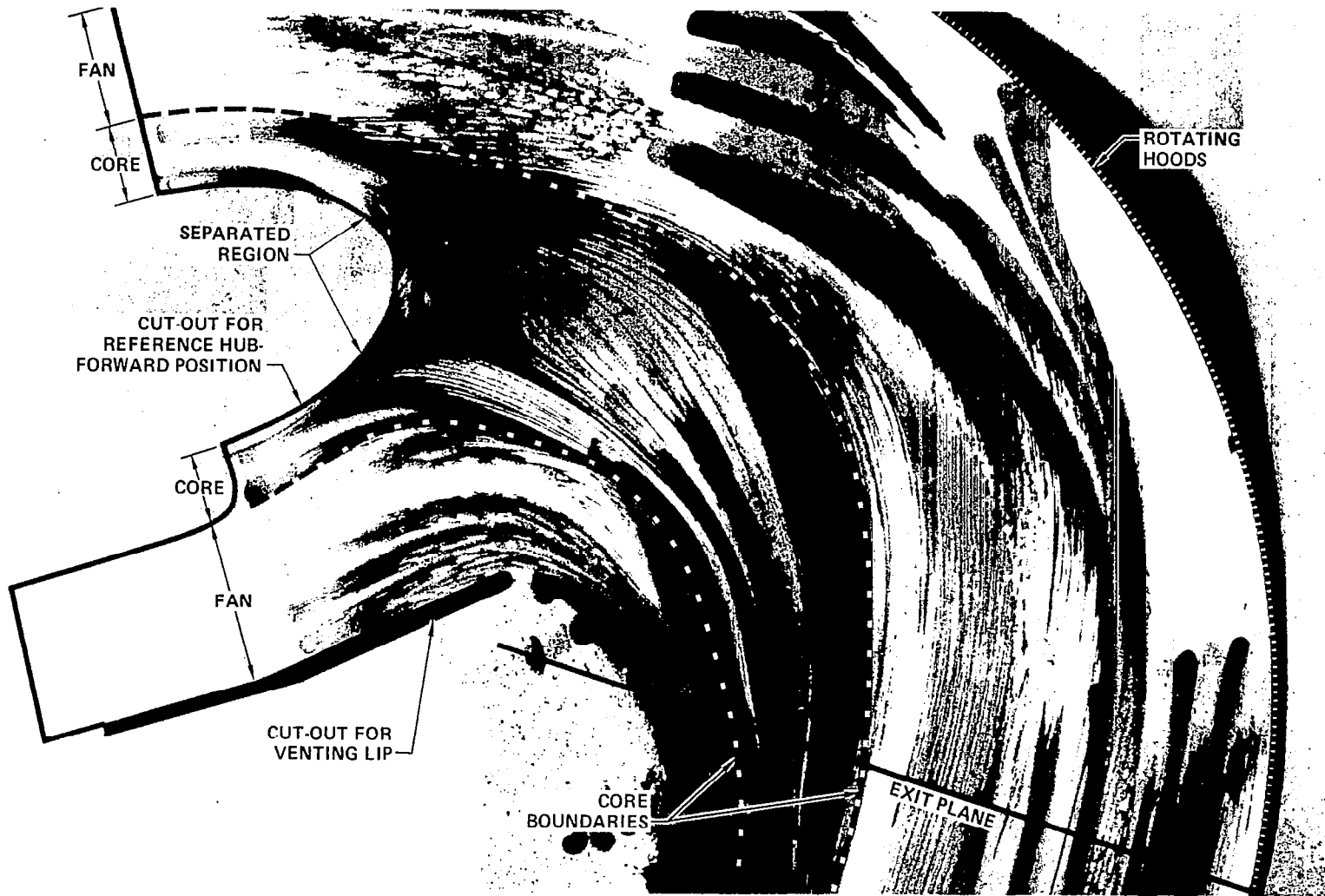


FIGURE 52
EFFECT OF EXIT AREA VARIATION ON THRUST MOMENT ARM
 NPR16 = NPR56 Reference Core - Forward $\phi = 90^\circ$

GP13-0272-26

59



FLOW VISUALIZATION RESULTS - CORE LOCATION

Matched NPR \approx 1.3 120° Hood $A_8/A_7=1.578$

TABLE 3
RUN SCHEDULE

CORE CONFIGURATION	HOOD POSITION (DEG)	A ₈ /A ₇	RUN	FIGURE	NPR SCHEDULE			COMMENTS
					MATCHED	ENGINE OUT	MISMATCHED	
REFERENCE CORE-FORWARD	35.5 (CRUISE)	—	1, 8	54	XX	X	XX	
	35.5	1.654	2	55	X	X	X	
	90	1.578	18	56	X			
		1.654	3, 6	57	XX	X	XX	
		1.706	16	58	X		X	
	100	1.386	10	59	X	X	X	
		1.489	11	60	X	X		
	110	1.489	13	61	X	X	X	
		1.578	9	62	X	X	X	
		1.578	51		X	X	X	FLOW VISUALIZATION
		1.654	4, 5	63	XX	XX	XX	
	120	1.706	14	64	X	X	X	
		1.489	12	65	X			
		1.578	17	66	X			
		1.578	51		X			FLOW VISUALIZATION
REFERENCE CORE-MID	90	1.578	20	69	X	X		
	110	1.578	19	70	X	X	X	
	120	1.578	21	71	X	X		
REFERENCE CORE-AFT	35.5	1.578	25	72	X	X	X	
	60	1.578	26	73	X	X	X	
	75	1.578	27	74	X	X	X	
	90	1.578	23	75	X	X	X	
	100	1.578	28	76	X	X	X	
	110	1.578	22, 29	77	XX	XX	XX	
	120	1.578	24	78	X	X	X	

GP13-0272-30

TABLE 3 (Continued)
RUN SCHEDULE

CORE CONFIGURATION	HOOD POSITION (DEG)	A ₈ /A ₇	RUN	FIGURE	NPR SCHEDULE			COMMENTS
					MATCHED	ENGINE OUT	MISMATCHED	
ALTERNATE 1	35.5 (CRUISE)	—	32	79	X	X	X	CORE TEMPERATURE = 250°F CORE TEMPERATURE = 300°F
	35.5	1.578	37	80	X	X	X	
	75	1.578	36	81	X	X		
	110	1.578	33	82	X			
	110	1.578	34	83	X	X	X	
	120	1.578	35	84	X	X	X	
ALTERNATE 2	35.5 (CRUISE)	—	42, 52	85	XX	XX	X	YAW VANE OUT
	35.5	1.300	74	86		X		
		1.386	59	87		X		
		1.578	41	88	X	X		
		1.578	67	89	X	X	X	
	60	1.300	73	90		X		
		1.386	60	91		X		
		1.578	61	92	X	X		
	75	1.300	72	93		X		
		1.386	56	94		X		
		1.578	40	95	X	X		
		1.578	66	96	X	X	X	
	90	1.300	71	97		X		
		1.386	57	98		X		
		1.578	65	99	X	X		
	100	1.300	70	100		X		
		1.386	58	101		X		
		1.578	64	102	X	X		
	110	1.300	68	103		X		
		1.386	54	104		X		
		1.578	38, 53	105	XX	XX	XX	YAW VANE OUT
		1.578	62	106	X	X	X	
		1.654	87	107	X			
		1.706	86	108	X			
	120	1.300	69	109		X		
		1.386	55	110		X		
		1.578	39	111	X	X	X	
		1.578	63	112	X	X		

GP13-0272-31

TABLE 3 (Concluded)
RUN SCHEDULE

CORE CONFIGURATION	HOOD POSITION (DEG)	A ₈ /A ₇	RUN	FIGURE	NPR SCHEDULE			COMMENTS
					MATCHED	ENGINE OUT	MISMATCHED	
SLOTTED MIXER	35.5 (CRUISE)	—	79, 80	113	XX	X	X	MIXER OPEN
	35.5 (CRUISE)	—	81	114		X		MIXER CLOSED
	60	1.578	82	115	X	X		
	90	1.578	83	116	X	X		
	110	1.578	84	117	X		X	MIXER 80% OPEN
		1.578	85	118		X		MIXER CLOSED
		1.578	78	119	X	X	X	MIXER OPEN
90° ELBOW	110	1.578	77	120	X	X	X	
REFERENCE CLOSURE HUB	35.5 (CRUISE)	—	43, 45	121				FAN STREAM ONLY
	35.5	1.578	49	122				FAN STREAM ONLY
	75	1.578	48	123				FAN STREAM ONLY
	110	1.578	46	124				FAN STREAM ONLY
	120	1.578	47	125				FAN STREAM ONLY
CONVERGENT CALIBRATION NOZZLE	—	—	88	126	X	X		

GP13-0272-32

CORE NOZZLE RESEARCH MODEL TEST

STM	TEST	RUN	HOOD	R8/R7	DESCRIPTION
○	54	1001	35.500	0.8163	REF. CORE - FWD CRUISE NOZZL
▲	54	2001	35.500	0.8163	REF. CORE - FWD CRUISE NOZZL
△	54	2008	35.500	0.8163	REF. CORE - FWD CRUISE NOZZL

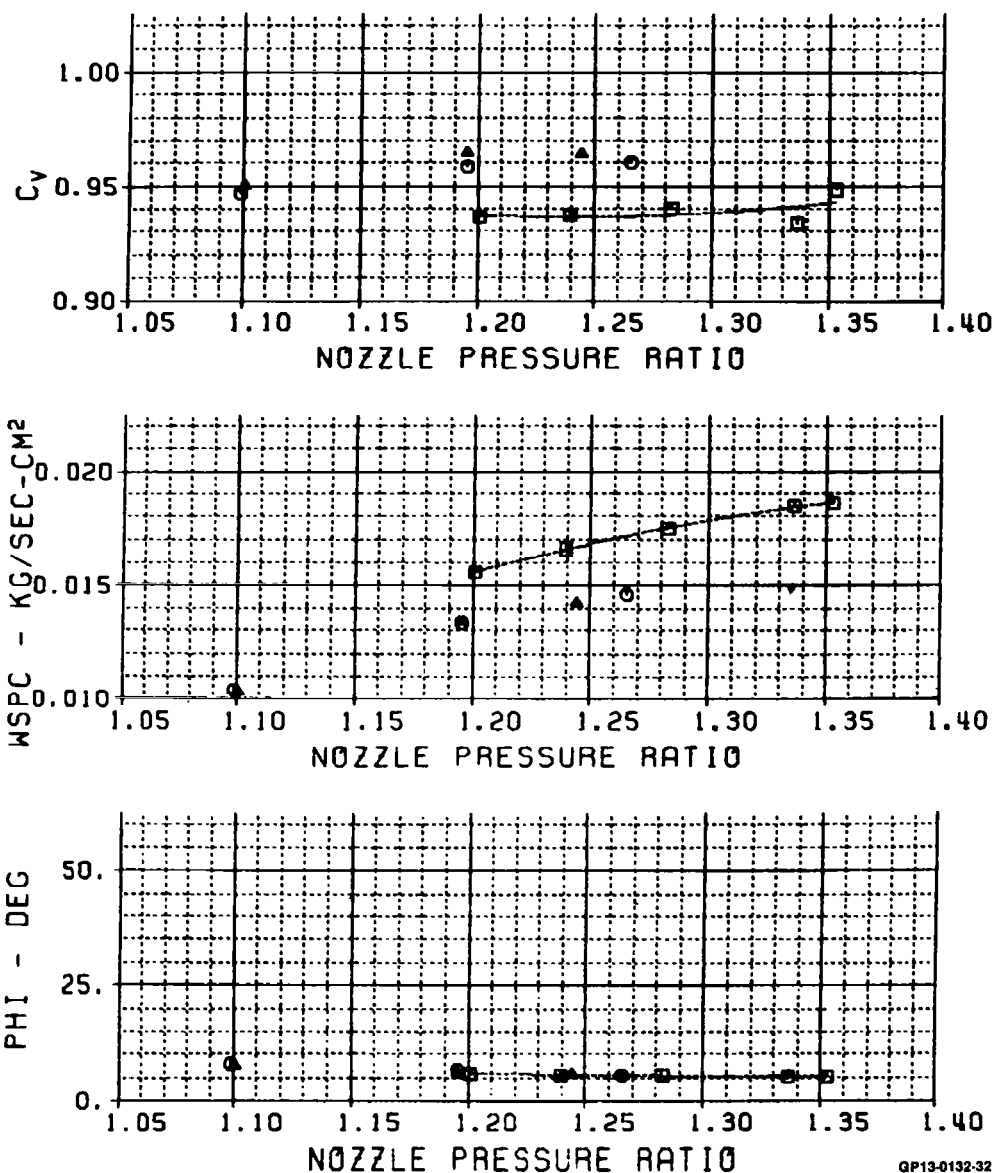


FIGURE 54

CORE NOZZLE RESEARCH MODEL TEST

SYM	TEST	RUN	HODD	AB/A7	DESCRIPTION
□	54	1002	35.500	1.6536	REF. CORE - FWD
○	54	2002	35.500	1.6538	REF. CORE - FWD

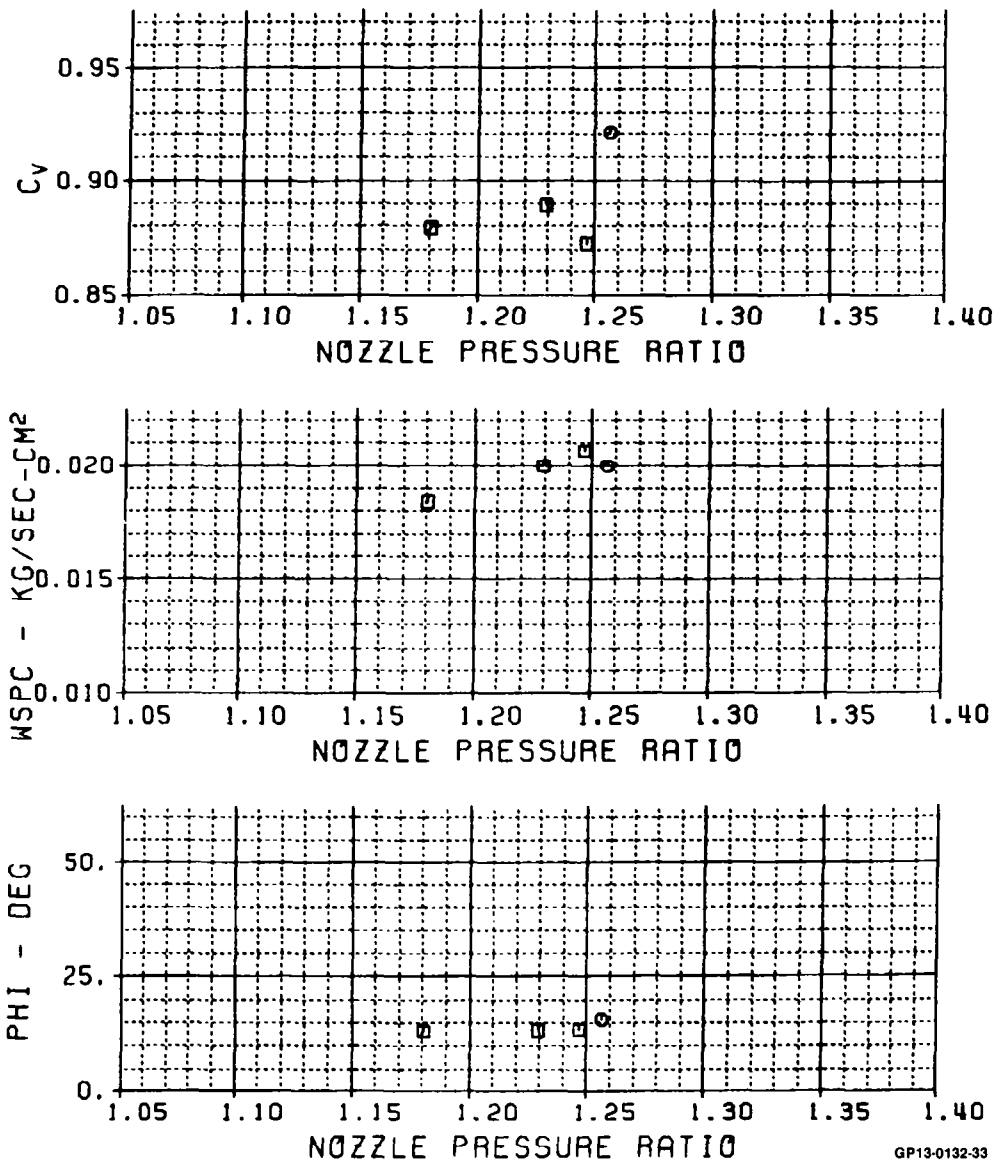


FIGURE 55

CORE NOZZLE RESEARCH MODEL TEST

SYM	TEST	RUN	HOOD	A8/A7	DESCRIPTION
□	54	2018	90.000	1.5781	REF. CORE - FWD

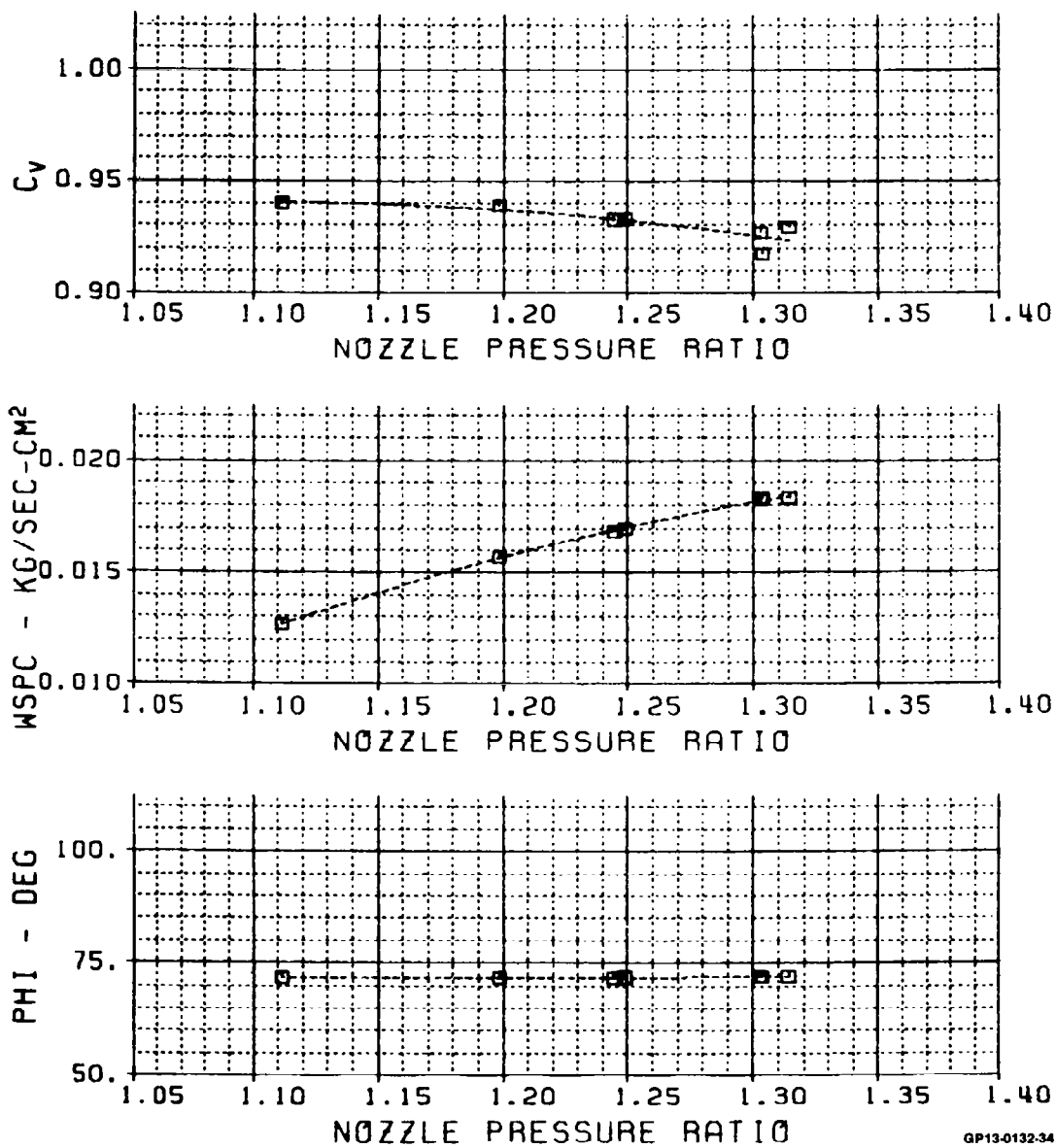


FIGURE 56

CORE NOZZLE RESEARCH MODEL TEST

STM	TEST	RUN	MOOD	AB/AT	DESCRIPTION
CB	54	1003	90.000	1.6536	REF. CORE - FWD
CB	54	2003	90.000	1.6536	REF. CORE - FWD
▲	54	2006	90.000	1.6536	REF. CORE - FWD

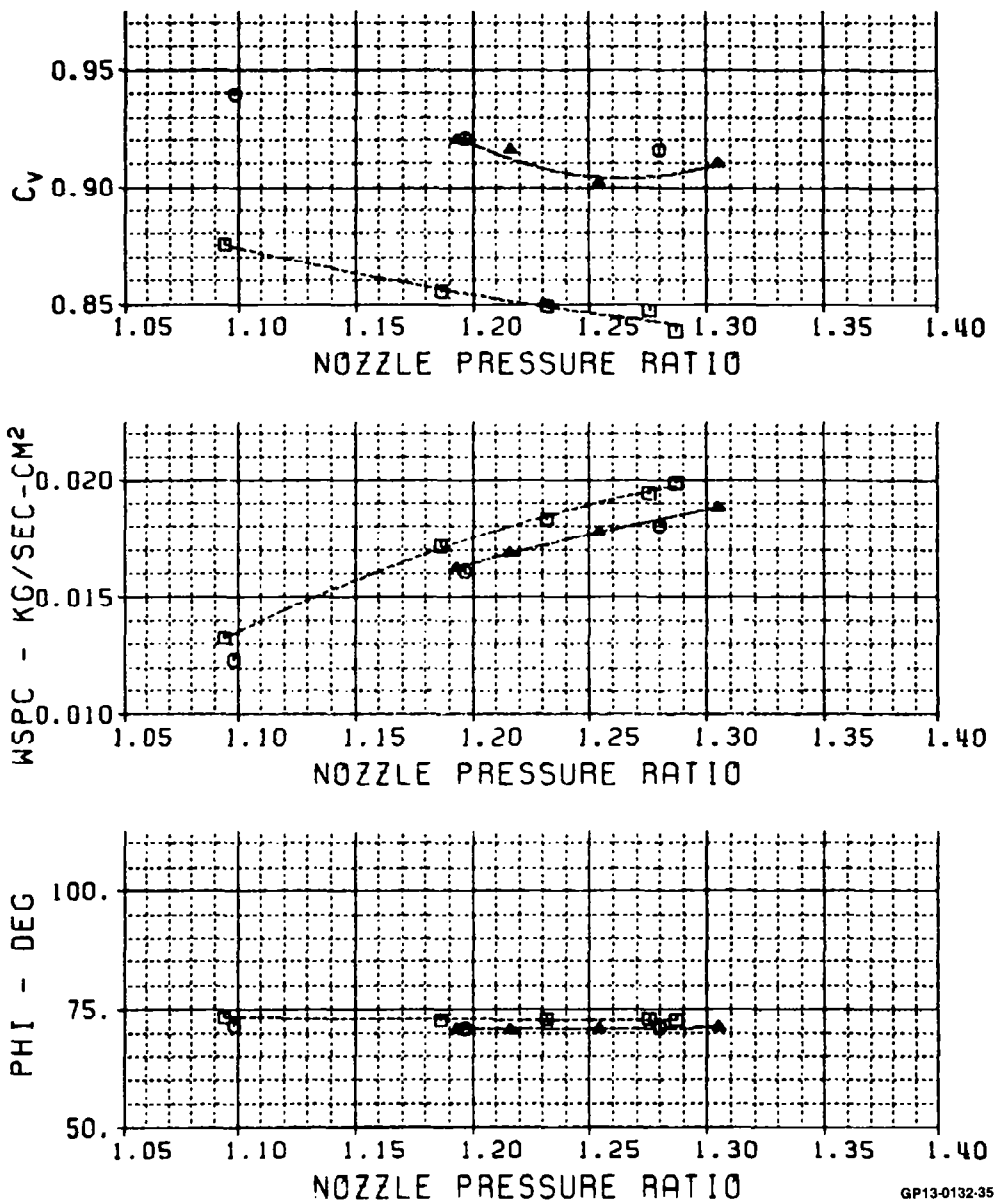


FIGURE 57

CORE NOZZLE RESEARCH MODEL TEST

SYM	TEST	RUN	HODD	R8/R7	DESCRIPTION
□	54	2016	90.000	1.7063	REF. CORE - FWD

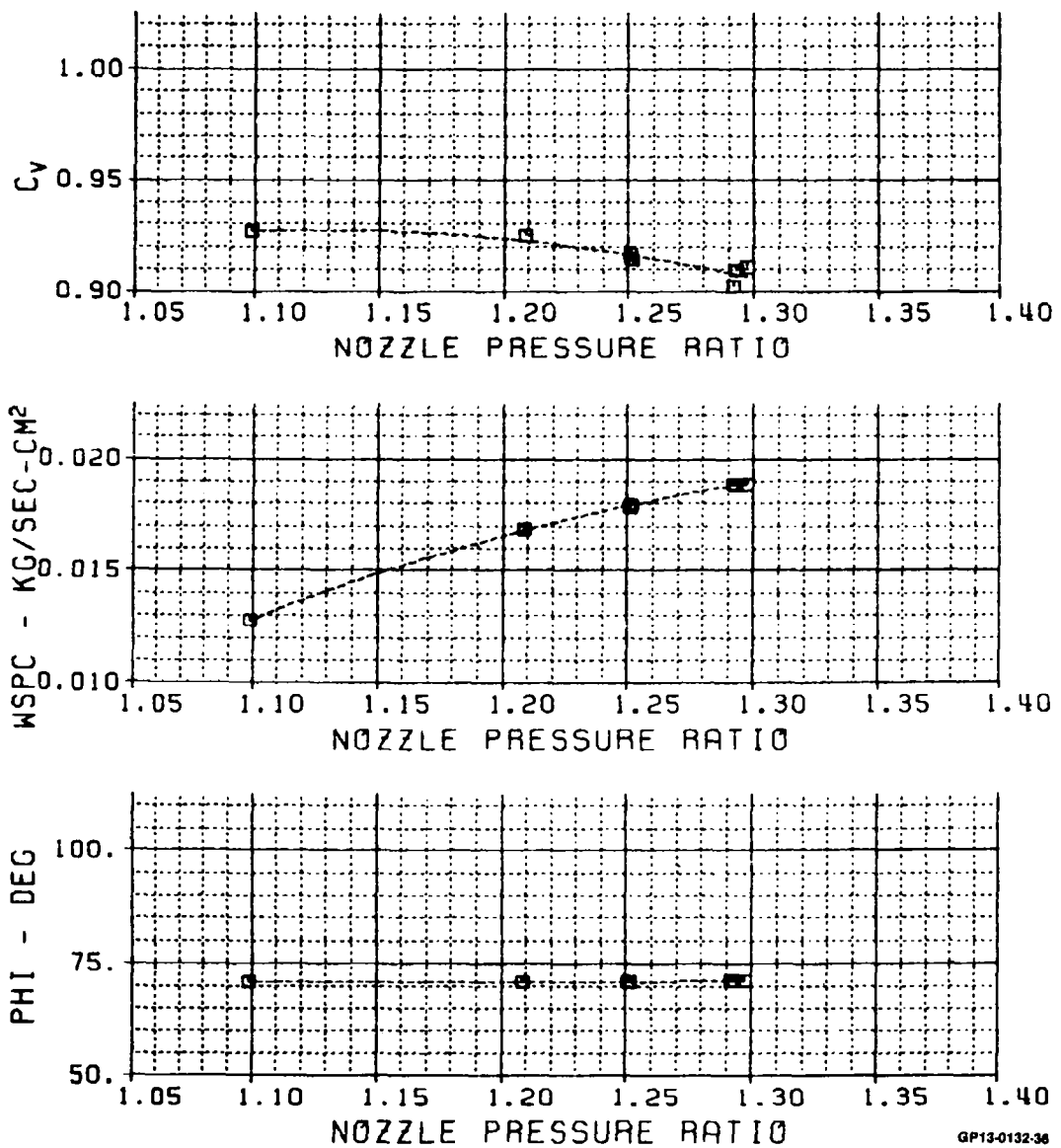


FIGURE 58

CORE NOZZLE RESEARCH MODEL TEST

SYM	TEST	RUN	HOOD	A8/A7	DESCRIPTION
■	54	1010	100.00	1.3861	REF. CORE - FWD
○	54	2010	100.00	1.3861	REF. CORE - FWD

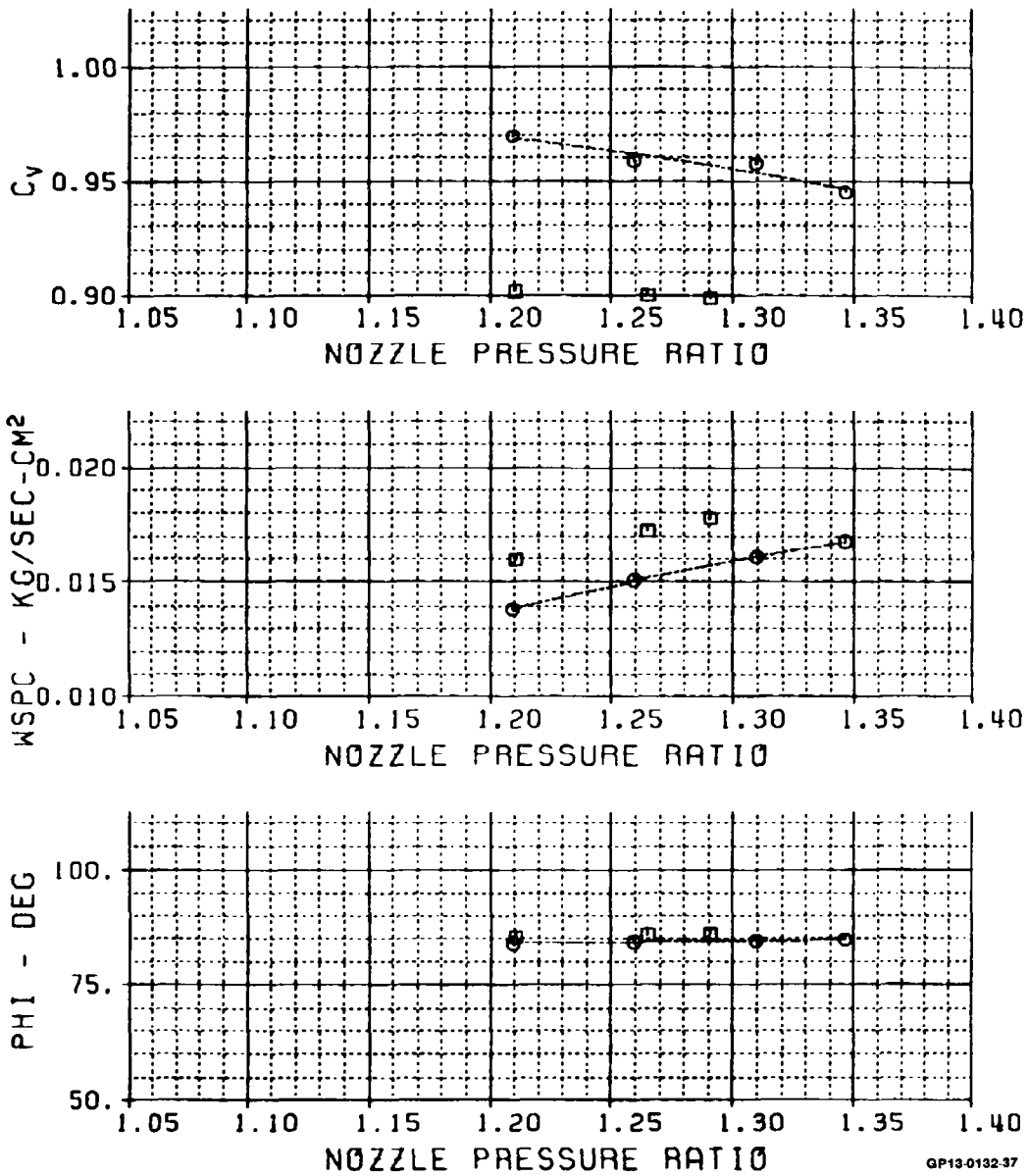


FIGURE 59

CORE NOZZLE RESEARCH MODEL TEST

SYM	TEST	RUN	HODD	R8/R7	DESCRIPTION
□	54	1011	100.00	1.4889	REF. CORE - FWD
○	54	2011	100.00	1.4889	REF. CORE - FWD

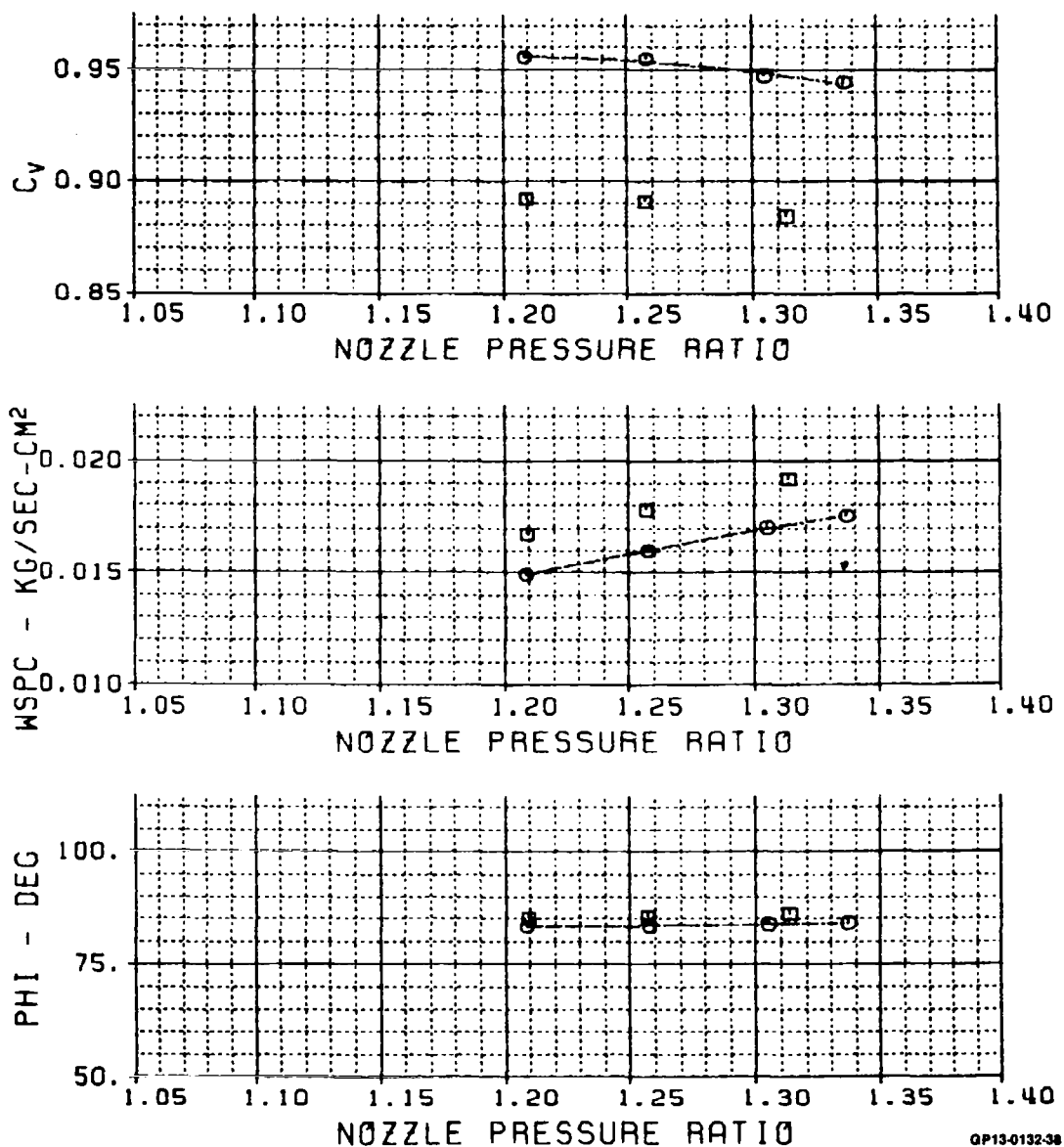


FIGURE 60

CORE NOZZLE RESEARCH MODEL TEST

STM	TEST	RUN	MOOD	A8/A7	DESCRIPTION
□	54	1013	110.00	1.4889	REF. CORE - FWD
○	54	2013	110.00	1.4889	REF. CORE - FWD

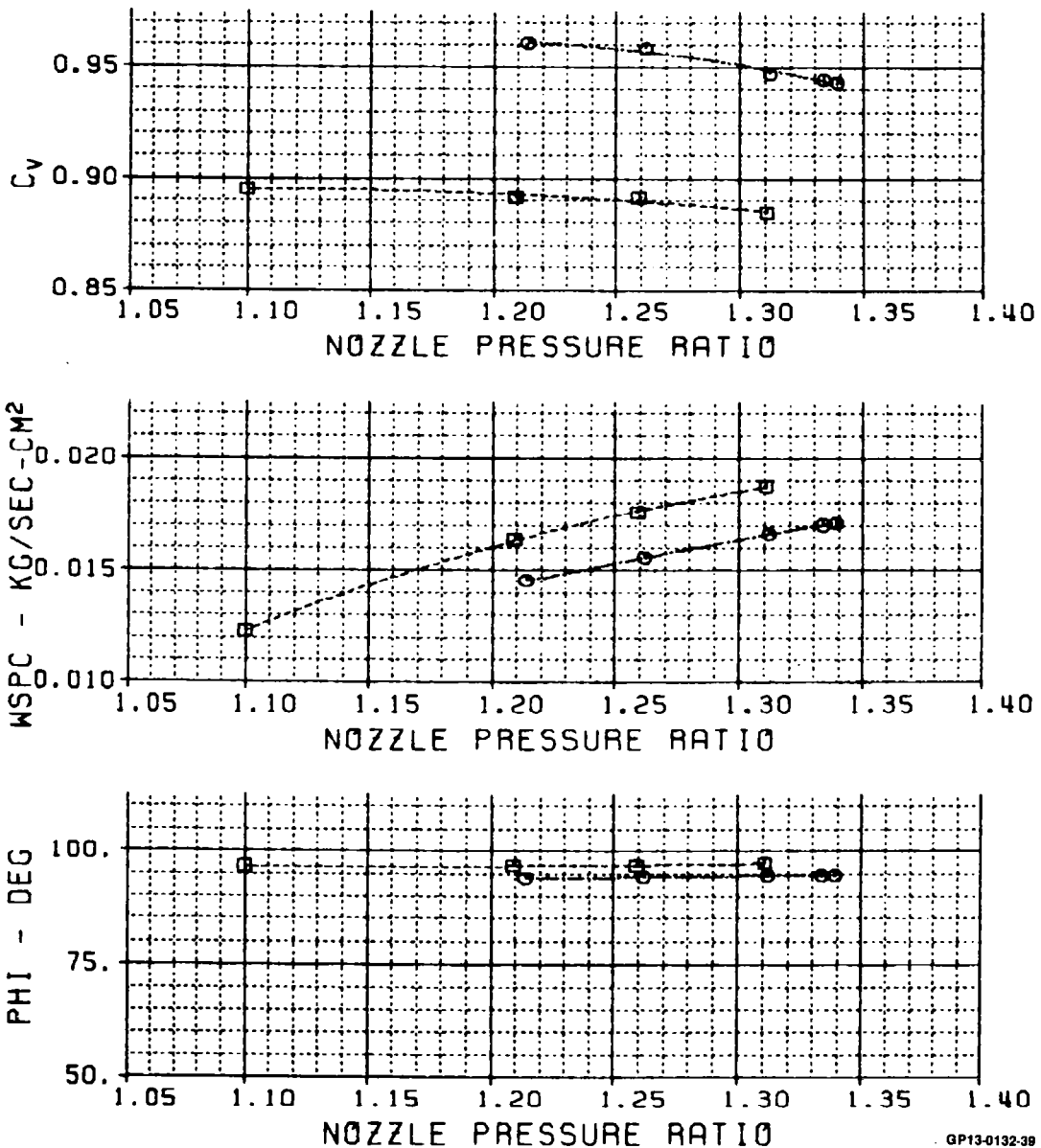


FIGURE 61

CORE NOZZLE RESEARCH MODEL TEST

SYM	TEST	RUN	HODD	R8/R7	DESCRIPTION
□	54	1009	110.00	1.5781	REF. CORE - FWD
○	54	2009	110.00	1.5781	REF. CORE - FWD

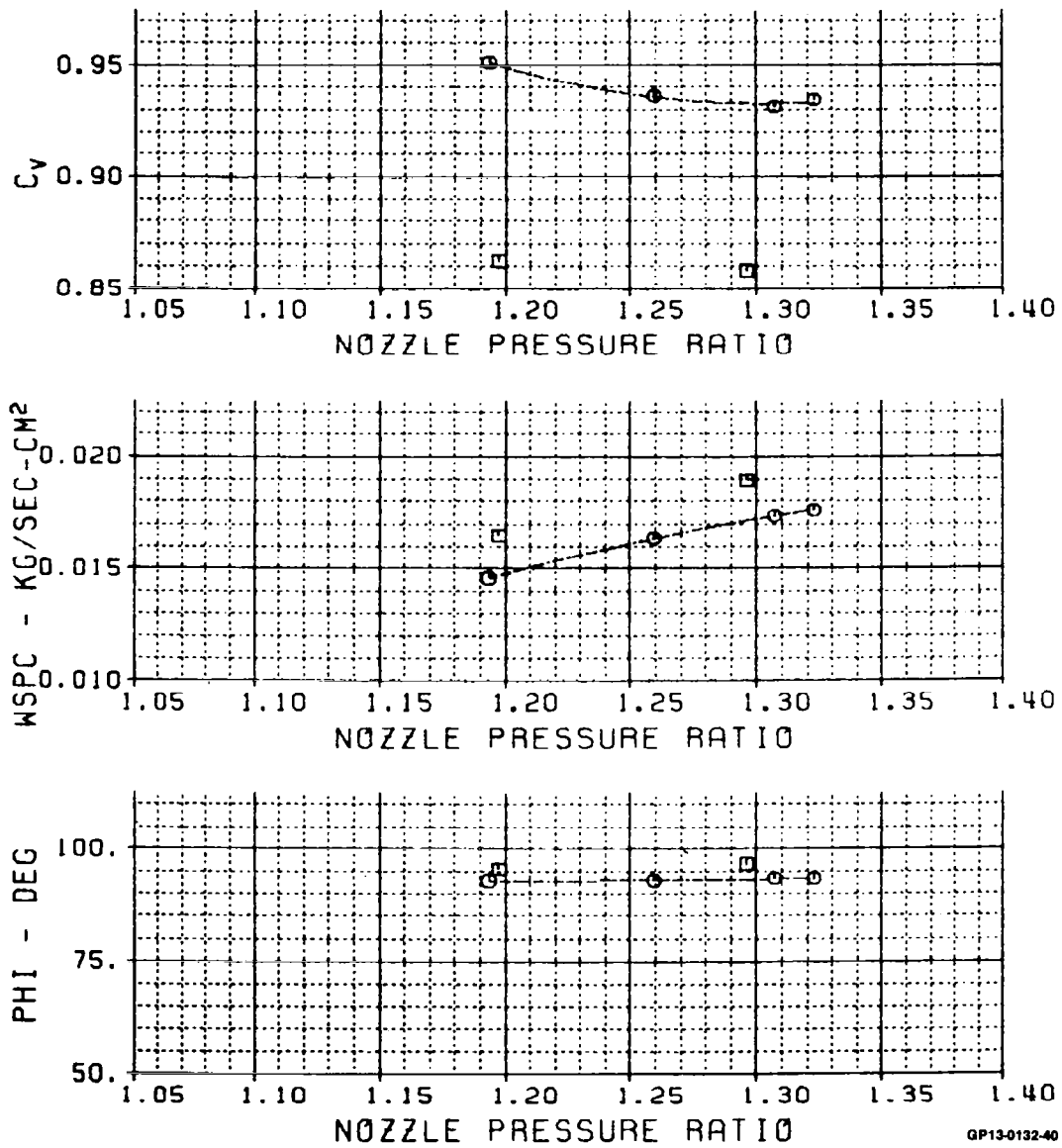
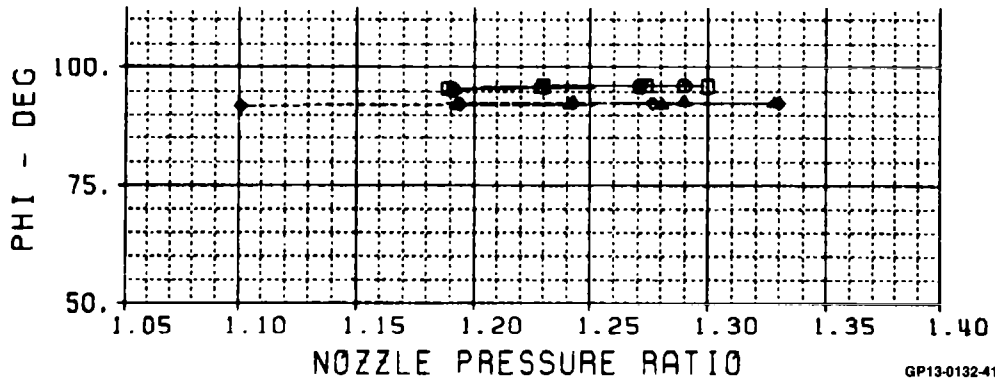
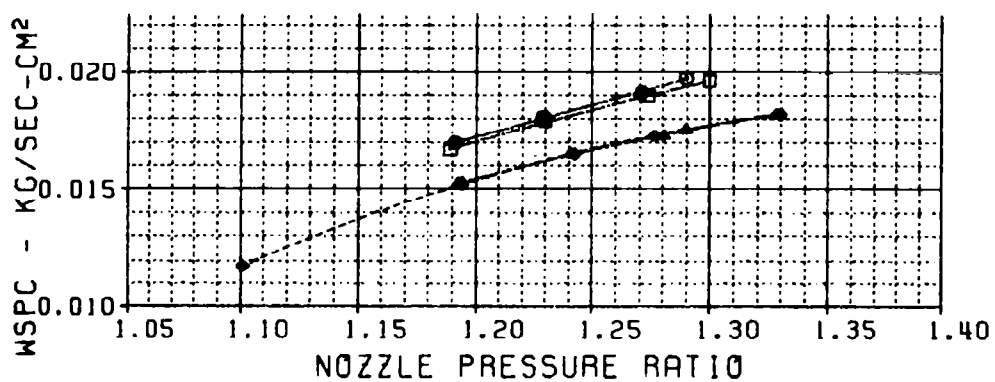
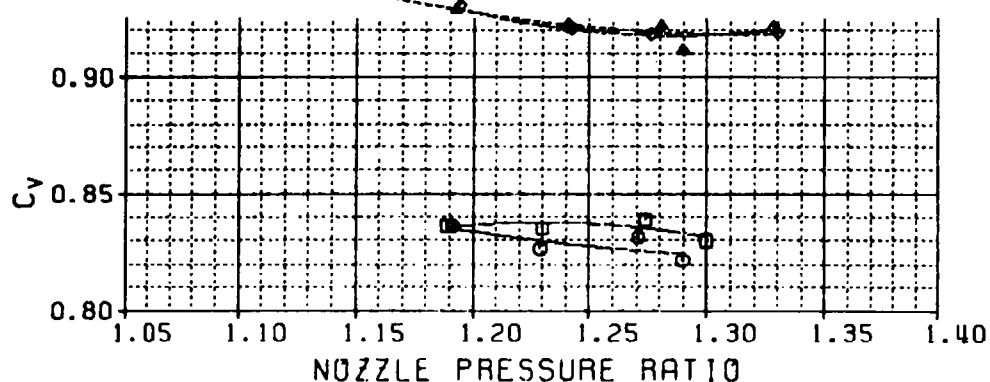


FIGURE 62

CORE NOZZLE RESEARCH MODEL TEST

SYM	TEST	RUN	HOOD	A8/A7	DESCRIPTION
□	54	1004	110.00	1.6536	REF. CORE - FWD
○	54	1005	110.00	1.6536	REF. CORE - FWD
△	54	2004	110.00	1.6536	REF. CORE - FWD
◊	54	2005	110.00	1.6536	REF. CORE - FWD



GP13-0132-41

FIGURE 63

CORE NOZZLE RESEARCH MODEL TEST

SYM	TEST	RUN	HOOD	R8/R7	DESCRIPTION
G	54	1014	110.00	1.7063	REF. CORE - FWD
O	54	2014	110.00	1.7063	REF. CORE - FWD

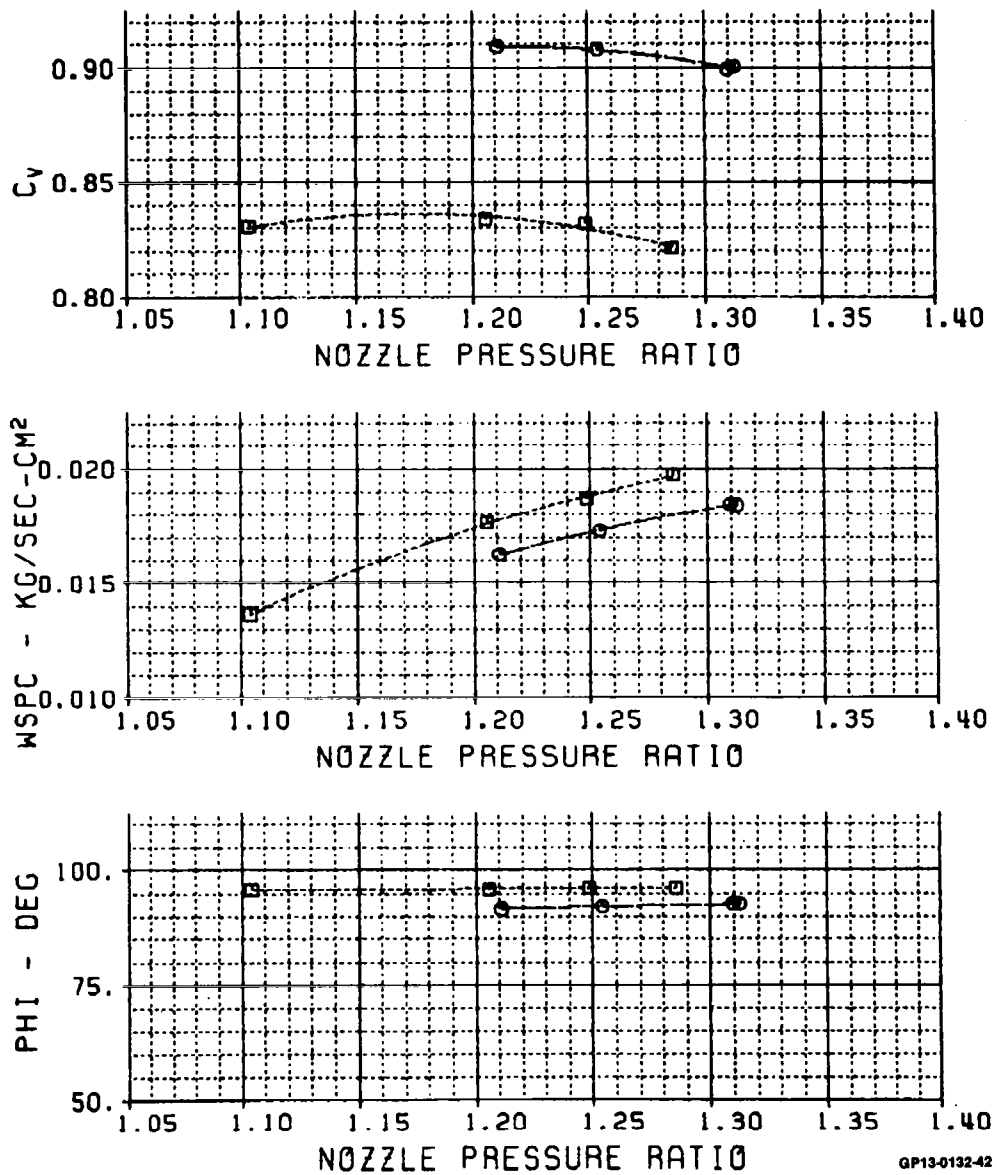


FIGURE 64

CORE NOZZLE RESEARCH MODEL TEST

SYM	TEST	RUN	HOGO	A8/A7	DESCRIPTION
□	54	2012	120.00	1.4889	REF. CORE - FWD

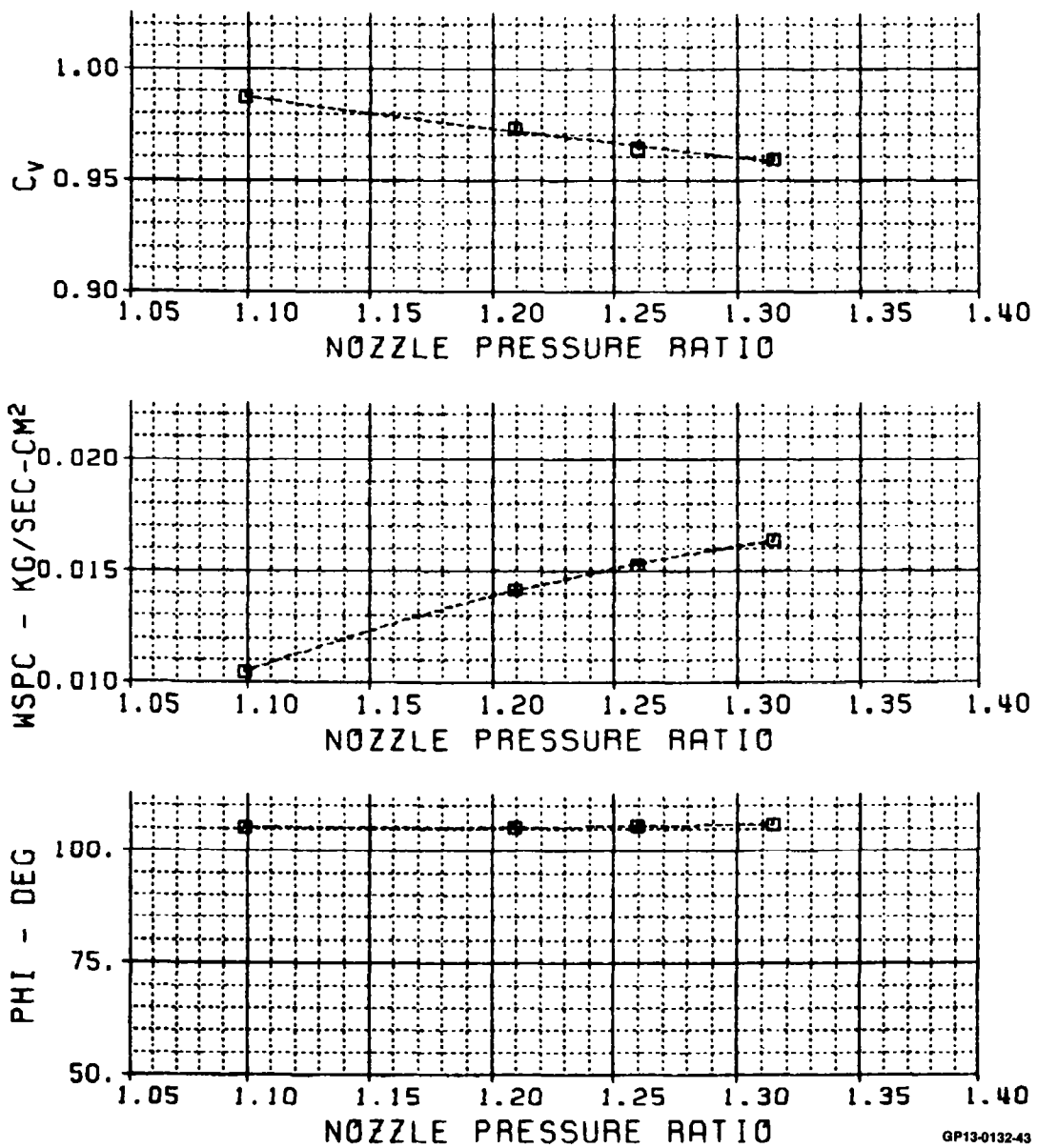


FIGURE 65

CORE NOZZLE RESEARCH MODEL TEST

SYM	TEST	RUN	HDD	A8/A7	DESCRIPTION
■	54	2017	120.00	1.5781	REF. CORE - FWD

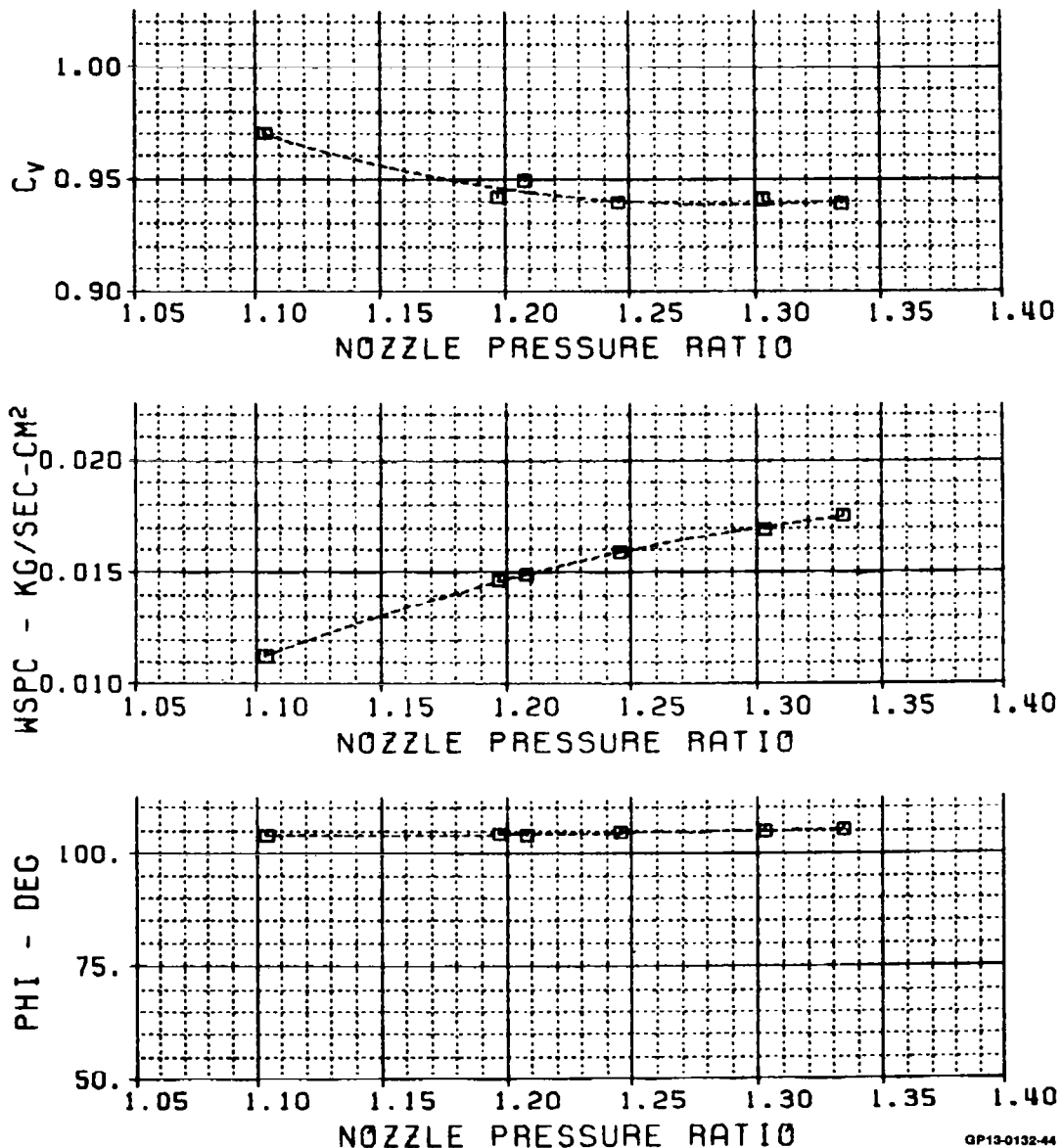


FIGURE 66

CORE NOZZLE RESEARCH MODEL TEST

SYM	TEST	RUN	HODD	AB/A7	DESCRIPTION
□	54	2007	120.00	1.6536	REF. CORE - FWD

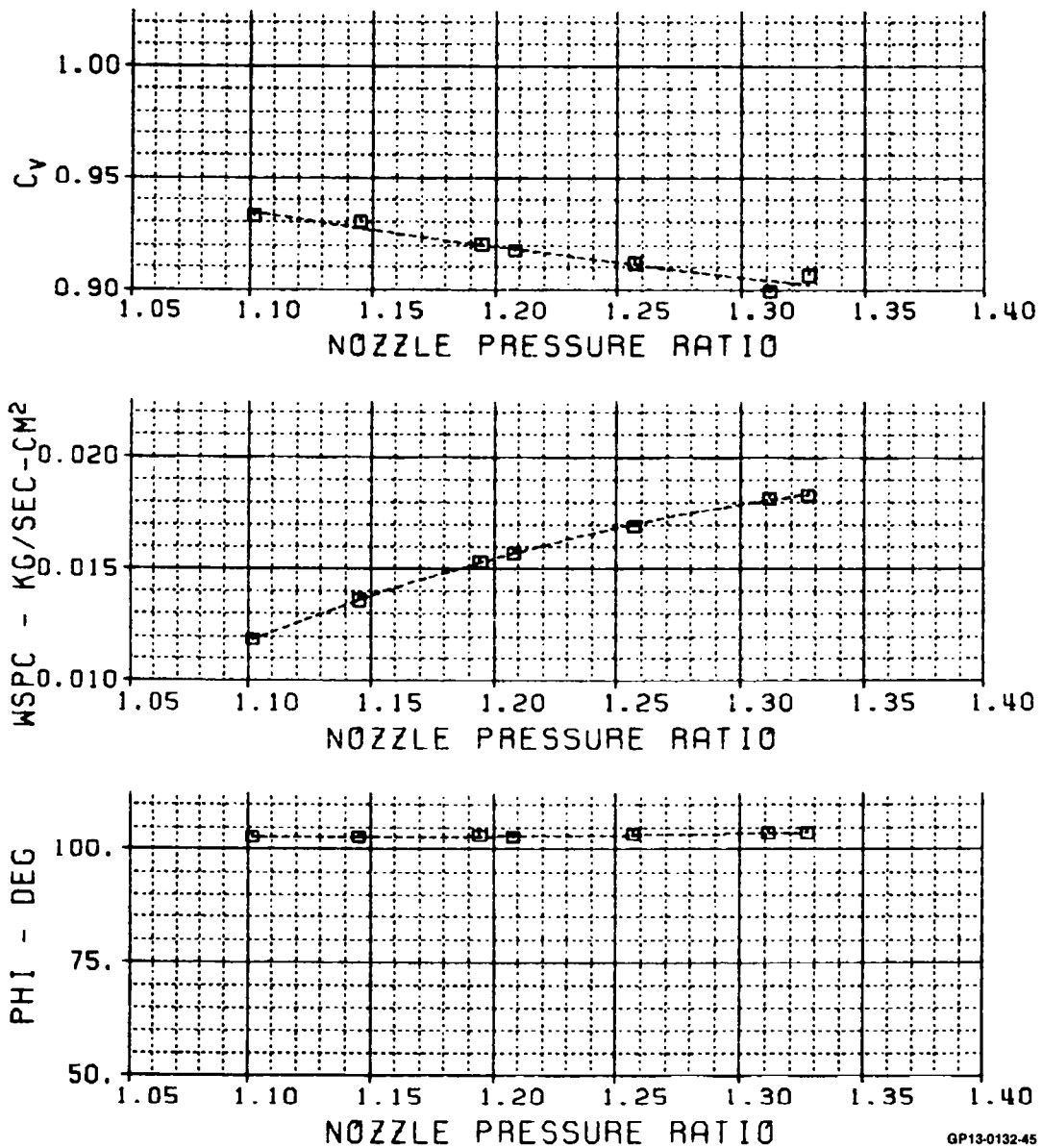


FIGURE 67

CORE NOZZLE RESEARCH MODEL TEST

SYM	TEST	RUN	HODD	AB/R7	DESCRIPTION
□	54	2015	120.00	1.7063	REF. CORE - FWD

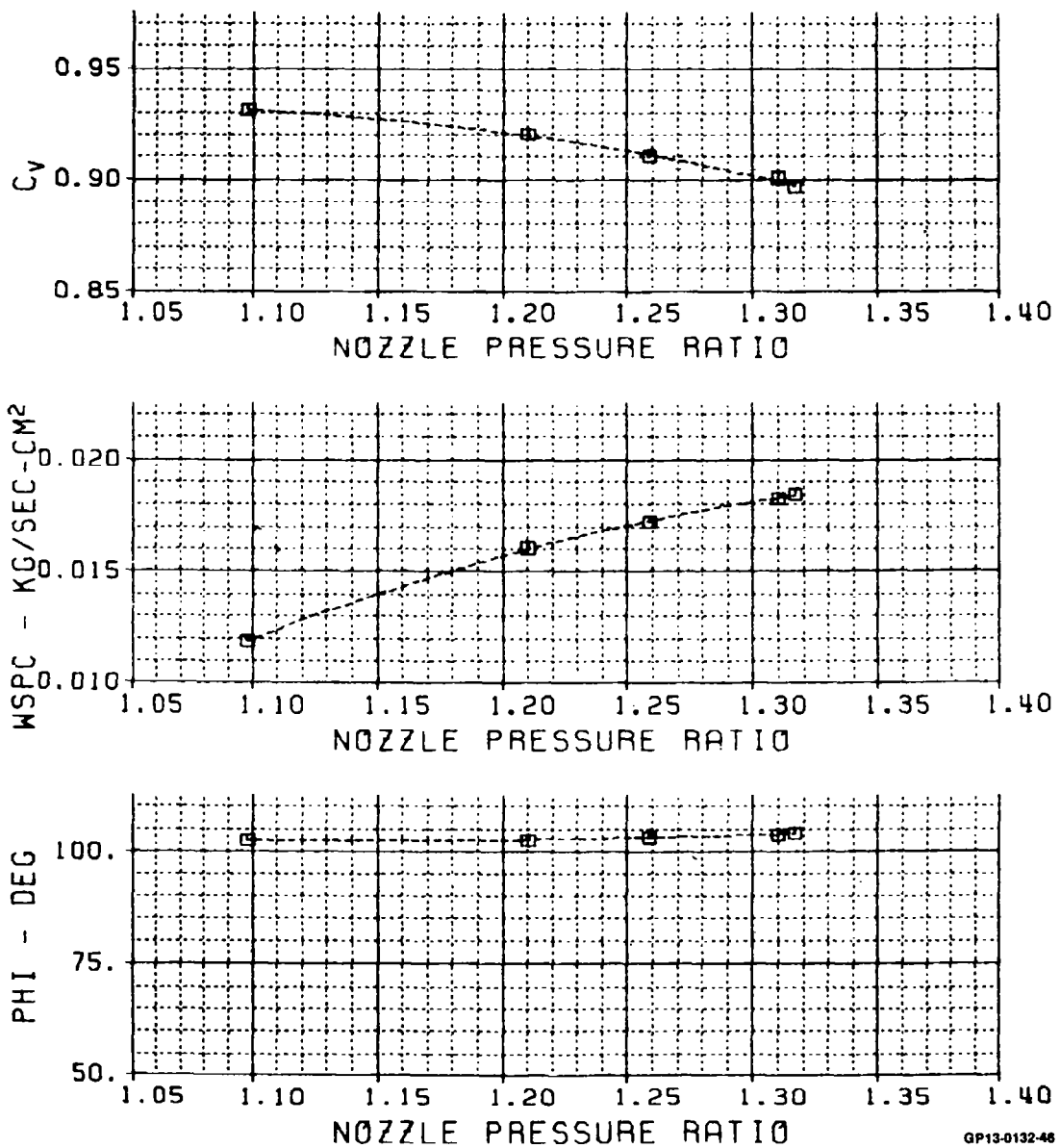


FIGURE 68

CORE NOZZLE RESEARCH MODEL TEST

SYM	TEST	RUN	H000	A8/A7	DESCRIPTION
■	54	1020	90.000	1.5781	REF. CORE - MID
○	54	2020	90.000	1.5781	REF. CORE - MID

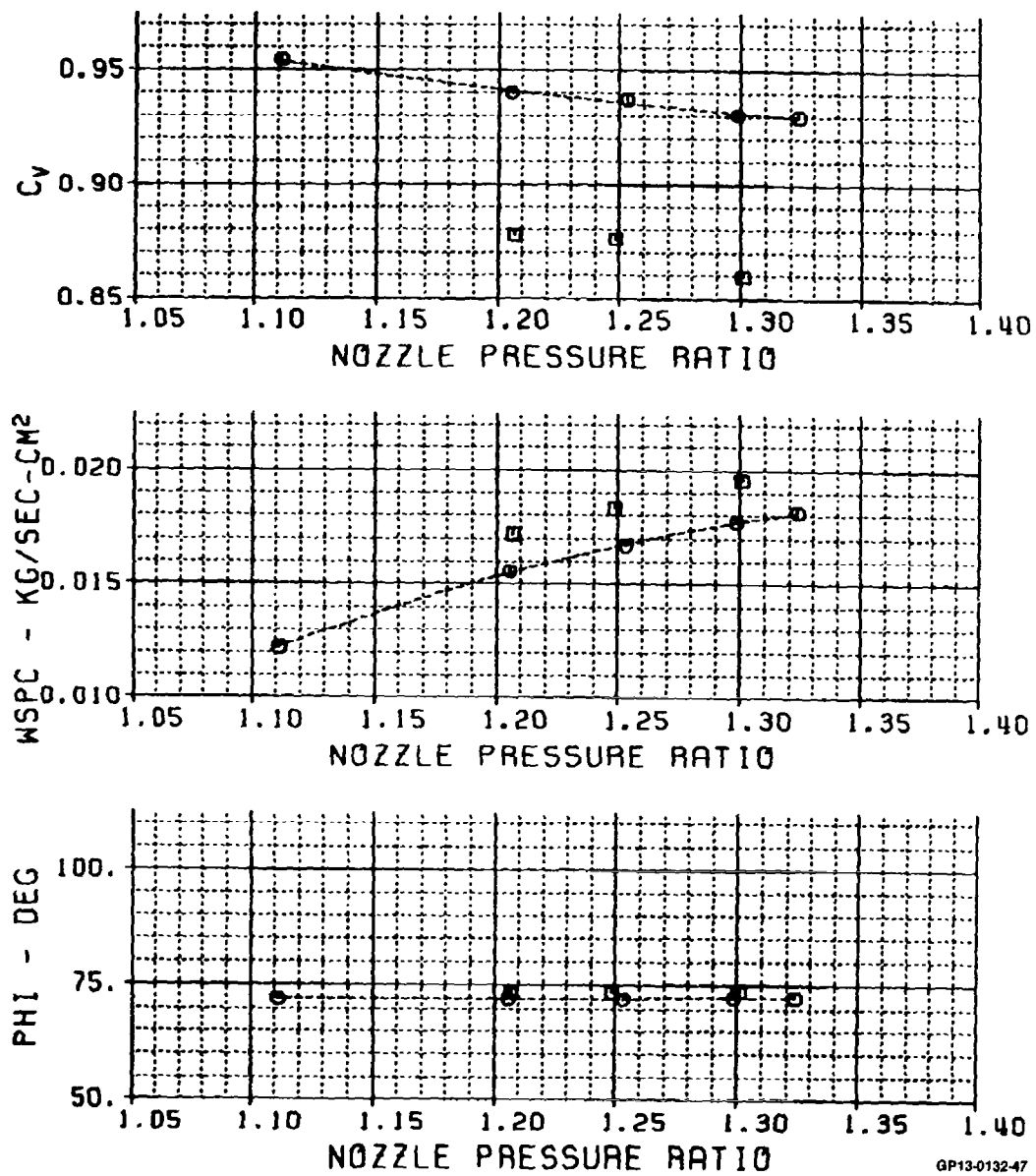


FIGURE 69

CORE NOZZLE RESEARCH MODEL TEST

STM	TEST	RUN	HODD	R8/R7	DESCRIPTION
■	54	1019	110.00	1.5781	REF. CORE - MID
○	54	2019	110.00	1.5781	REF. CORE - MID

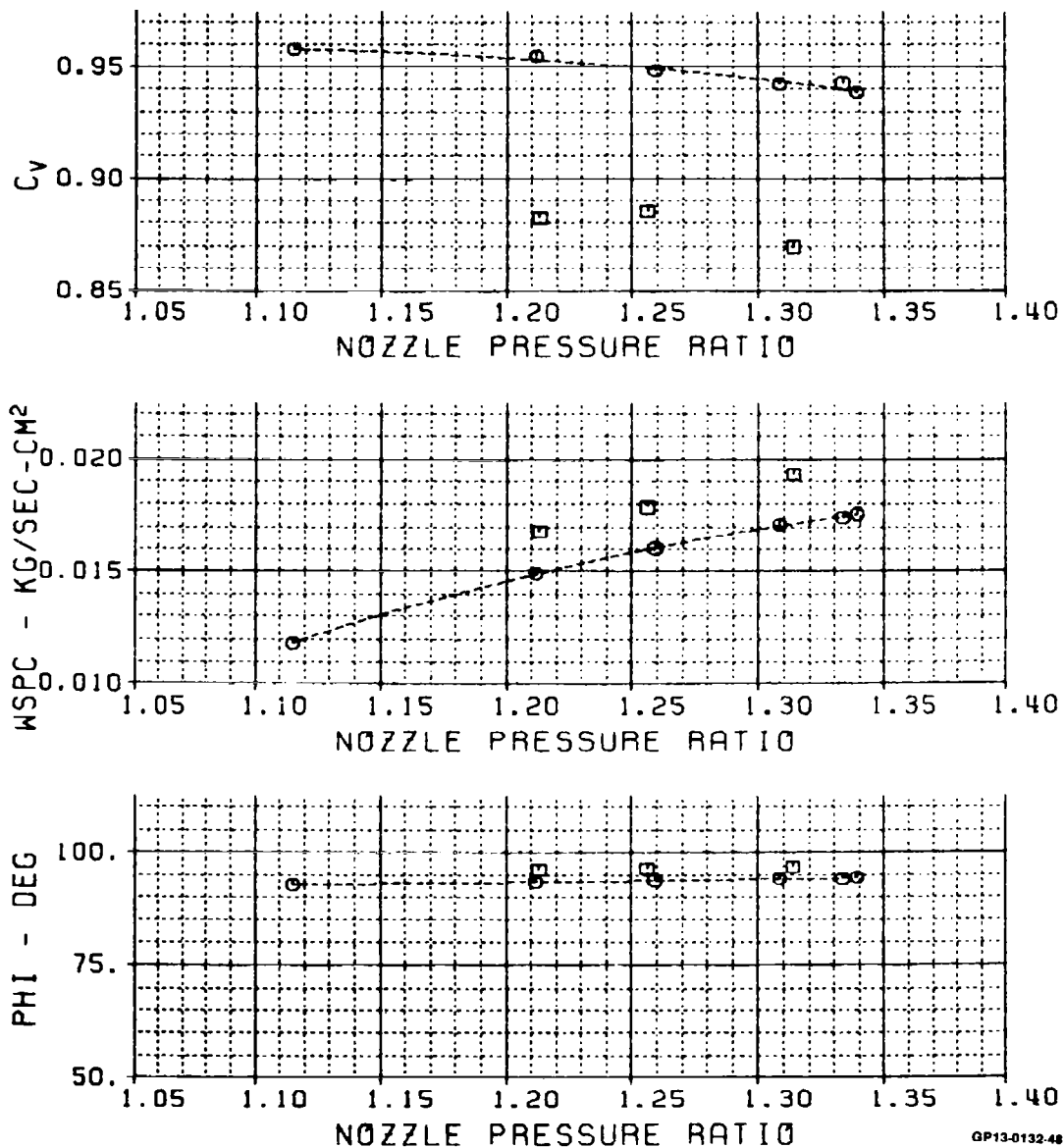


FIGURE 70

CORE NOZZLE RESEARCH MODEL TEST

SYM	TEST	RUN	HDDO	AB/A7	DESCRIPTION
□	54	1021	120.00	1.5781	REF. CORE - MID
○	54	2021	120.00	1.5781	REF. CORE - MID

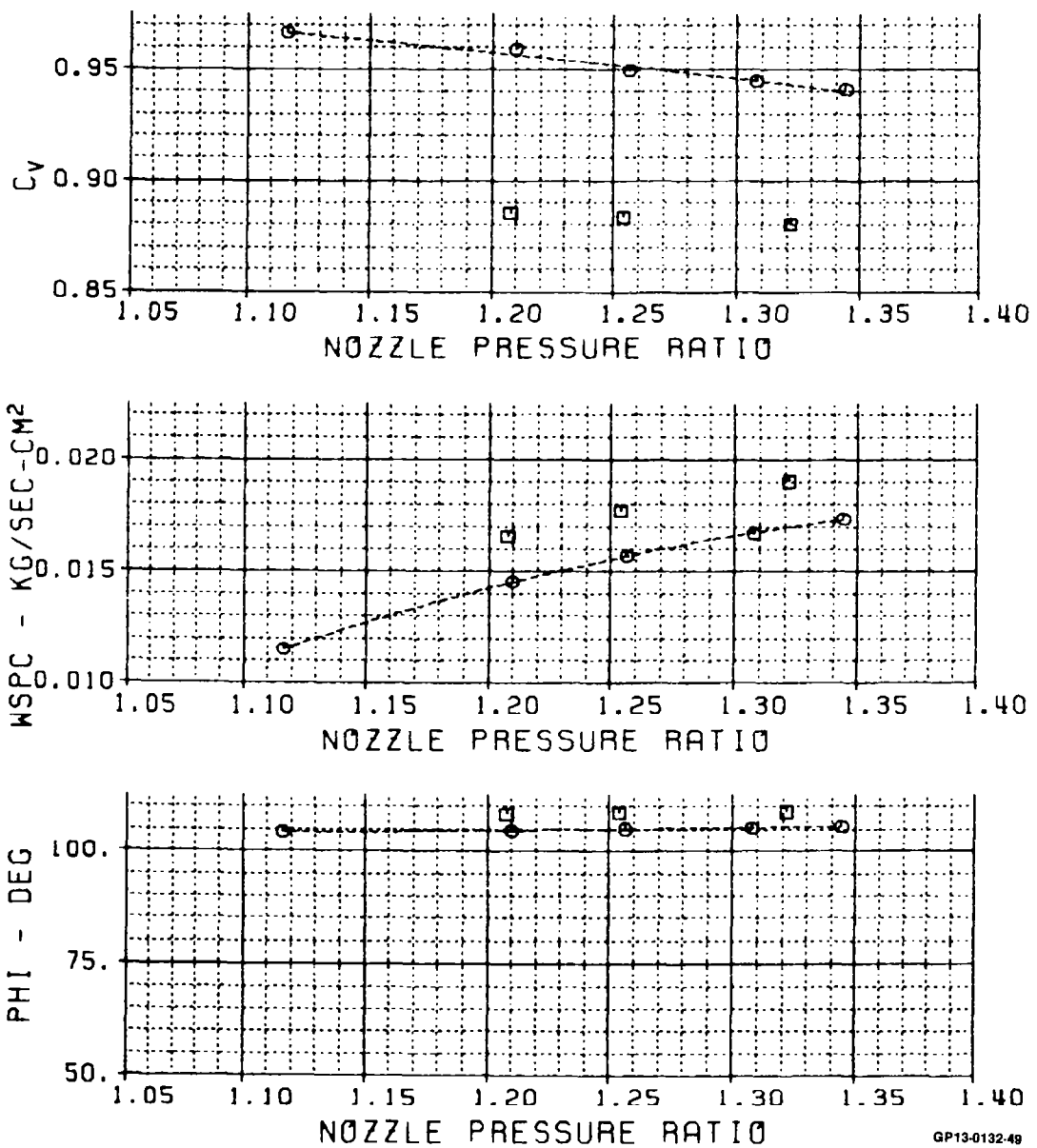


FIGURE 71

CORE NOZZLE RESEARCH MODEL TEST

SYM	TEST	RUN	HOOD	A8/A7	DESCRIPTION
■	54	1025	35.500	1.5781	REF. CORE - AFT
○	54	2025	35.500	1.5781	REF. CORE - AFT

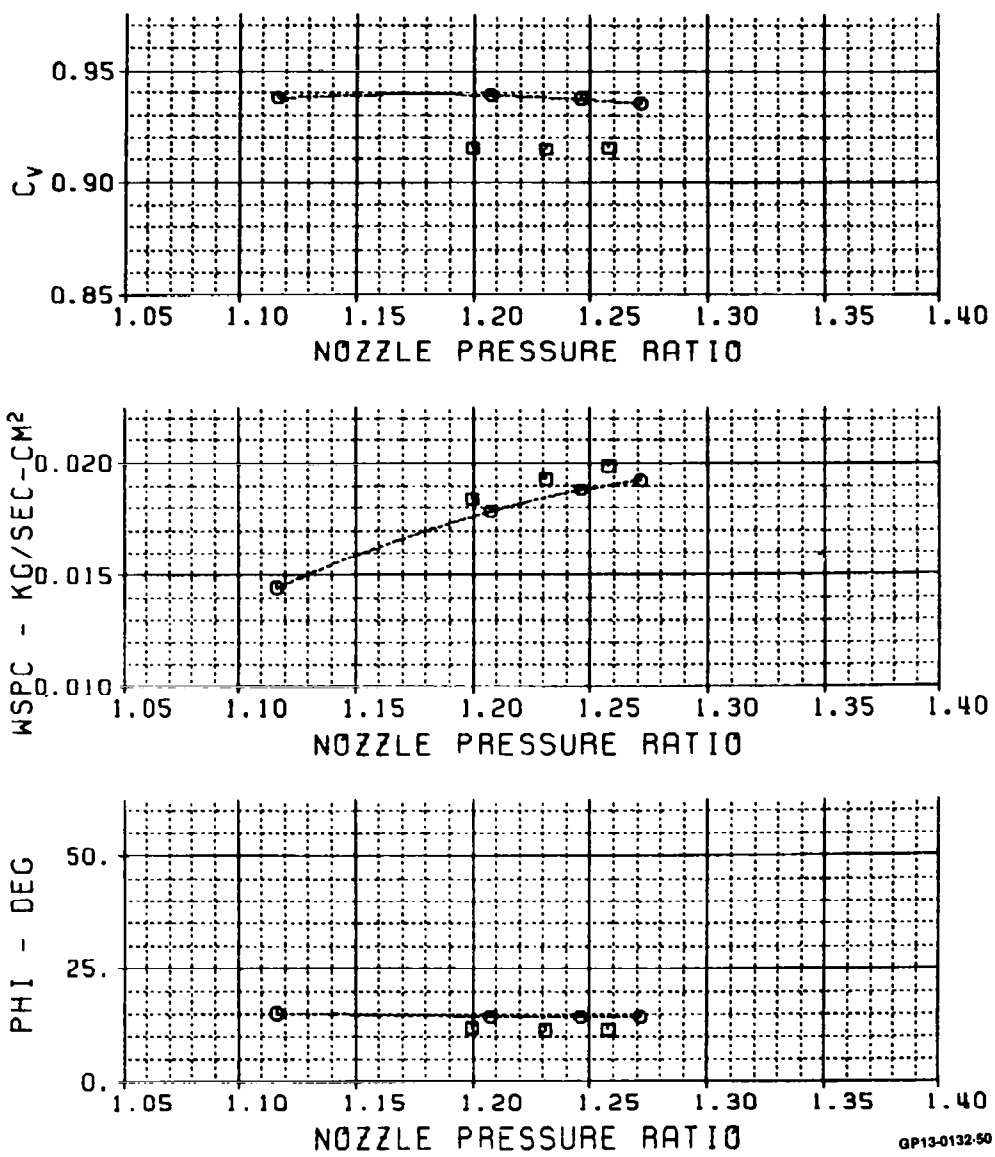


FIGURE 72

CORE NOZZLE RESEARCH MODEL TEST

STM	TEST	RUN	HOOD	R8/A7	DESCRIPTION
□	54	1026	60.000	1.5781	REF. CORE - AFT
○	54	2026	60.000	1.5781	REF. CORE - AFT

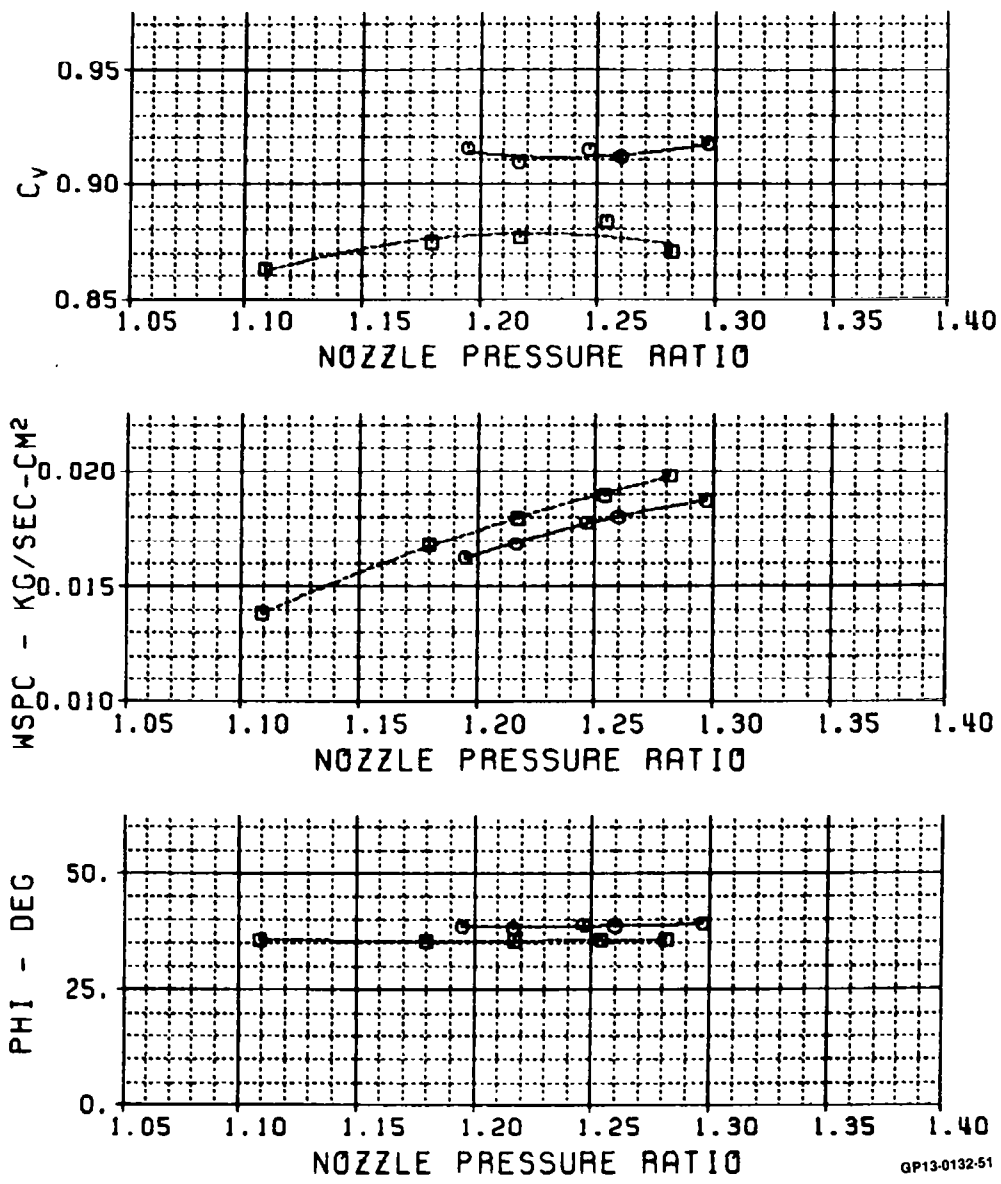


FIGURE 73

CORE NOZZLE RESEARCH MODEL TEST

SYM	TEST	RUN	HOOD	RB/R7	DESCRIPTION
Q	54	1027	75.000	1.5781	REF. CORE - AFT
O	54	2027	75.000	1.5781	REF. CORE - AFT

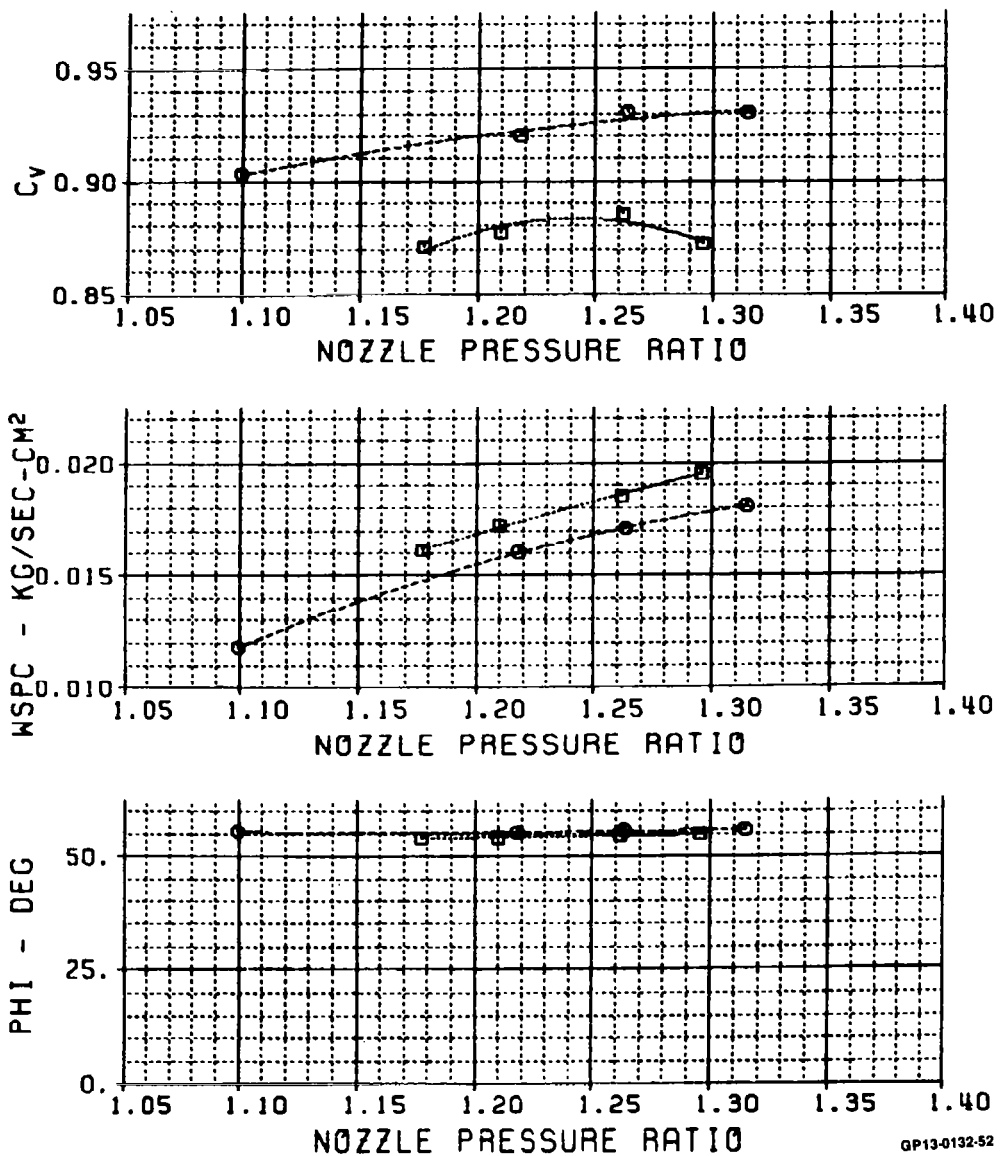


FIGURE 74

CORE NOZZLE RESEARCH MODEL TEST

SYM	TEST	RUN	HODD	AB/A7	DESCRIPTION
□	54	1023	90.000	1.5781	REF. CORE - AFT
○	54	2023	90.000	1.5781	REF. CORE - AFT

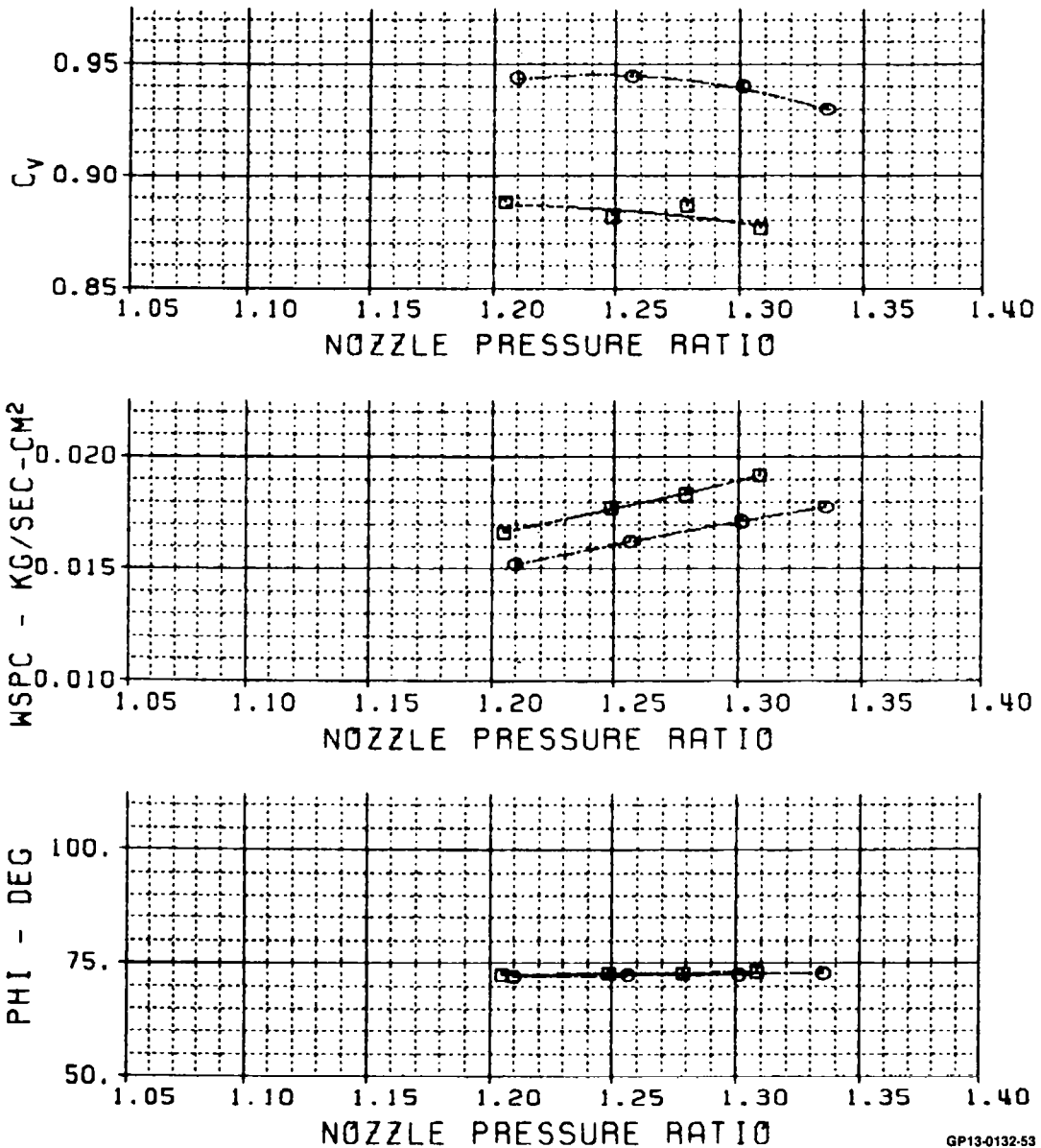


FIGURE 75

CORE NOZZLE RESEARCH MODEL TEST

STM	TEST	RUN	HODD	R8/R7	DESCRIPTION
□	54	1028	100.00	1.5781	REF. CORE - AFT
○	54	2028	100.00	1.5781	REF. CORE - AFT

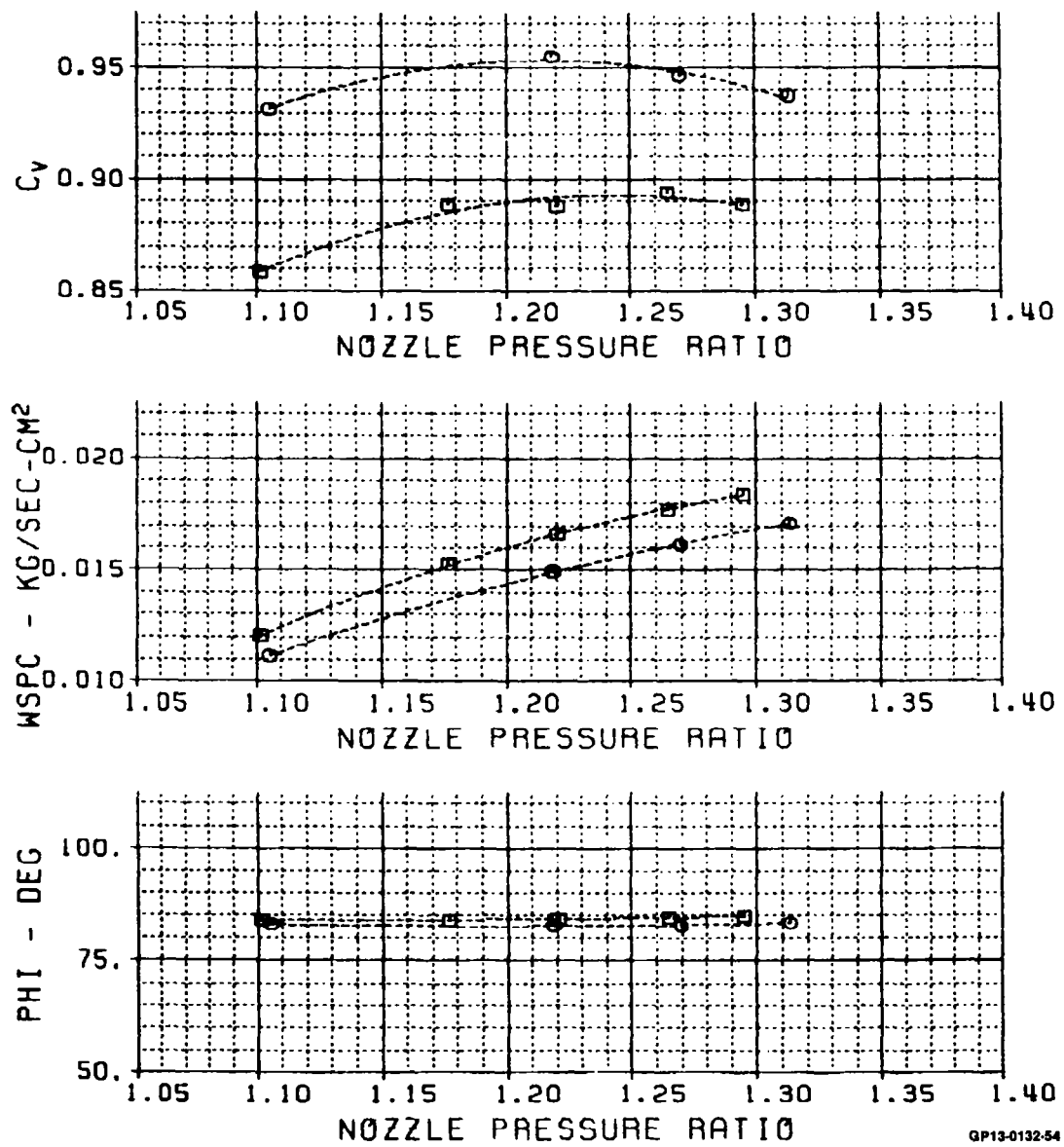


FIGURE 76

CORE NOZZLE RESEARCH MODEL TEST

SYM	TEST	RUN	HOOD	AB/A7	DESCRIPTION
□	54	1022	110.00	1.5781	REF. CORE - AFT
○	54	1029	110.00	1.5781	REF. CORE - AFT
▲	54	2022	110.00	1.5781	REF. CORE - AFT
◆	54	2029	110.00	1.5781	REF. CORE - AFT

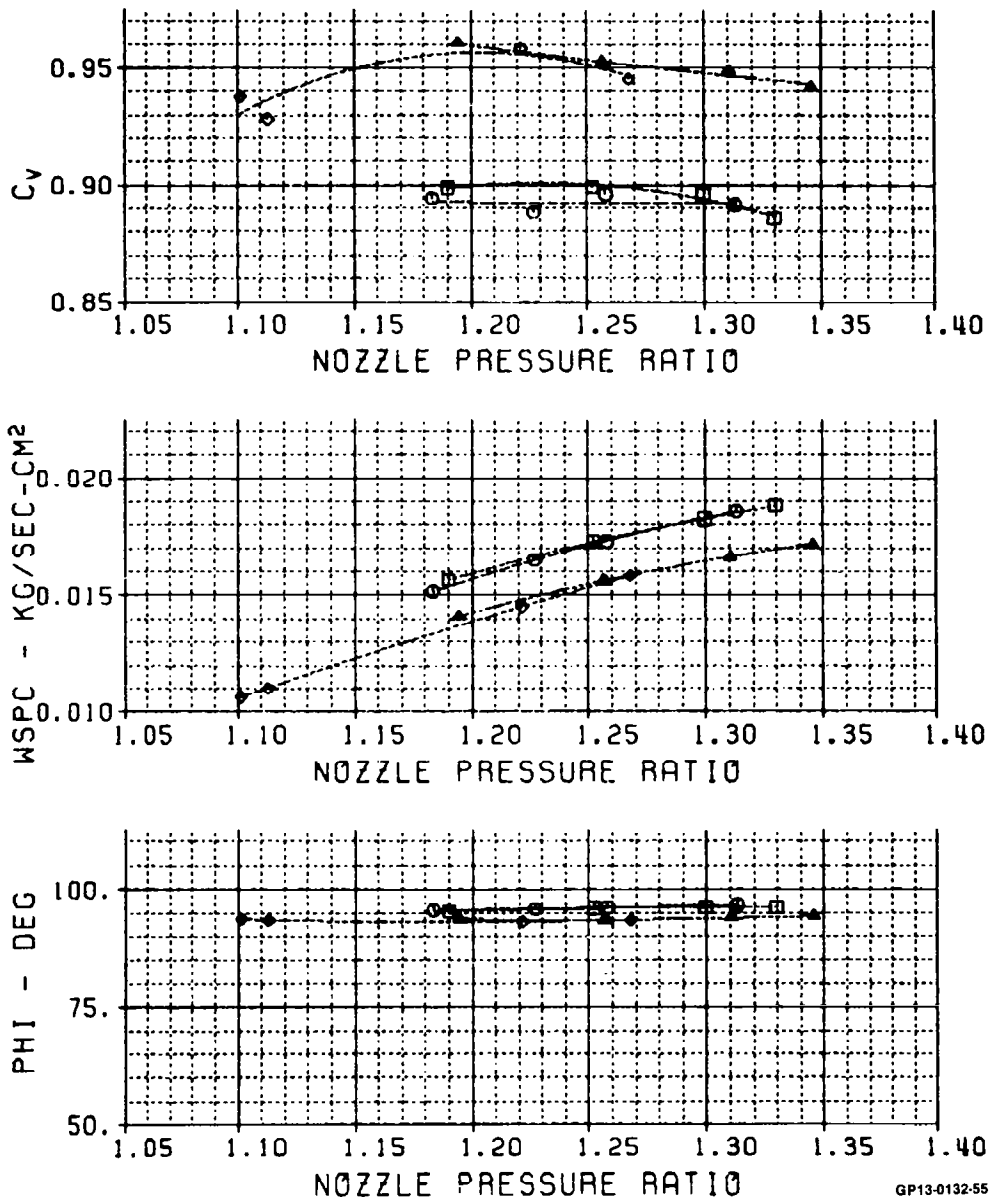


FIGURE 77

CORE NOZZLE RESEARCH MODEL TEST

SYM	TEST	RUN	HODD	R8/R7	DESCRIPTION
■	54	1024	120.00	1.5781	REF. CORE - AFT
○	54	2024	120.00	1.5781	REF. CORE - AFT

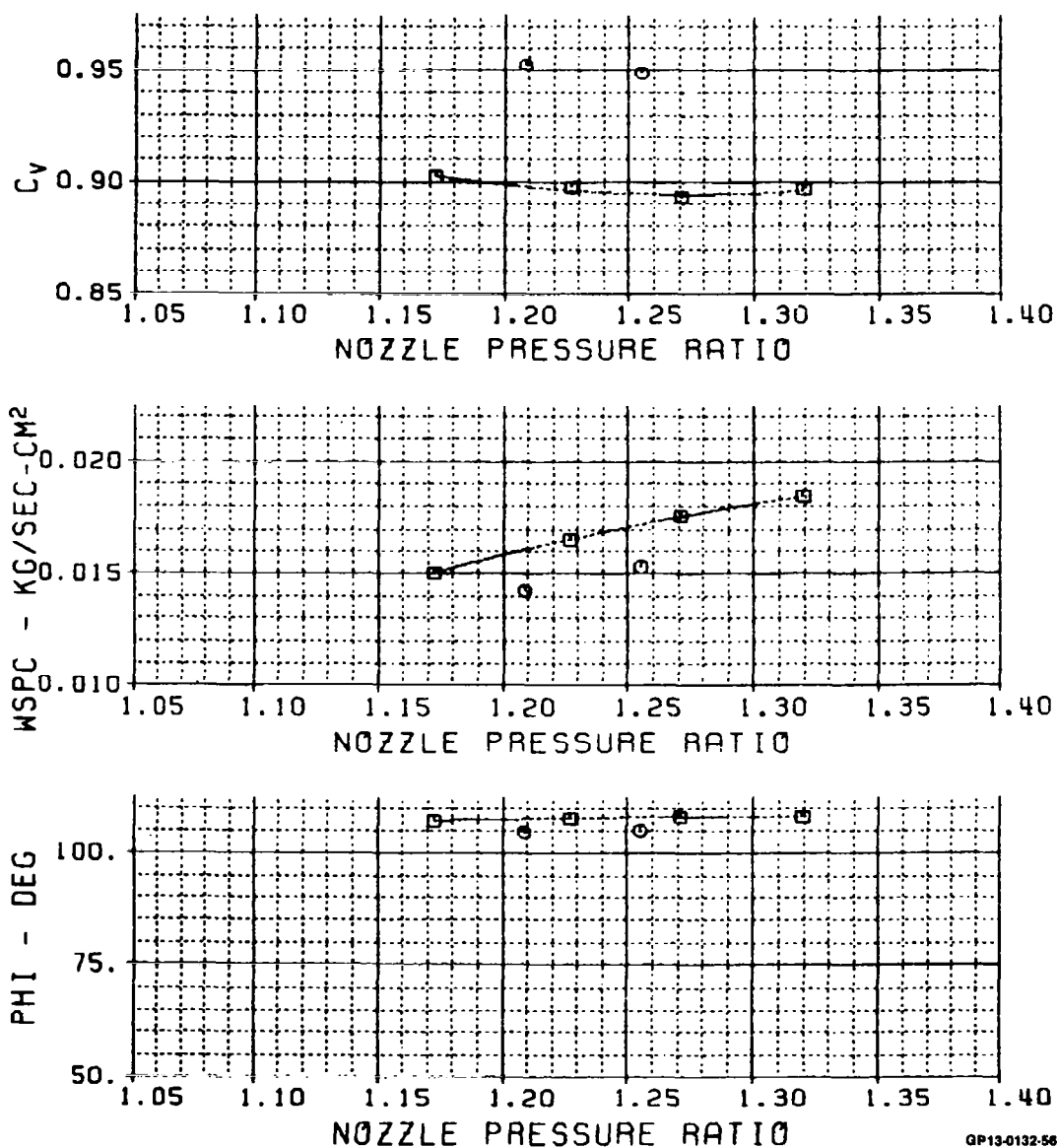


FIGURE 78

CORE NOZZLE RESEARCH MODEL TEST

SYM	TEST	RUN	HOOD	R8/R7	DESCRIPTION
□	54	1032	35.500	0.8163	ALT. NO.1 CORE CRUISE NOZZLE
○	54	2032	35.500	0.8163	ALT. NO.1 CORE CRUISE NOZZLE

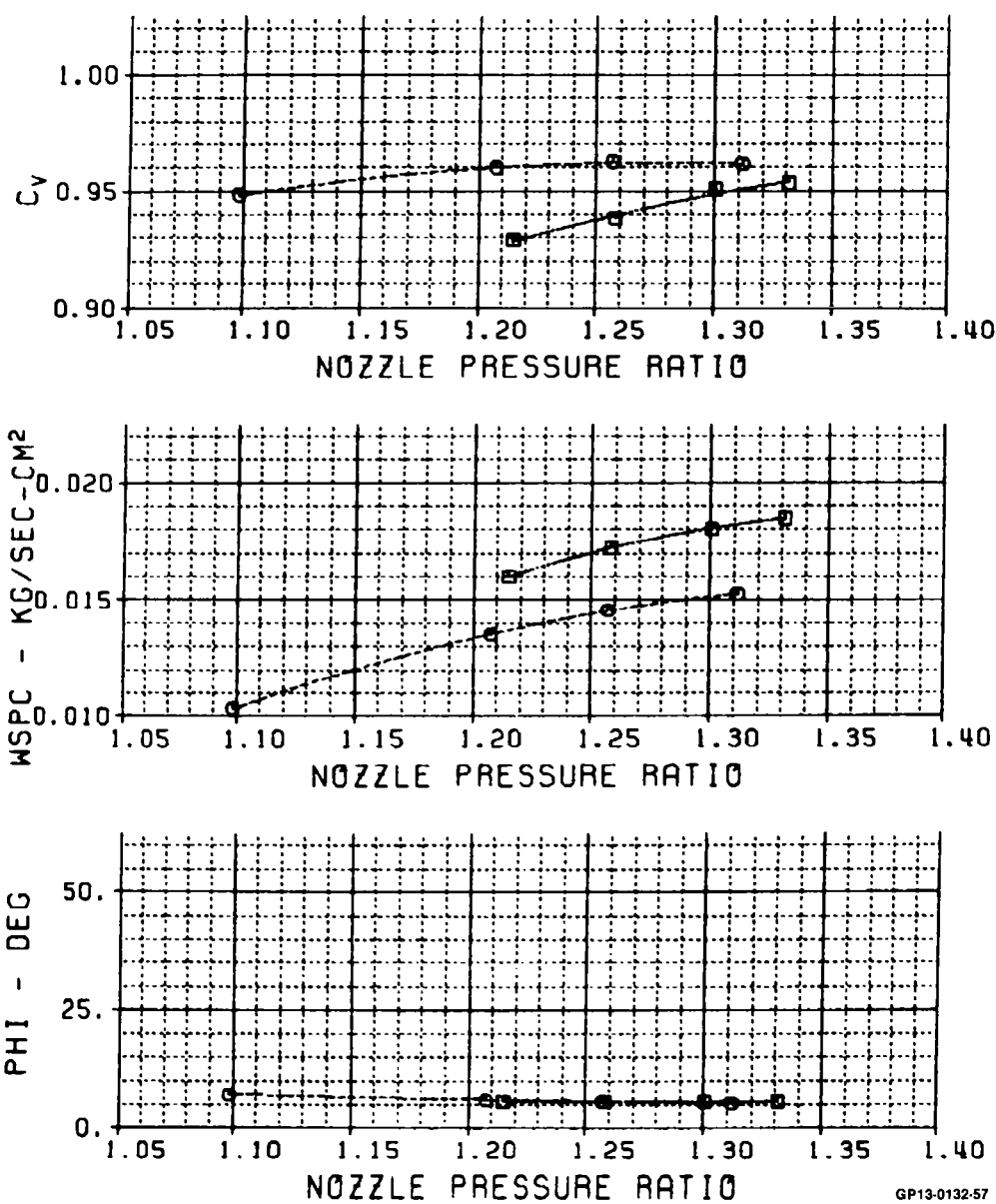


FIGURE 79

CORE NOZZLE RESEARCH MODEL TEST

STM	TEST	RUN	HOOD	AB/R7	DESCRIPTION
□	54	1037	35.500	1.5781	ALT. NO.1 CORE
○	54	2037	35.500	1.5781	ALT. NO.1 CORE

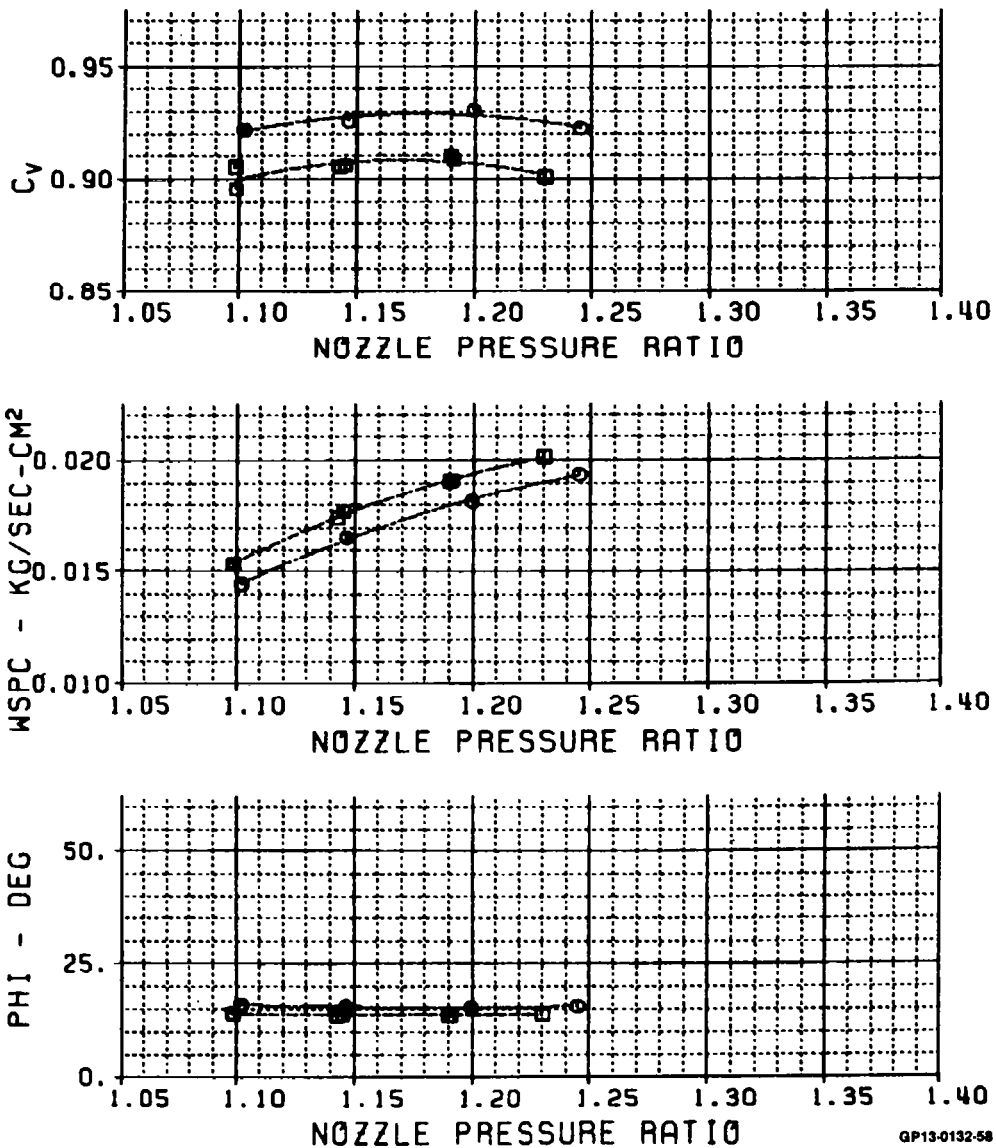


FIGURE 80

CORE NOZZLE RESEARCH MODEL TEST

SYM	TEST	RUN	HOOD	AB/A7	DESCRIPTION
■	54	1036	75.000	1.5781	ALT. NO.1 CORE
○	54	2036	75.000	1.5781	ALT. NO.1 CORE

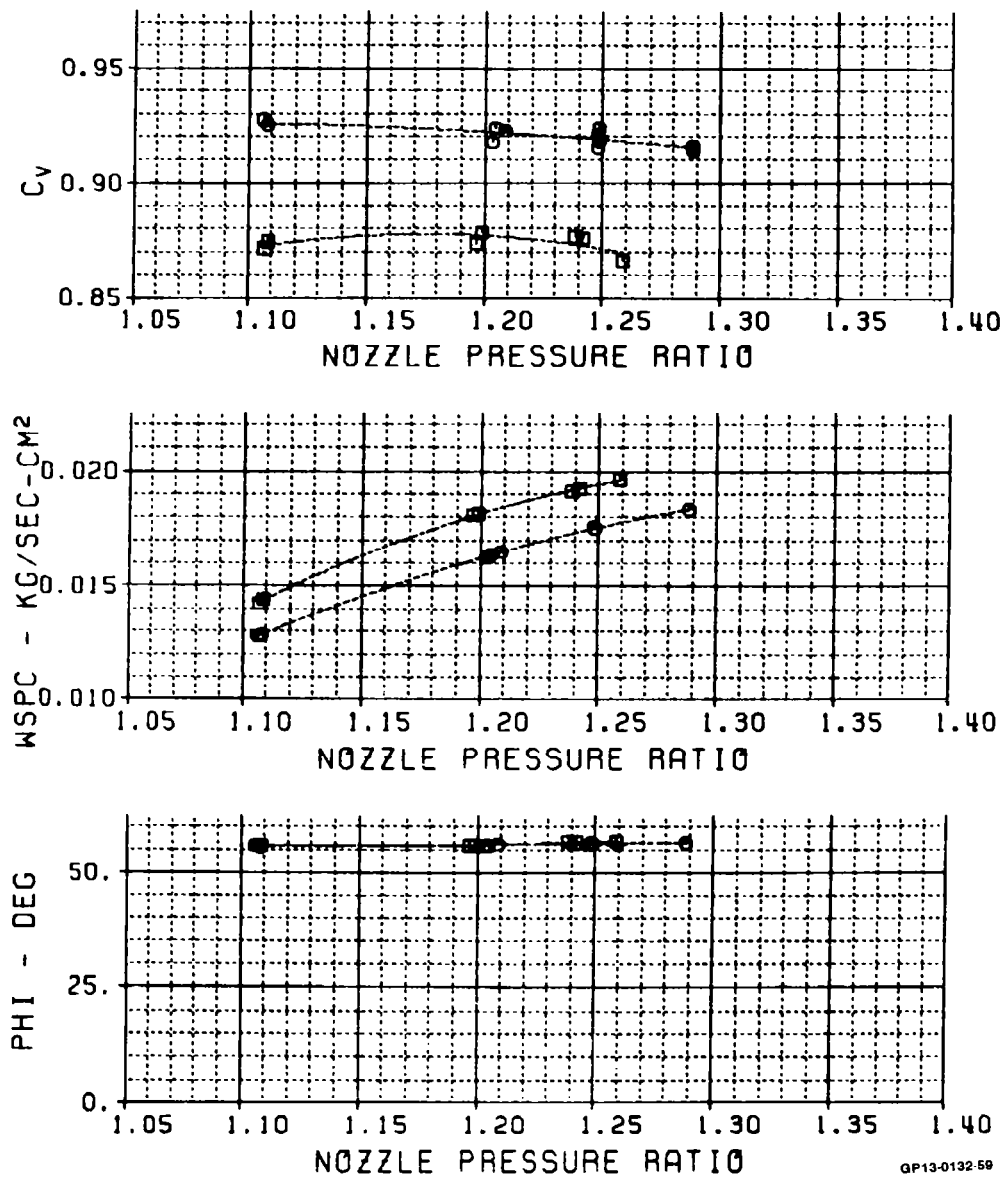


FIGURE 81

CORE NOZZLE RESEARCH MODEL TEST

SYM	TEST	RUN	HOOD	RR/R7	DESCRIPTION
■	54	2033	110.00	1.5781	ALT. NO.1 CORE

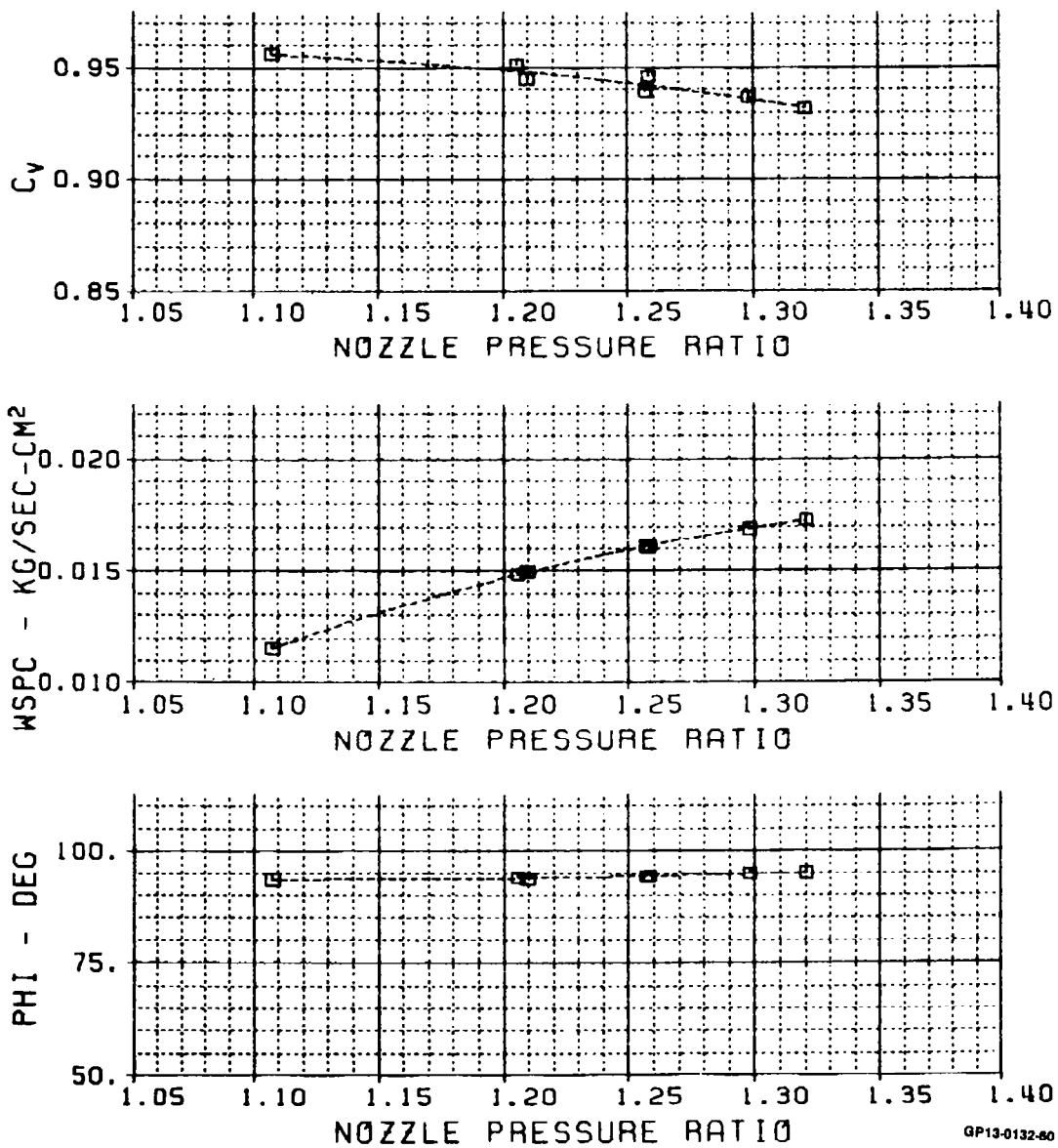


FIGURE 82

CORE NOZZLE RESEARCH MODEL TEST

STM	TEST	RUN	HOOD	A8/A7	DESCRIPTION
54	54	1034	110.00	1.5781	ALT. NO.1 CORE
		2034	110.00	1.5781	ALT. NO.1 CORE

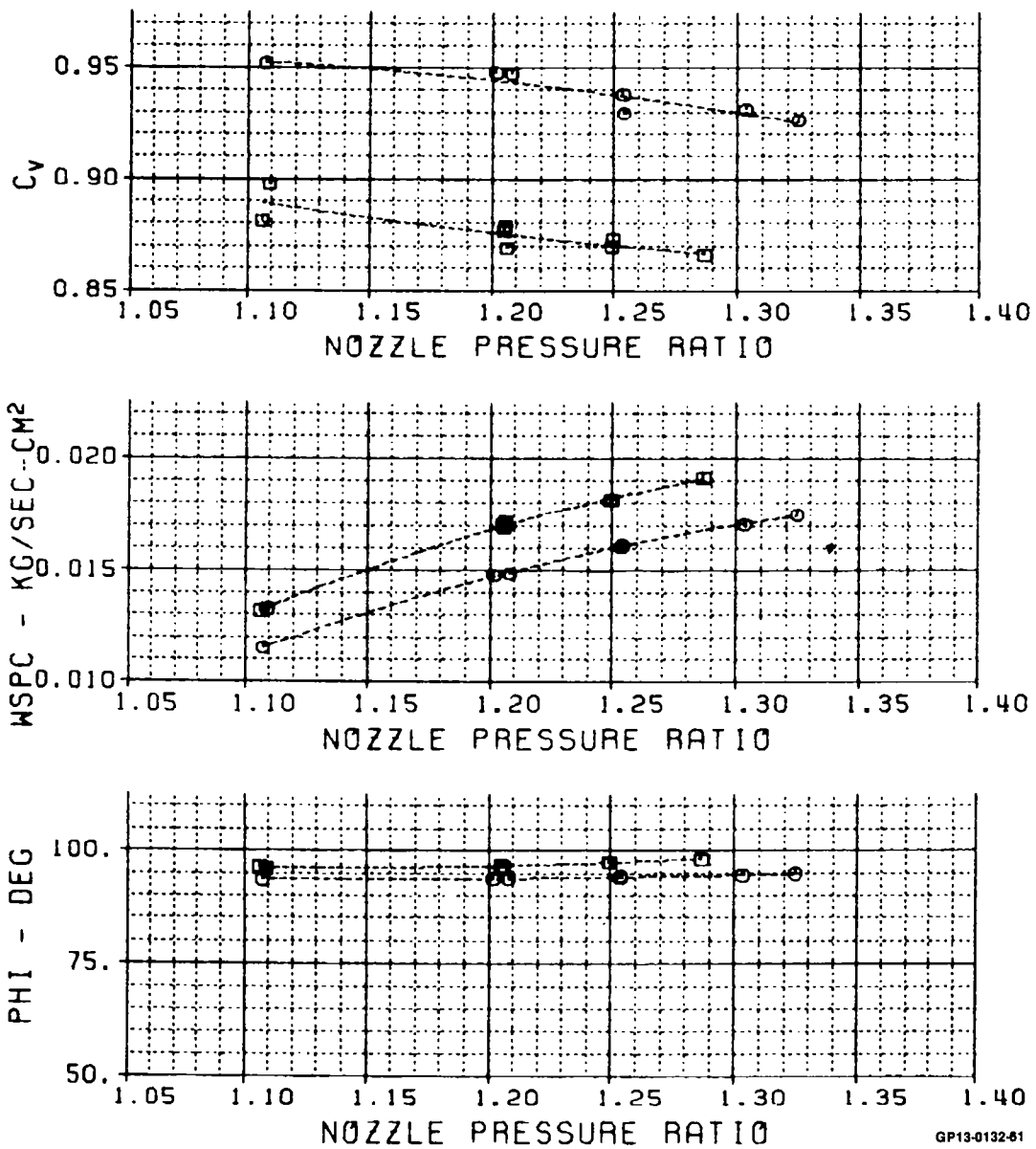


FIGURE 83

CORE NOZZLE RESEARCH MODEL TEST

STM	TEST	RUN	HOOD	AB/A7	DESCRIPTION
■	54	1035	120.00	1.5781	ALT. NO.1 CORE
○	54	2035	120.00	1.5781	ALT. NO.1 CORE

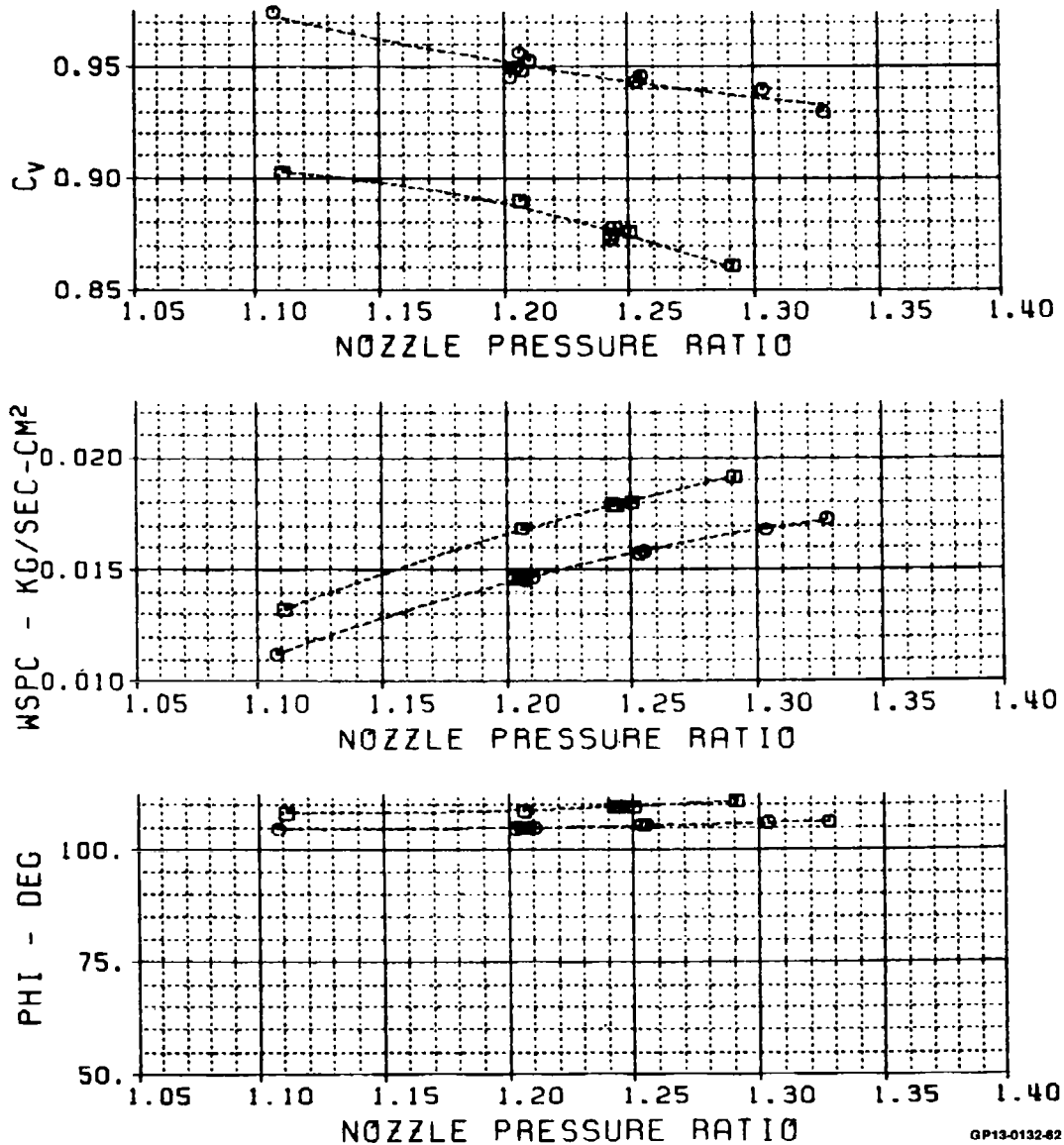


FIGURE 84

CORE NOZZLE RESEARCH MODEL TEST

SYM	TEST	RUN	HODD	RR/R7	DESCRIPTION
□	54	1042	35.500	0.8163	ALT. NO.2 CORE CRUISE NOZZLE
○	54	1052	35.500	0.8163	ALT. NO.2 CORE CRUISE NOZZLE
▲	54	2042	35.500	0.8163	ALT. NO.2 CORE CRUISE NOZZLE
◆	54	2052	35.500	0.8163	ALT. NO.2 CORE CRUISE NOZZLE

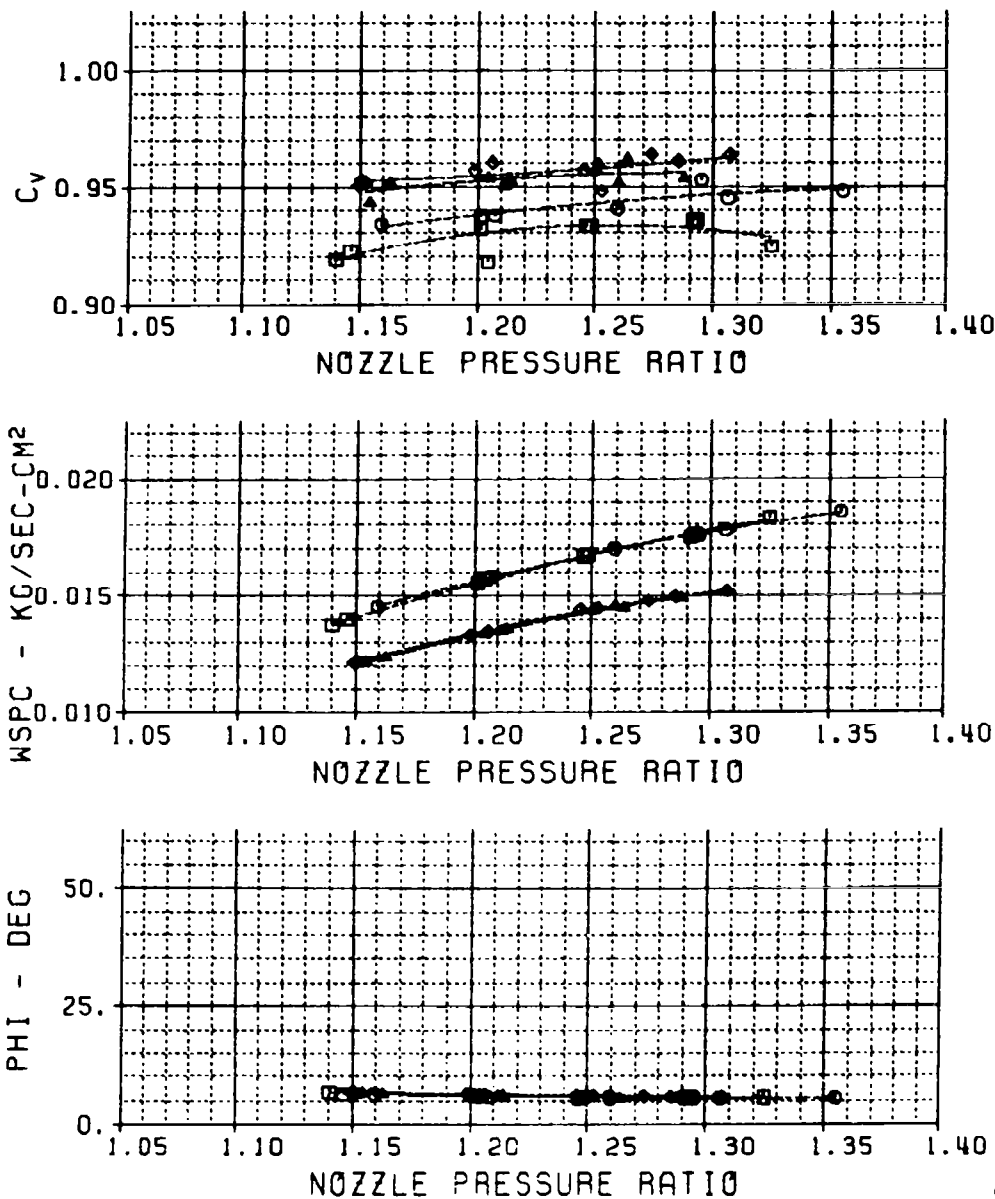


FIGURE 85

CORE NOZZLE RESEARCH MODEL TEST

SYM	TEST	RUN	HOOD	R8/R7	DESCRIPTION
□	54	1074	35.500	1.3003	ALT. NO.2 CORE

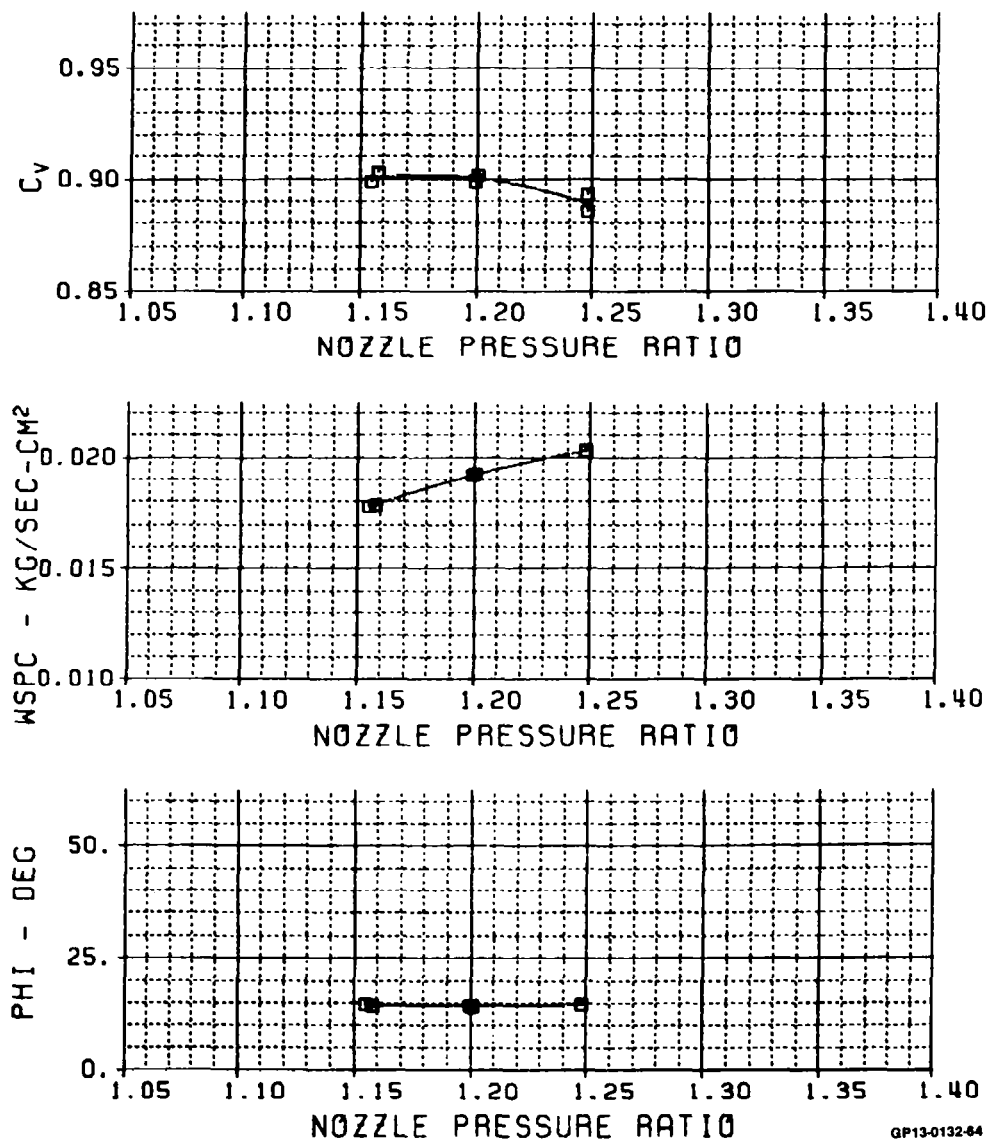


FIGURE 86

CORE NOZZLE RESEARCH MODEL TEST

STM	TEST	RUN	HOOD	A8/A7	DESCRIPTION
■	54	1059	35.500	1.3861	ALT. NO.2 CORE

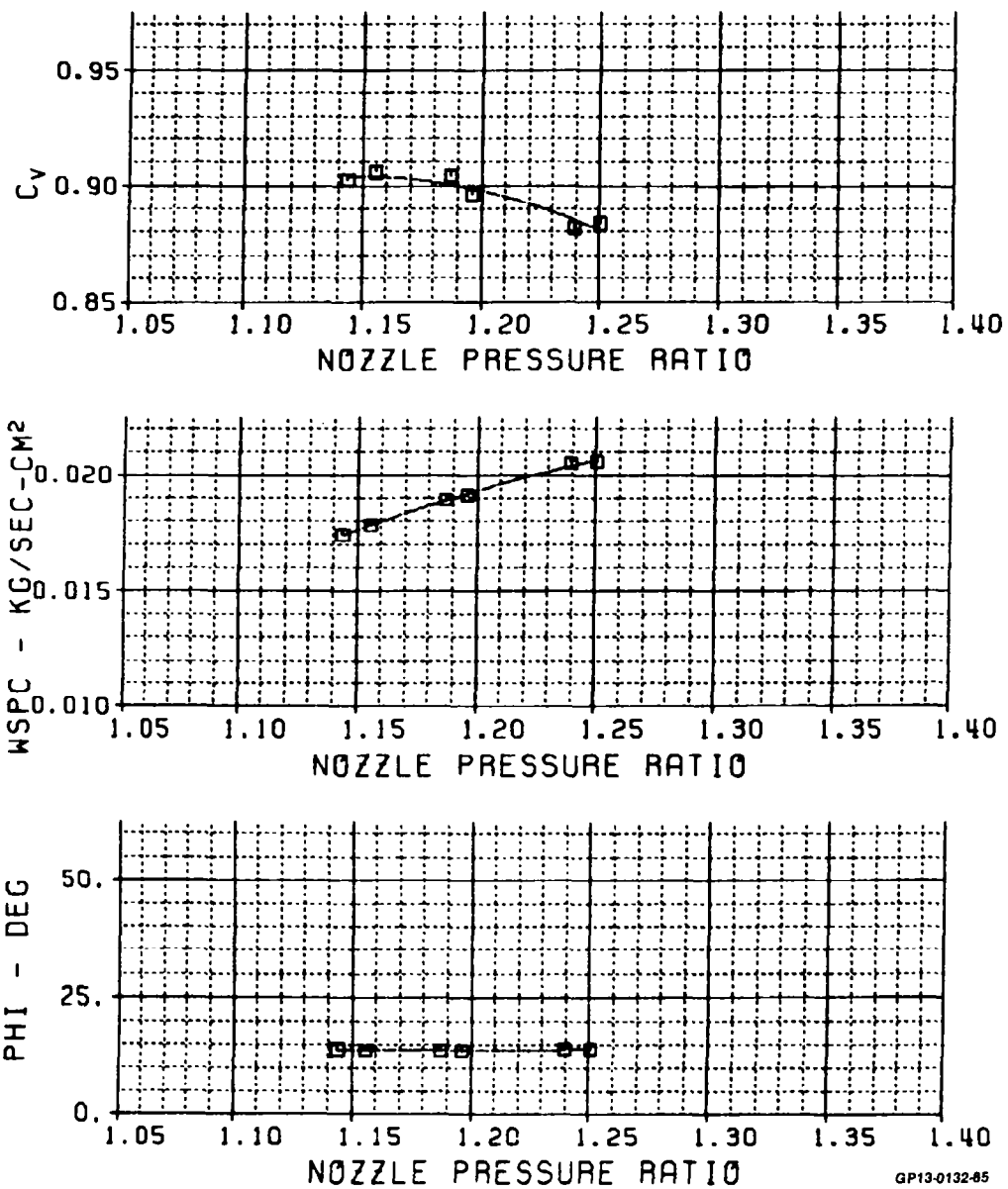


FIGURE 87

CORE NOZZLE RESEARCH MODEL TEST

SYM	TEST	RUN	HODD	R8/R7	DESCRIPTION
○	54	1041	35.500	1.5781	ALT. NO.2 CORE
○	54	2041	35.500	1.5781	ALT. NO.2 CORE

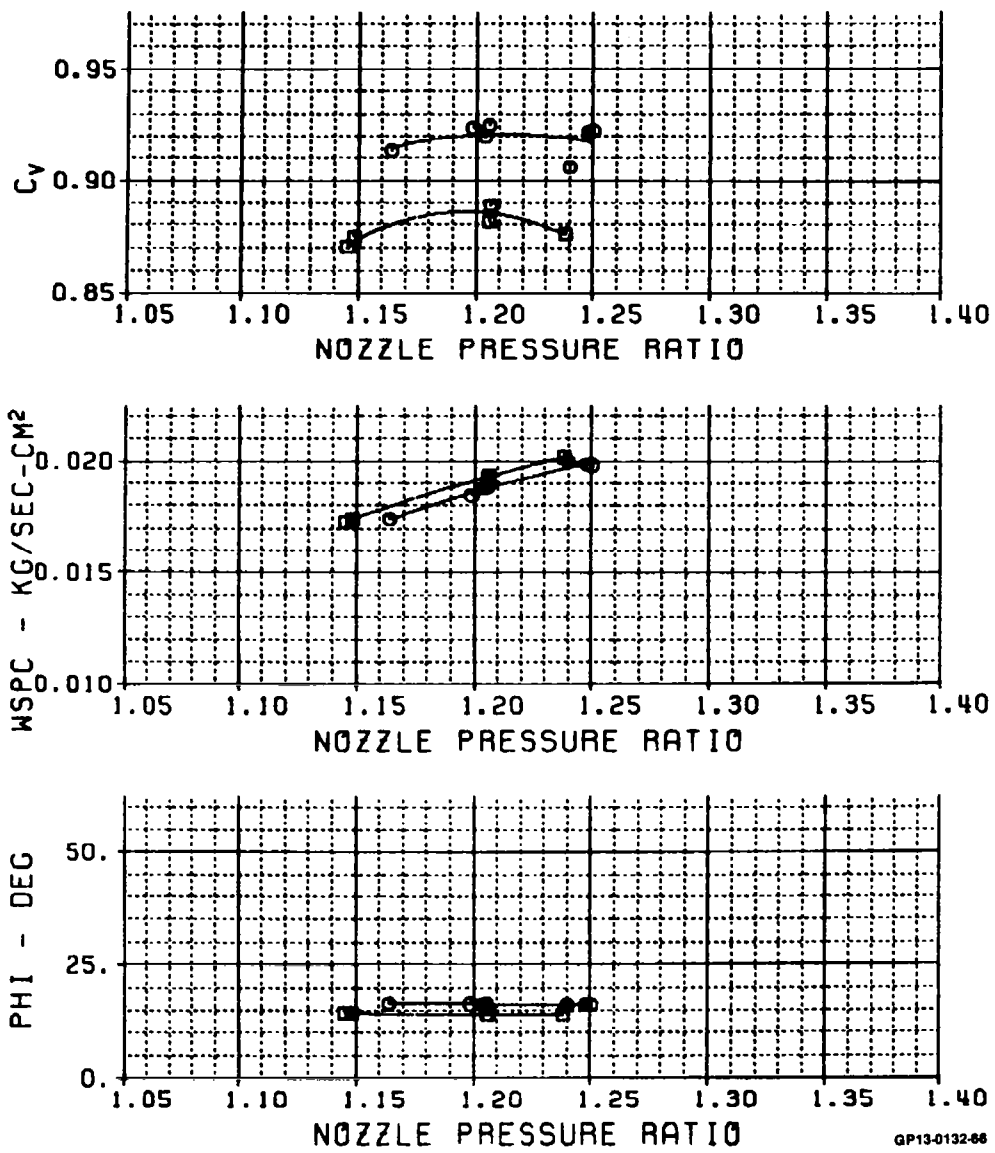


FIGURE 88

CORE NOZZLE RESEARCH MODEL TEST

STM	TEST	RUN	HOOD	AB/R7	DESCRIPTION
<input checked="" type="checkbox"/>	54	1067	35.500	1.5781	ALT. NO.2 CORE
<input type="checkbox"/>	54	2087	35.500	1.5781	ALT. NO.2 CORE

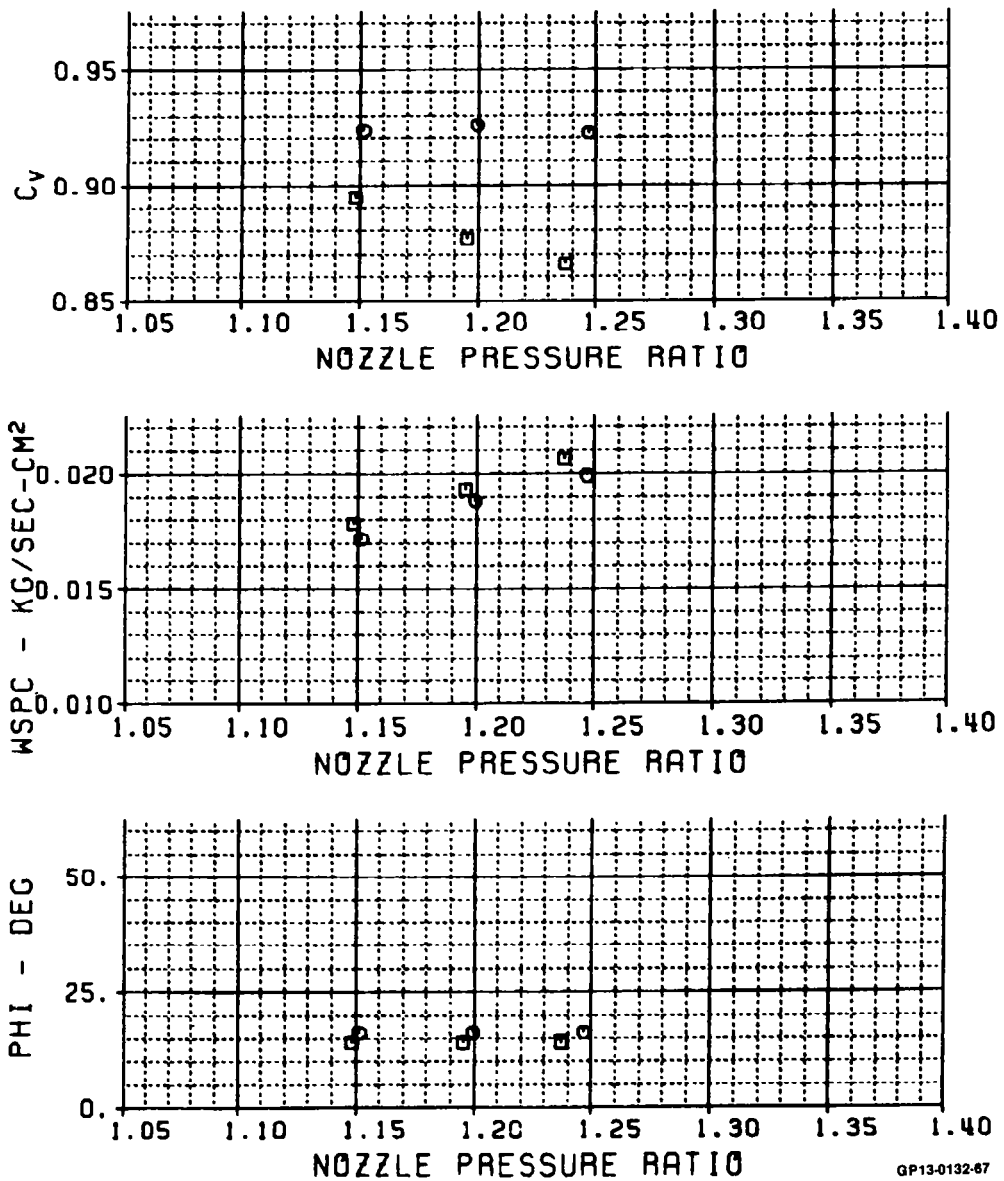


FIGURE 89

CORE NOZZLE RESEARCH MODEL TEST

SYM	TEST	RUN	HODD	A8/A7	DESCRIPTION
□	54	1073	60.000	1.3003	ALT. NO.2 CORE

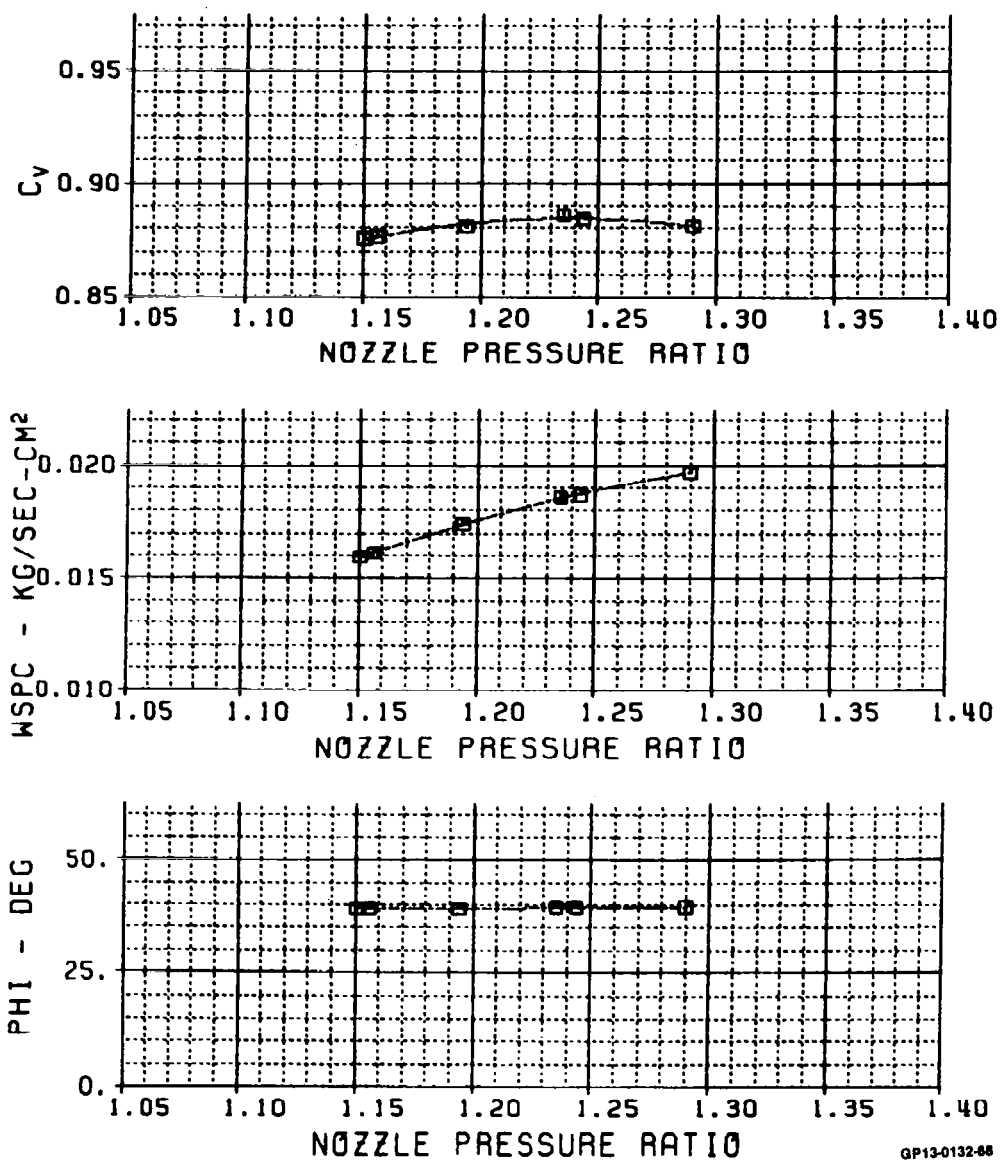


FIGURE 90

CORE NOZZLE RESEARCH MODEL TEST

SYM	TEST	RUN	HOOD	R8/R7	DESCRIPTION
□	54	1060	60.000	1.3861	ALT. NO.2 CORE

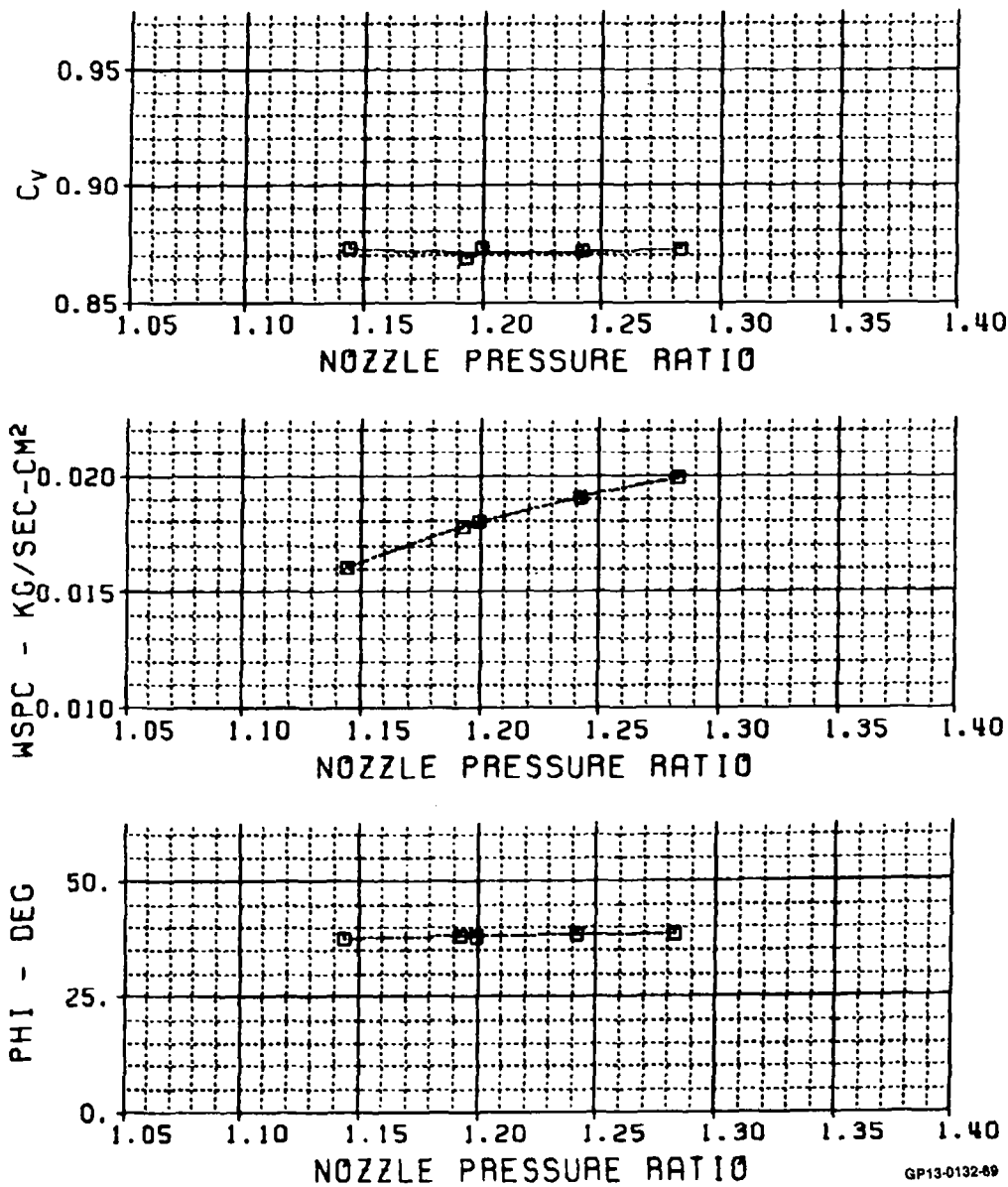


FIGURE 91

CORE NOZZLE RESEARCH MODEL TEST

SYM	TEST	RUN	HOOD	R8/R7	DESCRIPTION
■	54	1061	60.000	1.5781	ALT. NO.2 CORE
○	54	2081	80.000	1.5781	ALT. NO.2 CORE

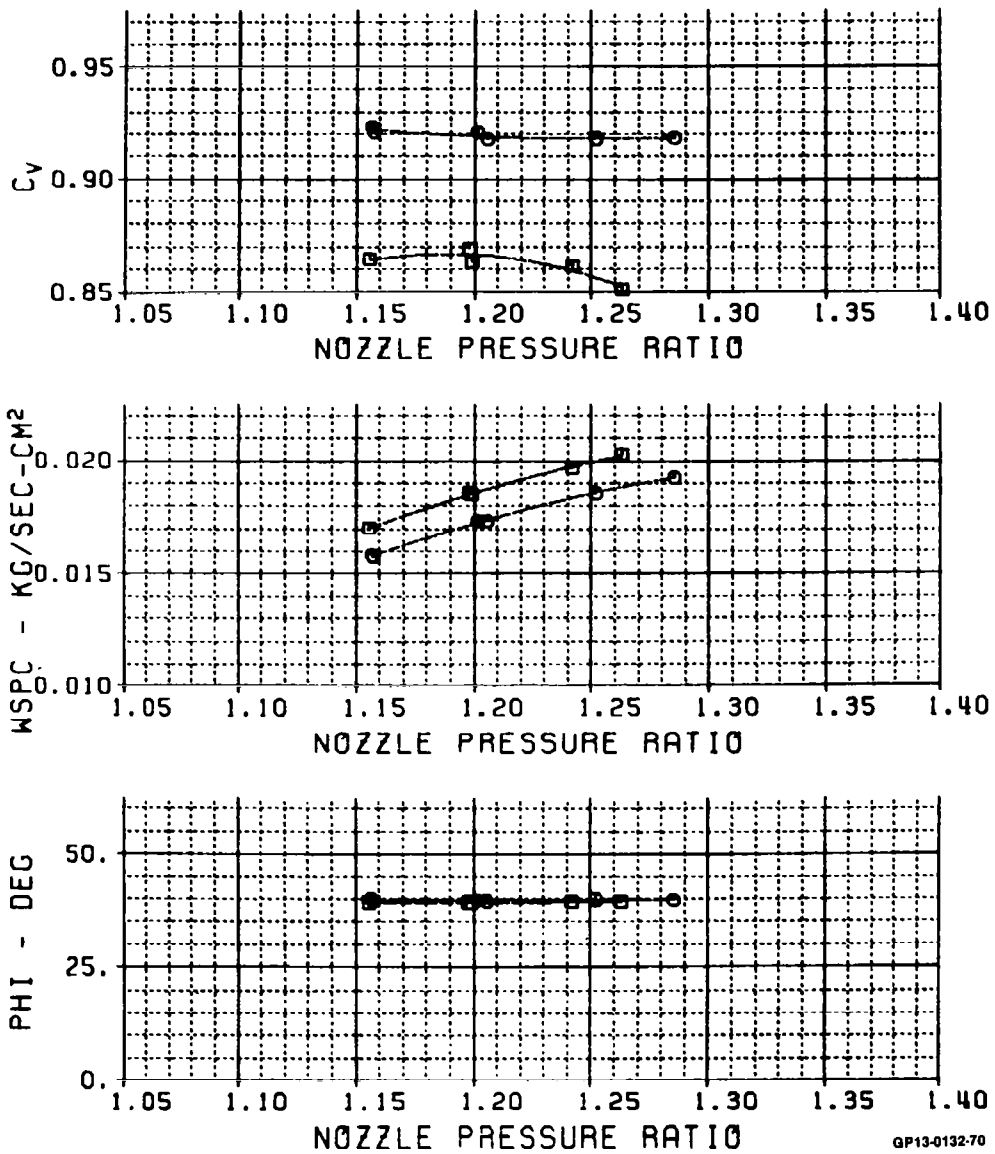


FIGURE 92

CORE NOZZLE RESEARCH MODEL TEST

SYM	TEST	RUN	HODD	AB/A7	DESCRIPTION
□	54	1072	75.000	1.3003	ALT. NO.2 CORE

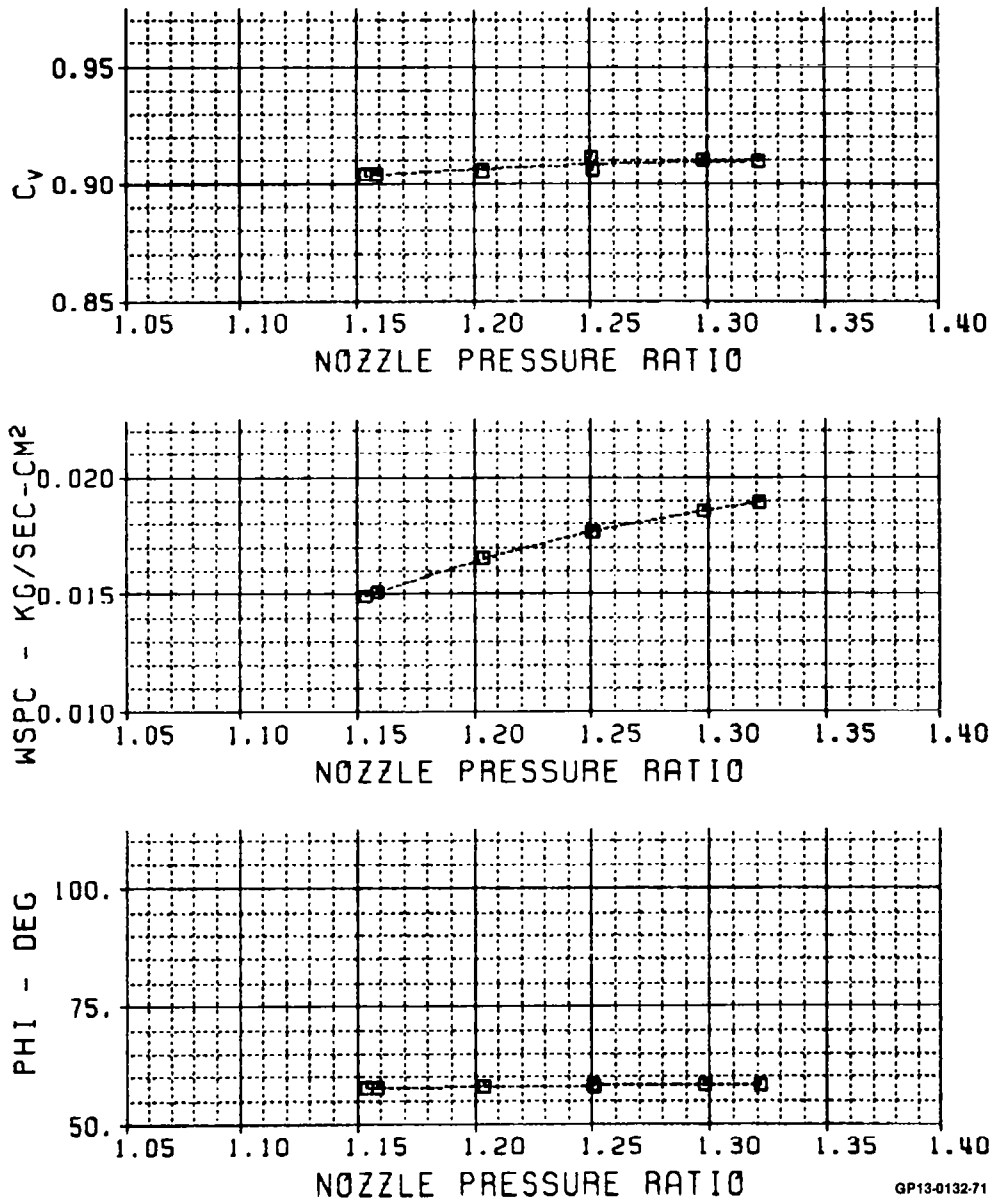


FIGURE 93

CORE NOZZLE RESEARCH MODEL TEST

SYM	TEST	RUN	HODD	A8/A7	DESCRIPTION
■	54	1056	75.000	1.3861	ALT. NO.2 CORE

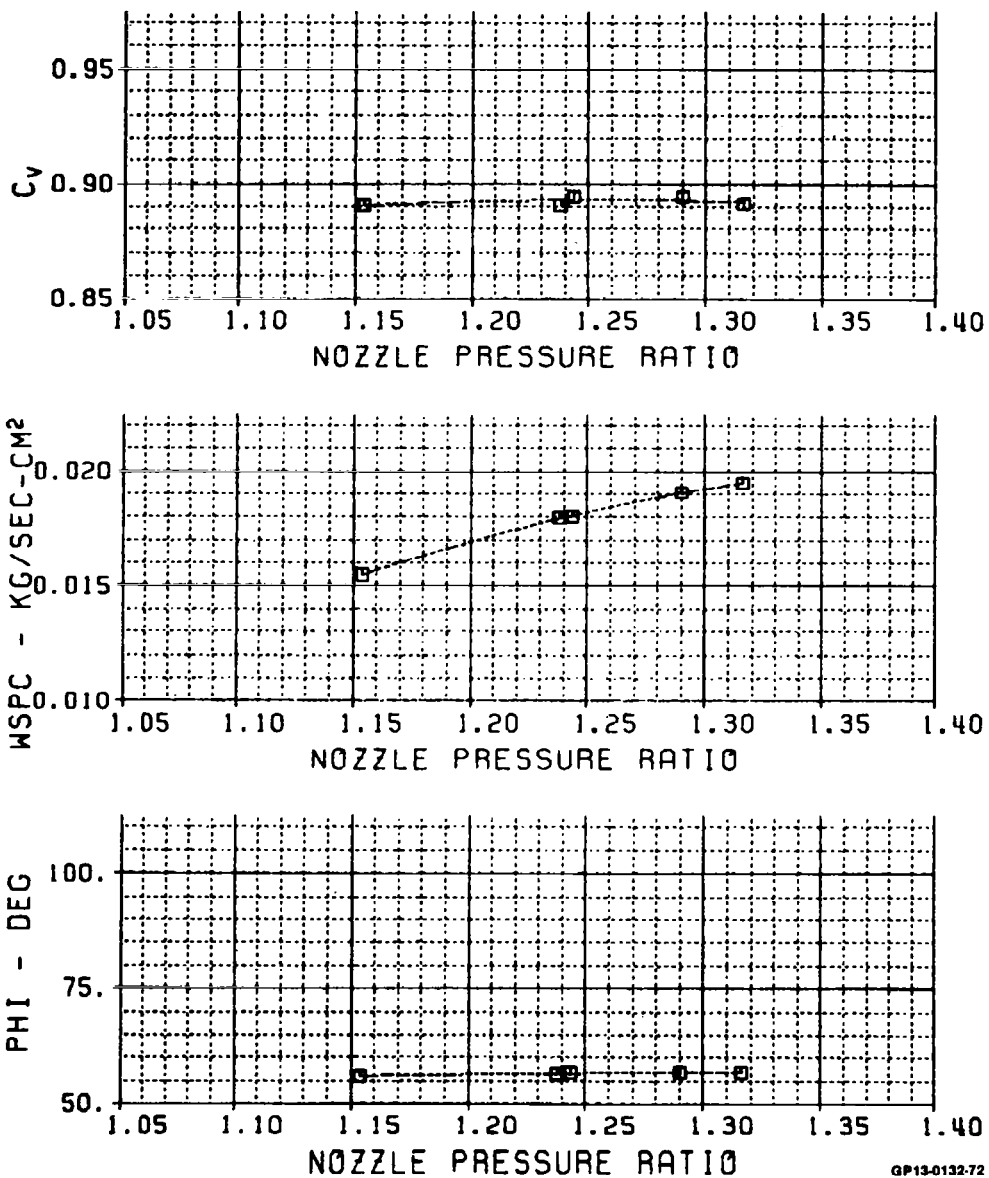


FIGURE 94

CORE NOZZLE RESEARCH MODEL TEST

SYM	TEST	RUN	HODD	A8/A7	DESCRIPTION
CB	54	1040	75.000	1.5781	ALT. NO.2 CORE
O	54	2040	75.000	1.5781	ALT. NO.2 CORE

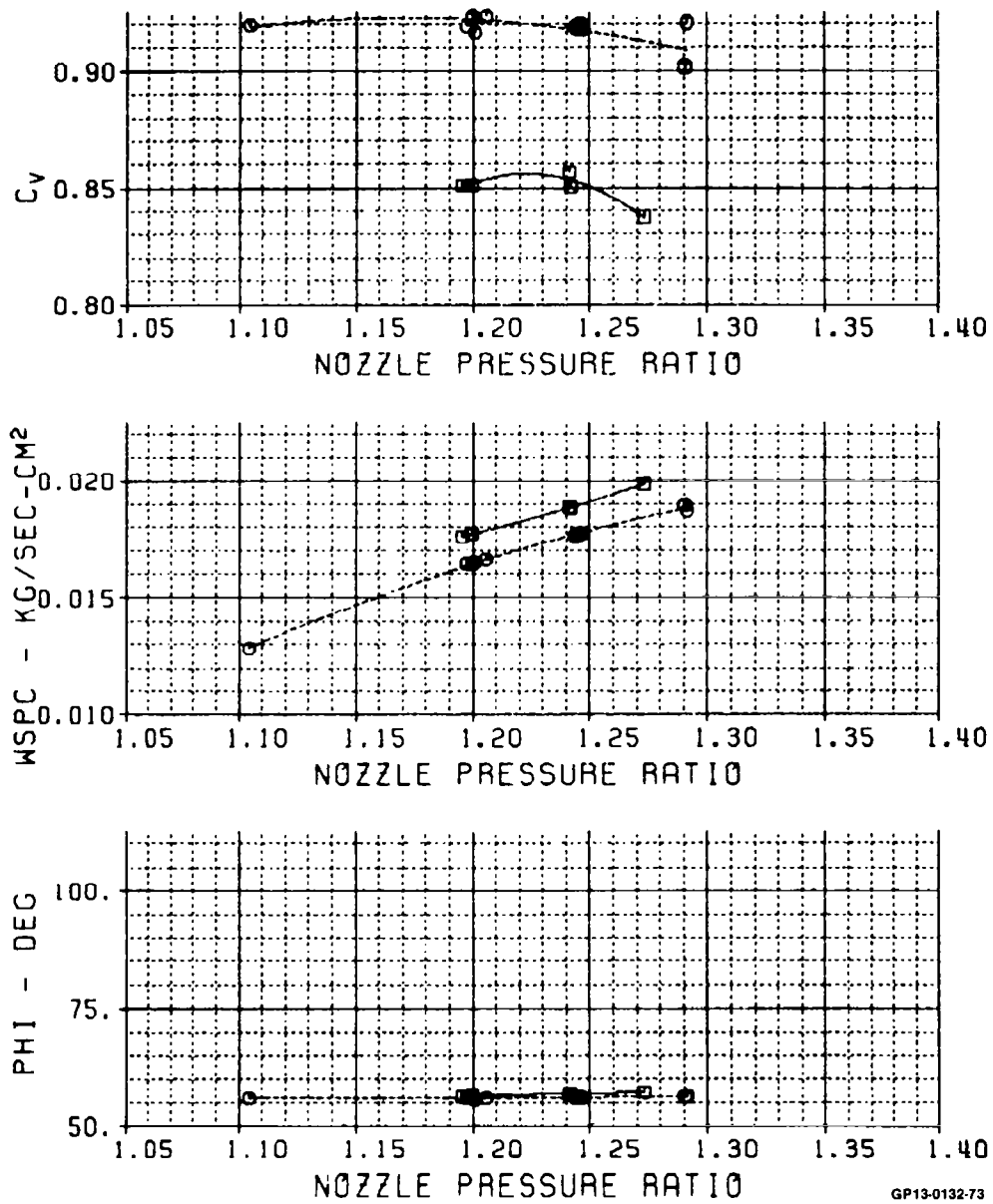


FIGURE 95

CORE NOZZLE RESEARCH MODEL TEST

STM	TEST	RUN	HOOD	R8/R7	DESCRIPTION
54	54	1066	75.000	1.5781	ALT. NO.2 CORE
	54	2086	75.000	1.5781	ALT. NO.2 CORE

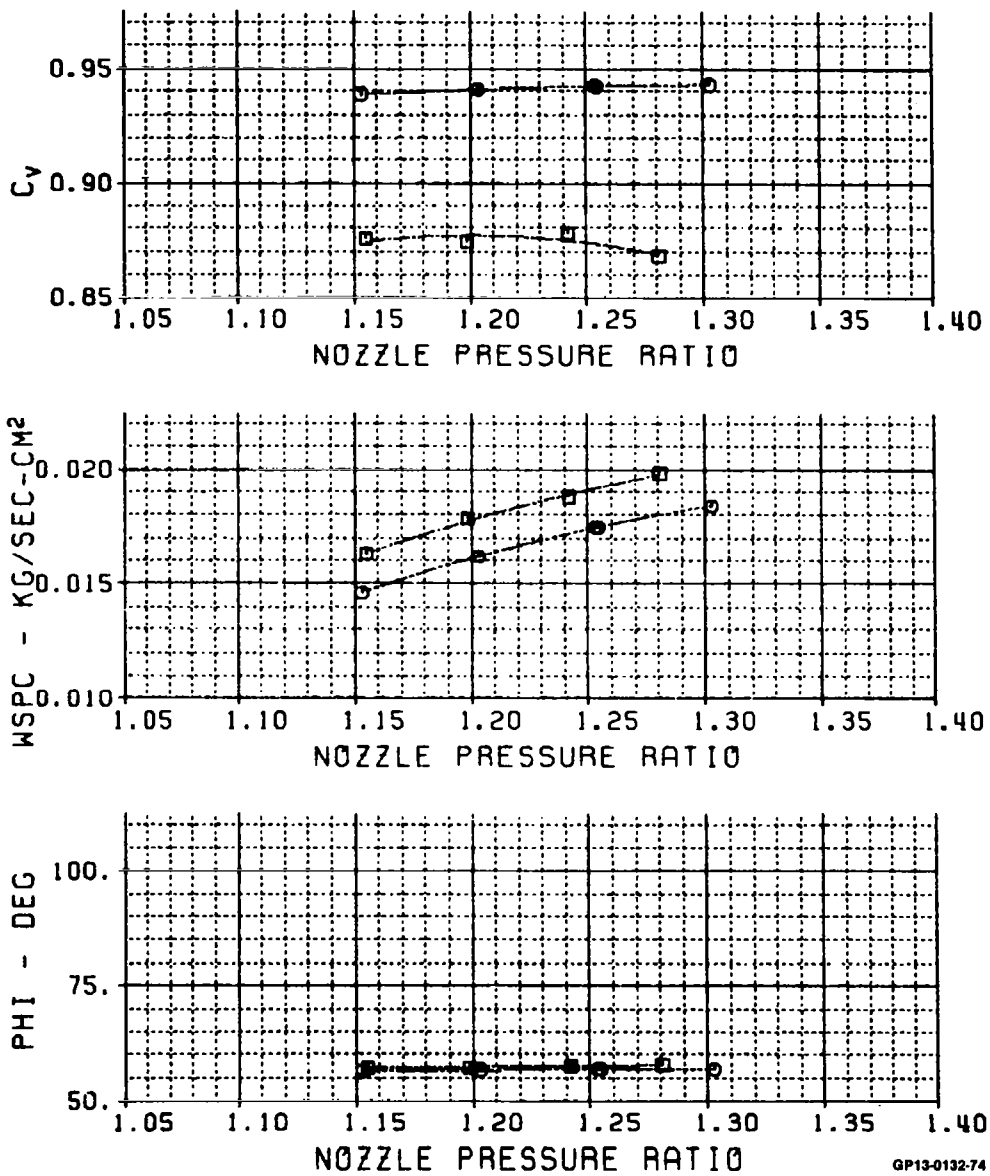


FIGURE 96

CORE NOZZLE RESEARCH MODEL TEST

SYM	TEST	RUN	HODD	R8/A7	DESCRIPTION
□	S4	1071	90.000	1.3003	ALT. NO.2 CORE

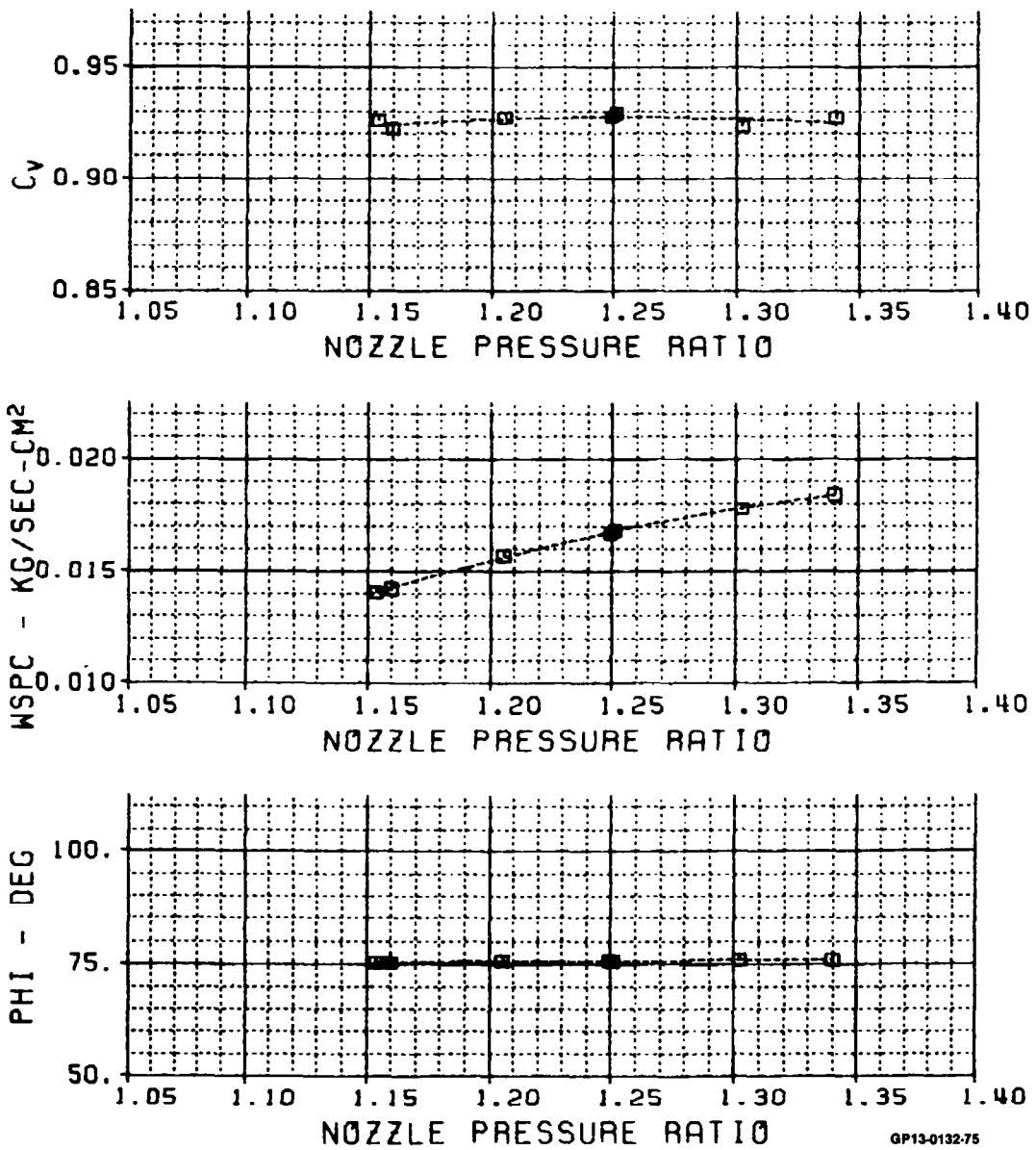


FIGURE 97

CORE NOZZLE RESEARCH MODEL TEST

STM	TEST	RUN	HOOD	AB/AT	DESCRIPTION
□	54	1057	90.000	1.3861	ALT. NO.2 CORE

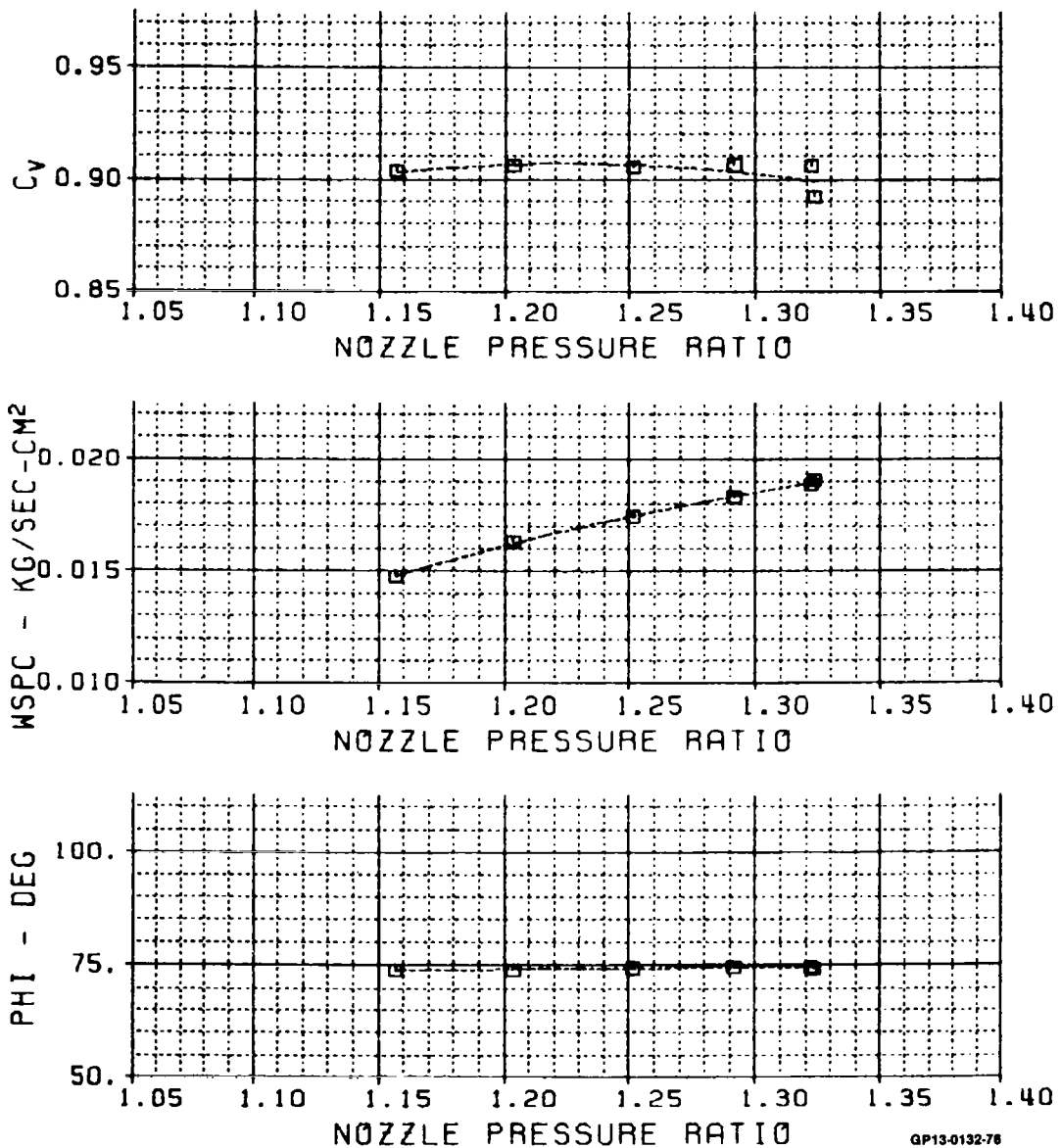


FIGURE 98

CORE NOZZLE RESEARCH MODEL TEST

SYM	TEST	RUN	HODD	R8/A7	DESCRIPTION
■	54	1065	90.000	1.5781	ALT. NO.2 CORE
○	54	2065	90.000	1.5781	ALT. NO.2 CORE

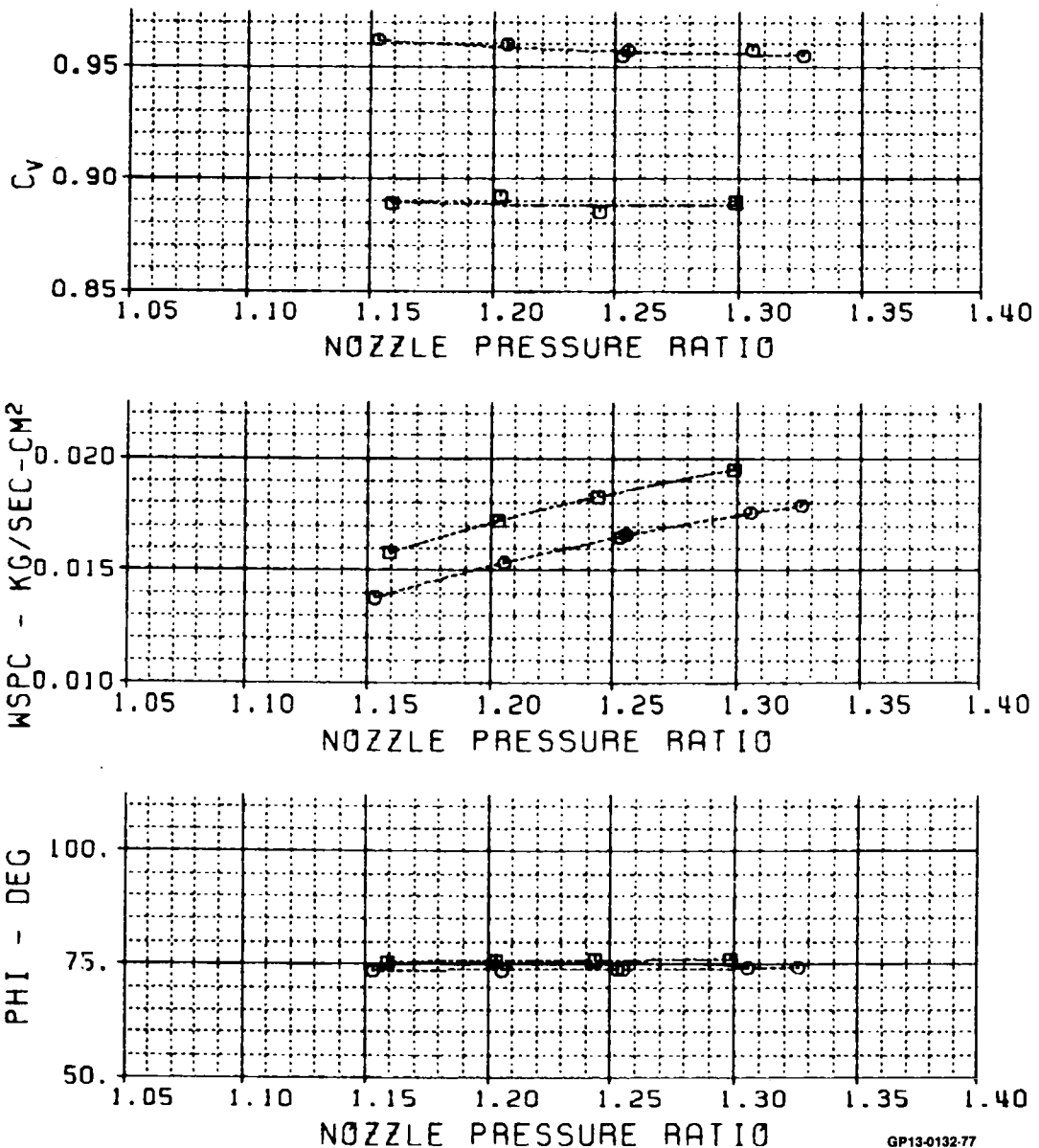


FIGURE 99

CORE NOZZLE RESEARCH MODEL TEST

STM	TEST	RUN	HOOD	AB/A7	DESCRIPTION
■	54	1070	100.00	1.3003	ALT. NO.2 CORE

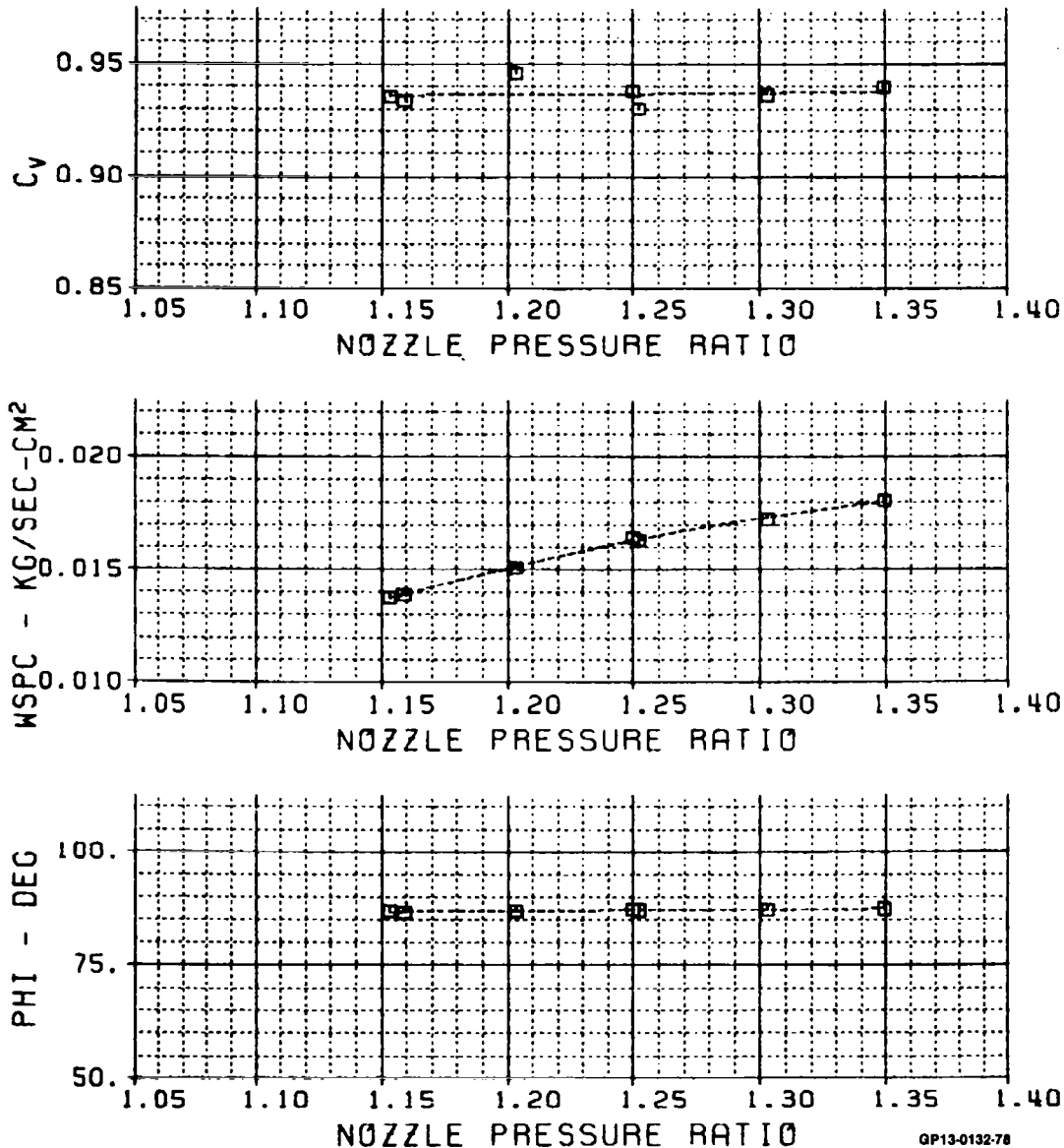


FIGURE 100

CORE NOZZLE RESEARCH MODEL TEST

SYM	TEST	RUN	HOOD	AB/A7	DESCRIPTION
□	54	1058	100.00	1.3861	ALT. NO.2 CORE

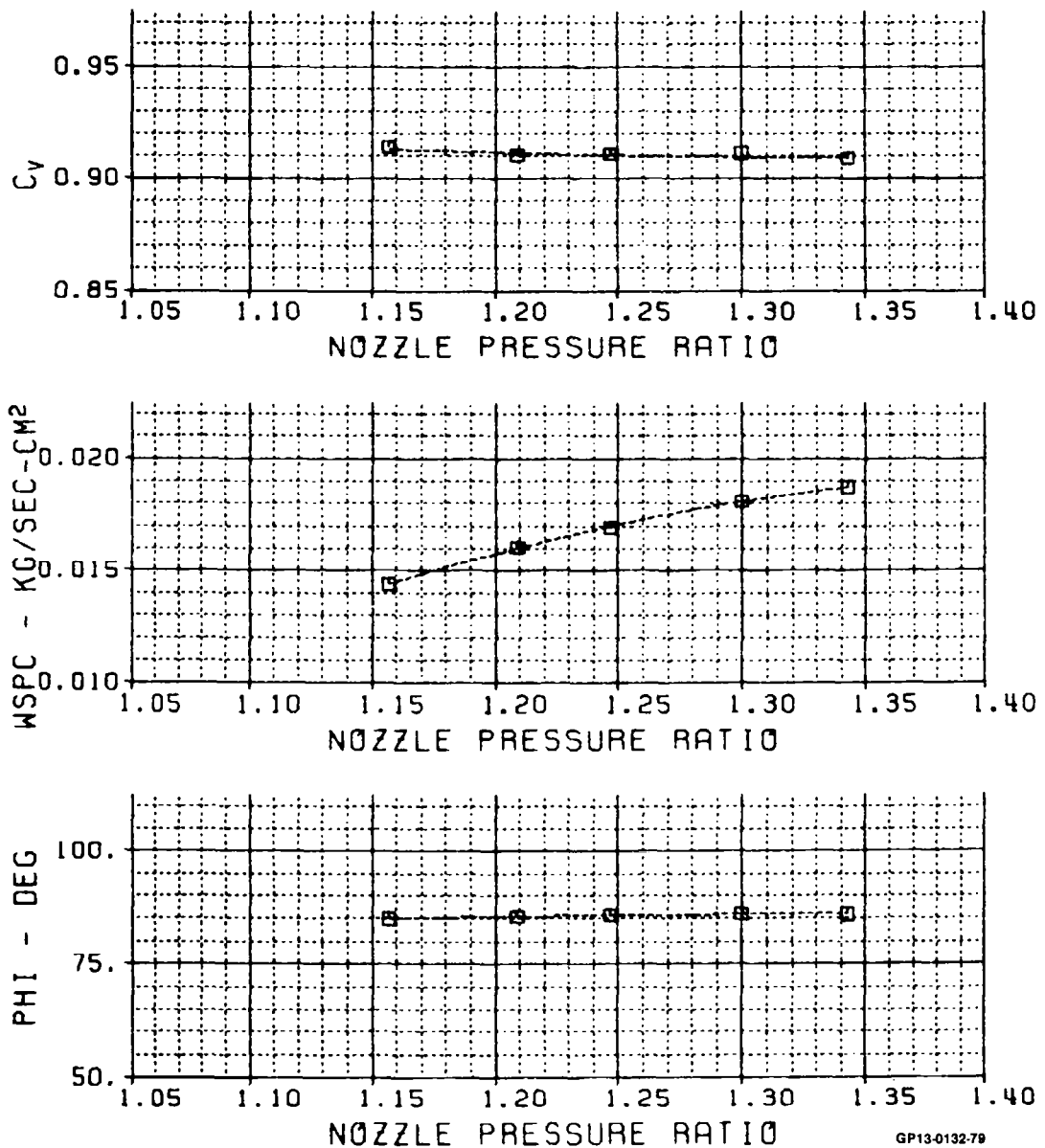


FIGURE 101

CORE NOZZLE RESEARCH MODEL TEST

SYM	TEST	RUN	HODD	AB/A7	DESCRIPTION
□	54	1064	100.00	1.5781	ALT. NO.2 CORE
○	54	2064	100.00	1.5781	ALT. NO.2 CORE

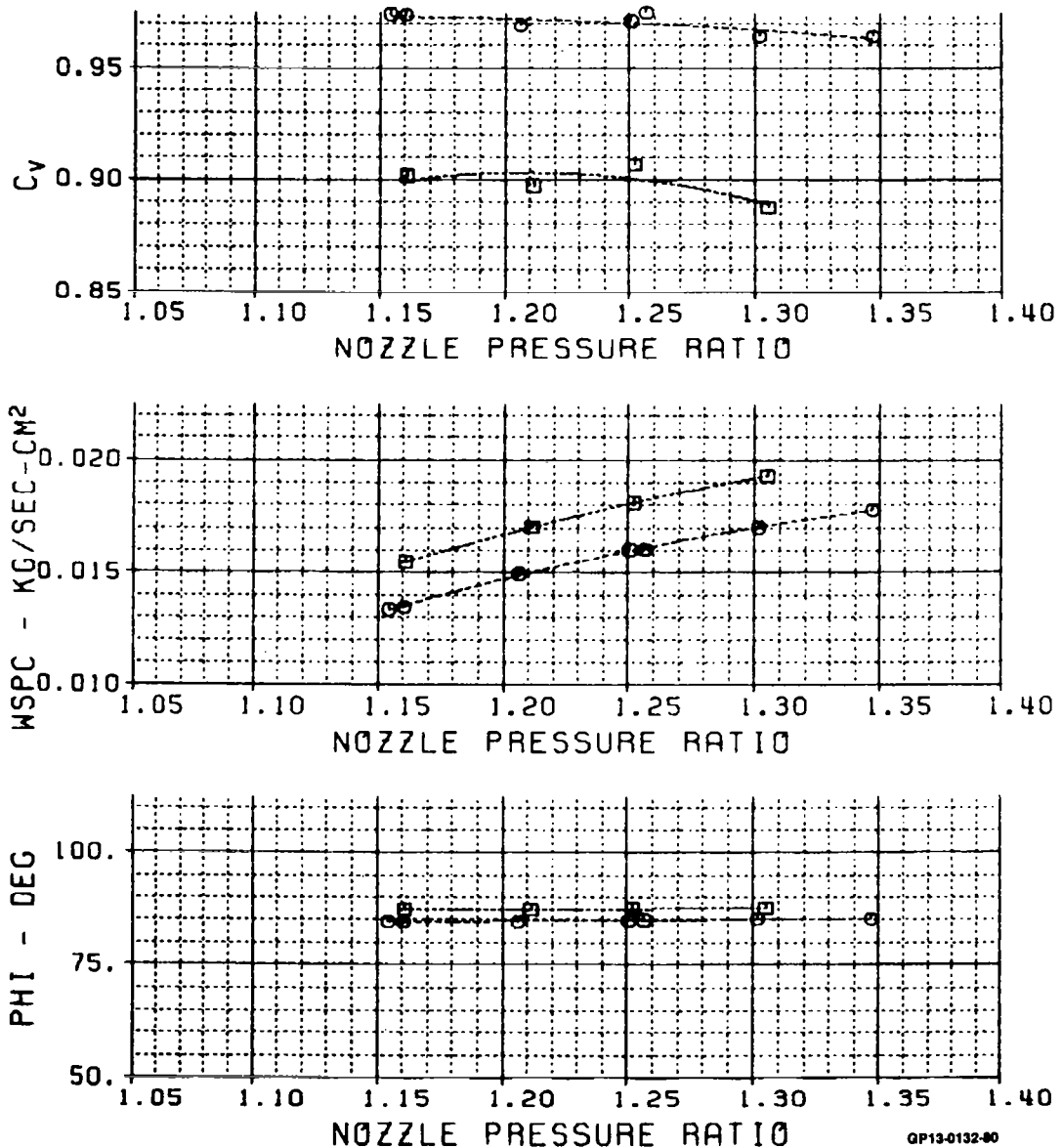


FIGURE 102

CORE NOZZLE RESEARCH MODEL TEST

SYM	TEST	RUN	HOOD	R8/R7	DESCRIPTION
□	54	1068	110.00	1.3003	ALT. NO.2 CORE

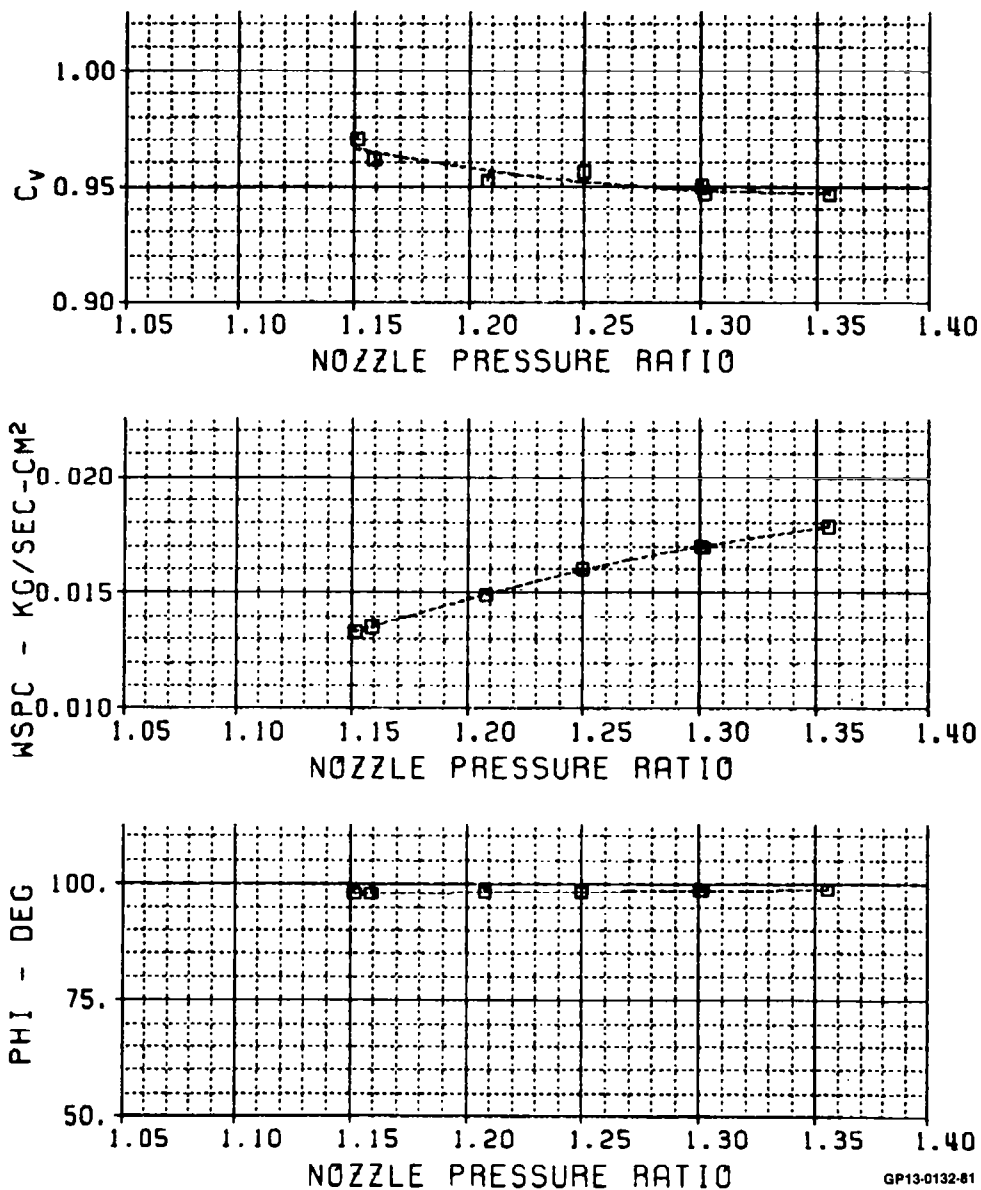


FIGURE 103

CORE NOZZLE RESEARCH MODEL TEST

SYM	TEST	RUN	HOOD	AB/A7	DESCRIPTION
□	54	1054	110.00	1.3861	ALT. NO.2 CORE

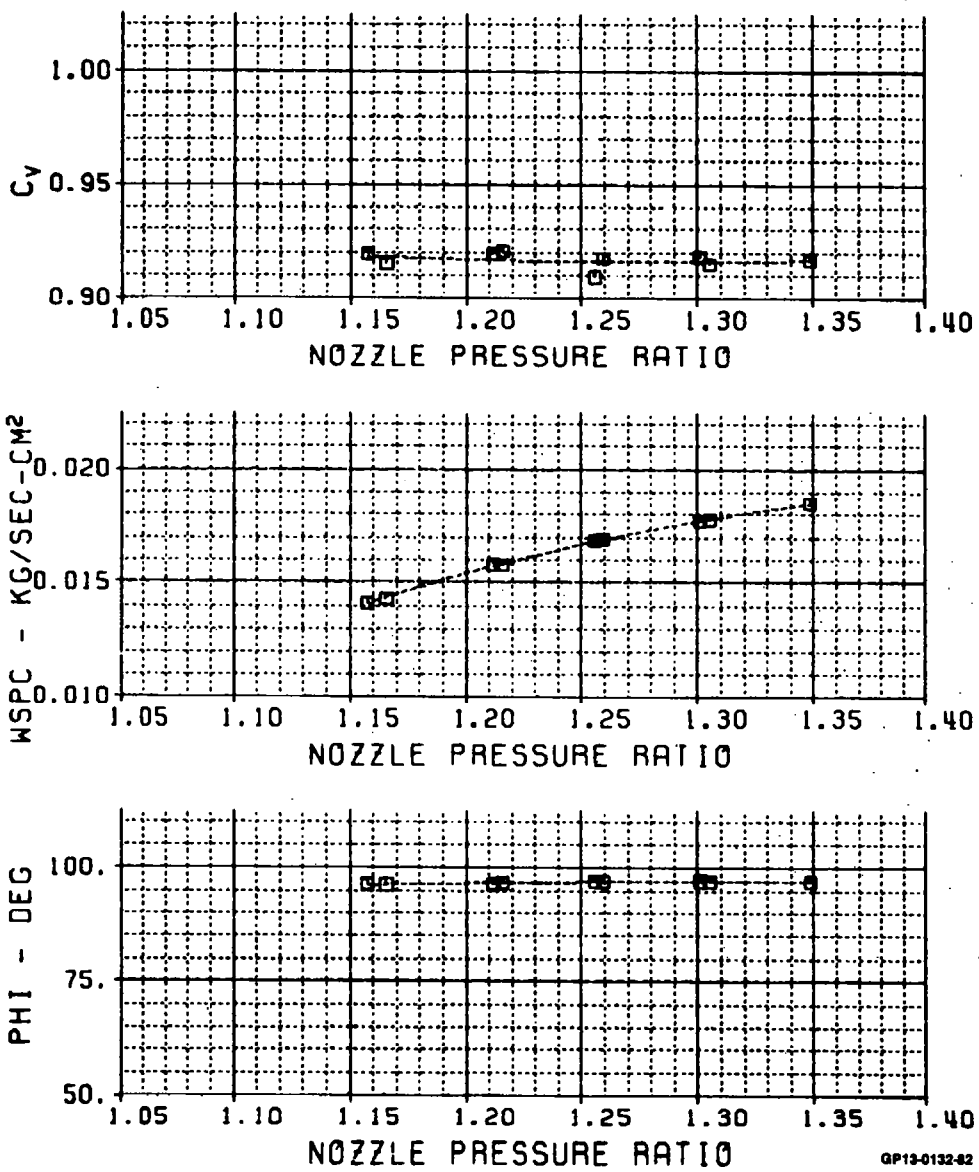


FIGURE 104

CORE NOZZLE RESEARCH MODEL TEST

SYM	TEST	RUN	HOOD	R8/A7	DESCRIPTION
□	54	1038	110.00	1.5781	ALT. NO.2 CORE
○	54	1053	110.00	1.5781	ALT. NO.2 CORE
▲	54	2038	110.00	1.5781	ALT. NO.2 CORE
◆	54	2053	110.00	1.5781	ALT. NO.2 CORE

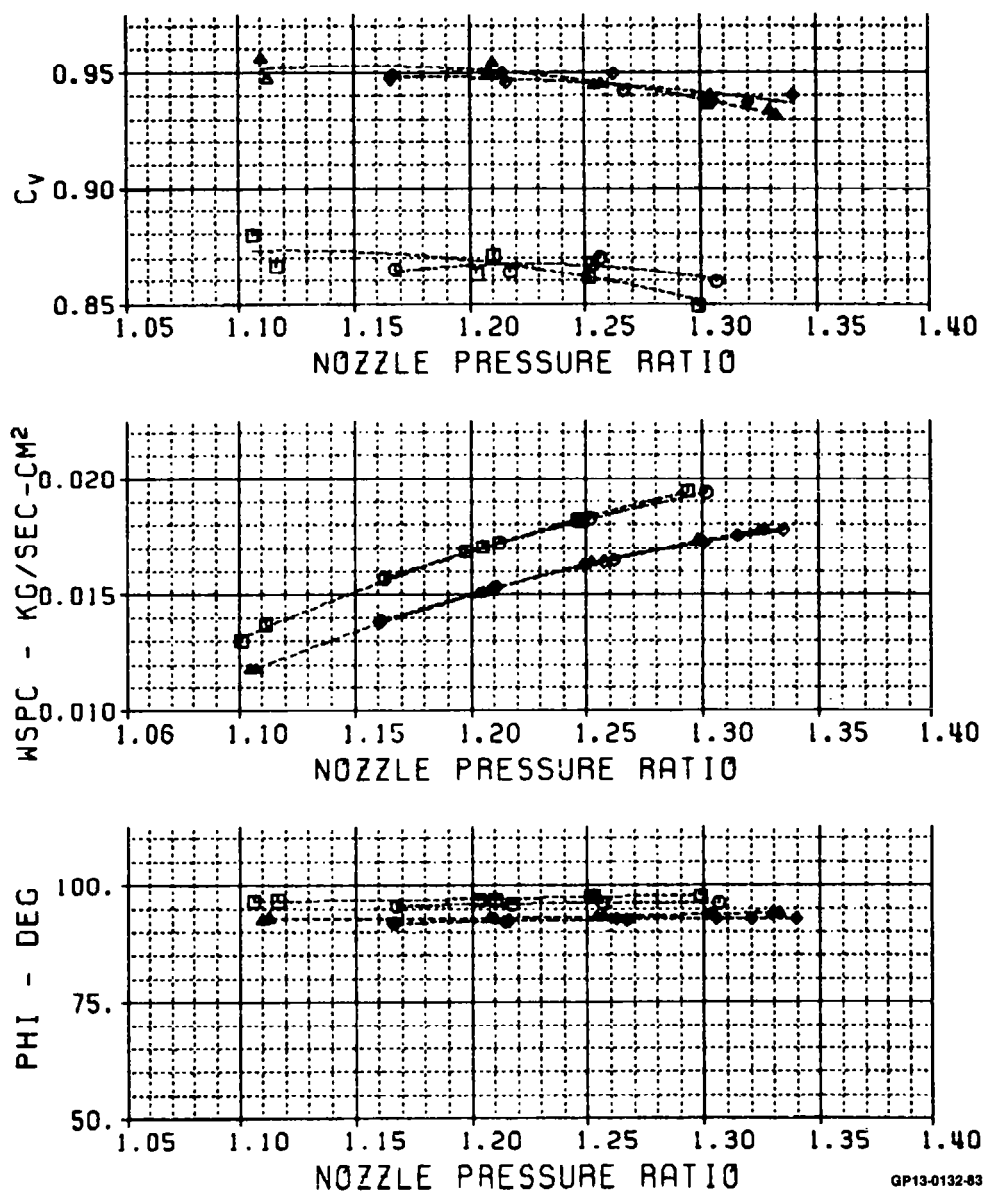


FIGURE 105

GP13-0132-83

CORE NOZZLE RESEARCH MODEL TEST

STM	TEST	RUN	HOOD	AB/R7	DESCRIPTION
□	54	1062	110.00	1.5781	ALT. NO.2 CORE
○	54	2082	110.00	1.5781	ALT. NO.2 CORE

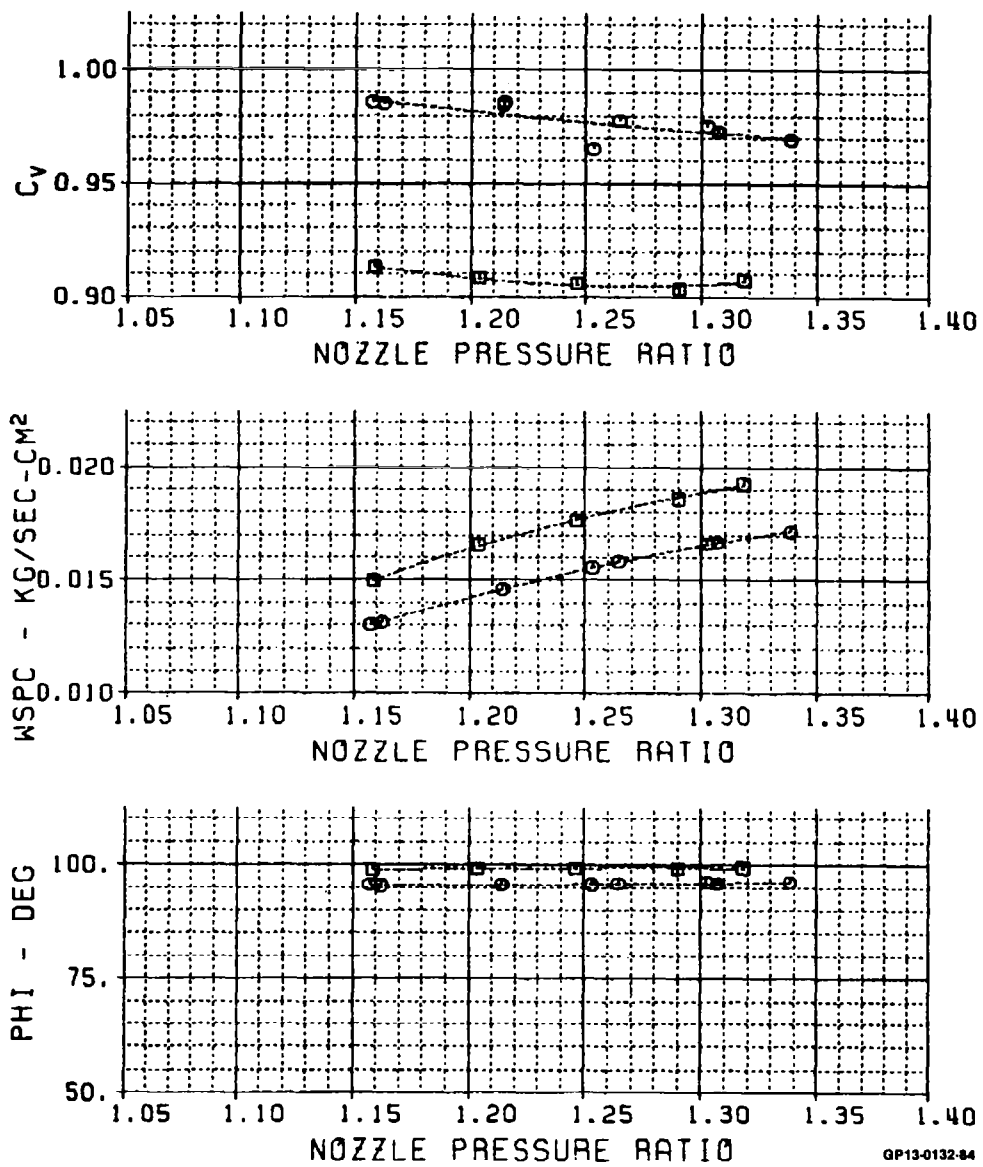


FIGURE 106

CORE NOZZLE RESEARCH MODEL TEST

SYM	TEST	RUN	HODD	AB/A7	DESCRIPTION
□	54	2087	110.00	1.6536	ALT. NO.2 CORE

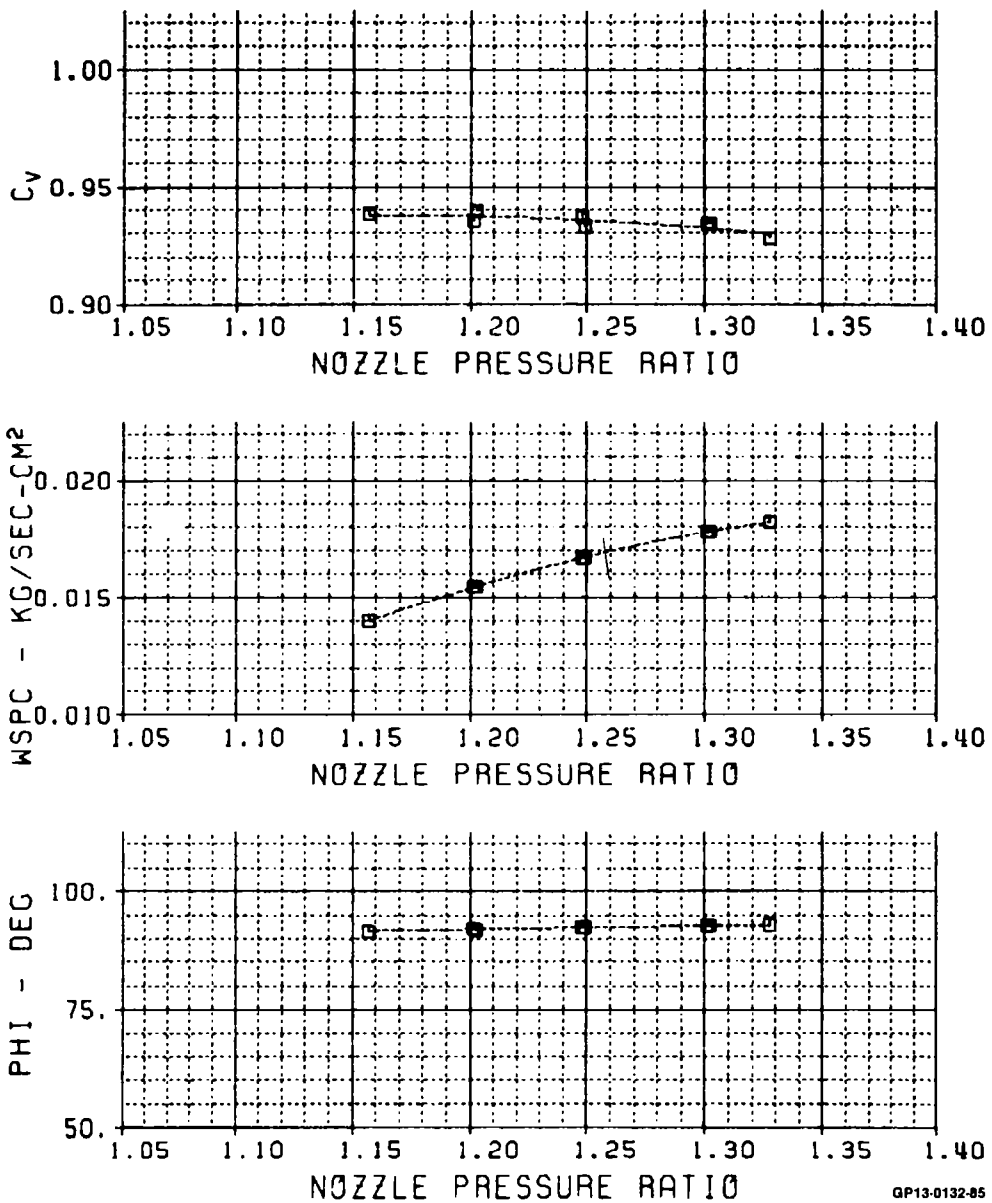


FIGURE 107

CORE NOZZLE RESEARCH MODEL TEST

SYM	TEST	RUN	HOOD	PB/P7	DESCRIPTION
□	54	2086	110.00	1.7063	ALT. NO.2 CORE

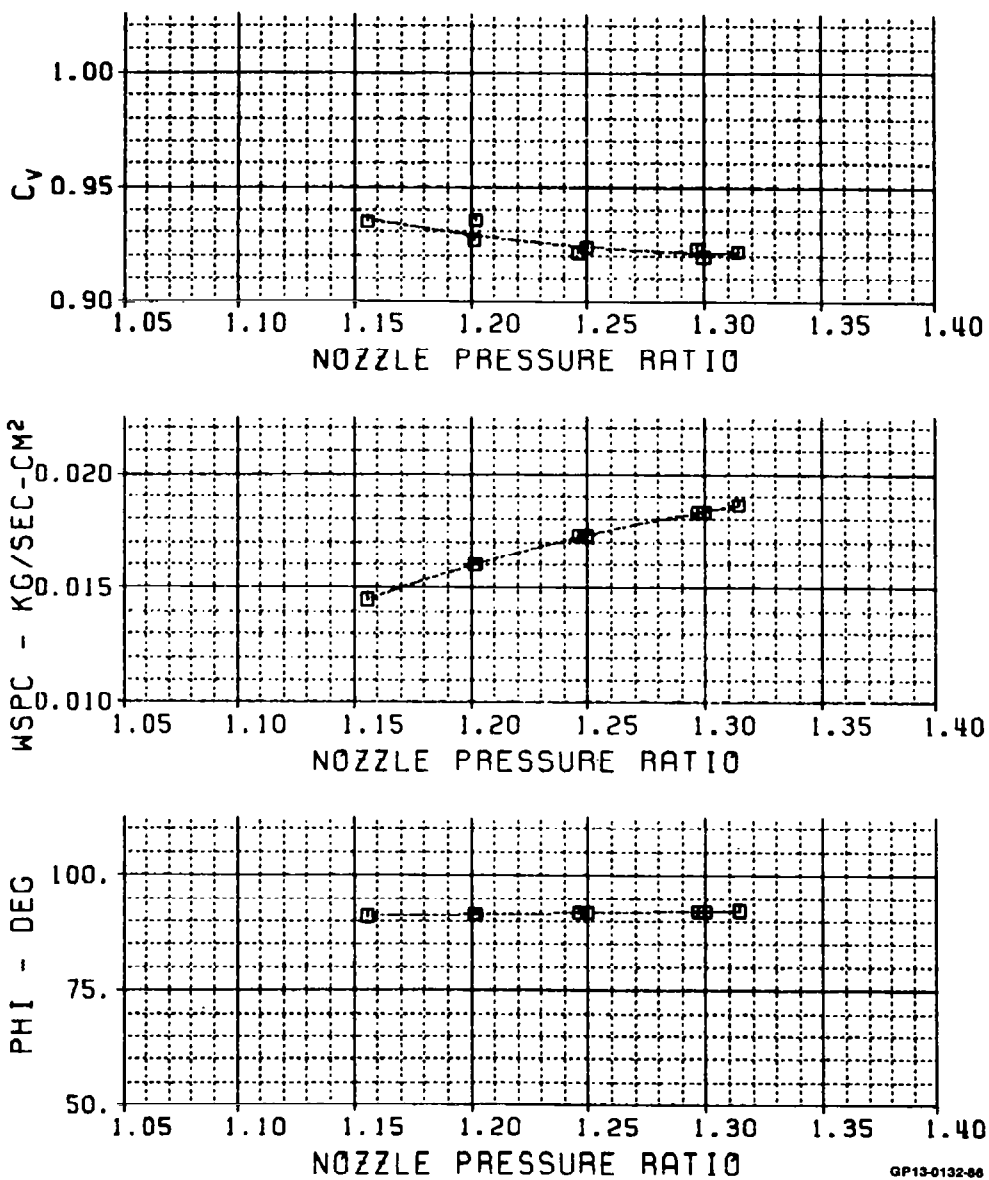


FIGURE 108

GP13-0132-86

CORE NOZZLE RESEARCH MODEL TEST

SYM	TEST	RUN	HOOD	A8/A7	DESCRIPTION
□	54	1069	120.00	1.3003	ALT. NO.2 CORE

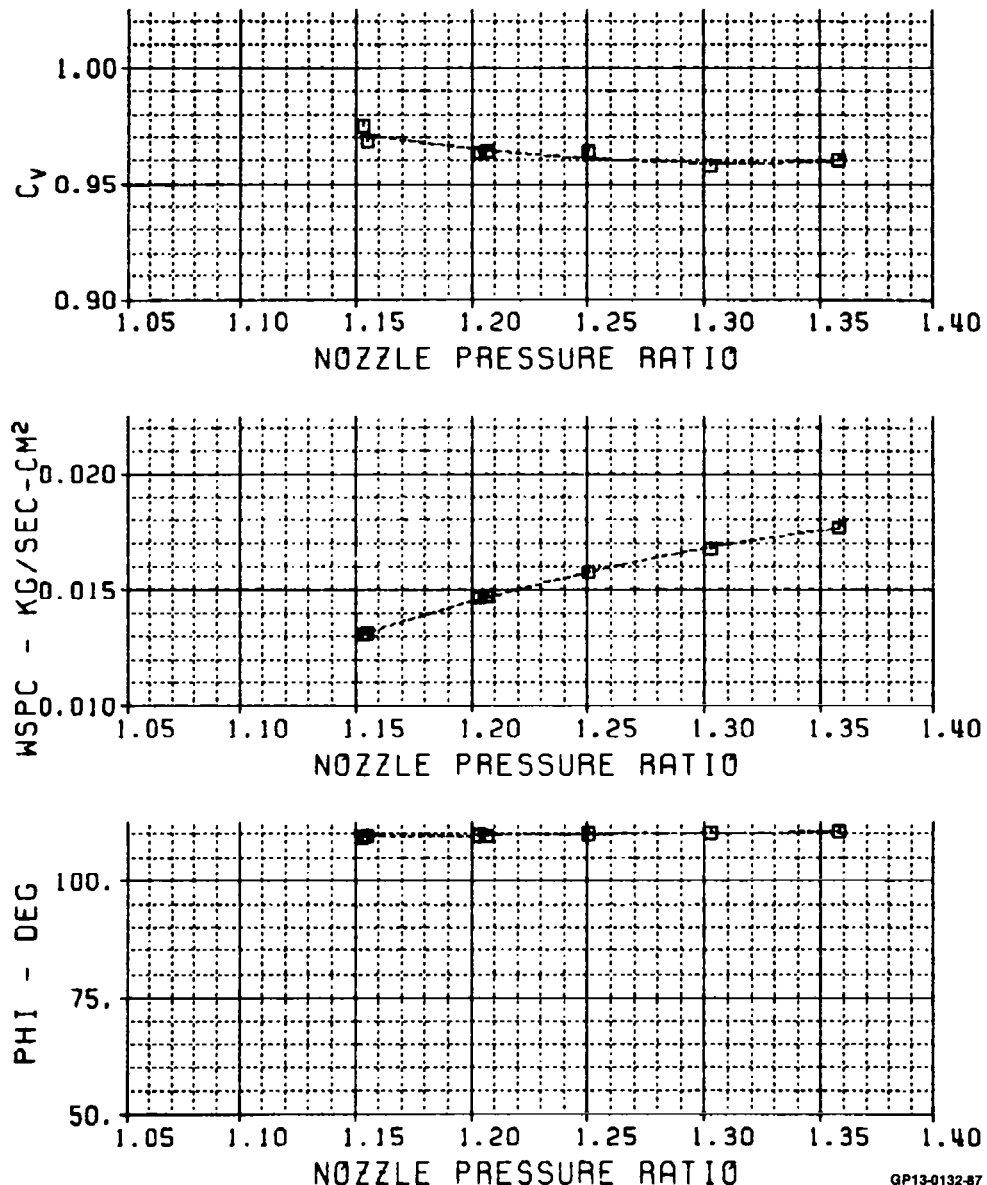


FIGURE 109

CORE NOZZLE RESEARCH MODEL TEST

SYM	TEST	RUN	HOOD	AB/AB7	DESCRIPTION
□	54	1055	120.00	1.3861	ALT. NO.2 CORE

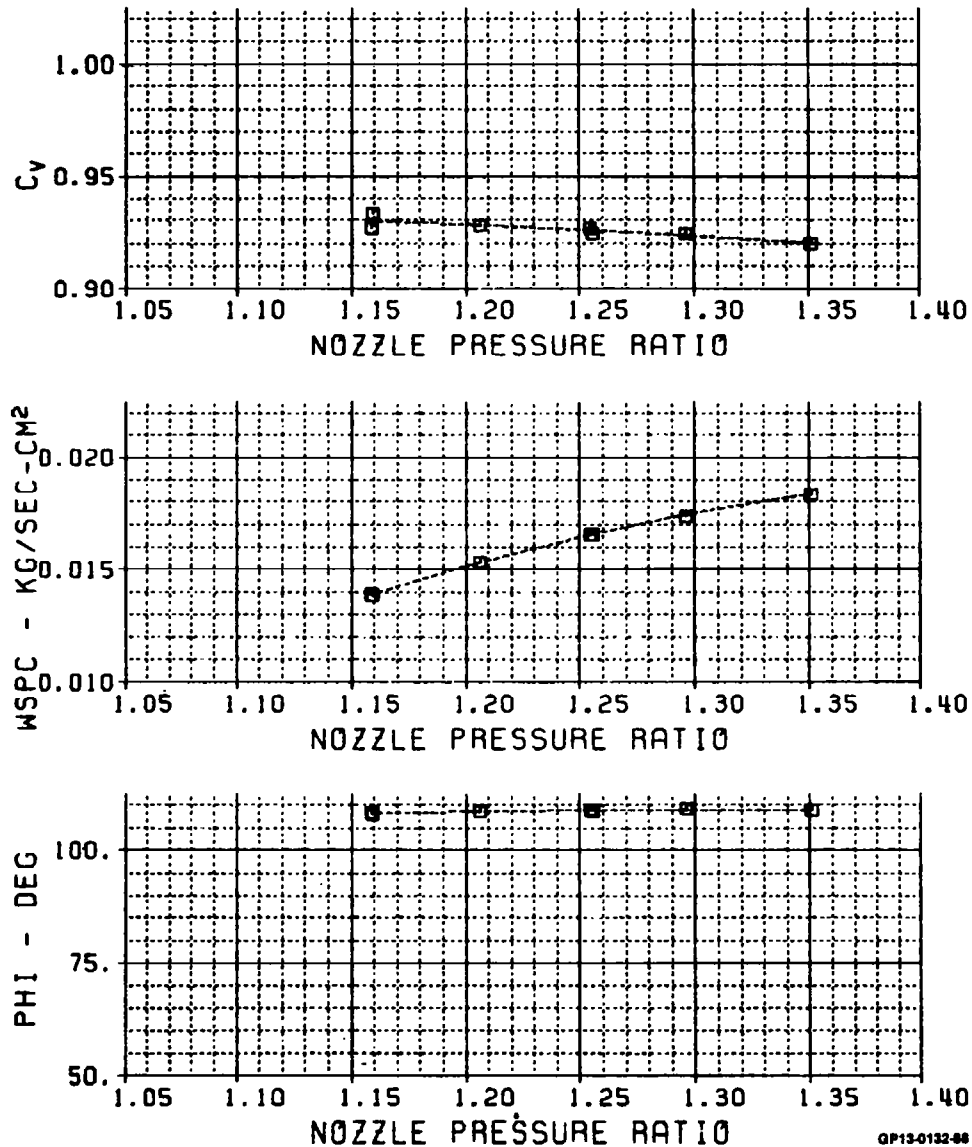


FIGURE 110

CORE NOZZLE RESEARCH MODEL TEST

SYM	TEST	RUN	HODD	A8/A7	DESCRIPTION
□	54	1039	120.00	1.5781	ALT. NO.2 CORE
○	54	2039	120.00	1.5781	ALT. NO.2 CORE

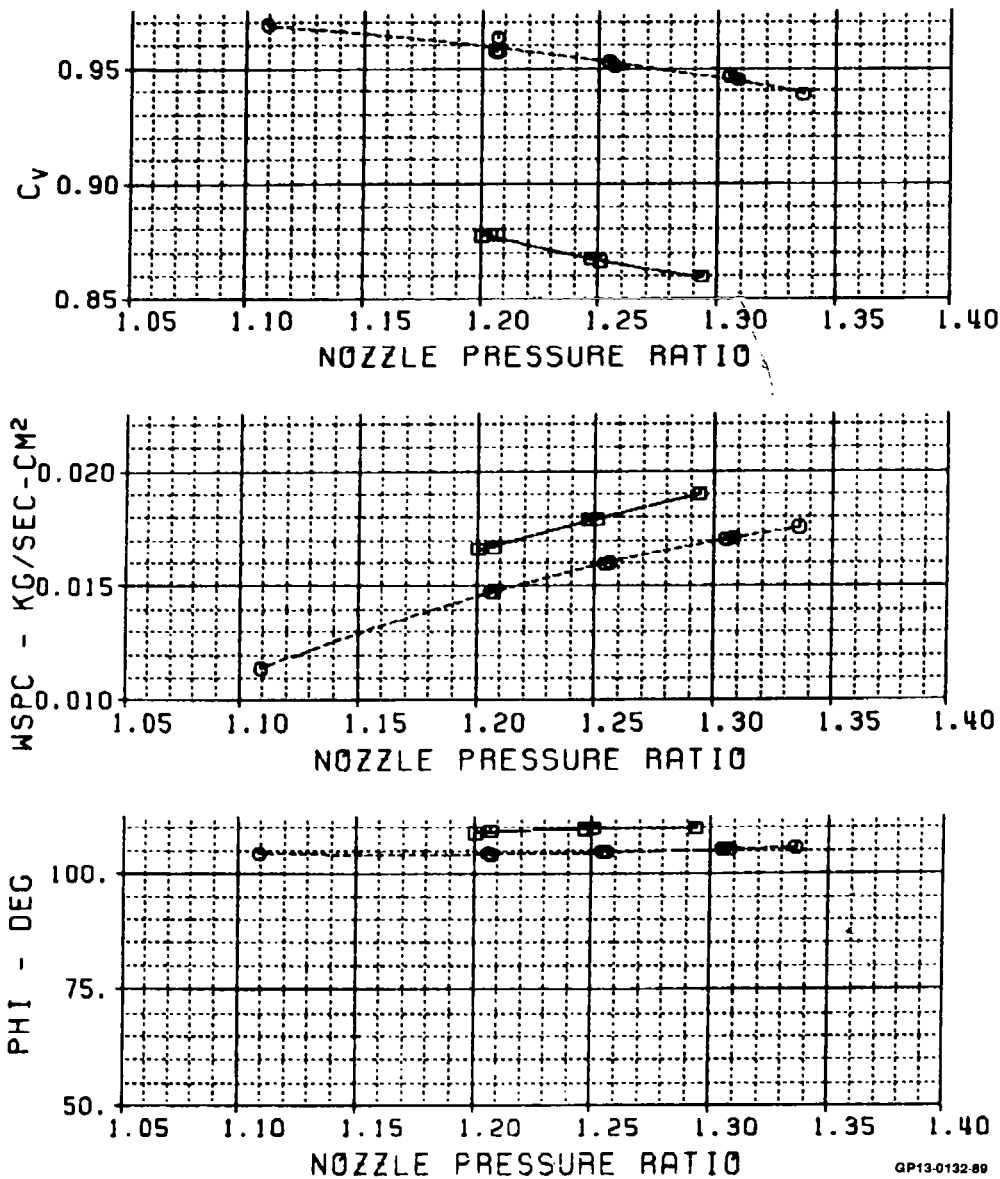


FIGURE 111

CORE NOZZLE RESEARCH MODEL TEST

SYM	TEST	RUN	HOOD	A8/A7	DESCRIPTION
□	54	1063	120.00	1.5781	ALT. NO.2 CORE
○	54	2063	120.00	1.5781	ALT. NO.2 CORE

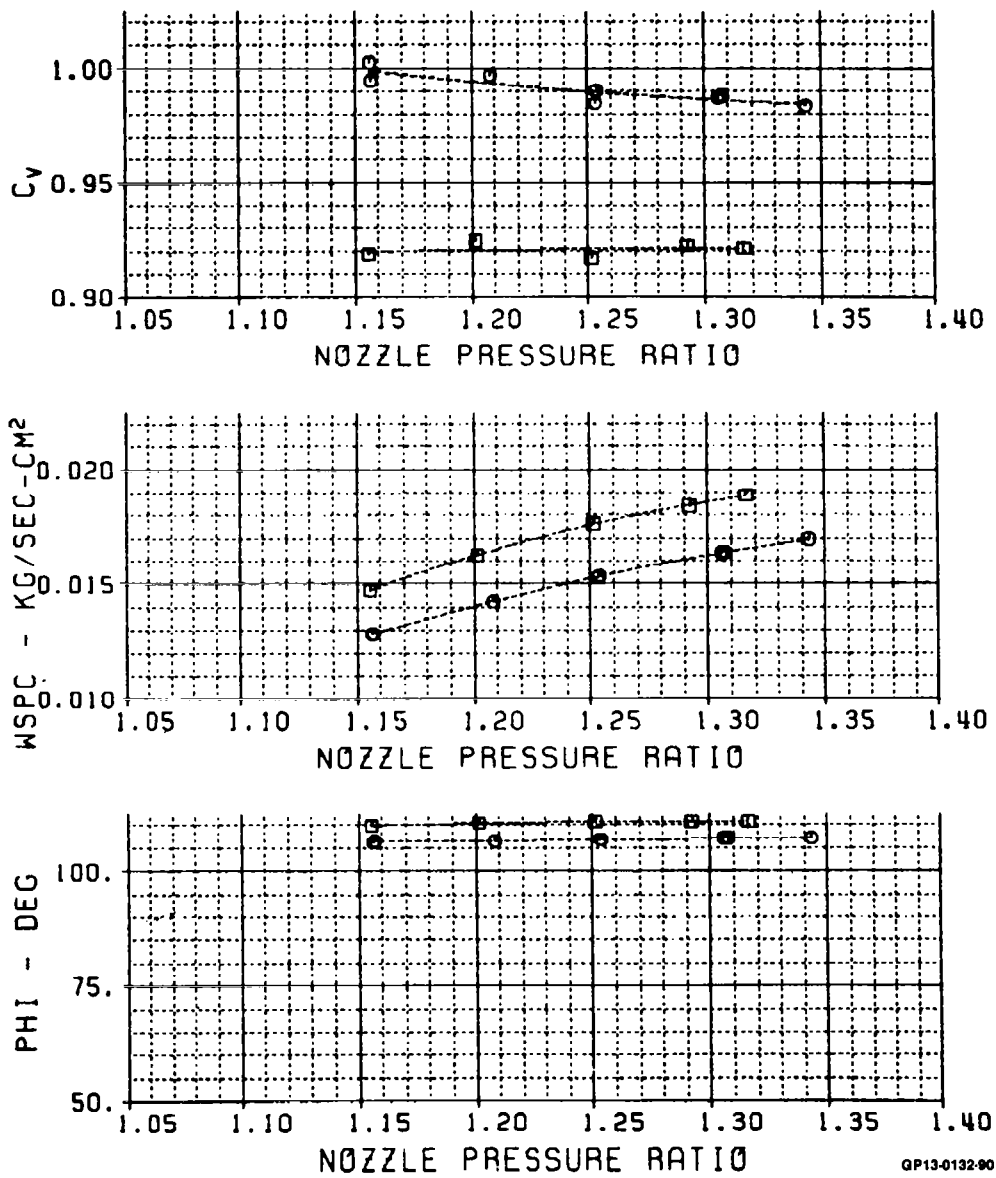


FIGURE 112

CORE NOZZLE RESEARCH MODEL TEST

STM	TEST	RUN	HOOD	RR/R7	DESCRIPTION	
■	54	1080	35.500	0.8163	SLOT. MIX. - 100% OPEN	CRUIS
○	54	2079	35.500	0.8163	SLOT. MIX. - 100% OPEN	CRUIS
▲	54	2080	35.500	0.8163	SLOT. MIX. - 100% OPEN	CRUIS

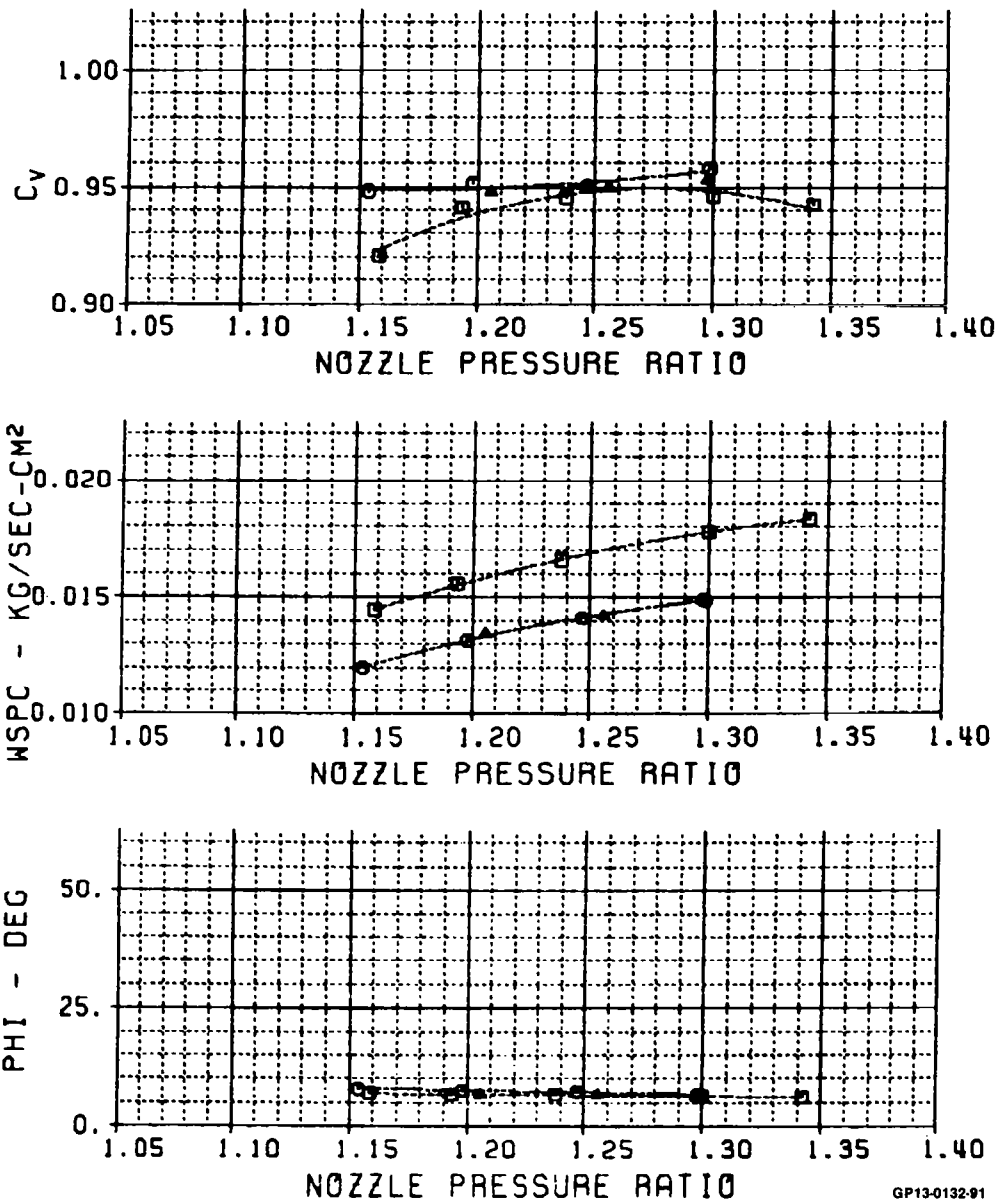


FIGURE 113

CORE NOZZLE RESEARCH MODEL TEST

SYM	TEST	RUN	HOOD	RR/R7	DESCRIPTION
□	54	1081	35.500	0.8163	SLOT. MIX. - CLOSED CRUISE I

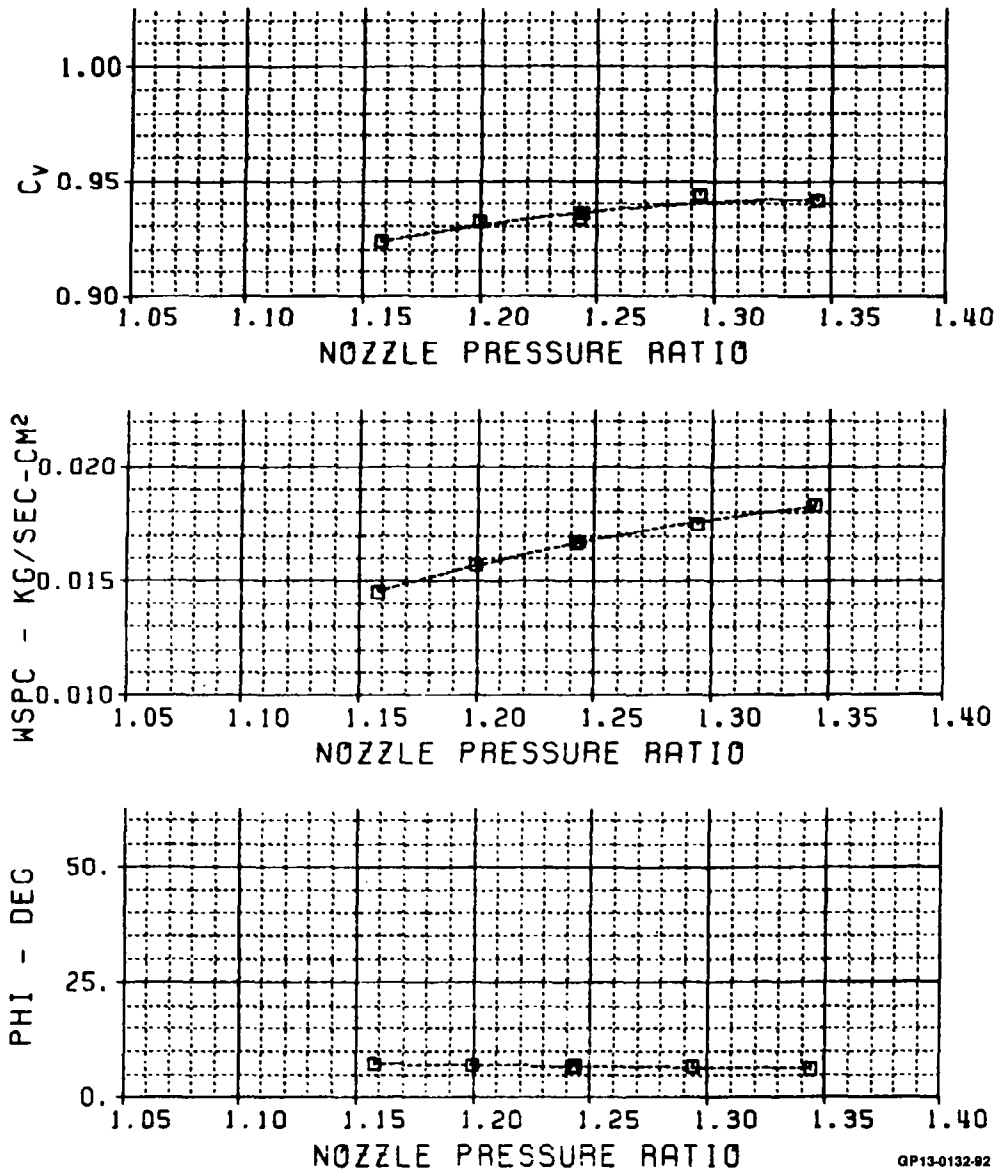


FIGURE 114

CORE NOZZLE RESEARCH MODEL TEST

SYM	TEST	RUN	HODD	R8/R7	DESCRIPTION
□	54	1082	60.000	1.5781	SLOT: MIX: - 100% OPEN
○	54	2082	60.000	1.5781	SLOT: MIX: - 100% OPEN

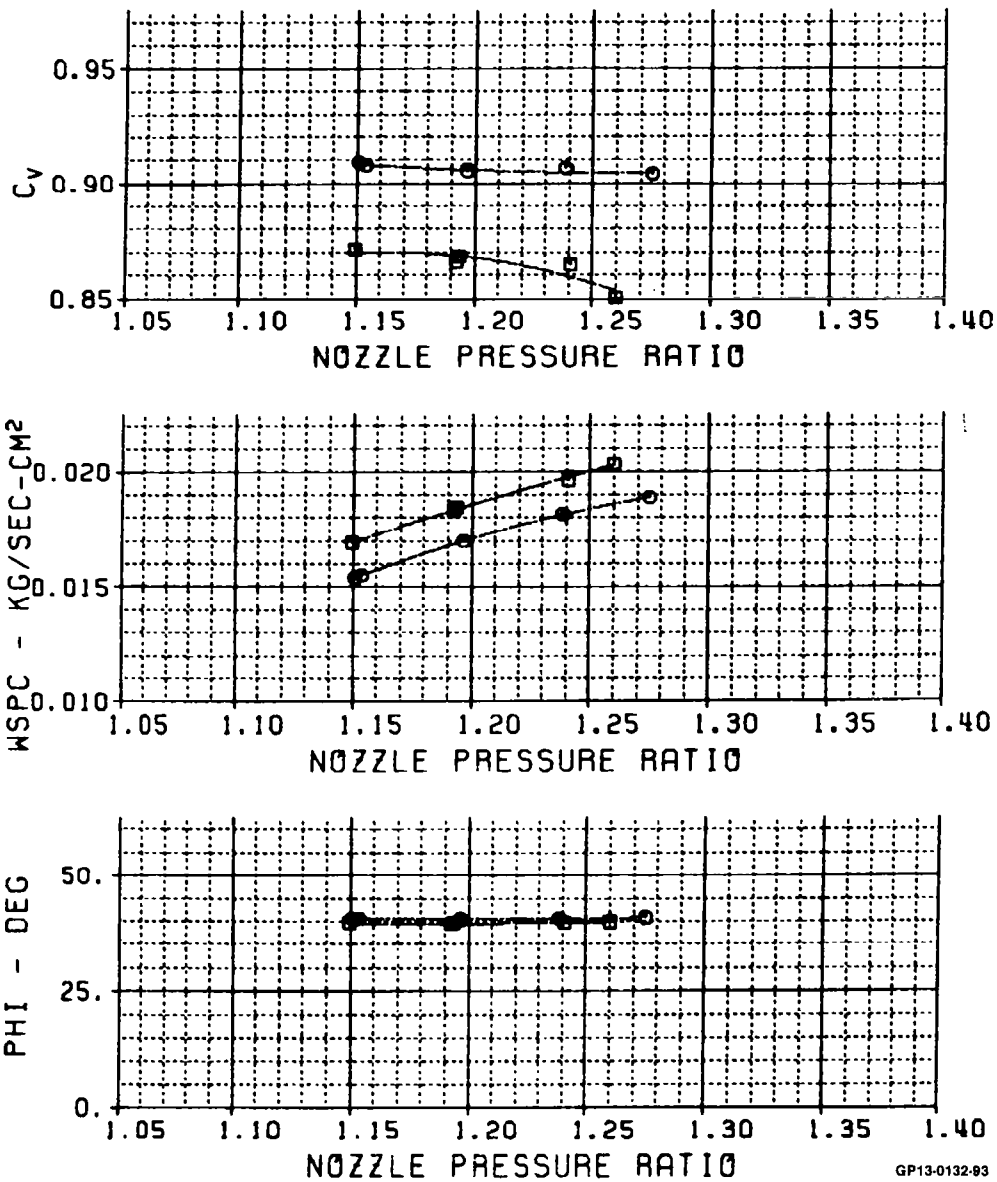


FIGURE 115

CORE NOZZLE RESEARCH MODEL TEST

STM	TEST	RUN	HOOD	R6/R7	DESCRIPTION
54	1083	90.000	1.5781	SLOT. MIX. - 100% OPEN	
54	2083	90.000	1.5781	SLOT. MIX. - 100% OPEN	

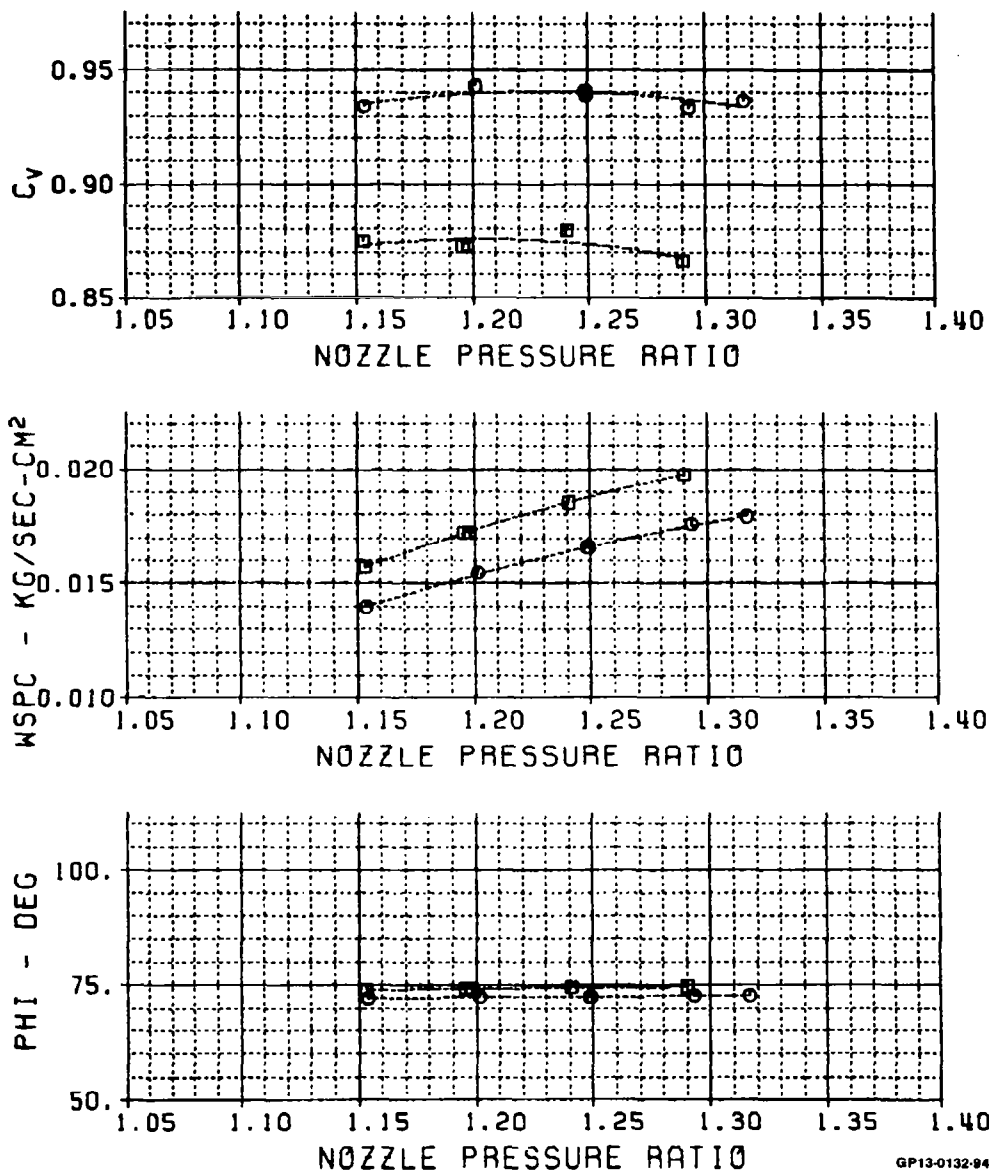


FIGURE 116

CORE NOZZLE RESEARCH MODEL TEST

SYM	TEST	RUN	HOOD	A8/A7	DESCRIPTION
□	54	2084	110.00	1.5781	SLOT. MIX. 88% OPEN

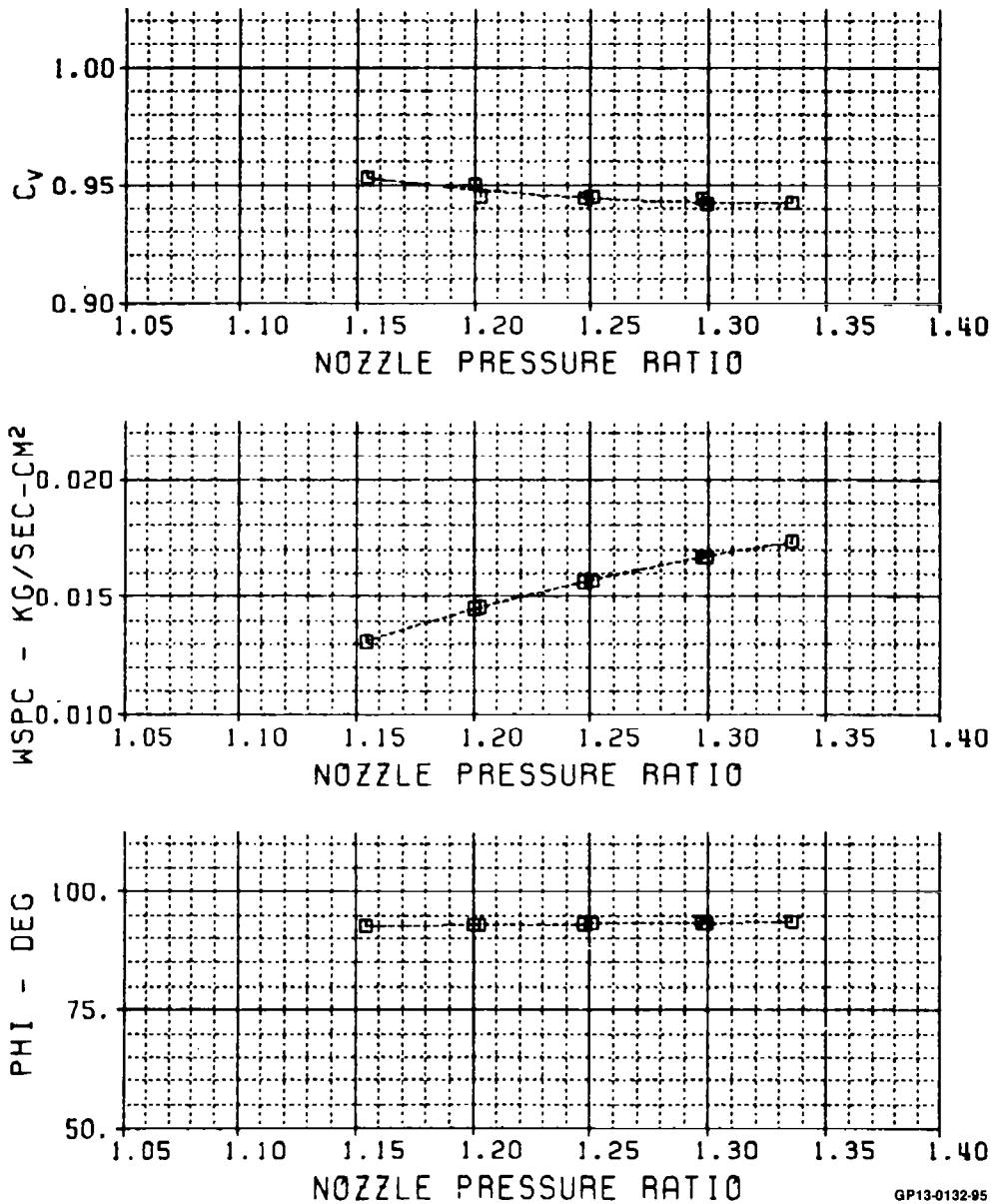


FIGURE 117

CORE NOZZLE RESEARCH MODEL TEST

SYM	TEST	RUN	HOOD	A8/A7	DESCRIPTION
□	54	1085	110.00	1.5781	SLOT. MIX. - CLOSED

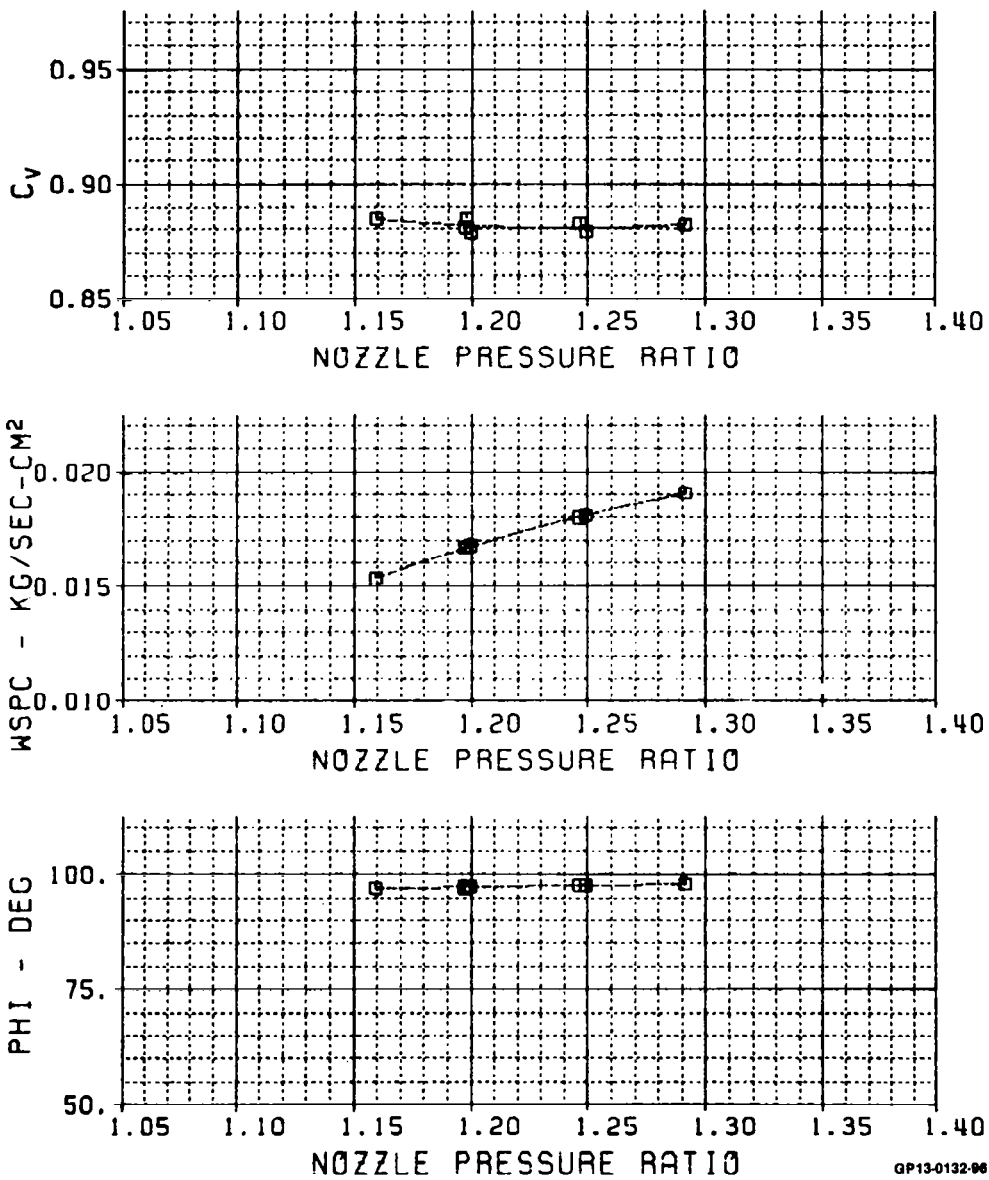


FIGURE 118

CORE NOZZLE RESEARCH MODEL TEST

SYM	TEST	RUN	HODD	RB/R7	DESCRIPTION
□	54	1078	110.00	1.5781	SLOT. MIX. - 100% OPEN
○	54	2078	110.00	1.5781	SLOT. MIX. - 100% OPEN

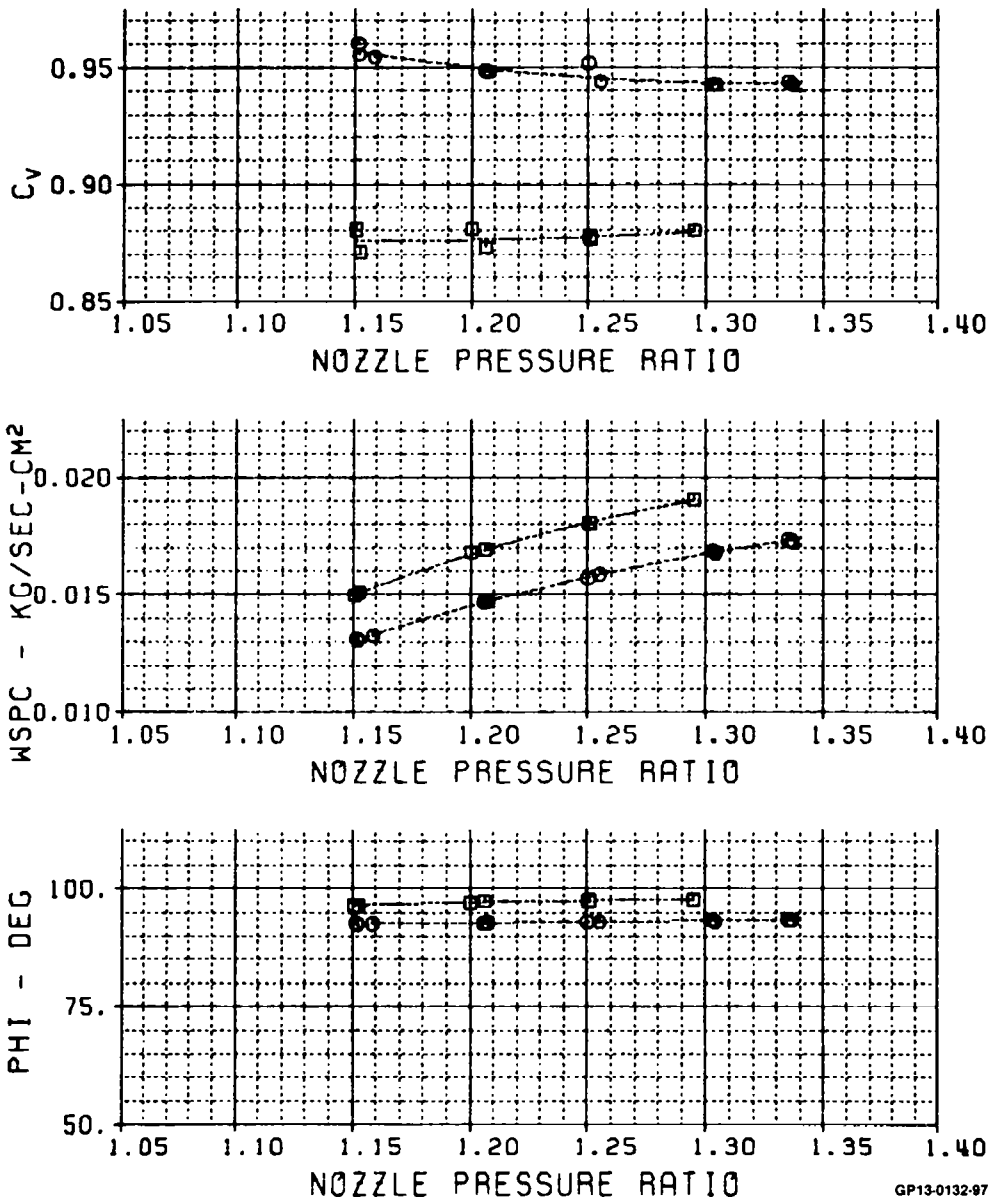


FIGURE 119

CORE NOZZLE RESEARCH MODEL TEST

STM	TEST	RUN	HOOD	AB/AT	DESCRIPTION
□	54	1077	110.00	1.5781	90 DEG. ELBOW
○	54	2077	110.00	1.5781	90 DEG. ELBOW

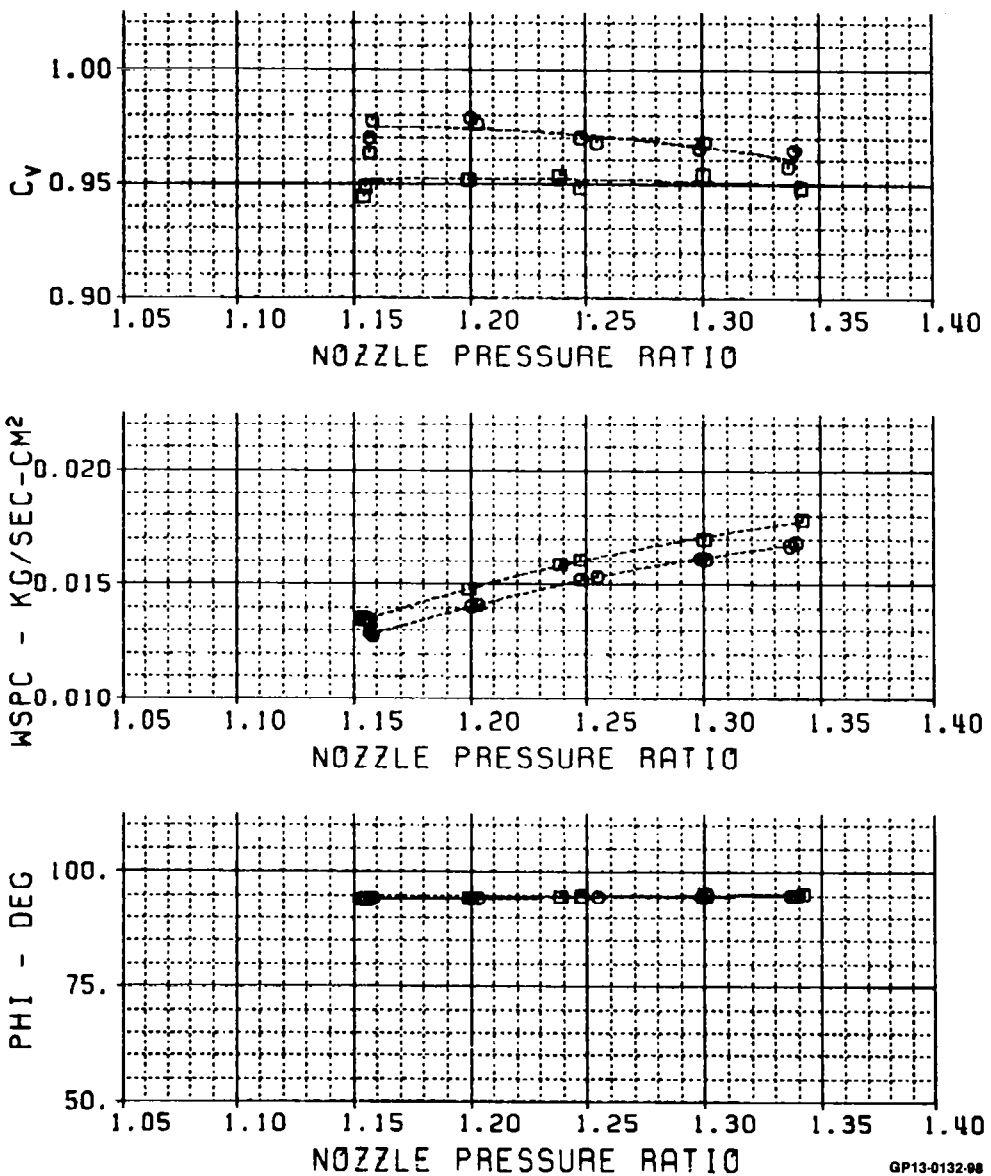


FIGURE 120

CORE NOZZLE RESEARCH MODEL TEST

STM	TEST	RUN	HODD	A8/A7	DESCRIPTION
□	54	1043	35.500	0.8163	REF. CLOS. HUB CRUISE NOZZLE
○	54	1045	35.500	0.8163	REF. CLOS. HUB CRUISE NOZZLE
▲	54	3045	35.500	0.8163	REF. CLOS. HUB CRUISE NOZZLE

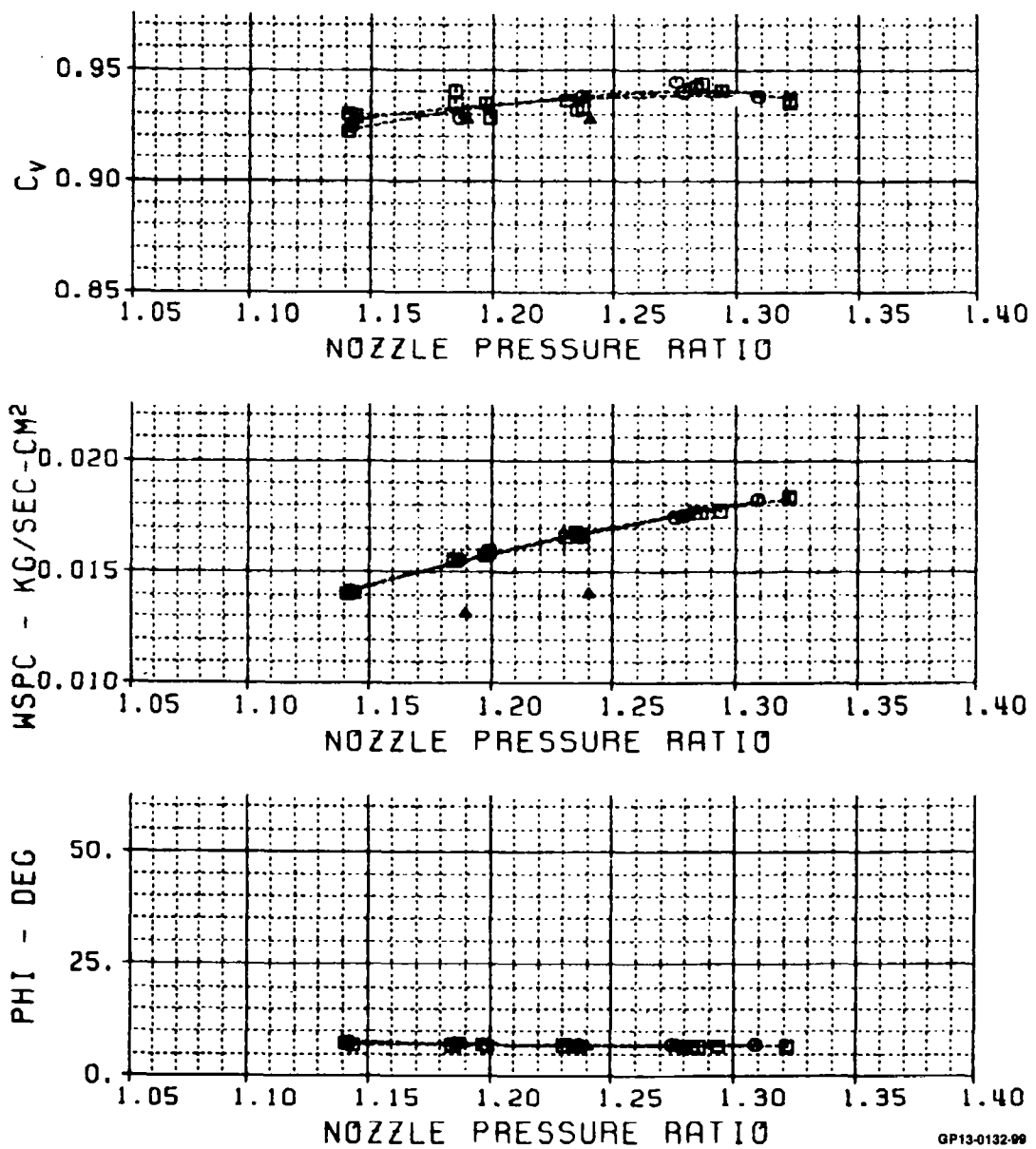


FIGURE 121

CORE NOZZLE RESEARCH MODEL TEST

SYM	TEST	RUN	HODD	AB/AT	DESCRIPTION
□	54	3049	35.500	1.5781	REF. CLOS. HUB

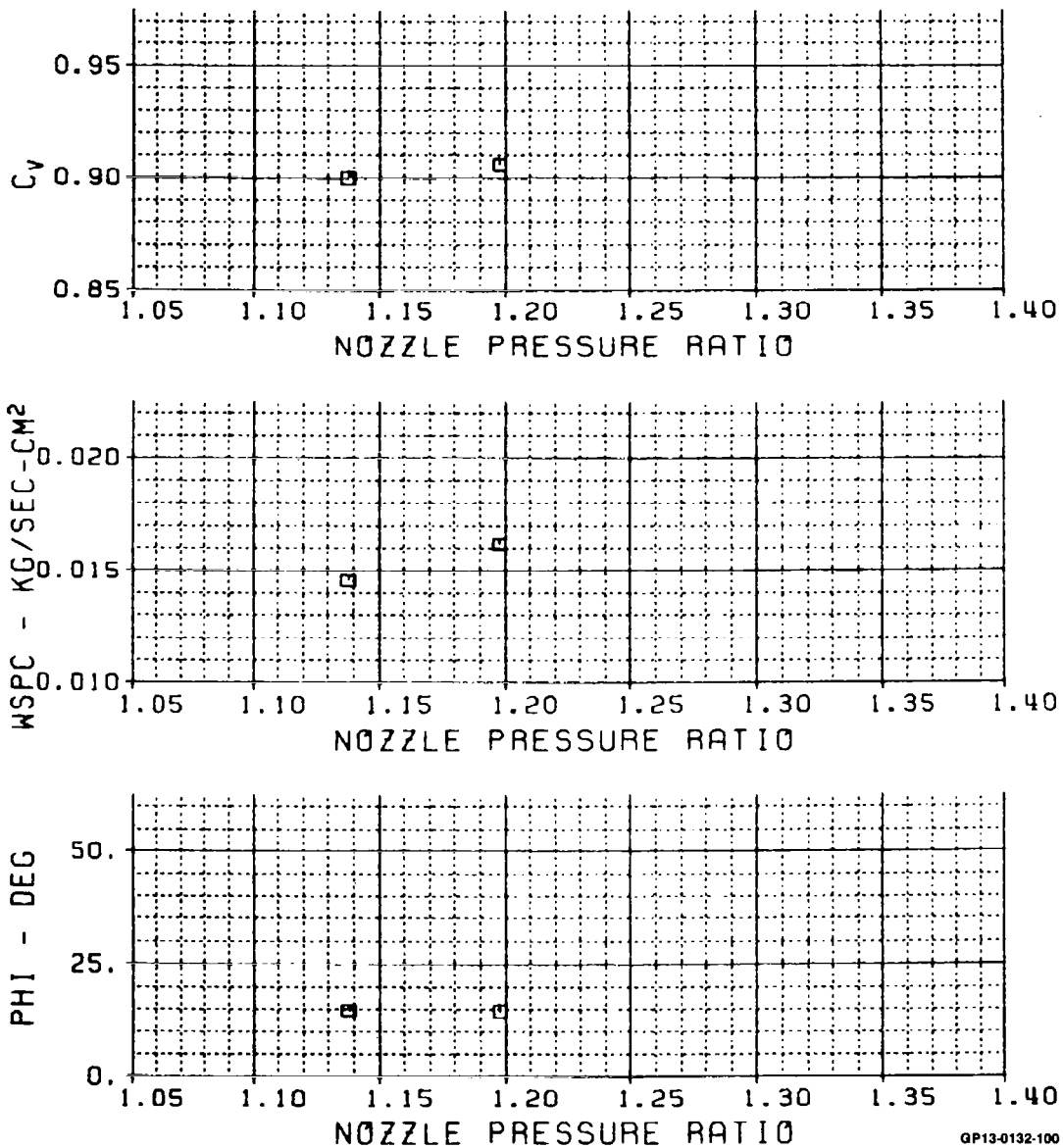


FIGURE 122

CORE NOZZLE RESEARCH MODEL TEST

SYM	TEST	RUN	HOOD	R8/R7	DESCRIPTION
□	54	3048	75.000	1.5781	REF. CLOS. HUB

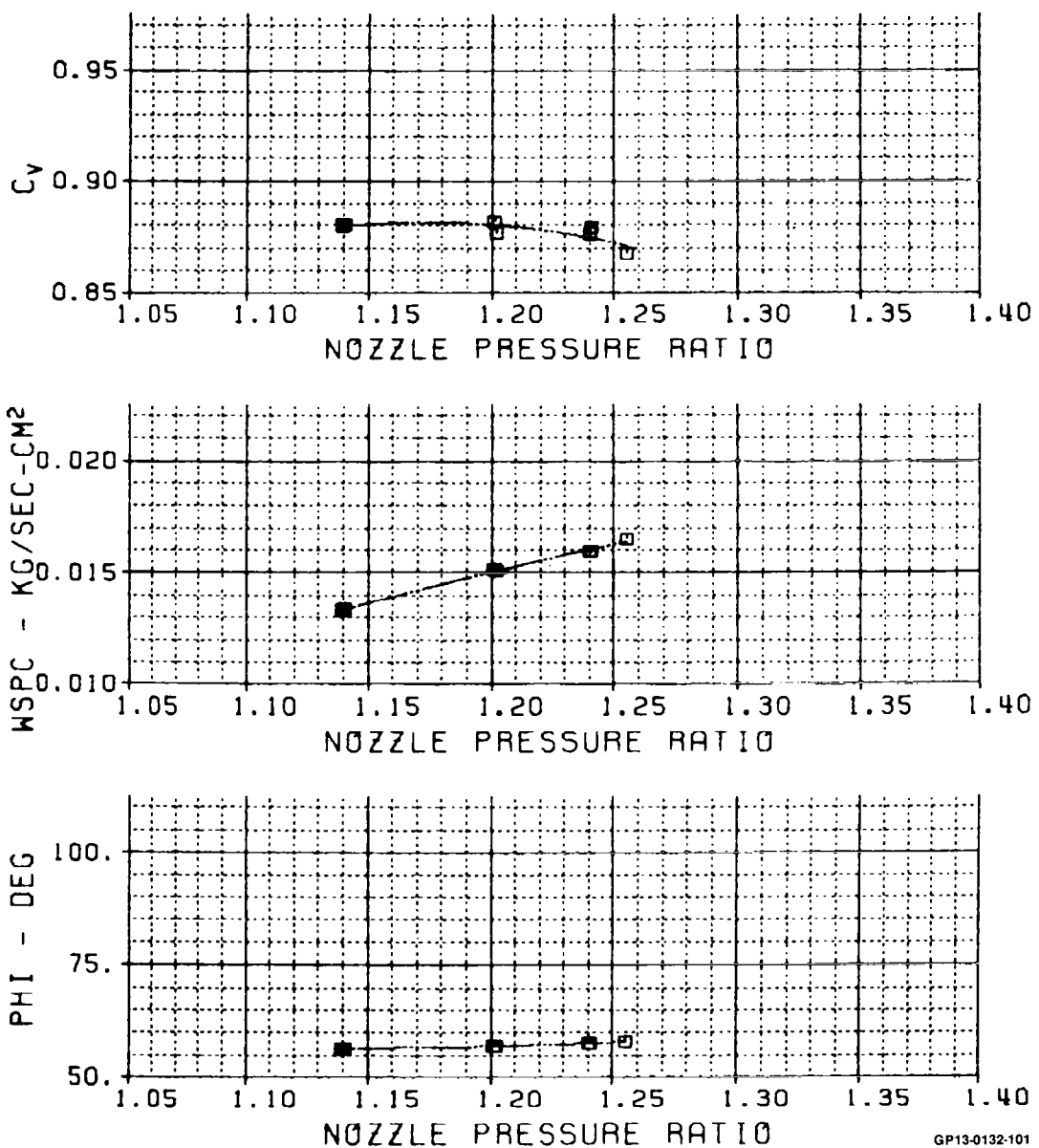


FIGURE 123

CORE NOZZLE RESEARCH MODEL TEST

STM	TEST	RUN	HOOD	AB/AB	DESCRIPTION
54	304G	110.00		1.5781	REF. CLOS. HUB

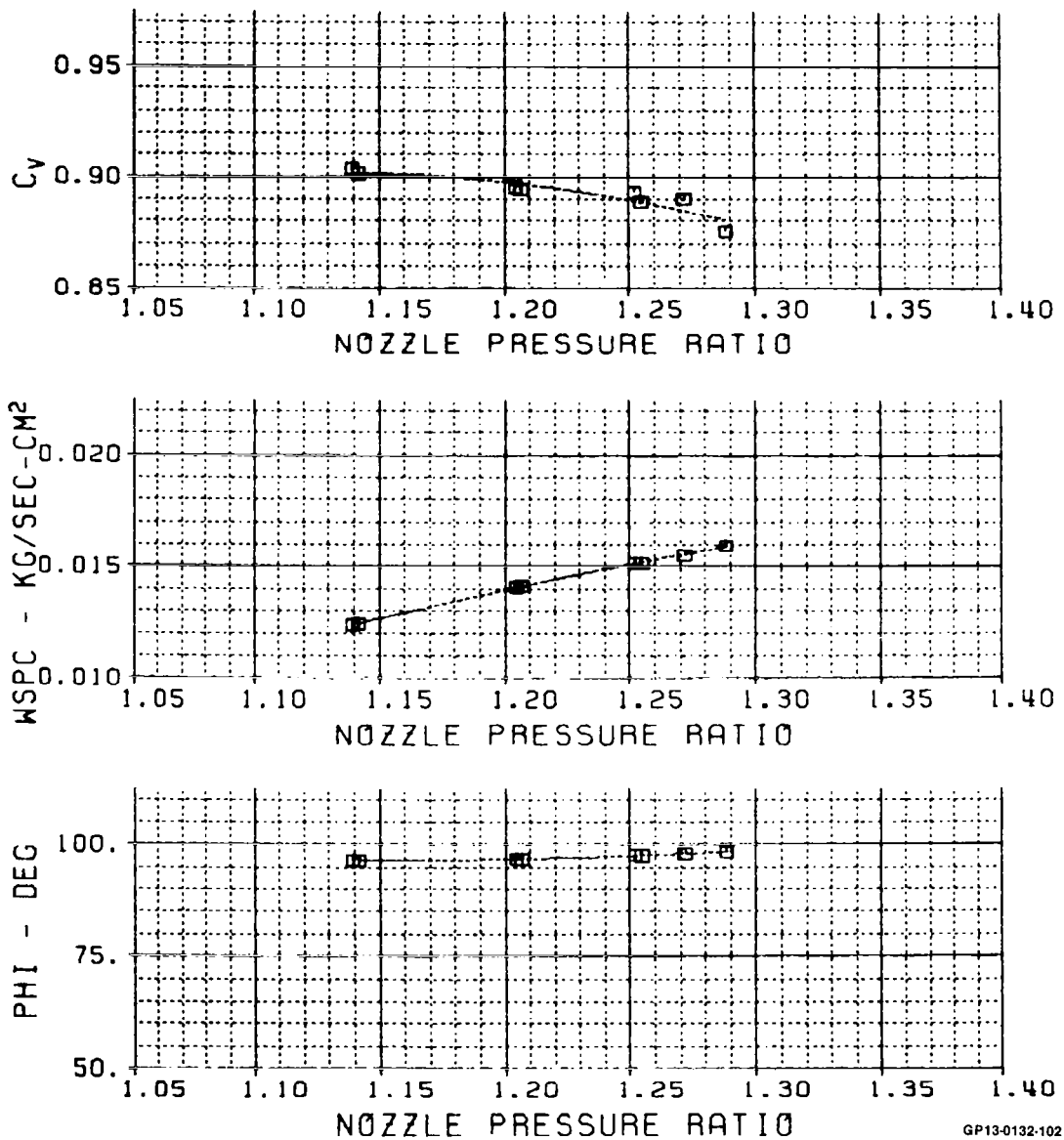


FIGURE 124

CORE NOZZLE RESEARCH MODEL TEST

SYM	TEST	RUN	HOOD	RB/R7	DESCRIPTION
□	54	3047	120.00	1.5781	REF. CLOS. HUB

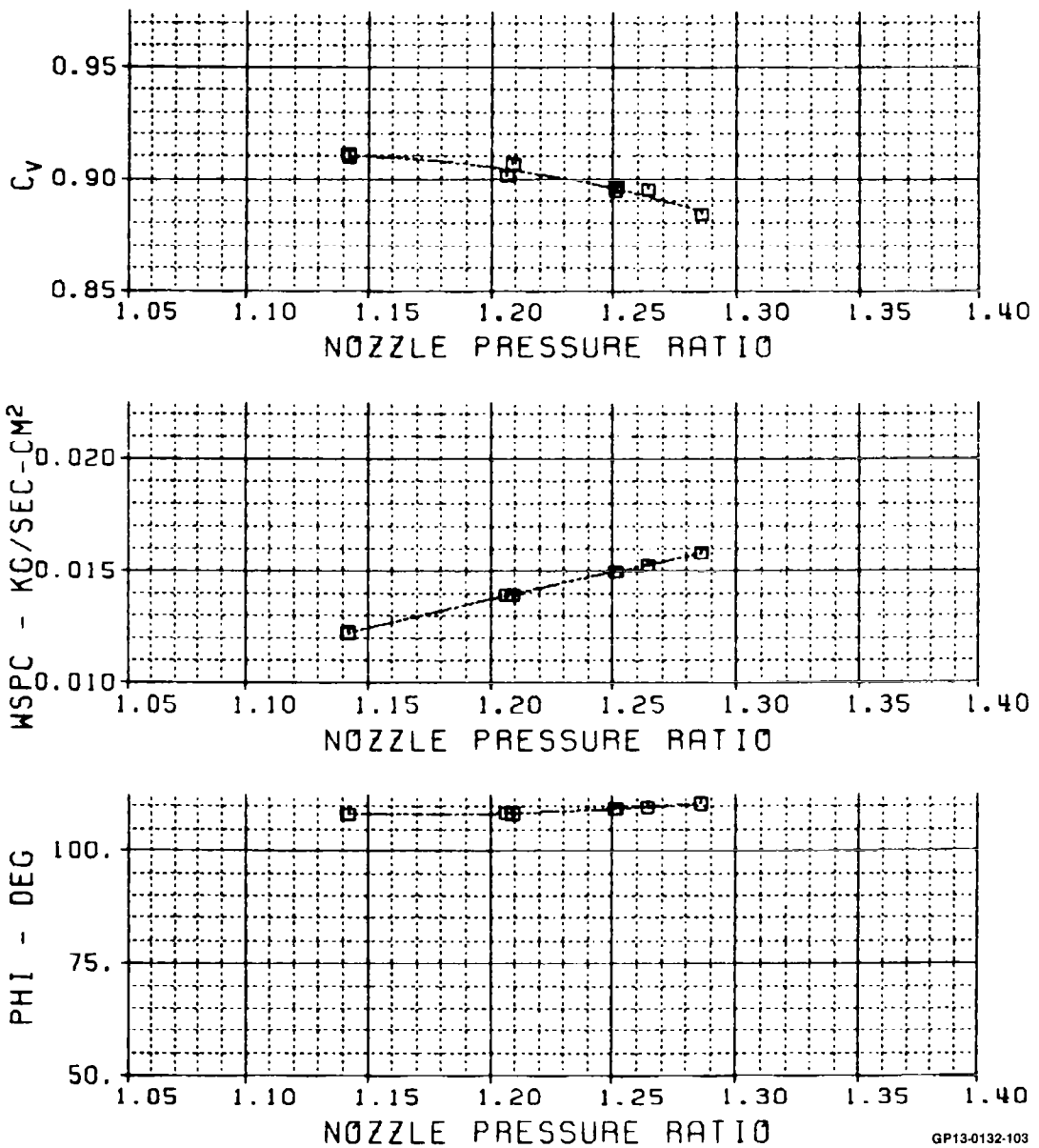


FIGURE 125

CORE NOZZLE RESEARCH MODEL TEST

STM	TEST	RUN	HOOD	R8/R7	DESCRIPTION
■	54	1088	0.000	0.7783	ALT. NO.2 CORE
○	54	2088	0.000	0.7783	ALT. NO.2 CORE

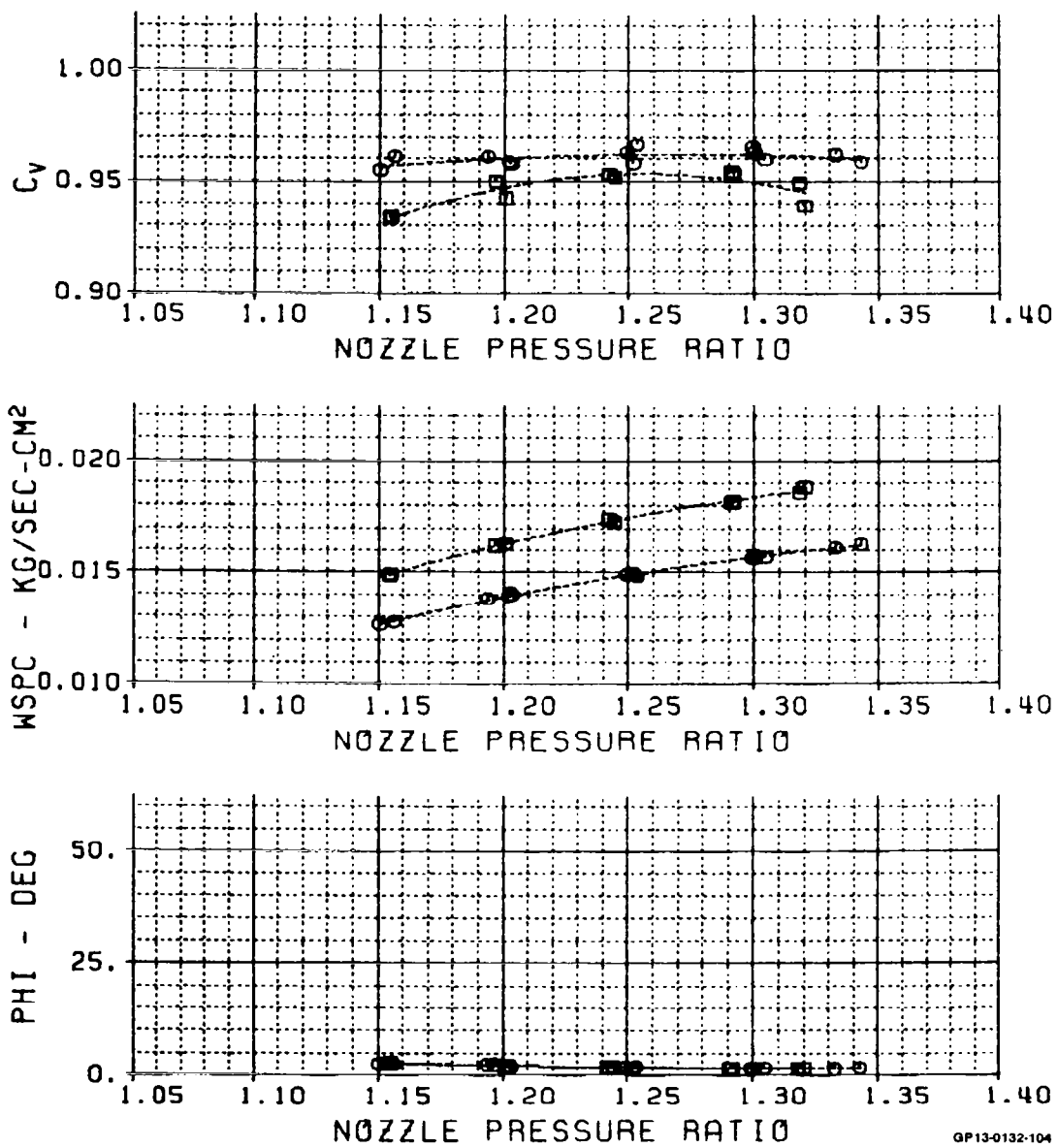


FIGURE 126

1. Report No. NASA CR-3508	2. Government Accession No.	3. Recipient's Catalog No.	
4. Title and Subtitle TESTS OF A "D" VENTED THRUST DEFLECTING NOZZLE BEHIND A SIMULATED TURBOFAN ENGINE		5. Report Date January 1982	
7. Author(s) T. L. Watson		6. Performing Organization Code	
9. Performing Organization Name and Address McDonnell Douglas Corporation McDonnell Aircraft Company Box 516 St. Louis, Missouri 63166		8. Performing Organization Report No. MDC A6930	
12. Sponsoring Agency Name and Address National Aeronautics and Space Administration Washington, D.C. 20546		10. Work Unit No.	
		11. Contract or Grant No. NAS3-21733	
		13. Type of Report and Period Covered Contractor Report	
		14. Sponsoring Agency Code 505-42-62	
15. Supplementary Notes Final report. Project Manager, Paul L. Burstadt, Propulsion Systems Division, NASA Lewis Research Center, Cleveland, Ohio 44135.			
16. Abstract A 20% scale "D" vented thrust deflecting nozzle applicable to subsonic V/STOL aircraft was tested behind a simulated turbofan engine in the Vertical Thrust Stand at the NASA Lewis Research Center. Fan flow was provided by a 30.5-cm (12-in.) diameter tip-turbine fan. An independently controlled hot air source simulated turbofan engine core flow. The model was instrumented to permit measurement of nozzle thrust, fan operating characteristics, nozzle entrance conditions, and static pressures. Nozzle pressure ratio of the fan stream was varied between 1.1 and 1.35 while that for the core stream was varied between engine out (no flow) and 1.6. Nozzle performance was measured for variations in exit area and thrust deflection angle. Six core nozzle configurations were evaluated as were the effects of core exit axial location, mismatched core and fan stream nozzle pressure ratios, and yaw vane presence. Core nozzle configuration affected performance at normal and engine out operating conditions. A mixer type configuration improved engine out performance. Highest vectored nozzle performance resulted for a given exit area when core and fan stream pressures were equal. High nozzle performance can be maintained at both normal and engine out conditions through control of the nozzle entrance Mach number with a variable exit area.			
17. Key Words (Suggested by Author(s)) Nozzle Thrust deflecting Low pressure ratio Turbofan engine nozzle V/STOL nozzle		18. Distribution Statement Unclassified - unlimited STAR Category 02	
19. Security Classif. (of this report) Unclassified	20. Security Classif. (of this page) Unclassified	21. No. of Pages 138	22. Price* A07

* For sale by the National Technical Information Service, Springfield, Virginia 22161